UNIVERSITÀ DEGLI STUDI FIRENZE

DOTTORATO DI RICERCA IN SCIENZE DELLA TERRA

CICLO XXIX

COORDINATORE Prof. LORENZO ROOK

Dating Late Cenozoic glacial variations with Surface Exposure Dating.

Datazione delle variazioni glaciali cenozoiche tramite età di esposizione superficiale.

Settore Scientifico Disciplinare GEO/04

Dottorando
Dott. Stefano Casale

Tutore
Prof. Carlo Baroni

Co-Tutore
Prof.ssa Maria Cristina Salvatore

Co-Tutore
PD Dr. Susan Ivy-Ochs

Coordinatore
Prof. Lorenzo Rook

Anni 2013/2016

INDEX

Abstract

The main goal of the research project was the reconstruction of a more detailed chronology of significant stages of the glacial history in key sites characterized by different geographical location (middle and high latitutes): the Ortles-Cevedale and Adamello-Presanela massifs (Rhaetian Alps) and Victoria Land (East Antarctica). The work was conducted to define the chronology of the sequence of glacier expansions that occurred during the Late Cenozoic, relevant for the reconstruction of the palaeoclimate evolution at local and global scale. We used a geomorphological and glacial-geological approach supported by cosmogenic isotope dating techniques (Surface Exposure Dating, SED) applied on glacial deposits and relict surfaces.

Alps

We studied key sites of the Ortles-Cevedale and Adamello-Presanella massifs. In detail, we focused on the Alta Val di Peio (Ortles-Cevedale) and on the upper Sole, Malga and Adamè valleys (Adamello-Presanella). Different glacial advances have been reconstructed and correlated to the alpine Lateglacial stages. The reconstructions obtained conducted to the generation and analysis of new morphometric parameters of the palaeo-glaciers in terms of areal extension, volume and Equilibrium Line Altitude (ELA). The reconstructed phases have been chronologically constrained trough the Surface Exposure Dating (SED) technique. New ^{10}Be ages, related to the geomorphological context, allowed to define the chronology of different glacial phases in the studied valleys. In particular, we identified the Lateglacial phases of Gschnitz, Daun and Egesen for the Sole, Malga and Adamè valleys. Furthermore in the upper Val di Peio and Val di Sole we found evidences of a double glaciers response to the last climate deterioration event of the Pleistocene, the Younger Dryas (YD). The alpine glacial Gschnitz stadial has been chronologically constrained before 15.7±1.2 ka. The Egesen stadial was bracketed in the 13.2±1.2 ka – 9.9±0.6 ka time interval and produced a double response correlable to the Younger Dryas. The two cited late glacial phases bracket the Daun stadial advance.

Antarctica

Concerning the antarctic context a georeferenced database of the available SED ages of the Victoria Land was implemented. The database made easier the overview on the disposition and entity of the available data. The archive was completed with the samples collected in several Antarctic expeditions by the Research Group of Geomorphology of Università di

Pisa. Forty samples of the latter group have been selected and dated at the ETH Zurich laboratory. The obtained ages allowed us to provide new insight on the long-lasting glacial history ranging from thousands to millions of years.

We are able to provide new evidences concerning the Last Glacial Maximum (LGM) and the subsequent deglaciation trend both for northern (Cape Sastrugi) and southern (Ross Island) Victoria Land sectors. A poliphasic evolution of the Younger Drift (Terra Nova Drift) allowed us to identify different glacial advances during the Late Pleistocene (LGM, ca 40 ka and older than 70 ka).

Furthermore, we obtained new data related to glacial phases occurred during the Middle Pleistocene. The latter group of ages covers a time interval of ca. 430-120 ka and derives from the dating of erratic boulders located on Ross Island and on the Miller Butte and Frontier Mountains nunataks and from a bedrock sample collected at Brien Rocks. In this time interval it is possible to speculate at least two glacial phases that can be confined in the 180-120 ka and 280 ka time intervals.

The dating of relict surfaces from Miller Butte and the Frontier Mountains told an older story, in the order of millions of years of exposition to cosmic radiation (the oldest age was obtained from the Frontier Mountains, ca. 5.1 Ma). The data obtained, correlated with available ages from other sites (i.e. Mount Keinath, Mount Abbott, Mount Pollock, Archambault Ridge), allowed us to speculate for this sector, located at the margin of the East Antarctic Ice Sheet (EAIS), the persistence of hyper-arid and cold desert conditions since at least 5-7 Ma, as documented by very reduced erosion rates (few cm/Ma).

Riassunto

Obiettivo principale del progetto di ricerca è stata ricostruzione di una più dettagliata cronologia di alcune tappe significative della storia glaciale di siti chiave che si caratterizzano per diversa posizione geografica (medie e alte latitudini): i massicci Ortles-Cevedale ed Adamello-Presanella nelle Alpi Retiche e la Terra Vittoria (Antartide Orientale). La ricerca è rivolta alla definizione, anche cronologica, delle fasi di massima e di minima espansione dei ghiacciai occorse nel tardo Cenozoico, che risultano determinanti per la caratterizzazione dell'evoluzione paleoclimatica anche a scala globale. La ricostruzione della storia glaciale nei due siti si basa su di un approccio prettamente geomorfologico e geologico glaciale che si avvale delle tecniche di datazione tramite isotopi cosmogenici (*Surface Exposure Dating*, SED) applicate a campioni di roccia provenienti da depositi glaciali e superfici relitte.

Alpi

Sono stati studiati siti chiave dei massicci dell'Ortles-Cevedale e dell'Adamello-Presanella. Più precisamente, l'attenzione è stata focalizzata sull'Alta Val di Peio (Ortles-Cevedale) e sulle valli Sole, Malga ed Adamè (Adamello-Presanella). Per queste zone sono state ricostruite, utilizzando criteri geomorfologici, diverse fasi di avanzata dei ghiacciai occorse alla fine del Pleistocene ed ascrivibili agli stadi Tardoglaciali alpini. Le ricostruzioni eseguite hanno portato alla generazione ed analisi di nuovi dati morfometrici relativi ai paleo-ghiacciai per i quali sono stati ottenuti aree, volumi ed Equilibrium Line Altitude (ELA). Alle fasi ricostruite è stato dato un vincolo cronologico mediante la tecnica di datazione tramite età di esposizione superficiale (*Surface Exposure Dating*, SED). Le nuove date, messe in relazione con il contesto geomorfologico, hanno quindi permesso di definire la cronologia delle diverse fasi glaciali individuate nelle valli campionate. In particolare, sono state individuate le fasi Tardoglaciali di Gschnitz, Daun, Egesen nelle valli di Sole, Malga ed Adamè. Inoltre nella Val di Sole e nell'Alta Val di Peio sono state riscontrate evidenze di una doppia risposta dei ghiacciai all'ultimo evento di deterioramento climatico del Pleistocene, lo*Younger Dryas* (YD). Gli stadi Tardoglaciali di Gschnitz e Daun sono stati vincolati cronologicamente rispettivamente a prima di 15.7±1.2 ka e 15.0±1.0 ka. Lo stadio di Egesen è stato individuato nell'intervallo 13.2±1.2 ka – 10.5±0.8 ka. Nelle valli Sole e Peio la seconda risposta dei ghiacciai allo Younger Dryas è stata vincolata tra 11.1±0.8 ka e 9.9±0.6 ka e tentativamente correlata alla fase finale dell'Egesen

Antartide

In riferimento al contesto antartico è stato implementato un database georeferenziato delle età di esposizione superficiali disponibili in letteratura per la Terra Vittoria. Il database ha reso più semplice la visualizzazione della disposizione ed entità dei dati disponibili. L'archivio è stato completato con i campioni del Gruppo di Ricerca di Geomorfologia dell'Università di Pisa. Quaranta di questi campioni sono stati selezionati e datati tramite SED presso i laboratori dell' ETH di Zurigo. Le datazioni ottenute, contestualizzate a livello geomorfologico e confrontate con il materiale bibliografico, ci hanno permesso di raccontare una storia che va da migliaia a milioni di anni. Più in dettaglio siamo in grado di fornire nuove evidenze in merito all'ultimo massimo glaciale (LGM) ed alla seguente deglaciazione sia per settori della Terra Vittoria Meridionale (Ross Island) che della Terra Vittoria Settentrionale (Cape Sastrugi). Altri dati (Lichen Hillse Cape Sastrugi, Terra Vittoria Settentrionale) ci hanno permesso di individuare una polifasicità dell'evoluzione dello *Younger Drift* (*Terra Nova Drift*) come conseguenza di diverse avanzate glaciali durante il Pleistocene, anche antecedenti (90-40 ka) l'ultimo massimo glaciale. Procedendo verso fasi più antiche è possibile fornire dati in merito a fasi glaciali relative al Pleistocene Superiore e Medio. Questo gruppo di età è confinabile in un arco temporale di circa 450-120 ka e deriva dalla datazione di massi erratici situati su Ross Island e presso i rilievi di Miller Butte e delle Frontier Mountains e da un campione di substrato di Brien Rocks. In questo arco temporale è possibile ipotizzare almeno due fasi glaciali confinabili a circa 180-120 ka e 280 ka. Infine, interessanti informazioni ci vengono fornite dalle datazioni eseguite su campioni di substrato provenienti da Miller Butte e dalle Frontier Mountains. Le età ottenute testimoniano un'esposizione alla radiazione cosmica nell'ordine di milioni di anni (il dato più antico deriva dalle Frontier Mountains, ca. 5.1 Ma). Quanto ottenuto, messo in relazione con altri siti quali Monte Keinath, Monte Abbotee Monte Pollock, ci ha permesso di ipotizzare per quest'area, situata al margine della calotta Est antartica (EAIS), il perdurare da circa 5-7 Ma di condizioni di deserto freddo, arido e con bassissimi tassi di erosione. In sintesi quanto ottenuto ci permette di meglio caratterizzare le fasi della storia glaciale e l'entità delle fluttuazioni nei diversi intervalli temporali individuati.

1- Introduction

Glaciers and ice sheets are fundamental indicators of the climate change because they respond directly to precipitation and temperature variations. Their sensitivity to the climate signals finds expression in variations of the mass balance and consequently in glacial advances or retreats. In fact, the extent and volume of past glaciers and the fluctuation of Equilibrium Line Altitudes (ELAs) represent the most direct response of the cryosphere to global and local climate changes (Oerlemans, 2001).

Ice sheets play a crucial role in driving climate change and in influencing the level of the oceans. In fact, even a modest change in ice heets mass balance could strongly affect future sea level (Lemke *et al.*, 2007). A detailed chronology of the events that marked the most significant steps of the Cenozoic glacial history is essential in the framework of the knowledge of the glacial history of the entire planet. The availability of a wider amount of dates for constraining the age of landforms related to glacial activity is absolutely necessary for identifying the main glacial phases and for bracketing the limits of glacier expansions. Defining the dynamics occurred in the past is a guide for better understanding the current status of the cryosphere and can contribute to hypothesize future scenarios induced by global warming.

In this context we studied, applying the same geomorphological and glacial-geological approach, two areas located in different geographic context, the Alps (Rethian Alps) and Antarctica (Victoria Land). Both study areas provide several well-preserved traces of the glacial activity from large time ranges, because were widely ice covered as a consequence of the past climate deterioration events. This condition configure them as invaluable archives for the study of glacial landscape evolution and the reconstruction of paleoclimate. The studied sectors (specially Antarctica) are potential agents in causing climate variations as a consequence of their capability to store large ice masses. Furthermore, the large volume of the Antarctic ice regulates the global sea level and the size of the landmasses

and continental shelves. Any eventual change of the sea level will certainly have influence on the oceans and atmospheric circulation patterns.

Furthermore, if the geomorphological and glacial geological reconstructions are supported by chronological constraints, it is possible to correlate the evolution of the cryosphere on land with climatic events recorded by other proxy data. The alpine glaciers (and in general the mountain glaciers) provide an high spatial and temporal resolution of their fluctuations as a response to the climate changes (IPCC, 2007; WGMS, 2008, 2014). This condition allow us to identify regional scale climatic trends beyond local influencing factors. Relevant climate variations were recorded by glaciers over the Alps and worldwide. These variations can be considered as a consequence of climate events occurred over the Northern Hemispere, the Dansgaard-Oescher events (D/O events). These events find a detailed chronology in the Greenland ice cores (Steffensen *et al*., 2008 and references therein). Nevertheless, the causes of the D/O events are still debated and one of the most important hypothesis is related to the release of fresh water derived from periodical detachments of consistent portions of icebergs from the Laurentide ice sheet. A large amounts of coarse-grained sediments eroded on land (Ice Rafted Debris, IRD) and detected in marine ice cores testified these events and are detected in marine ice cores (Heinrich, 1988). The great amounts of fresh waters derived from the ice melting forced changes in the North Atlantic circulation and caused climate deterioration periods. In this context the alpine glaciers responded to the climate signals with different glacial pulses. The most significant glacial advances were related to the Oldest Dryas and the Younger Dryas cold periods; a third and relatively short climate deterioration, occurred in between the other two, can be identified as the Older Dryas.

In this framework, continental proxies allow us to identify and investigate regional scale climate variability while marine and ice core stratigraphy can be used as reference at the global scale.

The continental records are less widespread on the Antarctic continent, they are related to the ice free areas that constitute only ca 2% of the total

Antarctic extension. On the other hand, the study and correlation with other proxy data of the terrestrial Antarctic records is crucial to enrich the knowledge of the past and future climate dynamics. In the past the majority of the studies on the Antarctic paleoclimate have been based on the ice-cores (e.g. Ciais *et al*., 1994; Blunier *et al*., 1998, Thompson *et al.*, 1998; Steig *et al.*, 1998, 2000; Petit *et al.*, 1999; Masson *et al.*, 2000, European Project for Ice Coring in Antarctica – EPICA community members, 2006) and marine records (e.g. Elverhøi, 1981; Anderson and Bartek, 1992; Shipp and Andersen, 1994; Licht *et al.*, 1996; Bentley and Anderson, 1998; Anderson, 1999; Domack *et al.*, 1991, 2001; Cape Roberts Science Team, 2000). In fact, Ice core records are continuous and with high resolution, but at the same time are limited to the drilling site and to a relatively short time range (i.e. 740 ka, EPICA community members, 2006, Jouzel *et al*, 2007).

It follows that the Surface Exposure Dating (SED) techniques is a valuable tool, applicable in both sectors (Alps and Antarctica) to date glacial features and provide chronological data useful to constrain events of the glacial history in key sites. In fact, in the glacial geology the Surface Exposure Dating was successfully applied since decades in several geographical contexts and conducted to the chronological constrain of the continental records (e.g. Gosse *et al.*, 1995; Ivy-Ochs, 1996; Ivy-Ochs *et al.*, 1996, 2006a, 2008, 2009; Kelly et *al.*, 2004, 2006; Akçar et *al.*, 2007, 2014, 2016; Oberholzer *et al.*, 2003, 2008; Strasky, 2008; Strasky *et al.*, 2009; Di Nicola *et al.*, 2009, 2012; Shulmeister *et al.*, 2010; Delmas *et al.*, 2011; Ballantyne and Stone, 2012; Hippe *et al.*, 2014; Wirsig *et al.*, 2016).

Structure of the thesis

In the first part (chapter 2), the methodology applied during the research is outlined. We describe the adopted approach and the techniques that conducted to the reconstruction of the glacial phases and the obtaining of the new morphometric parameters (areal extension, volume, ELA). Concerning the selected dating techniques, the Surface Exposure Dating, a short history of the method and the basic theoretical principles are

presented. In the second part of the chapter 2 the sampling approach adopted, the samples location and the preparation procedure followed are described. Analises were conducted at the Laboratory of Ion Beam Physics, ETH Zurich for obtaining new ^{10}Be and ^{26}Al ages.

Chapters 3 and 4 are dedicated to the study areas, Alps and Antarctica, respectively. Both chapters have the same structure that includes an introduction part of geographical, geological and geomorphological settings of the study areas, followed by the obtained results and by their discussion. Conclusions for both sectors are presented in the chapter 5 and in Appendix I are reported the thin section analysis of the dated samples.

2 - Material and methods

The reconstruction of the glacial evolution of our study areas was conducted following several steps that can be summarized as proposed in the following scheme.

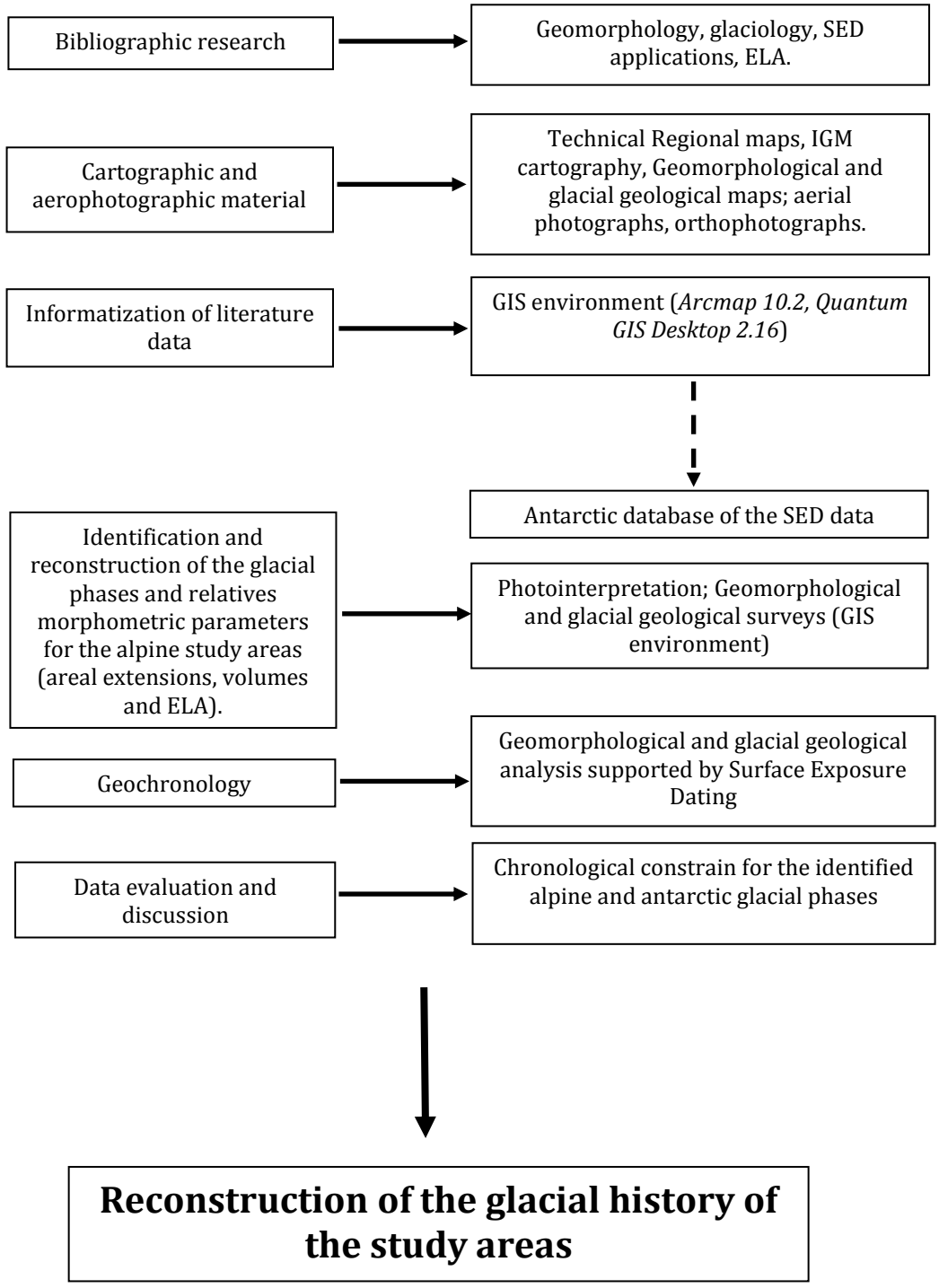

2.1 Bibliographic, cartographic and aerophotographic material

In a first phase previous works related to glacial–geological and geomorphological settings of Rhaetian Italian Alps and East Antarctic Ice Sheet were collected. At the same time a research on the bibliography related to the methodology and application of the Surface Exposure Dating techniques was conducted. The characteristics of the different cosmogenic nuclides were highlighted with the aim to find the most suitable to our purposes. The ^{10}Be radionuclide has been identified as the most appropriate for our study both in terms of time interval applicability that of the target mineral (samples lithology).

A collection of the basic topographical , geomorphological and geological cartography was conducted for the study areas.

For the Alpine sector the Technical Provincial maps (CTP) of Provincia di Trento (scale of 1:10.000) and the Technical Regional maps (CTR) of the Regione Lombardia (scale of 1:10.000) were used as principal cartographic support. As shown in table 2.1.1 we integrated the just mentioned cartography with IGM maps available as WMS service and with Digital Terrain Models (DTM). In particular we used a 5x5 m resolution DTM of Regione Lombardia and a 2x2 m Lidar of Provincia di Trento.

The cartographical material was collected in raster and vector format. These file extensions are suitable to be managed in a Geographic Information System (GIS) environment.

CARTOGRAPHIC DOCUMENT	SOURCE	SCALE	FORMAT
CTP Provincia di Trento	http://www.territorio.provincia.tn.it/portal/server.pt/community/cartografia_di_base/260/cartografia_di_base/19024	1:10.000	Raster/Shp/WMS
CTR Lombardia	http://www.geoportale.regione.lombardia.it/	1:10.000	Raster/Shp/WMS
IGM Map	www.minambiente.it	1:25.000	WMS
IGM Map	www.minambiente.it	1:100.000	WMS
DTM Regione Lombardia	http://www.geoportale.regione.lombardia.it/download-dati	1:5.000	Raster
Lidar Provincia di Trento	http://www.territorio.provincia.tn.it/portal/server.pt/community/lidar/847/lidar/23954	1:5.000	Raster

Table 2.1.1 - Cartographic documents covering the alpine study areas. CTP: Technical Provincial; Map CTR: Technical Regional Map; Shp: Shapefile. IGM: Istituto Geografico Militare; DTM:Digital Terrain Model.

Both for Antarctica and Central Italian Alps, available thematic maps

(geomorphological, geological and glacial elements maps) were collected and georepherenced using a GIS software (tab. 2.1.2).

Area	Type of map	Scale	Reference
Alta Val di Peio (Ortles-Cevedale Massif)	Geomorphological	1:15.000	GNGFG (1986)
Adamello-Presanella Maasif	Glacial elements	-	Castiglioni (1961)
Adamello-Presanella Maasif	Geological	1:50.000	CNR (1995)
Val Miller-Conca del Baitone	Geomorphological	1:15.000	Baroni and Carton (1988)
Adamello	Geological	1:50.000	Carta Geologica d'Italia – Monte Adamello- Foglio 058
Mt. Joyce Quadrangle (Victoria Land, Antarctica)	Geological	1:250.000	GIGAMAP (1999)
Mt. Melbourne Quadrangle (Victoria Land, Antarctica)	Geological	1:250.000	GIGAMAP (2012)
Mt. Murchison Quadrangle (Victoria Land, Antarctica)	Geological	1:250.000	GIGAMAP (1997)
Reeves Névé Quadrangle (Victoria Land, Antarctica)	Geological	1:250.000	GIGAMAP (2012)
Relief Inlet Quadrangle (Victoria Land, Antarctica)	Geological	1:250.000	GIGAMAP (1999)
Sequence Hills Quadrangle (Victoria Land, Antarctica)	Geological	1:250.000	GIGAMAP (2012
Freyberg Mts. Quadrangle (Victoria Land, Antarctica)	Geological	1:250.000	GIGAMAP (2012)
David and Mariner Glaciers (Victoria Land, Antarctica)	Geological	1:500.000	PNRA, CNR – ENEA
Northern Fooyhills (Terra Nova Bay, Antarctica)	Geomorphological	1:20.000	Baroni - PNRA, CNR – ENEA (1987)
Evans Cove (Victoria Land, Antarctica)	Geomorphological	1:50.000	Salvatore *et al.* (1997)
Mt. Murchison Quadrangle (Victoria Land, Antarctica)	Geomorphological	1:250.000	Baroni *et al.* (2004) - PNRA
Mt. Melbourne Quadrangle (Victoria Land, Antarctica)	Geomorphological	1:250.000	Baroni *et al.* (1996) - PNRA
Relief Inlet Quadrangle (Victoria Land, Antarctica)	Geomorphological	1:250.000	Baroni *et al.* (2000) - PNRA

Table 2.1.2 - List of the cartographic material that was scanned, georeferenced and digitalized in GIS environment.

All the maps were georeferenced using the UTM-WGS84 (Universal Transverse Mercator, World Geodetic System 1984 datum) coordinate system. Time-stable landscape features or directly coordinate grids, homogeneously spread along all the map extension were chosen as control anchorage points.

Once the maps were georeferenced, shapefiles provided of relative attribute tables were created in order to digitalize landforms and deposits of glacial origin. In the attribute tables information about the single

landforms are stored, together with geographical location and references. The digitalized data were organized in a database always updatable.

For Antarctica the bibliographic retrieval on the SED applications was conducted also to collect, in a GIS **database,** the available **exposure ages** for the Victoria Land**.** This operation was conducted with the goal to homogenize data from different sources, obtained with different techniques (different cosmogenic nuclides) and make more accessible the existing dataset. The first step was georeferencing the dated samples in the same coordinate system (UTM-WGS84) and create a shape file. To the shape file was associated an attribute table filled with information related to the samples characteristics. The selected data insert in the attribute table (fig. 2.1.1) concern the samples bibliographic references, their geographical attributes (Latitude, Longitude, altitude, locality name), sampling factors (i.e. sample thickness, topographic shielding) and Surface Exposure Dating parameters (used cosmogenic nuclide, cosmogenic nuclide concentration, exposure age). The database was implemented with the samples collected by the research group of Geomorphology of Università di Pisa (Prof. Carlo Baroni, Prof. Maria Cristina Salvatore) during past Antarctic expeditions (from 1997/98 to 2012/13). From the latter group of samples we selected and dated 40 samples collected from erratic boulders and ice free bedrock portions. These samples were collected during expeditions occurred from 2009/10 to 2012/13.

POINT_X	POINT_Y	LITHOLOGY	SAMPLE_DIM	TYPE	THICKNESS	Rho	SHIELDING	10Be_conc	10Be_error	10Be_Age	10Be_age_e
163,702967	-74,595928			erratic	1,5	2,65	0	0	9087,684293	8032	1400
163,703833	-74,596038			erratic	2	2,65	0	0	12459,268582	41820	2774
163,707351	-74,59832			erratic	0,5	2,65	0	0	4060	9124	759
160,743271	-73,200521			bedrock	0	2,65	0	0	0	0	0
160,744739	-73,200674			bedrock	0	2,65	0	0	0	0	0
161,375704	-73,215073			bedrock	1,5	2,65	0	0	327029,141393	357246	20834
160,348184	-72,988512			bedrock	0	2,65	0	0	0	0	0
160,344259	-72,98769			bedrock	2	2,65	0	0	2019590	4144042	726053
160,344489	-72,987499			bedrock	1,5	2,65	0	0	1937040	3643864	542310
160,348247	-72,987535			bedrock	2	2,65	0	0	2202670	5821745	1816640
160,347277	-72,987639			bedrock	0	2,65	0	0	0	0	0
160,35915	-72,974866			bedrock	0	2,65	0	0	0	0	0
160,357929	-72,974789			bedrock	0	2,65	0	0	0	0	0
160,359343	-72,975266			erratico	2	2,65	0	0	152360	180754	9999
160,359343	-72,975266			erratico	1,5	2,65	0	0	212170	273135	15319
160,360036	-72,975256			erratico	2,5	2,65	0	0	146400	185541	10177
163,679261	-74,603569			erratic	2,5	2,65	0	0	14114,926635	41359	3193
163,678461	-74,603488			erratic	1,5	2,65	0	0	8532,435297	16481	1666
163,678818	-74,60304			bedrock	2	2,65	0	0	12320	71246	4126
163,679071	-74,603147			erratic	1,5	2,65	0	0	6901,654468	10387	1279
163,678159	-74,603037			erratics	2	2,65	0	0	8970,239647	9398	1629
160,744739	-73,200674			bedrock	0	2,65	0	0	0	0	0
162,121903	-73,317713			erratic	2	2,65	0	0	83930,874629	90004	5120
162,153993	-73,312793			erratic	1,5	2,65	0	0	55493,664489	56091	3399
162,153895	-73,312781			erratic	1	2,65	0	0	52836,914968	69331	3908
160,237434	-72,70253			bedrock	3	2,65	0	0	1392013,836883	2418683	246037
160,301705	-72,706698			erratic	2,5	2,65	0	0	250606,914427	301018	17003
160,30014	-72,706811			erratic	3	2,65	0	0	114743,544846	123454	6750
160,302696	-72,706595			erratic	2,5	2,65	0	0	458812,783675	423591	26122
160,237432	-72,701313			bedrock	2	2,65	0	0	1238653,312372	1940980	2460370
160,218798	-72,708543			bedrock	2	2,65	0	0	687897,852792	847358	55220
160,217868	-72,708316			bedrock	3	2,65	0	0	2139020,219797	1764581	172068
160,220286	-72,708327			bedrock	2	2,65	0	0	901242,475242	1213758	87360
163,677051	-74,602337			erratic	2,5	2,65	0	0	5609,876983	5751	1008
163,677088	-74,602341			erratic	1,5	2,65	0	0	4340	7568	834
169,27845	-77,53078			erratic	2	2,65	0	0	4220	11987	946

Fig. 2.1.1 - Extract of the Antarctic SED Database attribute table.

2.2 Glaciers reconstruction in Rhaetian Alps

In Rhaetian Alps glacier positions were reconstructed in a relevant valley of the Ortles-Cevedale Massif (upper Peio Valley) and in selected valleys of the Adamello-Presanella Massif. The investigated landforms are located in a spatial interval that ranges from the early Lateglacial-related features until the once located immediately downstream of the LIA moraines.

Landscape analysis after the Last Glacial Maximum was conducted, on the basis of interpretation of aerial photographs, historical maps analysis, as well as Lidar data. Geometry and dimension of ice bodies related to the recognized glacial phases were reconstructed from detailed previous geomorphological studies (Castiglioni, 1961; GNGFG-CNR, 1986; Carturan *et al.,* 2013a, 2014, Baroni *et al.*, 2014), integrated and partially modified by photointerpretation and field surveys. Photointerpretation is a valuable tool in the framework of geomorphological studies and in particular in our case helps in the identification of the glacial features that are essential for reconstructing glacial outlines. The work with stereoscopic pairs of aerial photographs has its base on the principle that two adjacent overlapping photos of a flight line, endlapping for 60% of their extent, enable a 3-dimensional vision of the landscape (Paine and Kiser, 2003). Furthermore, a vertical exaggeration effect inherent in the binocular vision of stereoscopic photographs, allows to better analyse relief variations.

The aerophotographic material analyzed in this work consists in aerial photographs relative to distinct flights, with different ground resolution and nominal scale (tab. 2.2.1). Volo 1959 photograms are characterized by a nominal scale of 1:26.000, and refer to the Upper Peio Valley site. Instead, aerial photographs of Volo Tem.1 Lombardia 1980-83 with a nominal scale of 1:20.000 refer to the Adamello-Presanella Massif.

NAME	YEAR	SERIES	NOMINAL SCALE
-	1959	69	1:26.000
Tem.1 Lombardia 1980-83	1980-1983	63-68-70-71-72/a-72/b-73/c,74/c-75/c-75/d-77/c-79/c-81/b-83/b	1:20.000
Orthophotograps	2006	-	-
Orthophotograps	2012	-	-

Table 2.2.1 -. Characteristics of the aerophotographic and orthophotographic documents used.

Important instruments to support the photointerpretation were the orthophotographs 2006 and 2012 that are available as WMS service on the National Cartographic Portal (PCN, www.minambiente.it). The possibility to manage this digital product on a GIS system configures it as an important tool for the glacial feature identification and digitization.

Once glacial landforms were identified and digitalized in GIS database, glaciers were reconstructed in terms of extension (fig. 2.2.1), volume variation end ELA elevation. Relative position and shape of the moraines contributed to the identification of the different glacial phases and the delineation of a first preliminary relative chronology. Shapefiles were created for the different recognized phases and relative attribute tables filled with geographic information, areal extensions, volume variations and Equilibrium Line Altitude elevation.

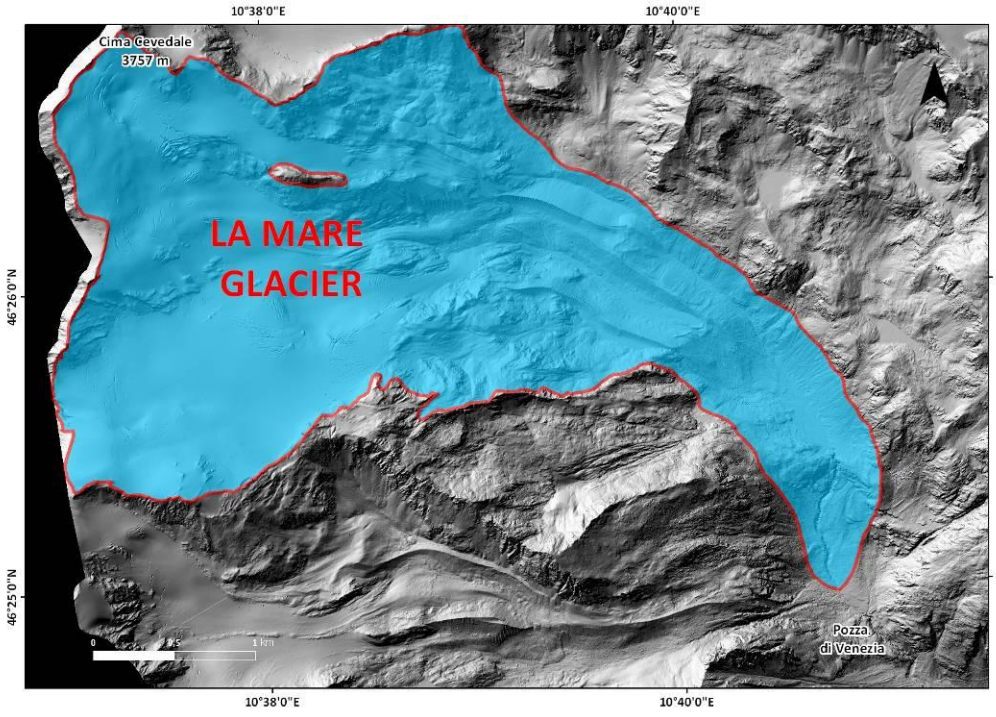

Fig. 2.2.1 - Reconstruction of glacial extension.

The topography of the paleoglaciers were reconstructed using the vectorial contour lines of Provincia di Trento and Regione Lombardia. Following Porter (1975) and Porter and Orombelli (1982). Ice surface topographies were reconstructed (fig. 2.2.2) and contour lines were drawn every 50 m altogether with reliable control points from the original

vectorial contours. Original contours were modified in the glaciated sectors, considering the ice – free bedrock unchanged over the whole time range. Volumes of single phases were calculated by comparing digital terrain models (cell size 10x10 m) in relation with reconstructed ice surface and present deglaciated topography.

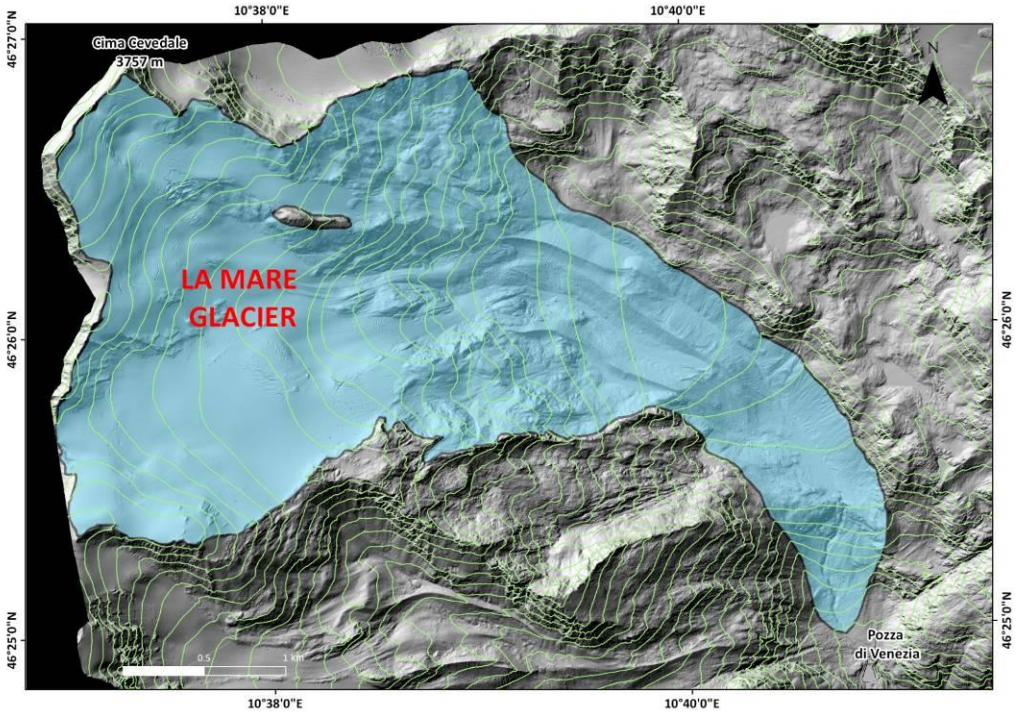

Fig. 2.2.2 - Reconstruction of the paleotopography.

Comparing digital terrain models (cell size 10x10 m) with the present deglaciated topography volumes of single glaciers in the different phases were estimated (fig. 2.2.5). The DTMs were elaborated by generating Triangular Irregular Networks (TIN) from the modified vectorial contour lines and reliable control points. 10x10 m resolution DTMs were also created starting from the unmodified original contour lines to represent the present deglaciated topography (figg. 2.2.3, 2.2.4).

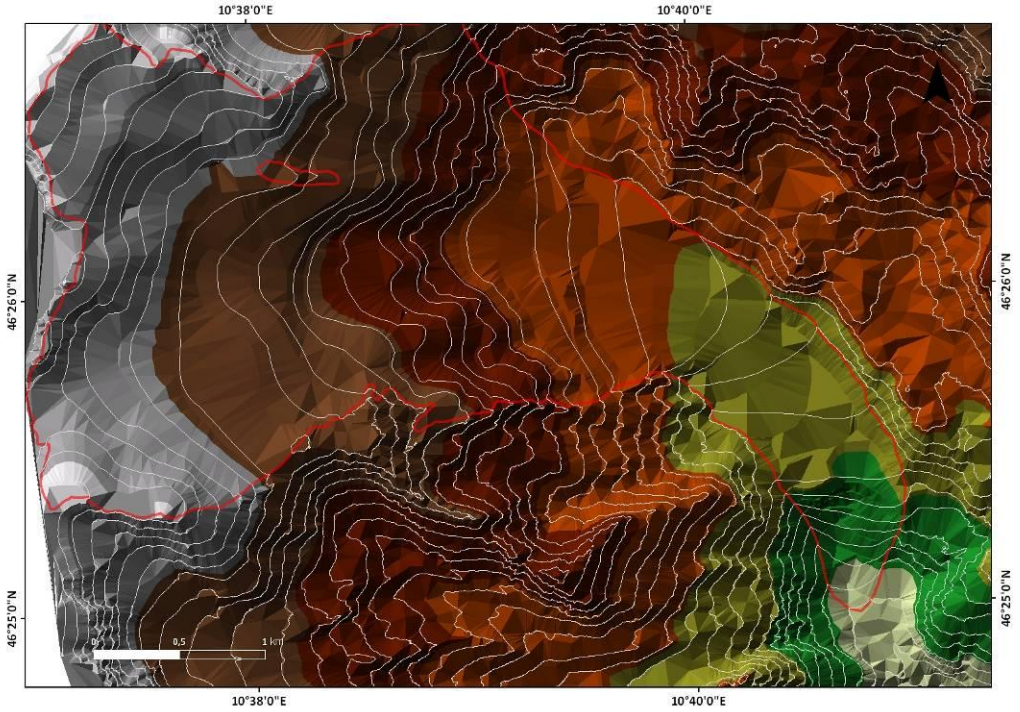

Fig. 2.2.3 - TIN elaboration.

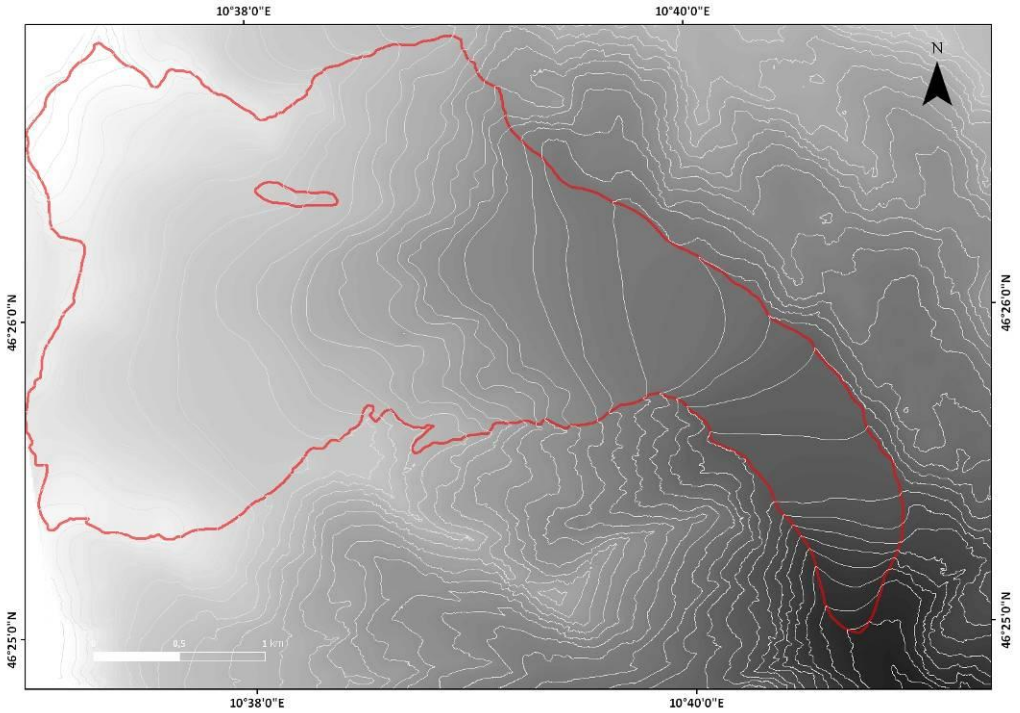

Fig. 2.2.4 - TIN to raster GRID conversion – DEM generation.

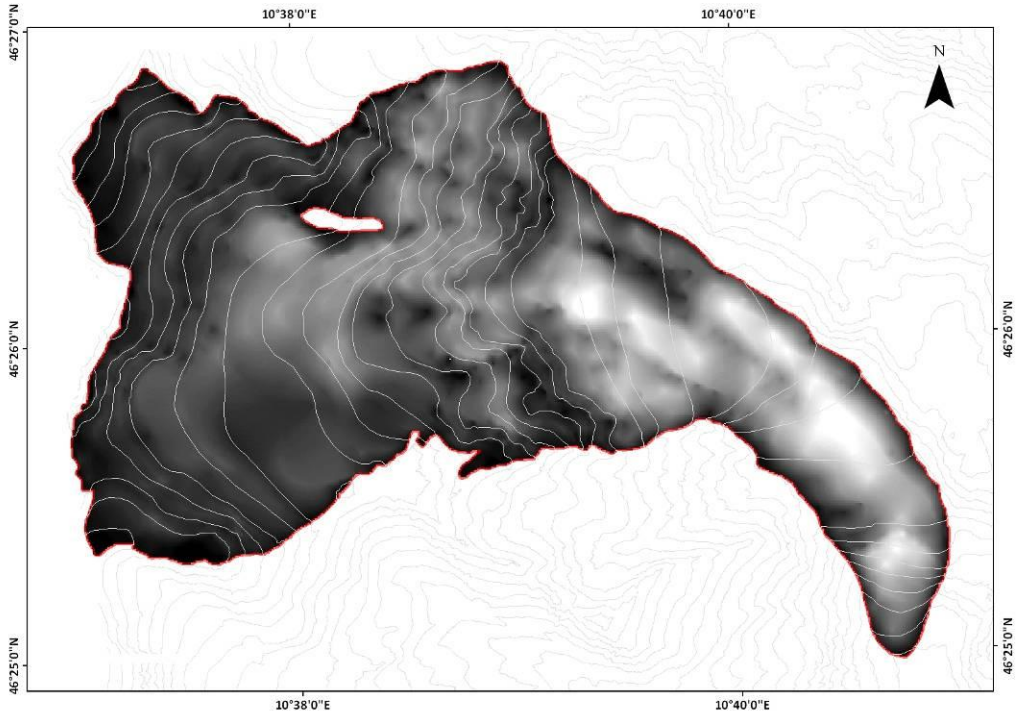

Fig. 2.2.5 - Comparison of the obtained DTM with the DTM relative to the present topography to estimate ice thickness, thus volumes

ELAs were calculated adopting an Accumulation Area Ratio (AAR) of 0.67 for valley glaciers, in line with standards used for the Alps (among others, Gross *et al.*, 1977; Braithwaite and Müller, 1980; Maisch, 1992; Baroni and Carton, 1990, 1996; Giraudi and Frezzotti, 1997; Ivy-Ochs *et al.*, 2008; Vieira, 2008; Kuhlemann *et al.*, 2009, 2013, Akçar *et al.*, 2016) and we applied an error of ±0.005. ELA elevations were extracted from the elaborated hypsographic curves, on the basis of the reconstructed paleotopography. ELA values were calculated as absolute elevations above sea level and, for the Ortles-Cevedale Massif, also as depression from LIA.

Geomorphological and glacial geological field surveys allowed us to reconstruct the geometry and extension of glacial bodies and to identify key sites suitable for dating distinct glacial phases applying ^{10}Be Surface Exposure Dating (SED) (Balco *et al.*, 2008, 2009). Equilibrium Line Altitude (ELA) were calculated adopting an Accumulation Area Ratio (AAR) for valley glaciers of 0.67±0.005.

2.3 Cosmogenic Surface Exposure Dating

2.3.1 A brief History of the method

The fact that nuclides of some isotopes are produced by the interaction of cosmic-ray particles with rock is known since early '50, but it found its application in Surface exposure dating (SED) only in the last three decades. Paneth *et al.*, (1952) discovered cosmogenic nuclides in iron meteorites. Cosmogenic nuclides were measured for the first time in terrestrial material by Davis and Schaeffer (1955) and Craig *et al.* (1979) discovered excess 3He and 21Ne in terrestrial metals.

This field of the research was strongly affected by the impossibility to measure the low concentrations of cosmogenic nuclides in terrestrial samples and the scientific community had to wait and improvement of the mass spectrometry technology.

1986 was a crucial year for the study of the Terrestrial Cosmogenic Nuclides (TCN) and a large number of pioneer and fundamental studies were published. In-situ produced cosmogenic radionuclides **^{10}Be, ^{26}Al** were detected in **quartz** by Nishiizumi *et al.* (1986) and Klein *et al.* (1986) and **^{36}Cl** in **volcanic rocks** was reported (Phillips *et al.*, 1986). **Volcanic olivine and pyroxene** were detected as mineral target for the cosmogenic noble gases **^{3}He and ^{21}Ne** in Kurz, 1986a,b; Craig and Poreda, 1986; Marti and Craig, 1987. This initial pulse was followed by improvement in many fields, from the dating techniques to the mass spectrometry technology.

Today, Surface Exposure Dating with TCN is a fundamental dating tool for the Earth Science useful to study many landscape elements and processes, for instance **glacial chronologies** (alpine, ice sheets), fluvial chronologies (terraces, incision), shoreline chronologies (terraces, lacustrine, marine), hillslope rates, catchment wide denudation rates, burial chronologies (caves, terraces, paleosoils), landslide chronologies, fault scarp chronologies (tectonic slip rates), volcanic eruption chronologies, desert chronologies, alluvial fan chronologies and archaeology

2.3.2 Principles of the Surface Exposure Dating

TCN have their origin from the radiation due to the supernova explosion in our galaxy. This cosmic radiation can by divided in two components, galactic and solar. The galactic radiation, that is fundamental for Suface Exposure Dating , originates outside our solar system and is made by high energy particles. The solar component has minimal influence and importance.

Cosmogenic Surface Exposure Dating techniques are based on **measuring the concentration of radionuclides** and stable nuclides as result of the interaction between cosmic rays and target minerals in the exposed rock surface (Ivy-Ochs and Kober, 2008). The concentration of the nuclides in the rock surface is the consequence of their production rate that is a function of the cosmic ray flux that reaches the earth's surface.

In space, the cosmic radiation is an almost isotropic flux made for ca. the ~90 % by protons and by smaller amounts of alpha particles (~8 %) and heavier nuclei (Gaisser, 1990).

The high energetic particles interact with other nuclei in the air generating spallation

reactions and the induction of further nuclear reactions. The cosmic ray flux is attenuate by the nucleon reactions exponentially with atmospheric depth and the final result is a cascade of secondary particles (neutrons) (fig. 2.3.2.1). More in detail, **secondary neutrons** are the product of the spallation reactions with the nuclides of the atmosphere and finally with the **matter on the Earth's surface.**

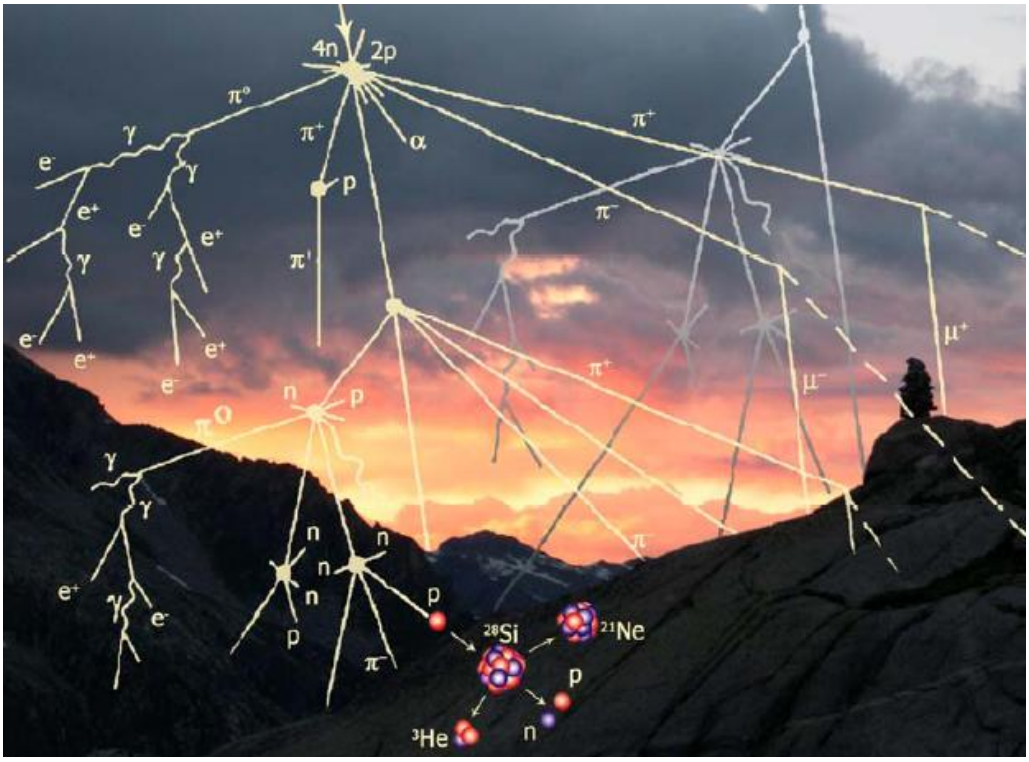

Fig. 2.3.2.1 - Schematic illustration of a cosmic ray air shower (cascade) and a spallation reaction (after Gosse and Phillips, 2001).

Crossing the atmosphere, the composition of the cosmic ray flux deaply changes and neutrons become predominant over protons (Lal and Peters, 1967) and secondary neutrons are the particles **ultimately responsible for TCN production** on the surface of our planet.

Surface Exposure Dating technique uses rare isotope of several elements and the most commonly used are the unstable radionuclides ^{10}Be, ^{26}Al and ^{36}Cl and the stable noble gases ^{3}He and ^{21}Ne. The cosmogenic isotopes concentration that we measure on the rock surface testify the range of time of the sample exposition to the cosmic radiation.

This concentration can be expressed with an equation:

$$N(t) = P_0 \cdot C \cdot \frac{1 - e^{-\left(\frac{\epsilon \cdot \rho}{\mu} + \lambda\right) \cdot t}}{\frac{\epsilon \cdot \rho}{\mu} + \lambda} + N(0) \cdot e^{-\lambda \cdot t}$$

N(t) represent the concentration of the cosmogenic nuclide; P0 is the isotope **production rate** (at/g/a) valid for the exposure time and normalized to sea-level, to high geomagnetic latitude (>60º) and open sky

conditions; C is a product of correction factors (scaling of P0 to the geographic position of the sample, shielding of the cosmic ray flux due topography of landscape and geometry of sample, any cover on the sample surface such as vegetation, snow, soil, additional rock, and the effective sample thickness); ρ is the density of the rock (g/cm3); ε describes an average erosion rate(cm/a) on the surface for the whole exposure time; μ is cosmic ray attenuation length in rock surface (g/cm2); λ is the decay constant of the radionuclide (1/years); N(0) is the inherited radionuclide concentration (at/g) at the beginning of the exposure. (Kubik *et al.*, 1998). For noble gases λ is zero.

Cosmogenic nuclides differ for target minerals and elements and of course for the applicable time range that depends on rock surface or landform weathering rate (tab. 2.3.2.1).

TCN	Target mineral	Target elements	Time range
^{10}Be	Quartz	O	To 5 Ma
^{26}Al	Quartz	Si	To 2.5 Ma
^{21}Ne	Quartz, olivine, pyroxene	Si, Mg	Tens of thousands to millions of years
^{3}He	Olivine, pyroxene	many	To millions of yers
^{14}C	Quartz	O	To 20 ka
^{36}Cl	All rock types	K, Ca, ^{35}Cl	To 1 Ma

Table.2.3.2.1 - Summary of nuclide characteristics (from Di Nicola PhD thesis, modified from Ivy-Ochs and Kober, 2007).

It is important to underline the differences between stable and radiogenic isotopes, the first increase with time unless chemical or diffuse loss occurs; the latter approach a steady-state concentration after 4 to 5 half-lives, limiting the application of those isotopes to cases where the exposure age is within 3 to 4 halflives.

The isotope production rate is a crucial factor to calculate the timing of exposure of a geological feature and is expressed in atoms/grams/years. Production rates of the different cosmogenic nuclides have been widely discussed (Balco *et al.*, 2009 and references therein) over time and must be corrected considering all the **potential influencing factors**.

The location of the sampled feature influences strongly and direcly the production of cosmogenic nuclides in the target minerals. Principal factor connected to the rate of production are **altitude**, **latitude** and the **shielding** due to the surrounding topography. The altitude factor is

related to the decrease of the particles flux strength with the atmosphere, and bigger production rates are related to higher altitude. The magnetic field deflects particles with lesser energies at lower latitudes and in consequence the production rate of cosmogenic nuclides decreases in line with latitude. The incoming radiation can be affected by the surrounding topography and the derived shielding can influence the final amount of cosmogenic nuclides product on the rock surface.

Important factor to consider is the sample thickness, in fact secondary particles are attenuated as they penetrate into the rock and the production rate of cosmogenic nuclides decreases with depth.

Secondary particles that penetrate into the rock are attenuated with depth and the production rate of cosmogenic nuclides decreases.

This relation can be expressed as: $\mathbf{Px = P0\ e\ -\rho x/\Lambda}$

Px is the production rate at depth x in at/g/a; P0 is the production rate at the surface, ρ is rock density in g/cm^3; x is the depth in cm; Λ is the cosmic ray attenuation length in g/cm^2.

Another relevant factor to take in account is the **temporary shielding** by biomass, snow, sediments and **ice** that can reduce or completely inhibit the production of cosmogenic nuclides. The biomass influence can be excluded for Antarctica and for our areas it is possible to exclude seasonal snow cover because of strong winds at the sampling sites; and sediment cover because of the lack of sedimentary deposits thick enough to shield samples from cosmic ray flux. Concerning ice cover, the thickness of ice required to completely inhibit production of cosmogenic nuclides in a rock surface can be calculated theoretically (Miller *et al.*, 2006), using established nuclide production proportions, appropriate attenuation lengths, and an ice density of 0.917 g/cm^3.

In this framework a multi-nuclide approach become an important tool to investigate the simple or complex exposure history of the sampled site. The combination of two nuclides (fig. 2.3.2.2) of different half-lives (or a stable and a radioactive nuclide) can define the continue exposition

(simple exposure History) or underline a story of coverage and exposition of the sample (complex exposure history). This is testified by the nuclides that were built up before the shielding period decay at different rates (or do not decay at all as the stable nuclides) during the shielding, they yield different ages.

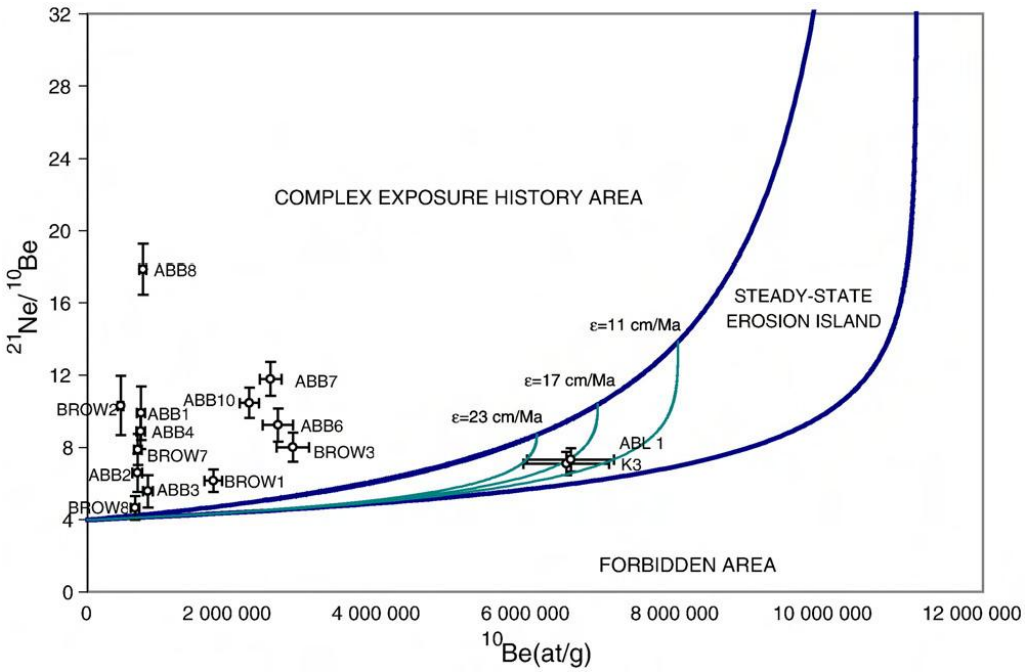

Fig. 2.3.2.2 - Example of two-nuclide diagram for interpreting 10Be and 21Ne measurements (Di Nicola *et al.*, 2009).

2.3.3 Sampling

Sampling is a crucial factor in the framework of Surface Exposure Dating. Reliable ages can be obtained only with an accurate sampling approach, precided from detailed geomorphological surveys (Oberholzer *et al.,* 2003, 2008; Ivy Ochs *et al.*, 2008; Di Nicola *et al.,* 2009; Strasky *et al.,* 2009). This approach lead to the identification of key sites and to the relative glacial features useful to our goals. Sampling criteria were focused to guarantee high reliability in terms of significance of the context and stability (i.e. erratic boulders) of the glacial feature over time.

In glacial geology, Surface Exposure Dating with cosmogenic nuclides was widely applied in providing geochronological constraints to reconstructed glacial histories and has been successfully applied in a large range of contexts worldwide (e.g. Gosse *et al.*, 1995; Ivy-Ochs, 1996; Ivy-Ochs *et al.*,

1996, 2006a, 2008, 2009; Kelly *et al.*, 2004, 2006; Akçar *et al.*, 2007, 2014, 2016; Oberholzer *et al.*, 2008; Strasky, 2008; Di Nicola *et al.*, 2009; Shulmeister *et al.*, 2010; Delmas *et al.*, 2011; Ballantyne and Stone, 2012; Hippe *et al.*, 2014; Wirsig *et al.*, 2016).

Dating different glacial phases, previously reconstructed by means of photointerpretation and geomorphological and glacial geological investigation, extend our knowledge of time ranges of past glacier variations. Suitable glacial features for applying cosmogenic radionuclide dating techniques, are erratic boulders located on moraines and glacially scoured bedrock surfaces. Minimum ages of deglaciation and rates of glacier downwasting can be provided by dating glacially scoured bedrock surfaces. However, in this case more attention must be paid to eventual glacial deposits that could have previously covered the surface and that could affect the exposure history of the sampled feature. On the other hand, erratic boulders located on moraine ridges and ice free bedrock concur in providing minimum ages of the relative glacial feature deposition. When the aim is to constrain a precise glacial phase, during sampling attention must be paid to obtain a single-age-exposure, avoiding nuclide inheritance that would overestimate the final age. The latter would be possible in case the boulder or the bedrock surface were already exposed to cosmic rays during previous times and buried again by a following glacial advance. Weathering rates significantly vary depending on the local climatic conditions and on the involved lithology. In the European Alps estimated surface erosion rates are of the order of mm/ka (among others, Ivy-Ochs *et al.* 2006a,b, 2007, 2008, 2009; Reuther, 2007; Moran *et al.* 2016)and in Antarctica are of the order of cm/Ma (Di Nicola *et al.*, 2009, 2012) An underestimated age could be related to the moraine degradation and the consequent exhumation of boulder tops that were buried since the moraine deposition. In this case the obtained age would represent the boulder exhumation rather than the moraine deposition time. Furthermore, boulders embedded in fine grained sediment can be affected by instability once the matrix is washed away. If the boulder

would change its orientation or position since its deposition a new surface would be exposed, giving a younger age.

The presence of vegetation can indirectly rejuvenate the final age by affecting the boulder or the bedrock in terms of mechanical weakening or destabilization and of chemical surface weathering. Finally, a partial shield of the exposed surface by vegetation and/or snow cover might also be taken into account in certain contexts. Because of all these factors it's always important remember the geomorphological criteria followed during our sampling campaigns, that allow us to exclude, or at least reduce, the influence of the above mentioned factors. For the Alpine context, during 2012-2014 field surveys, erratic boulders were sampled in valleys of Ortles-Cevedale (fig. 2.3.3.1) and Adamello-Presanella Massifs (fig. 2.3.3.2) for SED.Large and wide based erratic boulders located on top of moraine ridges were selected. Boulder size and location, altogether with weathering evidences, guaranteed stable positions and no post–depositional overturning of the sampled features. Samples were taken from the top surfaces of the boulders avoiding edges, potentially affected by loss of nuclides. Samples collected from the Ortles-Cevedale Massif were taken in Val de La Mare (LAM 13.1, LAM 13.2, LAM 13.3, LAM 13.4, LAM 13.5, LAM 13.6, LAM 14.1, LAM 14.2) and Val Venezia (POVE 1, POVE 2, POVE 3)(fig. 2.3.3.1, tab. 2.3.3.1). Samples from La Mare Valley we sampled one left lateral moraine and three right lateral moraines. In the Pozza di Venezia area we collected two samples from a right lateral moraine and one from a frontal moraine.

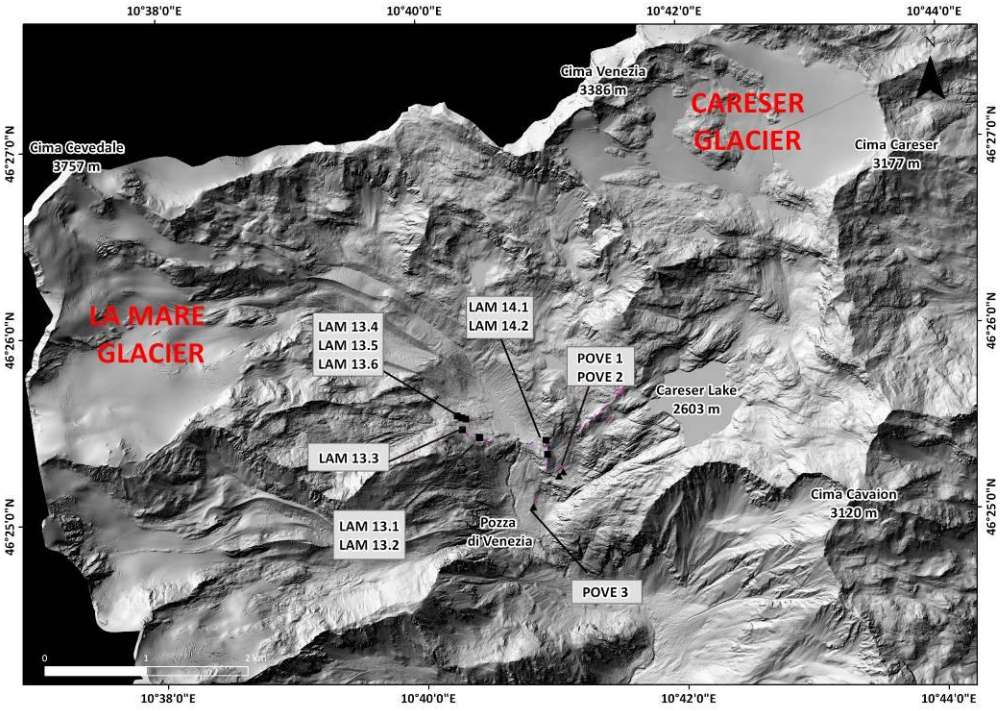

Fig. 2.3.3.1 - Location map of sampled and dated with ^{10}Be erratic boulders in Ortles-Cevedale Massif. Purple lines represent sampled moraines.

Sample ID	Massif	Latitude (°N)	Longitude (°E)	Altitude (m a.s.l.)	Boulder size (m)	Average sample thickness (cm)	Topographic shielding
LAM 13.1	Ortles-Cevedale	46°25'25"	10°40'26"	2346	6.0 x 4.5 x 3.0	2.8	0.980
LAM 13.2	Ortles-Cevedale	46°25'26"	10°40'26"	2346	3.0 x 2.5 x 2.0	2.1	0.980
LAM 13.3	Ortles-Cevedale	46°25'28"	10°40'18"	2384	8.0 x 5.0 x 4.0	1.7	0.964
LAM 13.4	Ortles-Cevedale	46°25'32"	10°40'15"	2375	4.0 x 3.0 x 2.5	1.0	0.974
LAM 13.5	Ortles-Cevedale	46°25'32"	10°40'17"	2369	4.8 x 4.0 x 2.0	1.5	0.974
LAM 13.6	Ortles-Cevedale	46°25'31"	10°40'19"	2362	6.5 x 3.0 x 3.0	2.4	0.976
LAM 14.1	Ortles-Cevedale	46°25'24"	10°40'56"	2350	3.3 x 3.0 x 1.8	1.5	0.960
LAM 14.2	Ortles-Cevedale	46°25'19"	10°40'57"	2309	2.4 x 2.1 x 0.9	1.0	0.974
POVE 1	Ortles-Cevedale	46°25'12"	10°41'02"	2203	5.0 x 3.5 x 2.5	2.0	0.965
POVE 2	Ortles-Cevedale	46°25'14"	10°41'04"	2214	3.5x2.0x1.5	2.0	0.961
POVE 3	Ortles-Cevedale	46°25'02"	10°41'50"	2022	3.0 x 2.2 x 2.5	2.0	0.980

Table 2.3.3.1 - Location of sampled sites in the Ortles-Cevedale Massif and main characteristics of the sampled erratic boulders.

In the Adamello-Presanella Massif we sampled six of the radial valleys departing from the summit of the mountain group (fig. 2.3.3.2). The goal was to obtain a good samples distribution. In this framework samples were collected in Val Presena (AP 14.1, AP 14.2, AP 14.4, AP 14.5, VP 14.1,

VOL 14.1), Val Stavel (STAV 14.1, STAV 14.3), Val Rendena (SANT 14.1, SANT 14.2), Val Breguzzo (BRE 14.01), Val Adamè (ADA 3, ADA 9, ADA 11, ADA 20) and Val Malga (MAL 14.1, MAL 14.2, MAL 14.6)(tab. 2.3.3.2).

All the AP, VP and STAV samples collected in the Upper Val di Sole derive from left lateral moraines (sample AP14.5 is on la left lateral-frontal moraine) while VOL14.1 was sampled on a right lateral moraine. In Val Malga, samples MAL14.1 and MAL14.2 have been collected on a right lateral moraine and MAL14.6 on a left lateral. Samples of Val Adamè derive from two different left lateral moraines (ADA9, ADA11, ADA20) and one right ridge (ADA3).

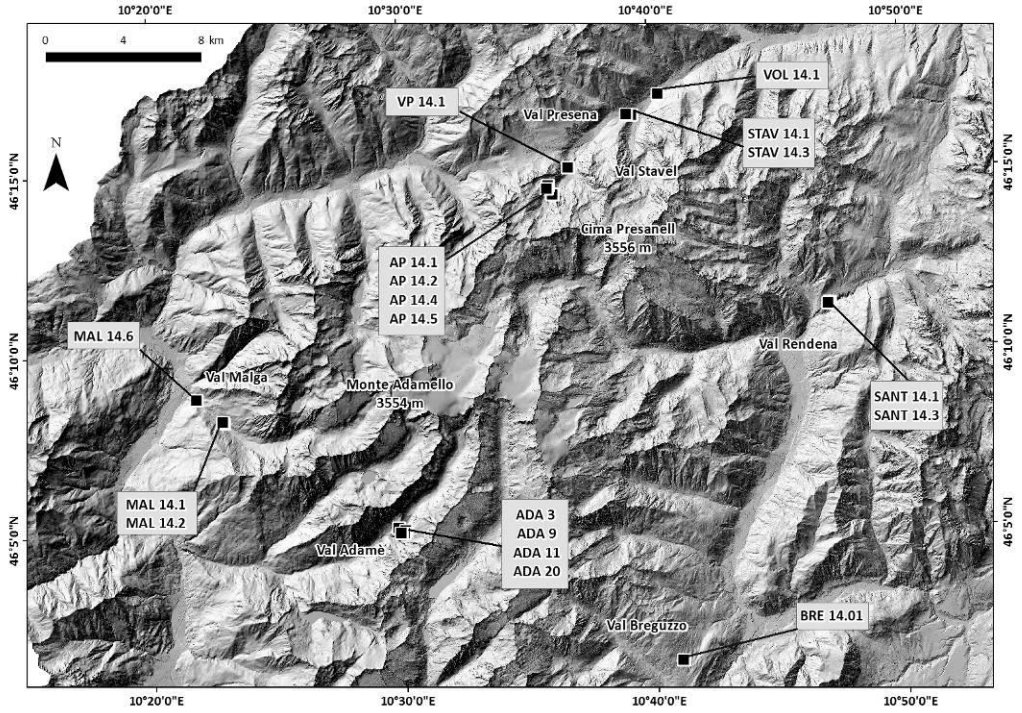

Fig. 2.3.3.2 - Location map of sampled and dated with ^{10}Be erratic boulders in Adamello-Presanella Massif.

Sample ID	Latitude (°N)	Longitude (°E)	Altitude (m a.s.l.)	Boulder size (m)	Average sample thickness (cm)	Topographic shielding
AP 14.1	46°14'23"	10°36'07"	2196	5.5 x 4.2 x 4.5	2.0	0.952
AP 14.2	46°14'22"	10°36'07"	2191	3.9 x 2.3 x 1.7	3.0	0.948
AP 14.4	46°14'37"	10°35'57"	2204	3.4 x 2.1 x 1.8	2.0	0.958
AP 14.5	46°14'32"	10°35'55"	2184	3.8 x 2.5 x 2.5	2.5	0.942
VP 14.1	46°15'05"	10°36'47"	1745	3.1 x 2.0 x 1.8	1.0	0.949
VOL 14.1	46°17'07"	10°40'26"	1238	2.1 x 1.6 x 1.4	1.0	0.943
STAV 14.1	46°16'32"	10°39'20"	1320	3.5 x 2.5 x 2.3	1.5	0.926
STAV 14.3	46°16'34"	10°39'07"	1379	2.3 x 1.5 x 1.2	2.5	0.961
SANT 14.1	46°11'14"	10°47'07"	1112	3.1 x 1.3 x 1.1	1.0	0.958
SANT 14.3	46°11'11"	10°47'03"	1092	3.3 x 1.9 x 2.0	1.5	0.950
BRE 14.01	46°01'21"	10°41'00"	1415	3.0 x 2.2 x 2.5	2.5	0.993

ADA3	46°05'10"	10°29'46"	2055	-	2.0	0.960
ADA9	46°05'06"	10°30'02"	2120	-	2.5	0.955
ADA11	46°05'03"	10°29'59"	2088	-	3.5	0.956
ADA20	46°05'01"	10°29'51"	2027	-	2.5	0.952
MAL 14.1	46°08'10"	10°22'52"	1165	4.6 x 2.0 x 5.5	1.0	0.933
MAL 14.2	46°08'12"	10°22'50"	1155	3.5 x 2.7 x 3.0	1.0	0.935
MAL 14.6	46°08'49"	10°21'47"	879	3.2 x 2.3 x 2.0	0.5	0.942

Table 2.3.3.2 - Location of sampled sites in the Adamello-Presanella Massif and main characteristics of the sampled erratic boulders.

In Antarctica we selected and dated 40 (fig. 2.3.3.3) samples taken from erratic boulders and ice free bedrock (tab. 2.3.3.3). The samples distribution allow us to define two geographical domains. The Northern Victoria Land with samples from Cape Sastrugi, Lichen Hills, Brien Rocks, Miller Butte and Frontier Mountain.

Sample ID	Locality	Latitude (°S)	Longitude (°E)	Altitude (m a.s.l.)	Sampled feature	Average sample thickness (cm)	Topographic shielding
CB 09 12 18.03	Cape Sastrugi	74°36'	163°41'	183	Erratic boulder	2.5	0.98
CB 09 12 18.04	Cape Sastrugi	74°36'	163°41'	185	Erratic boulder	1.5	0.98
CB 09 12 18.05	Cape Sastrugi	74°36'	163°41'	187	Bedrock	2.0	0.98
CB 09 12 18.06	Cape Sastrugi	74°36'	163°41'	187	Erratic boulder	2.0	0.98
CB 10 01 03.01	Cape Sastrugi	74°36'	163°41'	168	Erratic boulder	1.5	0.98
CB 10 01 03.02	Cape Sastrugi	74°36'	163°41'	173	Erratic boulder	1.5	0.98
CB 10 01 03.03	Cape Sastrugi	74°36'	163°41'	179	Erratic boulder	2.5	0.98
CB 10 01 03.04	Cape Sastrugi	74°36'	163°42'	328	Erratic boulder	1.5	0.98
CB 10 01 03.05	Cape Sastrugi	74°36'	163°42'	332	Erratic boulder	2.0	0.98
CB 10 01 03.06	Cape Sastrugi	74°36'	163°42'	239	Erratic boulder	1.5	0.98
CB 09 12 28.14	Lichen Hills	73°19'	162°07'	2347	Erratic boulder	2.0	0.98
CB 09 12 28.16	Lichen Hills	73°19'	162°09'	2059	Erratic boulder	1.5	0.98
CB 09 12 28.17	Lichen Hills	73°19'	162°09'	2059	Erratic boulder	1.0	0.98
CB 09 12 06.03	Brien Rocks	73°13'	161°23'	2734	Bedrock	1.5	0.98
CB 09 12 29.01	Miller Butte	72°42'	160°18'	2748	Erratic boulder	2.5	0.98
CB 09 12 29.02	Miller Butte	72°42'	160°18'	2732	Erratic boulder	3.0	0.98
CB 09 12 29.03	Miller Butte	72°42'	160°18'	2740	Erratic boulder	2.5	0.98
CB 09 12 29.04	Miller Butte	72°42'	160°14'	2920	Bedrock	3.0	0.98
CB 09 12 29.06	Miller Butte	72°42'	160°14'	2915	Bedrock	2.0	0.98
CB 09 12	Miller	72°43'	160°13'	2913	Bedrock	2.0	0.98

29.07	Butte						
CB 09 12	Miller	72°42'	160°13'	2921	Bedrock	3.0	0.98
29.08	Butte						
CB 09 12	Miller	72°42'	160°13'	2904	Bedrock	2.0	0.98
29.09	Butte						
CB 09 12	Frontier	72°59'	160°21'	3164	Bedrock	2.0	0.98
06.09	Mountain						
CB 09 12	Frontier	72°59'	160°21'	3157	Bedrock	1.5	0.98
06.10	Mountain						
CB 09 12	Frontier	72°59'	160°21'	3178	Bedrock	2.0	0.98
06.11	Mountain						
CB 09 12	Frontier	72°59'	160°22'	2614	Erratic	2.0	0.98
06.17	Mountain				boulder		
CB 09 12	Frontier	72°59'	160°22'	2614	Erratic	1.5	0.98
06.18	Mountain				boulder		
CB 09 12	Frontier	72°59'	160°22'	2617	Erratic	2.5	0.98
06.19	Mountain				boulder		

Table 2.3.3.3 - Location of sampled sites in the Northern Victoria Land and main characteristics of the sampled features.

The Southern Victoria Land with sampled sites from Cape Bird, Cape Royds and Cape Crozier (tab. 2.3.3.4).

Sample ID	Locality	Latitude (°S)	Longitude (°E)	Altitude (m a.s.l.)	Sampled feature	Average sample thickness (cm)	Topographic shielding
CB 11 12 15.02	Cape Bird S. Colony	77°16'	166°23'	88	Erratic boulder	3.0	0.98
CB 11 12 20.05	Cape Bird-Inclusio Hill	77°15'	166°26'	338	Erratic boulder	3.5	0.98
CB 11 12 20.07	Cape Bird-Inclusio Hill	77°15'	166°25'	286	Bedrock	1.5	0.98
CB 11 12 21.01	Cape Bird	77°15'	166°25'	169	Erratic boulder	1.0	0.98
CB 11 12 21.06	Cape Bird	77°14'	166°24'	53	Erratic boulder	2.5	0.98
CB 12 01 01.03	Cape Royds	77°33'	166°11'	32	Erratic boulder	4.5	0.98
CB 12 01 01.06	Cape Royds	77°33'	166°10'	54	Erratic boulder	3.5	0.98
CB 12 12 20.03	Cape Crozier-Crozier Hut	77°32'	169°17'	155	Erratic boulder	2.0	0.98
CB 12 12 20.04	Cape Crozier-Crozier Hut	77°30'	169°19'	229	Erratic boulder	1.0	0.98
CB 12 12 20.07	Cape Crozier	77°29'	169°18'	158	Erratic boulder	1.5	0.98
CB 13 01 01.01	Cape Crozier	77°28'	169°11'	274	Erratic boulder	3.5	0.98
CB 13 01 01.02	Cape Crozier	77°28'	169°11'	278	Erratic boulder	1.0	0.98

Table 2.3.3.4 - Location of sampled sites in the Southern Victoria Land and main characteristics of the sampled features.

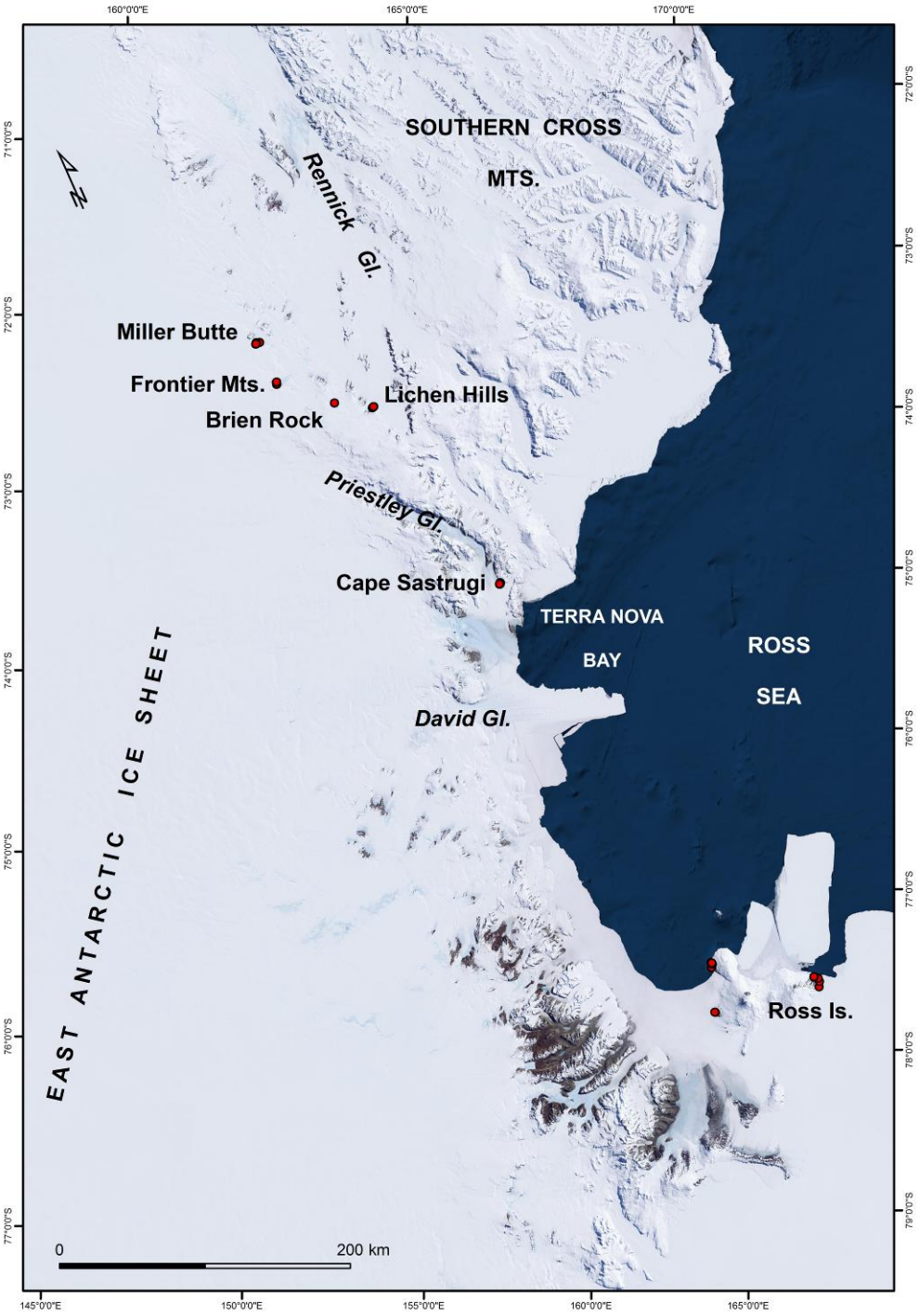

Fig. 2.3.3.3 - Location map of dated Antarctic samples.

The analysis of thin sections, for all the samples, provided to a qualitative minero - petrographic analysis and to the estimation of the amount of the possible target mineral (fig, 2.3.3.4). All the analyzed samples are described in detail in Appendix I.

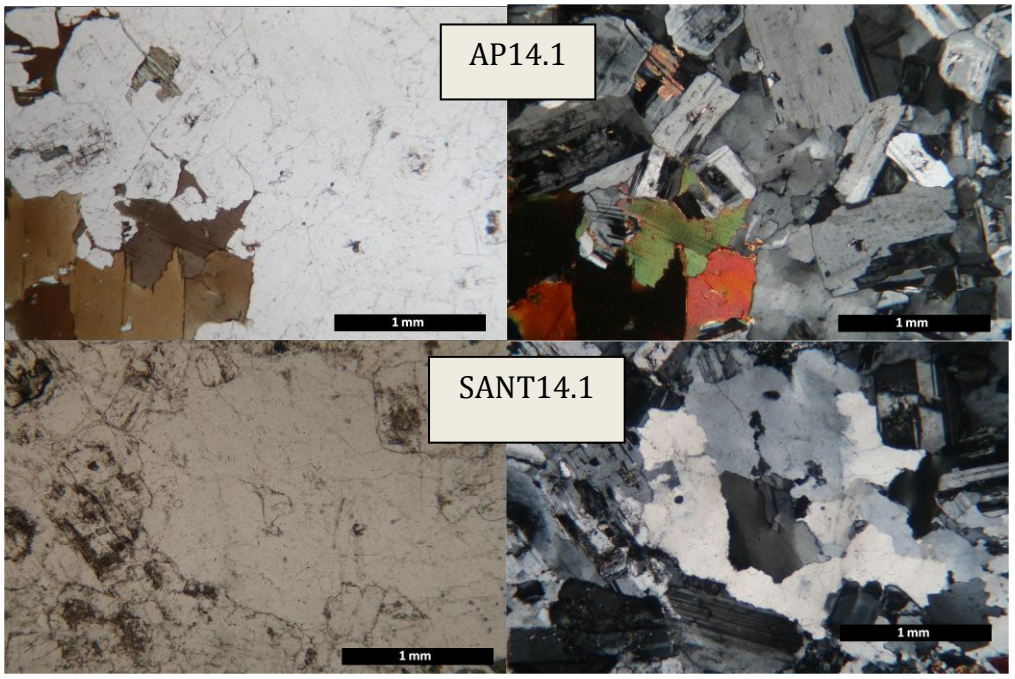

Fig. 2.3.3.4 - Particulars of two samples (Tonalite) in thin section.

Mineralogical and petrographic characteristics identified Quartz as target mineral and concentration of beryllium cosmogenic nuclide (^{10}Be) was measured. In this work we focused on the use of radionuclide ^{10}Be and for one Antarctic sample (CB 09 12 06.03) we used a multi-nuclide approach measuring the ^{10}Be and ^{26}Al concentration. Among long-lived radionuclides, ^{10}Be and ^{26}Al were considered suitable to the investigated time intervals. The sampled lithologies consist in micaschist for the Ortles-Cevedale Massif, in micaschist, tonalite, quartzite and gneiss for Adamello-Presanella Massif and in granite, granodiorite and tonalite for the Antarctic sampled sites.

2.3.4 Sample preparation

29 Alpine and 40 Antarctic Beryllium (1 Aluminum) samples were prepared (fig. 2.3.4.1) at the Laboratory of Ion Beam Physics (LIP) at ETH Zürich as shown in Ivy-Ochs *et al.* (2006), Ivy-Ochs and Kober (2008), Wirsig (2015) and Wirsig *et al.,* (2016), following Kohl and Nishiizumi (1992) and Ivy-Ochs (1996). Samples were crushed and sieved to a grain size <1 mm, treated with Hydrocloric acid (HCl) with the aim to dissolve the organic and carbonate components of the rock. Furthermore several cycles of diluted Hydrofluoric acid (HF) solution (ca. 4%) were done to

dissolve the other minerals and extract the clean quartz. To amplify the action of the acid samples were constantly mixed on a shakertable. In case of HF resistant minerals (i.e. muscovite, garnets, volcanic rock fragments), a magnetic separation was done using a Frantz magnetic separator, available at the Geology Department of ETH, Zürich. For other resistant but less magnetic minerals (i.e. feldspars) it was necessary to treat again the samples with weak HF cycle and ultrasonic baths. ^{9}Be carrier solution (ca. 0.25 mg) was added to the sample before dissolving the pure Quartz in concentrated HF and Nitric acid (HNO3). To determine the original concentration of ^{10}Be the addition of a known quantity of ^{9}Be is necessary. A blank sample of ^{9}Be solution was prepared and treated as the other samples since this phase with the aim to verify the good quality of the chemistry procedures and the absence of contamination. Concentrated HF (48%) and nitric acid (HNO3) were used to dissolve the pure quartz and the samples were heated and dried on hot plates to increase the acid action. After the quartz dissolution, samples were treated with several cycles of HNO_3 and HCl suprapure to avoid further presence of HF. In case of non dissolved minerals, samples were centrifuged and the amount of undissolved material was subtracted to the original quartz grams weighted before dissolving. Anion and cation – exchange columns and selective pH precipitation were used to purify the Beryllium. With this procedure the Beryllium was separated from other elements (e.g. Fe, Ti, Al). Beryllium samples were precipitated, transfered in quartz tiegels and pressed, ready to be measured.

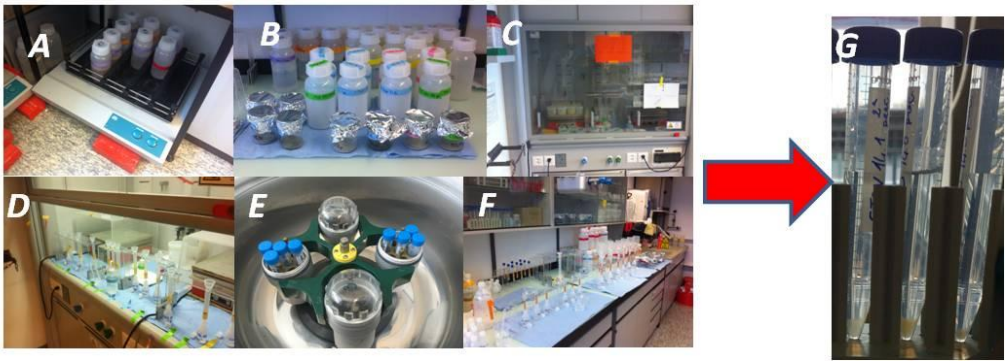

Fig. 2.3.4.1- Samples preparation: (A, B) quartz extraction, (C) quartz dissolution with HFand HNO_3, (D) anion columns, (E) centrifuge, (F) oxalic columns and final Beryllium samples.

$^{10}Be/^{9}Be$ ratios were measured by Accelerator Mass Spectrometry (AMS) on the 600 KV TANDY system (fig. 2.3.4.2) (Christl *et al.,* 2013) at the Laboratory of Ion Beam Physics (LIP) at ETH Zürich. ETH Zürich in house standard S2007N, in turn calibrated to the 07KNSTD standard of Nishiizumi *et al.,* (2007), was used to normalize the measured ratios.

Fig. 2.3.4.2 - TANDY system at LIP, ETH Zurich. Picture from: https://www1.ethz.ch/ams/.

Results were corrected by a weighted average value of long-term full chemistry process blank ratio of $(3.6 \pm 2.6)*10^{15}$. CRONUS-EARTH online calculator (Balco *et al.,* 2008; http://hess.ess.washington.edu/math/) was used to calculate ^{10}Be exposure ages (fig 2.3.4.3). Based on the Northeast North America calibration dataset ("NENA") from Balco *et al.* (2009), in agreement with other published production rate calibrations in Northern Hemisphere, a 3.87 ± 0.19 $at*g^{-1}*yr^{-1}$ sea level high latitude (SLHL) production rate was applied (Fenton *et al.,* 2011; Briner *et al.,* 2012; Gohering *et al.,* 2012; Hippe *et al.,* 2014; Young *et al.,* 2013; Heyman 2014, Wirsig 2015, Wirsig *et al.,* 2016). For Antarctic samples the version 2.3 of Cronus-Earth was used and the value related to the atmospheric pressure was changed, in the computation form, from *"standard"* (Std) to *"Antarctic"* (Ant). The time - dependent scheme of Lal (1991) and Stone (2000) was used to scale the spallogenic production rates to altitude and latitude.

sample	lat	long	elev	elev flag	d	rho	shielding	epsilon	Be10 conc	error	Be10 stand
LAM13_1	46.424000	10.674000	2346	std	2.8	2.65	0.980	0	260176.4469	16326	07KNSTD
LAM13_2	46.423899	10.673889	2346	std	2.1	2.65	0.980	0	274362.6253	21695	07KNSTD
LAM13_3	46.424526	10.671694	2384	std	1.7	2.65	0.964	0	307164.2469	10648	07KNSTD
LAM13_4	46.425778	10.671056	2375	std	1	2.65	0.974	0	282157.3305	13651	07KNSTD
LAM13_5	46.425611	10.671639	2369	std	1.5	2.65	0.974	0	258478.1854	12734	07KNSTD
LAM13_6	46.425472	10.672139	2362	std	2.4	2.65	0.976	0	244030.7319	10150	07KNSTD
LAM14_1	46.423443	10.682388	2350	std	1.5	2.65	0.960	0	262634.7228	21318	07KNSTD
LAM14_2	46.422180	10.682510	2309	std	1	2.65	0.974	0	254576.0723	13095	07KNSTD
POVE1	46.420222	10.683889	2203	std	2	2.65	0.965	0	206898.2573	9849	07KNSTD
POVE2	46.420611	10.684472	2214	std	2	2.65	0.961	0	235454.2278	9795	07KNSTD
POVE3	46.417520	10.680540	2022	std	2	2.65	0.980	0	197706.1691	8706	07KNSTD
BRE14_01	46.022522	10.683383	1407	std	2.5	2.65	0.993	0	204970.6907	9912	07KNSTD
SANT14_1	46.187200	10.785120	1109	std	1	2.65	0.958	0	96958.7881	5408	07KNSTD

Fig. 2.3.4.2 - CRONUS-EARTH input file.

A rock density value of 2.65 g/cm^3 was considered for all the collected samples. Corrections for sample thickness were applied assuming an exponential decrease of production by depth and an attenuation length for spallation in rock of 160 g/cm^2 (Gosse and Philips, 2001; Balco *et al.*, 2008) was adopted. Li (2013) ArcGis tool was used to evaluate the topographic shielding (fig. 2.3.4.3). The tool works on the DTM of the area surrounding the sample. A more detailed DTMs resolution brings to an higher accuracy of the results. We selected a 10x10 m resolution DTMs and we applied a 10° azimut interval and 5° elevation angle resolutions. The tool produces a digital terrain model of the topographic shielding and every single pixel has a value ranging from 0 to 1. The entity of the shielding decreases from 0 to 1. The results were compared with the topographic shielding factor values obtained using the tool available on the CRONUS-EARTH online calculator (http://hess.ess.washington.edu/; Balco *et al.*, 2008).

No corrections were applied because of snow cover and vegetation to boulders and surface erosion was considered neglectable as included in the external error ranges. Furthermore, we sampled boulders in dominant position and principally on top of moraine ridges, thus minimizing or eventually eliminating the effect of snow-covering.

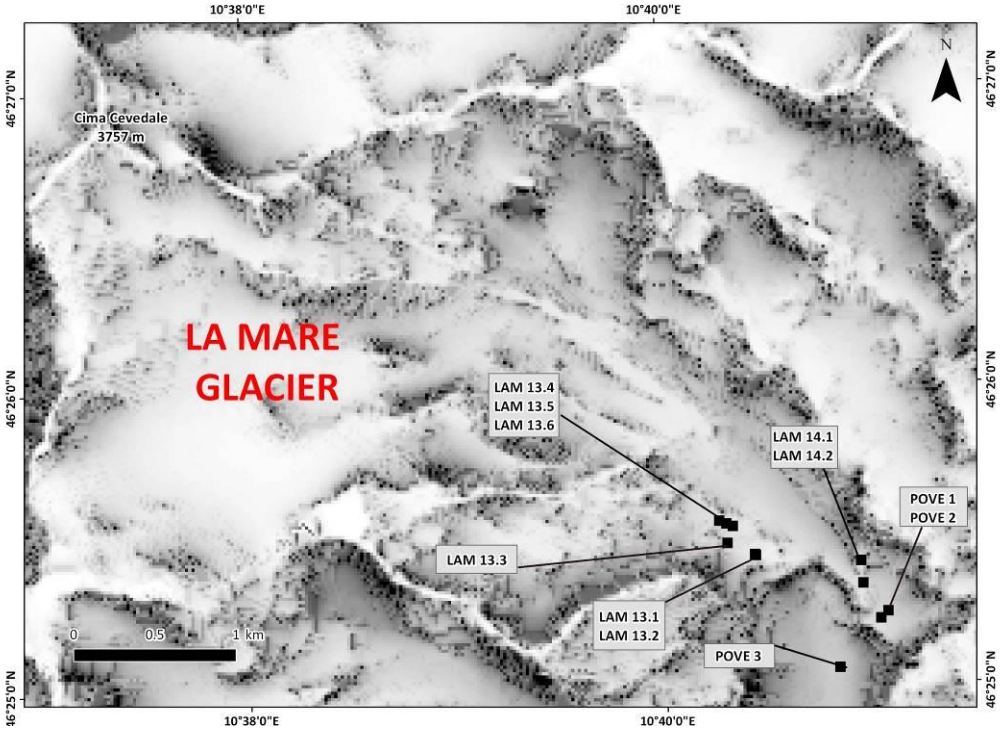

Fig. 2.3.4.3 - Topographic shielding of Ortles-Cevedale samples (Li,2013).

3 – Alps

3.1 - Alpine study areas (Rhaetian Alps): Geographical setting and climate

The Alpine sites studied in this work are located in the Ortles-Cevedale and Adamello-Presanella mountain groups and find their location in the Central Italian Alps, in particular in the Southern Rhaetian Alps at the border between Trentino Alto Adige and Lombardia regions (fig. 3.1.1).

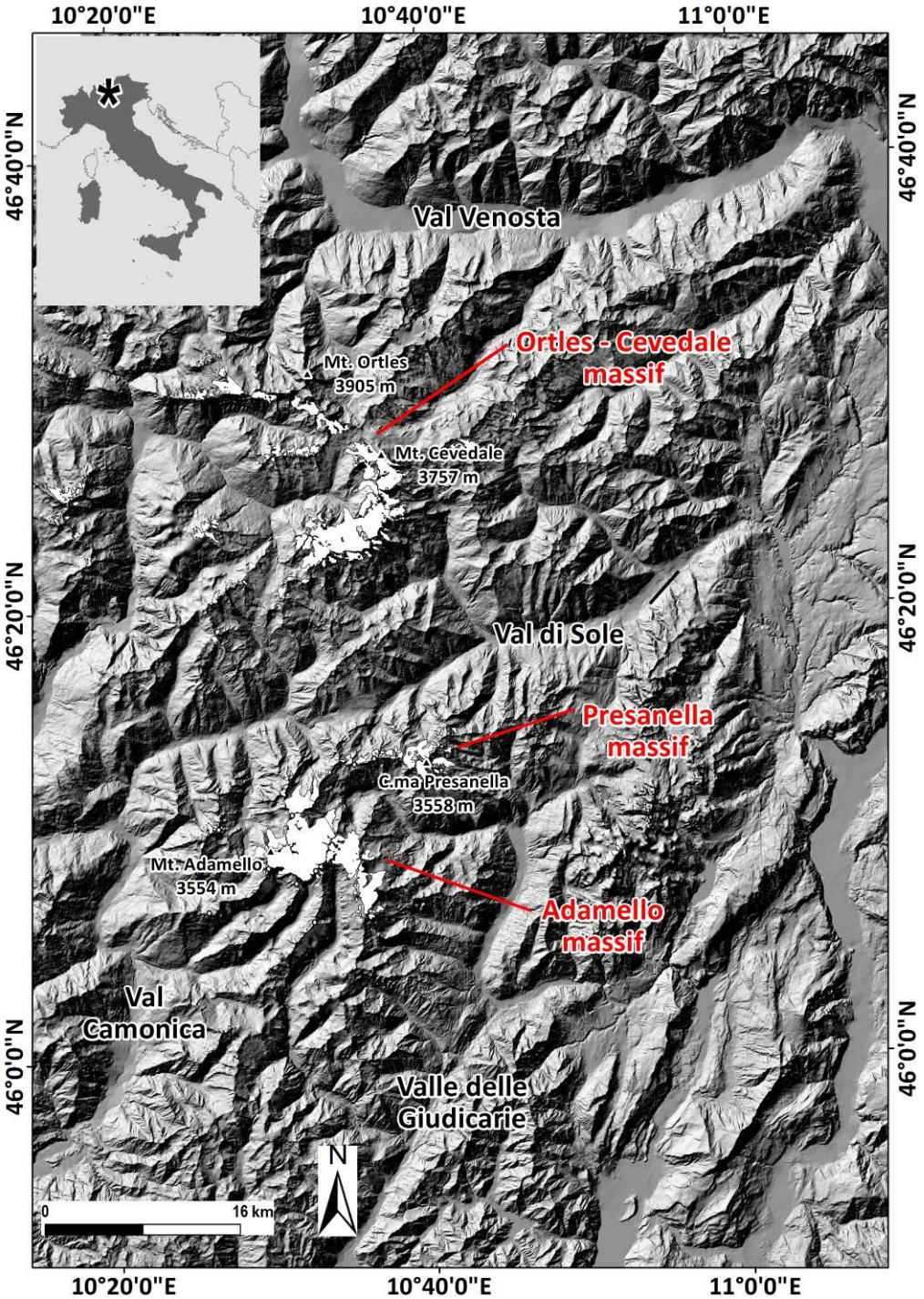

Fig. 3.1.1 - Location map of the Ortles-Cevedale and Adamello-Presanella massifs (Rhaetian Alps). In the background the hillshade derived from the 20x20 m DTM (www.pcn.minambiente.it)

The Ortles-Cevedale and Adamello-Presanella massifs constitute a strategic area in the framework of the glacial paleo-reconstructions in the alpine context and today host two of the three widest glaciers of the Italian Alps, according to Salvatore *et al.* (2015).

3.1.1 The Ortles-Cevedale group and the Upper Peio Valley

The **Ortles-Cevedale** mountain group (46°15' N - 46°40' N and 10°22' E - 11°09' E) exceeds 1600 km^2 extension (fig. 3.1.1.1) and culminates in the peaks of Mt. Ortles (3905 m), Mt. Gran Zebrù (3851 m) and Mt. Cevedale (3769 m), aligned in a NW–SE direction.

The massif is bordered by Val Venosta towards NNE, Valtellina on the W separates it from the Bernina Massif, Val d'Ultimo and Val di Rabbi define its oriental margin, whereas is separate towards S from the Adamello-Presanella Massif by Val Camonica and Val di Sole.

Several peaks along the massif exceed 3000 m a.s.l.. The backbone of the massif is constituted by four main branches that depart from Mt. Cevedale and C.no di Solda (3368 m). The western branch develops in E-W direction from C.no di Solda and hosts the highest peaks of Gran Zebrù (3851 m), Mt. Zebrù (3734 m) and P.ta Thurwieser (3657 m). On the southern sector the ridge culminates in Palon de la Mare (3700 m), P.ta Taviela (3611 m), P.ta Predanzini (3599 m) and Pizzo Tresero (3598 m) and finds its highest peak towards SW in P.ta S. Matteo (3678 m).

The hydrographic setting of the Ortles-Cevedale massif is characterized by several minor rivers with regimes strongly connected to glacial dynamics that take origin from the main basins and drain towards the Adige and the Adda rivers. The Adda basin is fed by waters collected in the western to southern valleys of the massif, in particular by Frodolfo River in Valfurva and Oglio River in Val Camonica. Instead, the hydrographic basins that constitute the northern and eastern sector of the range, the principal rivers represented by Rio Solda (Val di Solda), Rio Plima (Val Martello) and Torrente Noce (Val di Sole), drain their waters to the Adige basin.

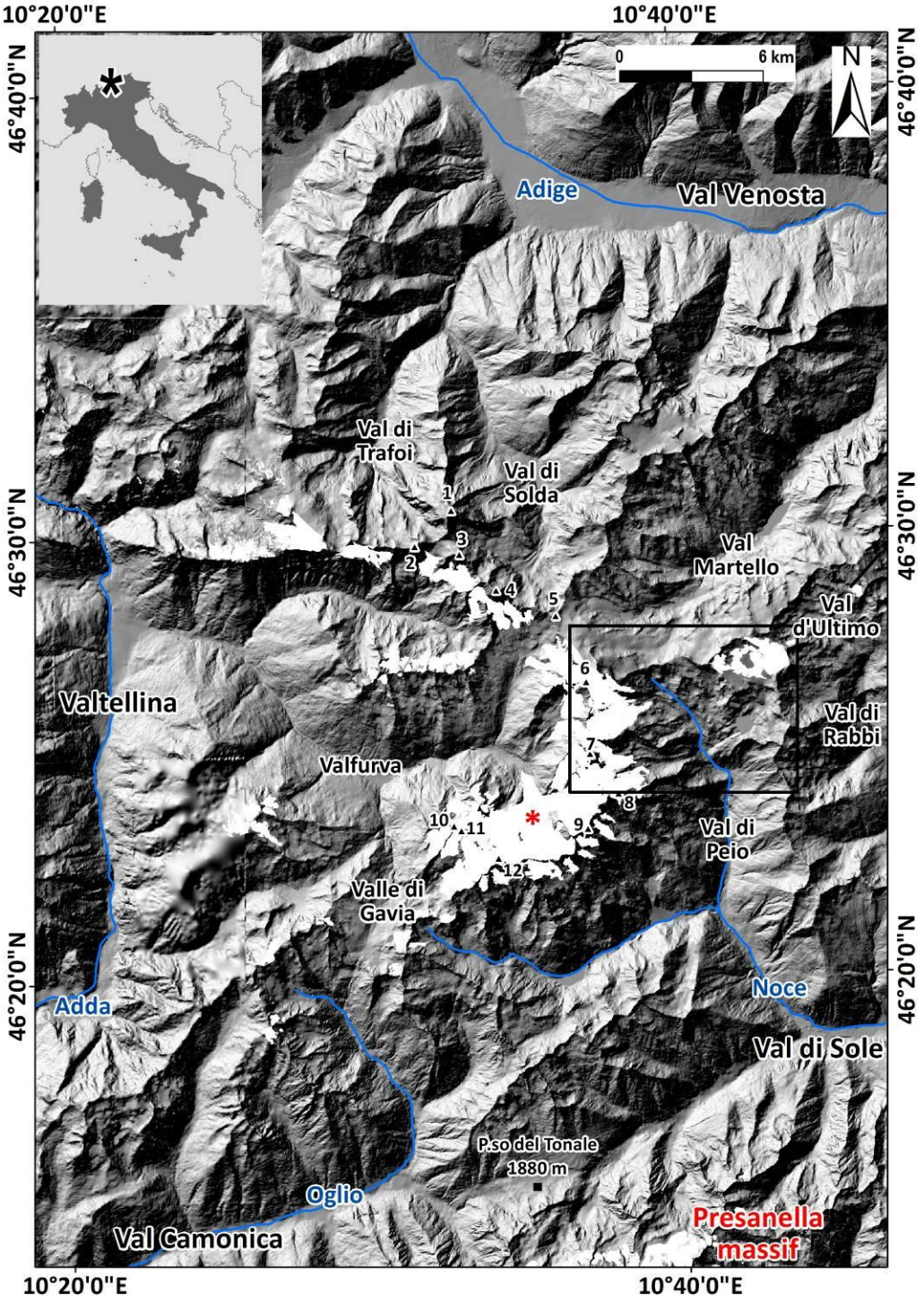

Fig. - 3.1.1.1 – Location map of the Ortles-Cevedale massif. 1- Mt. Ortles; 2 - P.ta Thurwieser; 3- Mt. Zebrù; 4- Gran Zebrù; 5- C.no di Solda; 6- Mt. Cevedale; 7- Palon de la Mare; 8- Mt. Vìoz; 9- P.ta Taviela; 10- Pizzo Tresero; 11- P.ta Predanzini; 12 - P.ta S. Matteo. In the black square the upper Peio Valley. Forni Glacier is marked by te red asterisk. In the background the hillshade derived from the 20x20 m DTM (www.pcn.minambiente.it). Glaciers limits from Nextdata (Salvatore *et al.*, 2015).

The Ortles-Cevedale massif constitutes one of the largest glaciated regions of the southern side of the European Alps (approximately 3.5% of the total Alpine glacierized area according to Carturan *et al.*, 2013a) and represents the most glaciated mountain group of the Italian Alps, hosting 134 glaciers

for a total extension of 76.5 km^2 (Salvatore *et al.*, 2015), included the largest Italian valley glacier (Forni Glacier, 11.3 km^2).

Glaciers of hosted in the Ortles - Cevedale massif were counted and inventoried since the second half of the XIX century (Mojsisovics, 1865; Payer, 1867 - 1872; Richter, 1888, in Desio, 1967). In the XX century, Desio (1967) counts and describes 132 glacial bodies. However, since the 1960s the general retreat that affected most of the alpine glaciers brought on one side to the extinction of several bodies, on the other hand to the fractionation of others, with a consequent increase of the number of elements(Ajassa *et al.* 1994, 1997; Baroni, 2010).

Today the majority of glaciers is concentrated in the tributary valleys of Valfurva, in the western sector of the massif, in the high Val Noce and in Val Martello, tributary of Val Venosta.

The **upper Peio Valley**, focus of our study, is located at the southeastern edge of the Ortles-Cevedale Massif (fig. 3.1.1.2) and hosts La Mare and Careser glaciers.

The watershed that confines the area, from SW rises up to Mt. Vioz (3645 m) and runs in a SSE-NNW direction. From Palon de La Mare (3703 m) the ridge develops N-S until reaching Mt Cevedale, where it drastically deviates in a E-W direction culminating in C.ma Marmotta (3330 m). The latter, together with C.ma Lagolungo (3165 m), defines the western head of Val Venezia, that today hosts La Mare Glacier. The western sector of the upper Peio Valley develops towards ENE from C.ma Marmotta to C.ma Venezia (3386 m) and C.ma Rossa di Saent (3347 m) for turning towards a N-S direction from C.ma Careser (3189 m) to C.ma Cavaión (3120 m).

La Mare Glacier (World Glacier Inventory code I4L00102517; WGMS 1989) is a valley glacier covering an area of 3.55 km^2, today divided in two ice bodies: the northernmost (1.44 km^2) faces SE, ranges from 3769 m a.s.l. (Mt. Cevedale) to a minimum elevation of 3070 m a.s.l.. At the terminus the northern ice body is in contact with the southern glacier (2.11 km^2), that faces NE and presents a small valley tongue. The elevation range of this ice body is from 3590 to 2660 m a.s.l.. The northernmost part

is characterized by steep areas with crevasses and an irregular surface morphology due to the shape of underlying bedrock; flat areas are typical of the southernmost body related to a more regular surface.

Careser Glacier (World Glacier Inventory code I4L00102519; WGMS, 1989) today covers an area 1.63 km^2 is a mountain glacier located in a wide, S facing cirque surrounded by peaks ranging from 3162 m a.s.l. (C.ma Lagolungo) to 3386 m a.s.l. (C.ma Venezia).

The glacier reaches a minimum elevation of 2865 m a.s.l. and a maximum of 3280 m a.s.l., is divided into three main ice bodies and three smaller patches (data related to 2012, Carturan *et al.*, 2013a). A small height difference between the glacier surface and the surrounding summits is the main reason of an almost absent debris cover.

Hydrographically the Upper Peio Valley belongs to the Adige basin. Melt waters originated in the upper valley mainly feed the Noce Bianco and the Rio Careser, that drain into the Noce River, tributary of the Adige River.

Currently both La Mare and Careser glaciers are subject to glaciological mass balance monitoring (Carturan *et al*. 2009, 2013a, 2014).

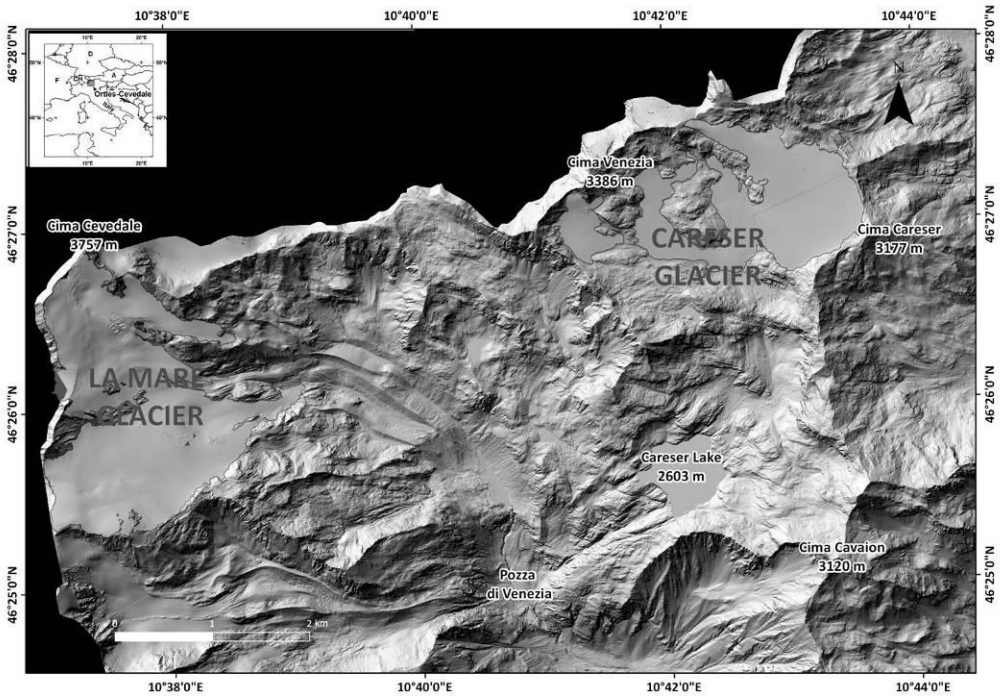

Fig. 3.1.1.2 - Geographical setting of the upper Peio Valley, with La Mare and Careser glaciers. In the backgroung the 2x2 m Lidar of Provincia di Trento (www.territorio.provincia.tn.it).

3.1.2 The Adamello - Presanella Group

The Adamello–Presanella Group (45°54'–46°19' N; 10°21'–10°53' E) represents the southernmost massif of the central Italian Alps and extends for more than 1100 km^2 (fig. 3.1.2.1). The massif is separated towards N from the Ortles-Cevedale massif by Val di Sole and Val Camonica, bordered by the latter on the W and by Val Rendena and Valle delle Giudicarie on the E. Val Camonica and Val Rendena isolate the massif from Alpi Orobie and Dolomiti di Brenta respectively.

The highest peaks, exceeding 3500 m, are represented by Cima Presanella (3558 m) and Mt. Adamello (3539 m), located at the northeastern border and on the central sector of the massif.

Several valleys depart from the summit of the massif describing a radial pattern from the main peaks of P.ta del Venerocolo (3323 m), C.no Bianco (3437 m), Mt. Adamello, C.no Miller (3373 m), Mt. Fumo (3418 m) and Mt. Carè Alto (3462 m). From N, directly W of Passo del Tonale (1880 m), Val Narcanello and Val d'Avio represent the main north facing valleys. From Val Rabbia and Val Miller, a series of valleys progressively faces from WSW to SSW (Val Salarno, Val Adamè-Val Saviore), until the SSW facing Val di Fumo-Val di Daone. The N-S oriented ridge that constitutes the watershed between Val di Fumo and Val Rendena finds on its eastern slope several smaller valleys, mainly E facing. Proceeding towards N, Val di Genova is clearly oriented towards NNE at its head, for abruptely deviating to SE and finally to ENE until Val Rendena. The Presanella ridge culminates in C.ma Presena (3068 m), C.ma Busazza (3225 m), C.ma Cercen (3282 m), C.ma Presanella, and C.ma Scarpacò (3254 m). On the northern slopes the main valleys of Val Presena and Val Stavel develop towards NNE whereas the minor Val Piana and Val di Barco mainly follow a N-S direction. The southern side correspond to the left slope of Val di Genova and, on the E develops in Val di Nambrone.

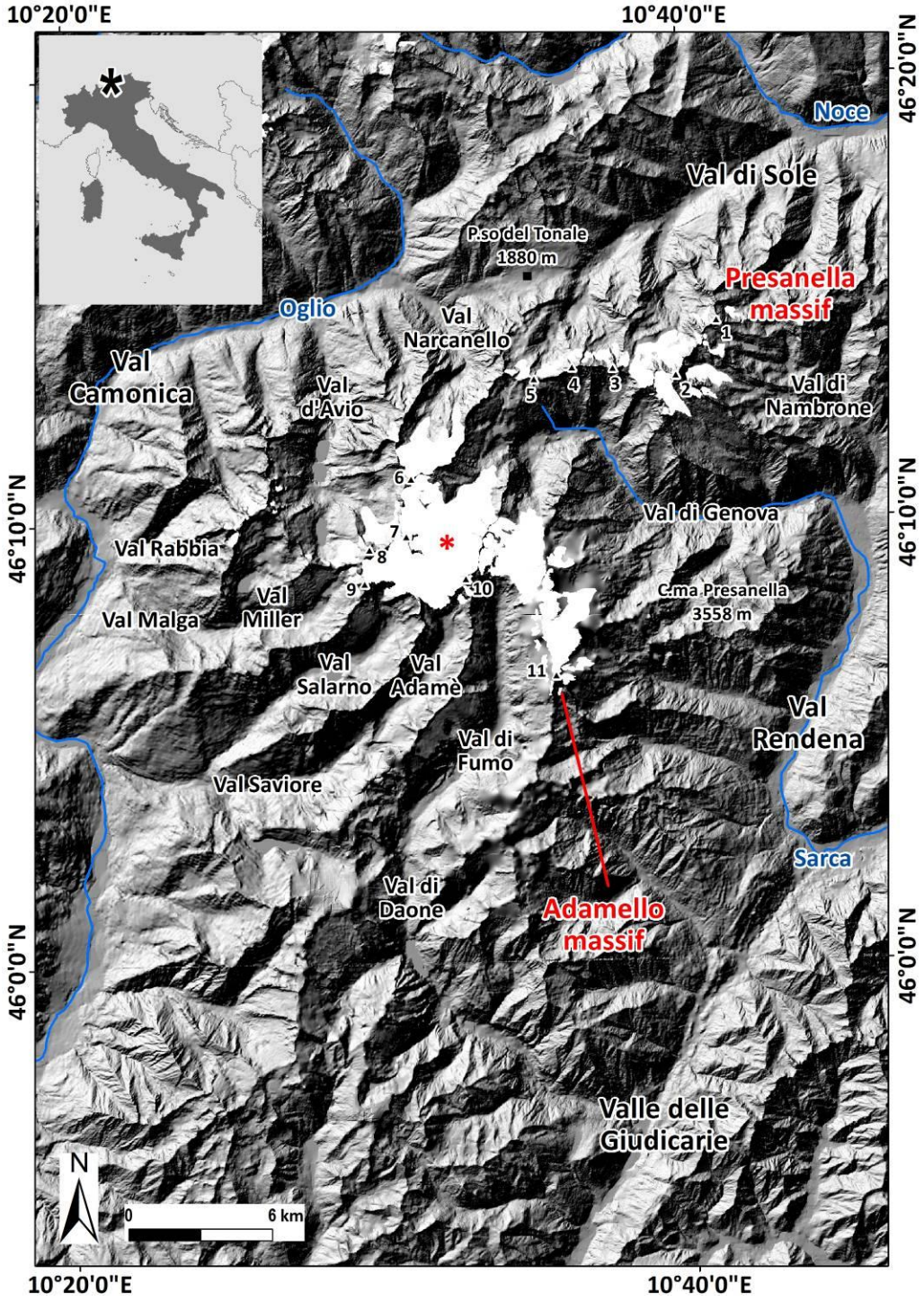

Fig. 3.1.2.1 - Location map of the Adamello-Presanella Group. 1 - C.ma Scarpacò; 2 - C.ma Presanella; 3 - C.ma Cercen; 4 - C.ma Busazza; 5 - C.ma Presena; 6 - P.ta del Venerocolo; 7 - C.no Bianco; 8 - Mt. Adamello; 9 - C.no Miller; 10 - Mt. Fumo; 11 - Mt. Carè Alto. The red asterisks marks the Adamello Glacier. In the background the hillshade derived from the 20x20 m DTM. (www.pcn.minambiente.it). Glaciers are from Trentino and Lombardia regions.

Principal hydrographic elements of the Adamello massif are represented by the rivers Adda, Sarca and Noce. Adda River collects the waters from the majority of the area, through the Oglio River on the NNW, until the

Poia River on the S (Val Adamè). Sarca River takes origin in Val di Genova and is fed by the rivers coming from the eastern valleys that flow into Val Rendena, the main represented by the Chiese River, that drains the waters of the southern Val di Fumo-Val di Daone. Instead, the waters collected on the northern slopes of the Presanella massif directly flow in Noce River, whereas the southern side drains to Sarca River. On the N Passo del Tonale separates the Oglio and the Noce basins.

According to Salvatore *et al.* (2015), 92 glaciers occupy the massif for a total area of ca. 43 km^2. The summit of the massif hosts the Adamello glacier, the largest glacier in the Italian Alps (16.4 km^2 in 2007, in Salvatore *et al.*, 2015). Adamello Glacier lies on a plateau at an average elevation of ca. 3000 m, feeding several frontal margins descending from the top (Baroni and Carton, 1996; Ranzi *et al.*, 2010, 2013) and is classified by Salvatore *et al.* (2015) as a Scandinavian-type glacier.

3.1.3 Climate overview

Temperature and precipitation distribution are crucial parameters in the framework of glacial and paleo-glacial studies as a control factor of ice masses melting.

The Southern Rhaetian Alps find their location at the boundary between the central and southern European climate regions and differ from other well characterized glacial areas of the Western Alps, especially for the precipitation amount and seasonality. Brunetti *et al*. (2006) classify the Italian Alps as one single homogenous air temperature region (Italian Alpine region, Liguria, and Piedmont), but consider two sub-regions based on different precipitation regimes: Northwestern Italy and the northern part of Northeastern Italy. The region of the Ortles-Cevedale massif is located close to a rain shadow known as the "inner dry Alpine zone" (Frei and Schär 1998; Schwarb, 2000). This area is in fact characterized by the lowest precipitation in the entire European Alps (500 mm/yr at the floor of Val Venosta). Instead southward, close to a wetter area affected by the influence of the Mediterranean Sea, precipitation does increase, reaching 900 mm/yr in the valleys at the southern edge of the mountain group. A

total annual precipitation of 1300–1500 mm/yr is instead estimated at 3000–3200 m a.s.l. in the area of La Mare and Careser glaciers (upper Peio Valley, Carturan 2010; Carturan *et al*. 2012).

At the scale of the Ortles-Cevedale massif, precipitation rates record a single maximum during the summer season and a low winter precipitation rate (Belloni in Desio, 1967; Gabrieli *et al*., 2010). This precipitation pattern can be explained as a possible consequence of the prevailing SW, W and NW cyclonic winds that provide significant precipitation to the southern and northern slope of the Alps and leave the innermost Alpine area in a rain shadow.

The Ortles-Cevedale region is characterized by a continental cool-temperate climate (Pelfini, 1992, Peel *et al.*, 2007, Salerno *et al.*, 2014), characterized by high daily temperature range but limited at the annual scale (RSA 2010/2011, 2011). In table 3.1.3.1 data of mean annual and monthly temperatures and mean annual precipitations available from the Forni weather station (2150 m) are listed (from Orombelli and Pelfini, in Cavallin *et al.*, 1997). Considering the data related to monthly regime average temperature and precipitation recorded in the upper Peio Valley, at Careser Dam (2605 m, 46°25'21.4"N, 10°41'57.7"E) for the time interval 1959-2009 (from Carturan *et al.*, 2013b, fig. 3.1.3.1), mean summer temperatures settle around 7°C, in contrast with negative peaks around -8.0°C reached during January and February. Instead, mean annual precipitations lightly above 1200 mm/yr are recorded, with maximum peaks reached during the months of May and November

If the Peio weather station is considered (1565 m, fig. 3.1.3.2), a mean annual precipitation of 920 mm is recorded for the time interval 1978-2005 and the annual precipitation distribution shows a minimum in winter, a principal maximum in autumn and a secondary maximum in spring (Carturan *et al.*, 2012).

Continuous seasonal snow cover is recorded from above 1000 m a.s.l. (Peel *et al.*, 2007). The mean annual 0°C isotherm is located at around 2500 m a.s.l. (ca. 2300 m a.s.l. during the 1960s, Belloni in Desio, 1967).

Weather station	Altitude (m a.s.l.)	MAT (°C)	January T (°C)	July T (°C)	MAP (mm)	Reference
Forni	2150	1.5	-6.8	11.1	807	Orombelli and Pelfini, in Cavallin *et al.* (1997)
Careser Dam	2605	-0.7	-7.9	8.5	873	-

Table. 3.1.3.1. - Temperature and precipitation data from Forni weather station.

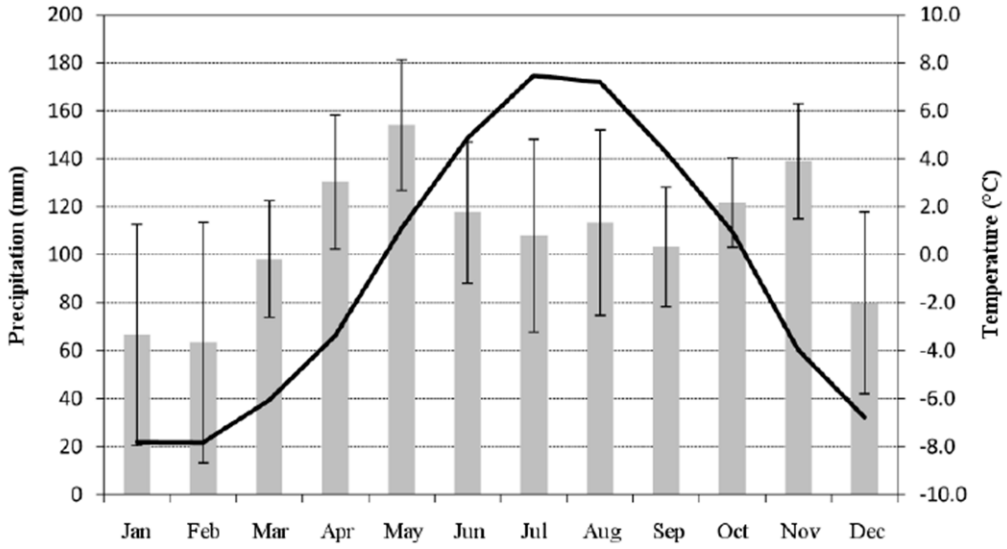

Fig. - 3.1.3.1 - Monthly regime of average temperature and precipitation at the Careser Dam weather station (2605 m), averaged for the interval 1959-2009. Bars indicate ± 1 standard deviation. From Carturan *et al.* (2013b).

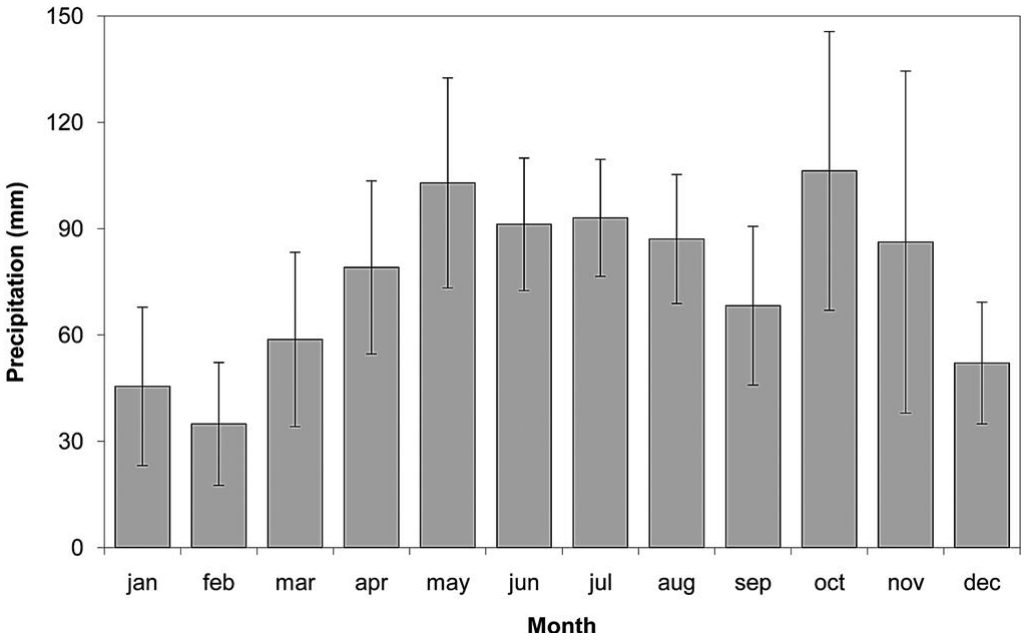

Fig. 3.1.3.2 - Average monthly precipitation at the Peio weather station(time interval 1978-2005). Bars indicate ± 1/2 standard deviation. From Carturan *et al.* (2012).

Precipitation distribution, intensity and temperature ranges are strongly related to the altitude and aspect of the different areas. Related to the altitude, Belloni, in Desio (1967) related with altitude the trend of mean annual precipitation amount and temperature gradient for the Ortles-Cevedale area. According to the Author, every 100 m of altitude precipitation regularly increases of 25 mm and a temperature gradient of ca.0.54°C is recorded, maximum in April and May, minimum between December and January.

Diolaiuti *et al.*(2012), analyzing the daily mean temperature for the 1976-2005 period referred to the Bormio weather station (1225 m, 46°28'13" N, 10°22'21" E), detected a significant increase of seasonal temperatures, of 1.60 °C, 2.51 °C and 1.21 °C for winter (TJFM), spring (TAMJ) and summer (TJAS) respectively, with an increase of 1.37 °C in terms of mean annual temperature (MAT)(fig. 3.1.3.3). This trend is supported by Salerno *et al.* (2014) that find a temperature rise of 0.012°C/yr considering the 1924-2007 period. The trend id better highlighted when the Authors consider the different time intervals of 1954- 1981 (0.014 °C/yr) and 1981-2007 (0,038 °C/yr), detecting a tripled increase for the latter.

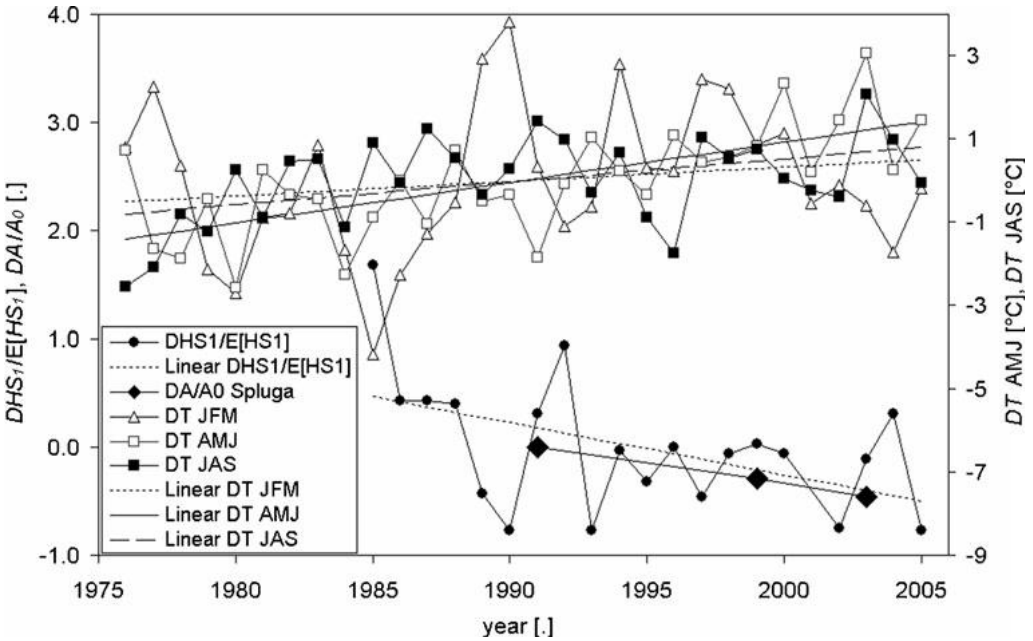

Fig. 3.1.3.3 - Temperature anomalies DTJFM, DTAMJ and DTJAS, relative snow depth variation DHS1/E[HS1], and relative area variation DA/A0 for Ortles-cevedale group (Diolaiuti *et al.*, 2012)

Available data for this area, processed by the *Historical instrumental climatological surface time series of the Great Alpine Region* (HISTALP) project, developed from Auer *et al.* (2007), made possible to reconstruct the Ortles-Cevedale temperature anomalies for the 1780-2009 period. The study underlines a progressive increase (especially since 1990) of positive mean annual temperature anomalies within the massif, in line with the global scale temperature variation (IPCC 2007, 2013). A general increase of temperatures was detected both considering mean summer (AMJJAS) and winter (OND+JFM$_{y+1}$) semester temperatures (fig. 3.1.3.3).

The local climate trend is related to larger scale phenomena. One of the most important indicators of the long term climate variation is the Sea Surface Temperature (SST) used for the monitoring of the Atlantic Multidecadal Oscillation (AMO) (Huang *et al.*, 2015). The latter is a climate variability model based on North Atlantic SST long-duration natural changes, occurring since at least 1000 yrs, with alternating cool and warm phases that may last for 20-40 years and a difference of about 1°F between extremes (NOAA, National Oceanic and Atmospheric Administration). Fluctuations of SST strongly influence precipitation and temperature distribution and entity over Europe. Since middle ’90 we are in a positive AMO that defines a warm period (NOAA).

Instead, no precipitation series datasets are available from HISTALP for the investigated area.

Compared to the Ortles-Cevedale massif, characterized by an average precipitation rate of 750-800 mm/yr, the Adamello-Presanella massif records an average mean annual precipitation around 1400 mm/yr (Baroni *et al*., 2004). The Adamello-Presanella group find in fact its location in a southern position compared to the Ortles-Cevedale, less close to the "inner dry alpine zone". According to Ceriani and Carelli (1999), considering the 1891-1990 time interval, the mean annual precipitation records its minimum around 800 mm/yr in the northern sector (Ponte di Legno weather station, 1200 m a.s.l.), rises to ca. 1000 mm/yr in the Val Camonica valley floor, reaches 1350 mm/yr in the highest portion of the

Adamè Valley and around 1500 mm /yr on the southern sector at the Bagolino weather station (ca. 800 m a.s.l.).
Mean Annual Tempeartures (MAT) range from ca. 8°C slightly above 1200 m, to ca. 0°C at ca. 2500 m (Seppi *et al.*, 2010). An average vertical termic gradient of 0.59°C/100 m was calculated by Baroni *et al.* (2004, 2007).
At 1900 m in Val d'Avio a mean annual temperature of 3.8 °C is recorded for the 1955–1987 time interval (Baroni *et al.*, 2014).

3.2- Geological and geomorphological setting of the Southern Rhaetian Alps

3.2.1 Geology

The Ortles-Cevedale mountain group is represented in the geological maps 8 “Bormio” and 9 “Monte Cevedale” at a scale of 1:100.000. In the framework of the geological cartography related to the CARG (CARtografia Geologica) project, the massif falls within the maps “Ponte di Legno”, "Bormio", "Rabbi" and "Malè", at the scale of 1:50.000.

The present geo-structural configuration of the Ortles-Cevedale massif is strictly related to the events that, since the Triassic, brought to the development of the Tethys Ocean and to its subsequent closure with the formation of the Alpine orogen. The different paleogeographic domains recognized along this sector of the Alps assumed their identity since the fragmentation of the Pangea supercontinent. During Permian – Triassic the first marine transgression on the hercynian basement took place, with a consequent imposition of carbonate platform environments in a rifting regime during the Triassic – Middle Jurassic, that progressively brought to the spreading of the Tethys Ocean. During the Jurassic from W to E the western branch of the Tethys, the neo-Ligure - Piemontese oceanic crust developed (Marroni *et al.*, 2001). On the Adria Plate continental passive margin thick sedimentary successions in the deeper basin areas associated to condensed successions on structural highs developed. Since the Late Cretaceous the between the European and African plates began to converge, progressively leading to the disappearance of the Tethys Ocean The complete closure of the ocean (Eocene) marked the onset of the

Adria/European plates collision and the consequent build-up of the Alpine orogen (Froitzheim *et al.*, 1996; Dal Piaz *et al.*, 2003; Chiesa *et al.* in press)). The deep asymmetry of the original passive continental margin strongly affected the following tectonic evolution, where rifting discontinuities were exploited in a compressive tectonic during the convergence phases (Marroni *et al.*, 2001). These processes brought to the development of a complex fold thrust belt (Casati, 2012). As depicted by Dal Piaz *et al.* (2003), the Alpine orogen is described by a double vergence structure, separated by the Insubric Line. The "Europe-vergent" belt is a thick collisional wedge of Cretaceous-Neogene age, consisting of continental and minor oceanic units displaced towards the European foreland; The Southern Alps consist in a minor, shallower (non-metamorphic) and younger (Neogene) fold-thrust belt displaced to the south (Adria-vergent), developed far from the oceanic suture.

The subduction and the subsequent collisional phase involved different paleogeographic domains, already defined since the end of Jurassic and identified in the Helvetic, Pennidic, Austroalpine and Sud-Alpine domains. The Helvetic and the Pennidic domains do not outcrop in the study area. The Helvetic Domain represents the externalmost unit and is part of the European continental margin, mainly constituted by shallow marine successions (Zanchi in Cavallin *et al.*, 1997). The Pennidic Domain (or Axial Domain) is constituted by the continental and oceanic nappes from the distal European continental margin and the Mesozoic ocean, all belonging to the subducting lower plate. Units related to this domain outcrop further N from the Ortles-Cevedale massif, from the Engadina and Tauri tectonic windows.

The Austroalpine Domain represents remnants of the continental margin of the African and Adria plates and is tectonically located above the oceanic units of the Pennidic Domain (Chiesa *et al.* in press). The Austroalpine Domain constitutes, therefore, the highest geological structure of the Alps and is constituted by the continental crystalline basement and the relative Mesozoic sedimentary cover (Zanchi in Cavallin *et al.*, 1997).

South-Alpine Domain

Both the Austroalpine and the South Alpine domains belong to the Adria plate paleomargin (Dal Piaz *et al*., 2003).

The area of the Ortles-Cevedale massif is confined between two of the most important tectonic alignments of the Alps, represented by the Engadina Line towards N and the Insubric Line (or Periadriatic alignment) towards S. The Insubric Line represents a major fault system of Oligocene-Neogene age consisting in a set of predominantly strike-slip faults (Zanchi in Cavallin *et al.*, 1997; Dal Piaz *et al*., 2003; Casati, 2012, Chiesa *et al.* in press) marked by a considerable milonitic band that crosses the entire Alpine extent developing ca. E-W. This great tectonic unit, constituted by several minor tectonic structures, assumes different local names. In particular, the southern boundary of the Ortles-Cevedale massif is represented by two main segments of the Insubric Line defined as Tonale Line, oriented WSW-ENE, that runs in correspondence of Val di Sole and the start of Val Camonica and Giudicarie Line (North and South), that follows a SSW-NNE direction and joins the latter close to the village of Dimaro. In this framework, the Austroalpine and South Alpine domains are defined depending on their position, respectively north and south of the Insubric line, and on the vergence. In fact, the Insubric Line separates the metamorphic units of the Pennidic and Austroalpine domains (NW-vergent) from the South Alpine Domain, the latter characterized by a S-vergence (Zanchi in Cavallin *et al.*, 1997; Dal Piaz *et al.*, 2003; Casati, 2012; Carminati *et al.*, 2012).

The Ortles-Cevedale Massif is characterized by lithologies belonging to the metamorphic basement of the Austroalpine Domain and the relative Permian-Mesozoic sedimentary cover. Among the Austroalpine units, crystalline schists, mostly paragneiss, mica schists and phyllites predominate, with abundant interbedded ortogneiss, amphibolites and subordinately marble horizons, metabasites, metaperidotites, migmatites, granulites, quartzites and pegmatites. Magmatic units are represented by

andesitic or basic bands and localized gabbro or tonalite intrusions. Also the Permian - Cretaceous sedimentary cover is largely represented. Relatively sharp ridges exist in the northwestern area, constituted by sedimentary rocks (dolomites and limestones), whereas metamorphic rocks (micaschists, paragneiss and phyllites) prevail elsewhere, forming more rounded reliefs. These lythologic differences play an important role on the present topography and significantly affect the distribution and morphology of the glaciers (Desio, 1967).

The lithological characteristics of the main units outcropping in the Ortles-Cevedale massif are described here Below. Figures are extracted from the Sheet No. 024 Bormio (CARG, 1: 50,000 scale). Following Montrasio *et al.* (2010), in the Ortles-Cevedale massif outcrop units from the Upper and Middle Austroalpine:

Upper Austroalpine

- Umbrail-Chavalatsch Zone (Ötztal)
  - Umbrail Sedimentary
  - Chavalatsch Crystalline

Middle Austroalpine

- Quattervals Unit
- Ortles Unit
- Campo Unit
  - Scaglia dello Zebrù
  - Peio Unit
  - Lasa Unit
- Languard Unit

The Umbrail-Chavalatsch zone represents the uppermost unit of the structure and is constituted by rocks of the crystalline basement (mainly migmatites, ortogneiss, paragneiss).

The Middle Austroalpine is mainly constituted by metamorphic units (marbles, prasinites, phyllites, paragneiss, granitic or granodioritic intrusions).

The "Campo Unit", named "Falda Campo" sensu Montrasio *et al.* (2010) or “Falda Ortles-Campo” sensu Chiesa *et al.* (2010) is mainly represented by phyllites and mica schists (pre-Permian basement) and younger elements,

(Permian to Cenozoic), represented in particular by andesitic - basaltic intrusions. The Campo Unit outcrops on most of the massif (Alta Valtellina, Valfurva, Valle dello Zebrù). This unit is tectonically identified from the uppermost Ortles Unit by the Zebrù Line and bounded at the base by the Blesaccia Line.

The Campo Unit is subdivided into three different metamorphic complexes, characterized by a different origin and separated by the Madriccio and Lasa lines. From bottom to top we identify "Lasa" Unit, "Peio" Unit and "Scaglia dello Zebrù" Unit.

The Peio Unit , mainly characterized by metamorphic elements, most frequently outcrops along the study area, in the High Valtellina and the Mt. Cevedale-Mt. Vioz sector. The "Sondalo Pluton" is a gabbro-dioritic intrusive complex outcropping in the High Valtellina and considered part of the Peio Unit.

The Lasa Unit represents the lowermost of the Campo Unit and results tectonically overlapped by the Peio Unit along the Zumpanell-Lasa Line. Is constituted by crystalline basement mainly consisting in pre-Varisican metamorphites in amphibolite facies and by an evident "Alpine" overprint in green schists facies Montrasio *et al.* (2010).

Towards S, according to Staub (1924, 1964, in Chiesa *et al.*, 2010) in correspondence of the Peio Line, the Ortles – Campo Unit is overlapped by three main units of the Upper Austroalpine that develop parallel to the Insubric Line. In particular, from SE to NW we meet the "Falda del Tonale *s.s.*", "*Nordliche Tonale Zone"* and *"Piazzi Decke"*. The Languard Unit tectonically overlaps the Campo Unit.

Permo-Mesozoic sedimentary successions are recognized for every structural unit, except Lasa and Peio. Sedimentary units constitute the "Ortles" and "Quattervals" units and are interbedded along secondary detatchment plans with pre-Permian basement units in the Umbrail-Chavalatsch Zone.

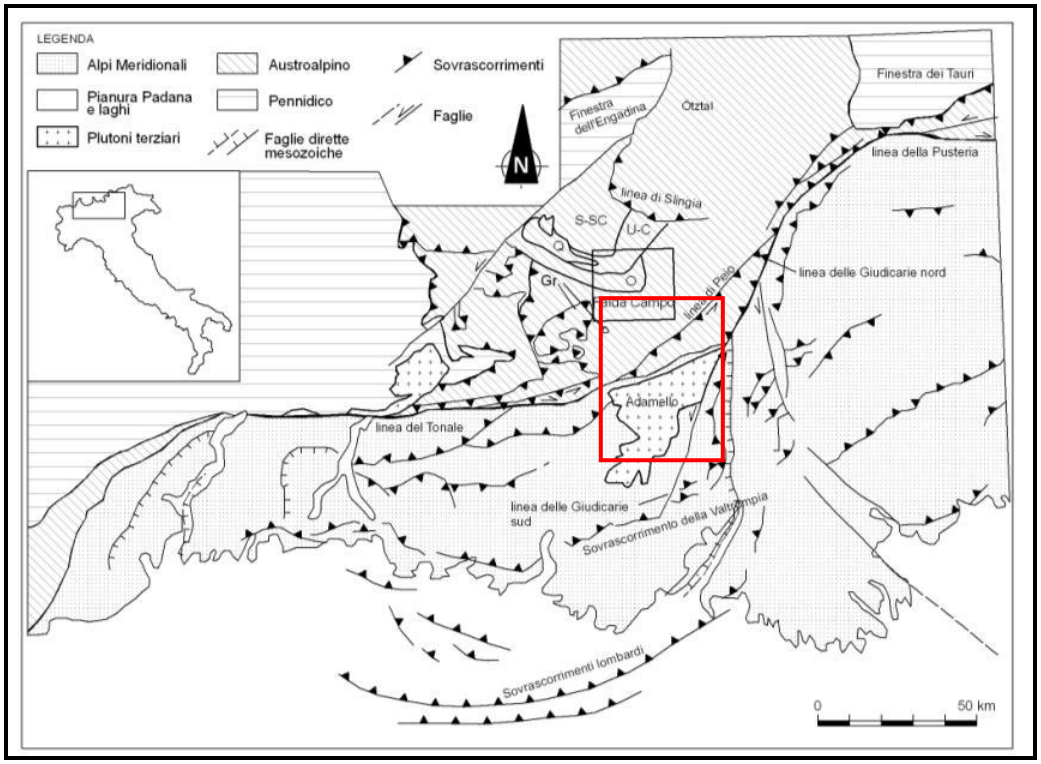

Fig. 3.2.1.1 – Geologica map of the central-eastern Alps.i. The black rectangle represents the Foglio (sheet) "*Bormio"* (1:50.000), the red rectangle refers to "Ponte di Legno" and "Adamello" sheets. C = Falda Campo, Gr = Falda Grosina, L = Falda Languard, S-SC = Complesso Sesvenna – S-charl, U-C=Zona a scaglie Umbrail Cavalatsch, Q = Falda Quattervals, O= Falda Ortles. From Montrasio *et alii* (2010).

As mentioned above, the Insubric Line marks the boundary between the Austroalpine and the Sud-Alpine domains. Crossing Val di Sole towards S, the Adamello-Presanella massif rises up, until ca. 3550 m a.s.l.. As evident from fig. 3.2.1.1 this sector is characterized by a different geological setting compared to the Ortles-Cevedale massif. The origin of this area is in fact related to post-collisional magmatic phenomena ("Periadriatic magmatic cycle" following Dal Piaz and Venturelli, 1983), expressed in the Adamello-Presanella batholith, the largest Cenozoic intrusion among the post-collision Tertiary plutonic bodies in the Alps (670 km^2; Callegari and Brack, 2002; Brack *et al.*, 2008; Dal Piaz *et al.*, 2008). The magmatic activity along the Insubric Line for all its extent occurred between the late Eocene and late Oligocene (42–29.4 Ma; Del Moro *et al.*, 1983; Callegari and Brack, 2002; Mayer *et al.*, 2003) and was generated by partial melting of lithospheric mantle sources, previously modified during the Cretaceous-Eocene subduction, and consequent ascent to upper crustal reservoirs, linked to slab break-off and related thermal perturbation, coupled with

extension and rapid uplift of the wedge during active plate convergence (Dal Piaz *et al.*, 2003).

In the context of our study area, the intrusion is enclosed within the Sud-Alpine structural unit and within a crustal structural wedge bounded towards N by the Tonale line, oriented approximately E–W, and on the W by the Giudicarie line, oriented NE–SW.

The geological setting of the Adamello-Presanella massif is greately represented in the geological map at the scale of 1:50.000 edited by Callegari *et al.* (1998).

More into detail, four major plutons of tonalite– granodiorite composition characterize the Adamello-Presanella batholith, identified in as much magmatic episodes (fig. 3.2.1.2). The oldest magmatic products (42–38 Ma) only outcrop in the southern sector of the Adamello batholith. The Periadriatic magmatism occurred in several stages during the Alpine orogeny and ceased in the Late Oligocene, when renewed collisional shortening (Neo-Alpine phase according to Dal Piaz and Venturelli, 1983) neutralized the magmatic sources (Dal Piaz *et al.*, 2003).

According to Callegari (1983), the four main phases of magmatic activity in the Adamello-Presanella area can be described as follows:

- Monte Re di Castello - Corno Alto Pluton (42- 40 Ma): the first in the series, represented in the S-SE portion of the Adamello massif. Mainly tonalite, with frequent granodioritic and gabbric bodies.

- Adamello Pluton (36-34 Ma): Located in the central sector of the batholith. Tonalite and presence of gabbric bodies at the margins.

- Avio Pluton (34-32 Ma): Outcrops in the northwestern sector of the batholith. Reported to be almost completely tonalite.

- Presanella Pluton (33-29 Ma): Final magmatic episodein the Southern Alps. Located in the N-NE sector of the massif, is composed of a large number of sub-units, mostly of tonalite nature.

Mayer *et al.* (2003) showed a progressive migration of the magmatic activity from SSW to NNE, accompanied by a gradual increase of the assimilation of crustal material by the same magma from S to N and from the central areas to peripheral portions of the batholith. According to Callegari (1983) the origin of the batholith would be due to a joined action of deep fractionate crystallization and contamination, with progressive assimilation, of crustal material. The latter would justify a lythological uniformity of the magma mineralogy, whereas the geochemical differences would depend on the nature of the fractionation stages, of the assimilated material and on the degree of assimilation. In addition, the several gabbro - dioritic bodies, together with frequent mafic inclusions in the tonalites would suggest a basic essentially mafic original magma.

The same Author thus interprets the prevailing outcrops of tonalites compared to gabbri as related to a higher density of the latter, that would lie deeper, and considers however the gabbric bodies outcrops as expression of a rapid rise of the magma as a result of temporary peaks of extensional tectonics.

Considering the host rocks, the thermo-metamorphic contact aureole was found in a band locally even 4 km wide (Callegari and Brack, 2002).

The great variety of rocks resulted from contact metamorphism reflects the variegated nature of the sources, from pre-Permian crystalline basement, both belonging to Sud-Alpine and Austroalpine domains to Permian volcano-sedimentary sequences (Sud-Alpine Domain) and Meso-Cenozoic sedimentary successions (for major details refer to Callegari and Brack, 2002).

Furthermore, the several veins that intrude and cross the batholith and the surrounding area are worth to be mentioned, realted to the Periadriatic magmatic phase or to older age, probably Permian-Triassic (Salomon, 1908-10).

Finally, phases of ductile and brittle deformation affected the area before, during, and after the Eocene–Oligocene intrusions of the Adamello batholith (Brack *et al.*, 2008, Baroni *et al.*, 2014). Fracture sets that cross the tonalite are primarily oriented NW–SE, WNW–ESE, and NE–SW and

affect the morphology of the valleys, driving selective erosion of rectilinear segments of secondary valleys, disrupting top relict surfaces, and localizing passes on sharp ridges. Callegari (1983) considered faults that cross the intrusive body to be expressions of recent tectonic activity.

Beyond the above discussed units, wide sectors of the study areas are covered by abundant continental quaternary deposits, mainly of glacial and gravitational origin. These deposits are related to the most recent evolution of the Alpine range and constitute the highest stratigraphic units of the Southern Rhaetian Alps. The shape of the landscape along the highest sectors of the chain, result of its tectonic evolution, favoured the development of glaciers during periods of climate deterioration throughout the Pleistocene and the Holocene. The glacial cirque shapes sculpted in the highest crests, quaternary glacial deposits and the relative sediment outwash that frequently characterize slopes and wider valleys represent the fingerprint of the past glaciations.

The Adamè Valley is nearly everywhere underlain by tonalitic rocks (Dal Piaz *et al.*, 2008), including (i) the 'Western Adamello Tonalite', which is exposed in the western and central portions of the valley, and (ii) the 'Avio and Central Adamello Tonalite', which is exposed at the head of the valley. Both tonalites are late Eocene and consist of medium- to coarse-grained rocks. The tonalites intruded into the metamorphic basement of the Edolo Schists (Paleozoic micaschists, phyllites, and paragneiss) and a sedimentary cover (Permo-Triassic contact metamorphosed clastic and carbonate rocks), which are exposed along the western margin of the study area .

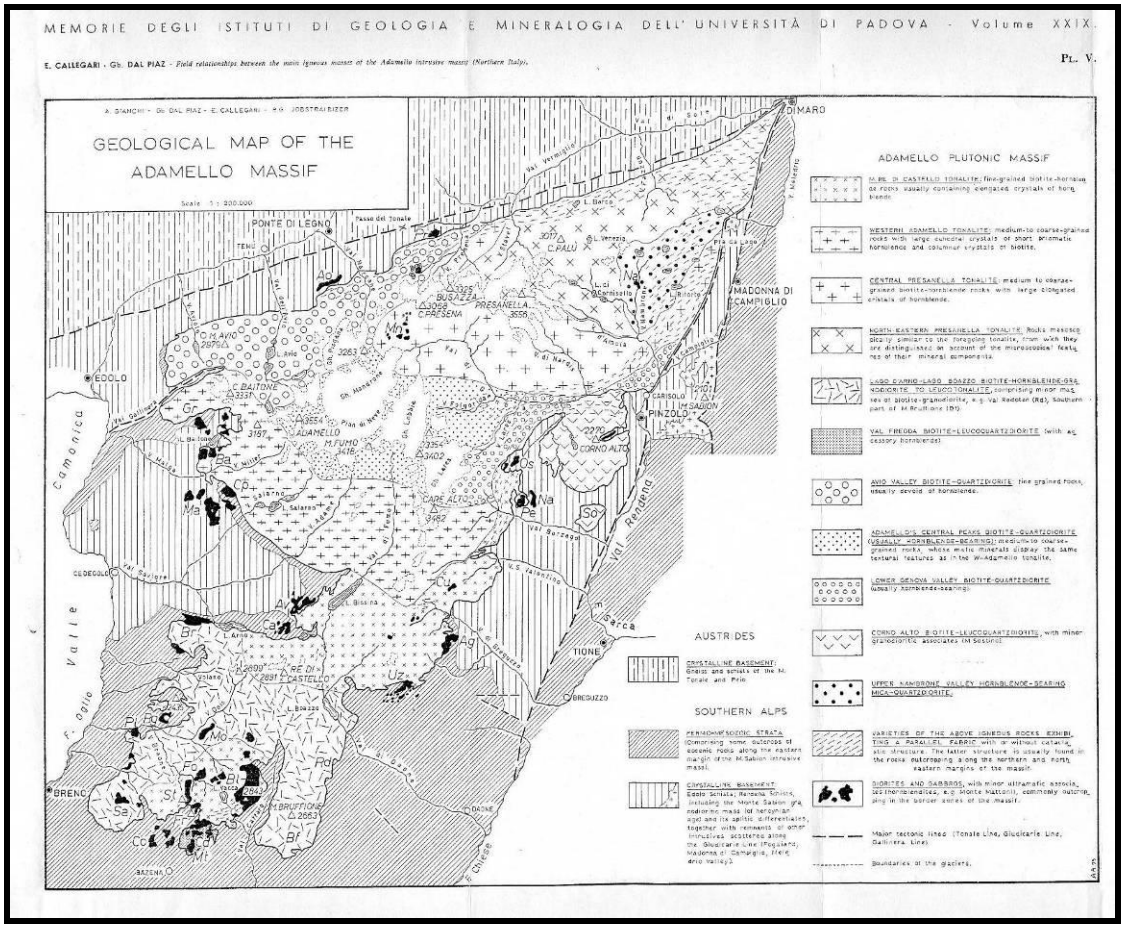

Fig. 3.2.1.2 – Geological map of the Adamello Batholith.

3.2.2 Geomorphological outlines of the Ortles-Cevedale and the Adamello-Presanella massifs

The present morphology of the Ortles-Cevedale (Upper Peio Valley) and the Adamello-Presanella massif is the typical of the high mountain environment. The most important morphogenetic agents that modeled the landscape are connected to the Quaternary glacialism, to the action of the surface waters, to the gravity and to the cryonival processes. The highest sectors, characterized by alpine morphologies, are occupied by glacial masses and the slopes are interested by the gravitative and cryonival action. The landscape presents a well-defined Alpine glacial morphology, with deep glacial troughs that are composed by successions of basins and steps, steep glacial shoulders, glacial cirques, sharp ridges and horns. The most important glacial morphologies of the study area are the typical glacial profile ("U" profile) of the valleys, the glacial cirques and the sharp crests. The transversal valley profiles have an almost regular shape in

relation with the lithology and the erosion capability. While the longitudinal profiles differ from the fluvial valleys and present glacial thresholds and depressions (Castiglioni, 1986; Baroni *et al.*, 2004). Often on the slopes of the principal valleys are located hanging valleys as, for instance, the Valle di Rosole and the Valle di Cedech on the right side of the Valle dei Forni. In many cases the glacial valleys present a terminal part with fluvial shape that testifies the recent fluvial erosion action.

In the southern sector of the Adamello Massif are located four big glacial valleys that represent the important past glaciers modeling. From the west to the East are located the Val Miller, the Val Salarno, the Val Adamè (fig. 3.2.2.1) and the Val di Fumo. The last are hanging valleys modeled by the glacial activity that flow in the main Val Camonica and Val di Daone.

Fig. 3.2.2.1 - The typical U shaped glacial valley of the Val Adamè.

In particular the Adamè–Saviore valley system is one of the most well-defined U-shaped valleys that radially diverge from the Adamello central peaks. Furthermore, during the late Pleistocene the southern extension of the Adamello glacier was hosted in this valley. The valley slopes have been interested by cryoclastic and gravitative processes that generated numerous debris cones and slopes and debris flow (Baroni and Carton,

1991). On the valley sides it is common find trimlines, glacial cirques, roche mountonnée and glacial deposits that testify the past glacial advances. Another typical erosional feature are the glacial cirques that find a reliable expression in the Alta Val Tellina. They are recognizable in the upper parts of the valley and today are occupied by mountain glaciers, permanent snowfields or are deglaciated. The glacial cirques(fig. 3.2.2.2) are often characterized by the presence of rock steps with a morphology defined whale back or by the typical roche mountonnée. (Sharp, 1988).

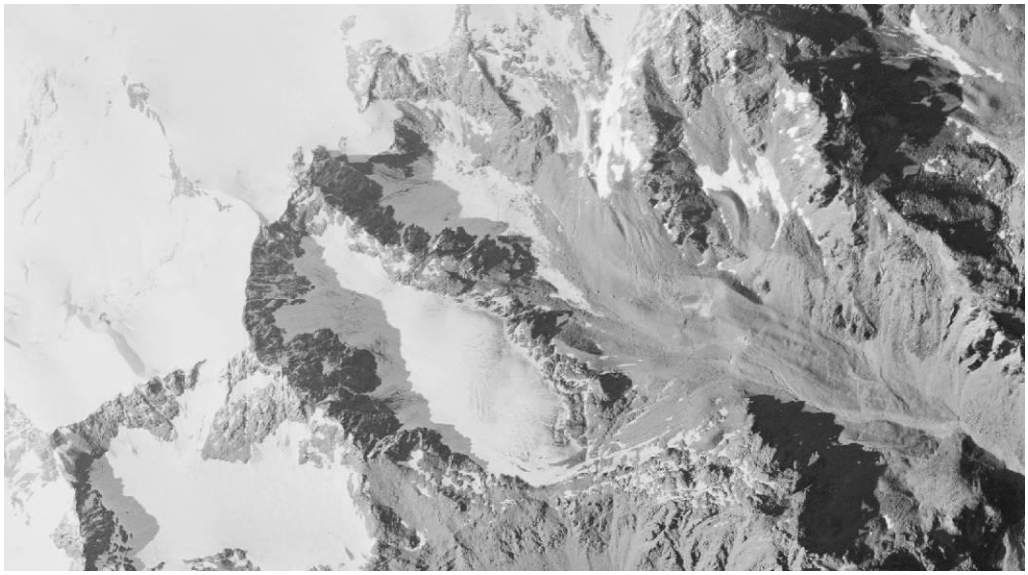

Fig. 3.2.2.2 - Example of glacial cirque (Vedretta Saline, Ortles-Cevedale Massif). Orthophotographs 1989 (www.minambiente.it)

The most important glacial feature on the entire study area is the moraine. The moraines are fundamental evidences of the glacial evolution and testify the different glacial phases over different time intervals. Several Holocene moraines are well preserved, in particular those related to the maximum Holocene glacial expansion moment (fig. 3.2.2.3), the Little Ice Age (LIA).

Fig. 3.2.2.3 – Example of LIA moraines in Val de La Mare (Ortles-Cevedale Massif). (photo R. Seppi, 21 September 2012 after Carturan *et al*, 2014)

Less widespread but still very important are older moraines related to Lateglacial events (fig. 3.2.2.4). These testify the glacial re-advances occurred at the end of the Pleistocene and were the most important glacial feature in our glacial reconstructions, concerning the alpine part of the research project. In fact shape and relative position of these ridges provided the basilar information about the Lateglacial history of the study areas.

These moraines are characterized by a sharp and well preserved ridge with evidences of deeper weathering of erratic boulders, thicker soils, and wider vegetation cover respect to the LIA moraines.

The majority of the slopes and valley floors are occupied by glacial deposits with variable thickness. This variability depends mainly on the bedrock morphology. These sedimementary rocks known as limestones, are characterized by a heterogeneous granulometry and can be described as massive diamicton constituted by rounded clasts of different dimensions.

Numerous erratic boulder can be found in several sectors of the valley floors and on the top of the moraines or in line defining a trimline. In other

cases isolate erratic boulders rest on glacial deposits on directly on the outcropping bedrock.

Fig. 3.2.2.4 – Lateglacial moraine in Val de La Mare (Ortles-Cevedale Massif)

In the higher sectors of the valleys the debris can be organized in cones or debris layers that are modeled by the winter snow and by the seasonal presence of ice in the ground. In the Ortles-Cevedale massif it is possible to find the latter kind of deposit with a flat shape. This conformation is mainly due to the characteristics of the bedrock (phyllites and micashists) that favor this configuration.

In most of the study area slopes are affected by mass wasting and cryoclastic processes. Rocky gullies originated by gravitational processes as well as snow avalanches and running water (e.g., debris flow, fig. 3.2.2.6) or derived from a combination of the three processes are common over the slopes. The poligenic origin of rocky channels is a consequence of the seasonal variability of geomorphological processes. Debris flows are widely diffused and originated deposits as insolated or coalescent lobes as well as composite debris cones. The debris flow events are triggered by the saturation of the debris that generate a debris-air-water mixture mobilized by the gravity action. The fluidized material can tread long

distances acquiring an high velocity. The derived deposit is characterized by a lower inclination, compared to the previous configuration, and by an imbricate structure.

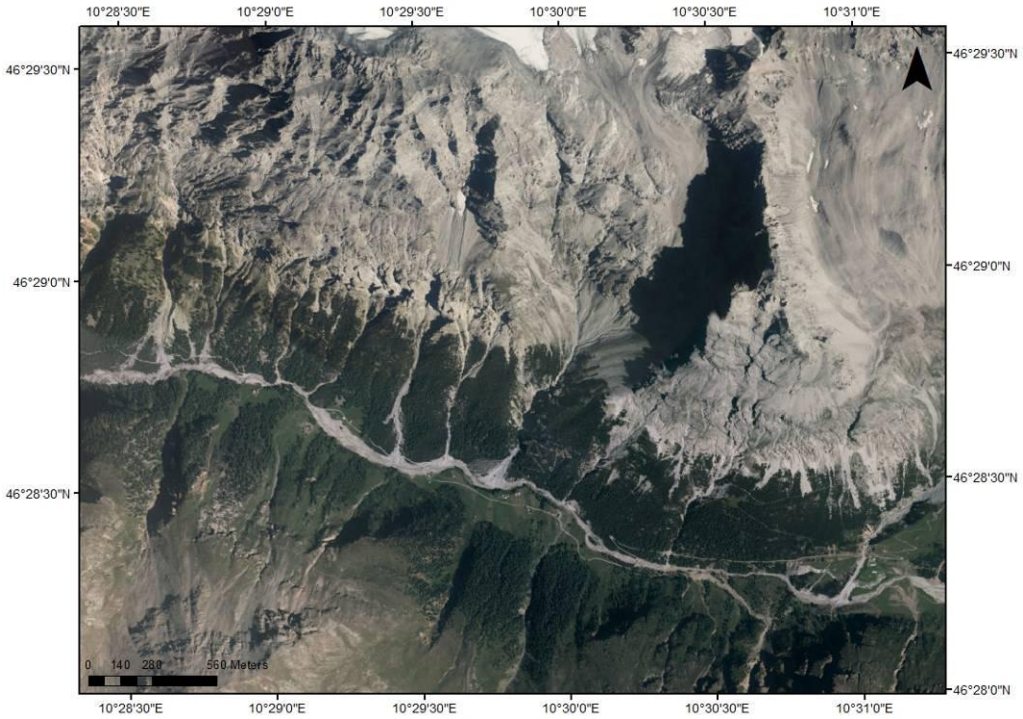

Fig. 3.2.2.6 - Example of an area interested by debris flow (ValZebrù, Ortles-Cevedale Massif) Orthophotographs 2012 (www.minambiente.it)

The numerous glaciers of the Ortles-Cevedale Massif are temperate glaciers characterized by a strong erosive capability. The glaciers of this massif are mainly valley and cirque glaciers, affected by crevasses and seracs on the ice surface.

In the Adamello-Presanella Massif, the high plateau hosts the Adamello Glacier that is the largest italian glacier (16.4 km^2 in 2007, Salvatore *et al.*, 2015). The plateau has an average elevation of ca. 3000 m and the Adamello Glacier (classified by Salvatore *et al.*, 2015 as a Scandinavian-type glacier) feed several frontal margins descending from the top (Baroni and Carton, 1996; Ranzi *et al.*, 2010, 2013). Because of the strong glacial reduction of occurred in the recent past and still acting, several glacial tongues are isolated from the main catchment basin. Other important glaciers are the Pisgana Glacier, the Vedretta della Lobbia, the Vedretta di Lares (fig. 3.2.2.7). The alpine glaciers, characterized by well defined catchment basins and tongues, are not the unique glacier typology of the

massif. Several other glaciers, with a small catchment basin and laking of a defined tongue, are diffused at the high elevation (e.g., Vedretta di Aviolo, Vedretta d'Avio, Vedretta del Venerocolo, Vedretta di Folgorida, Vedretta di Niscli, Vedretta di Passo di Monte Fumo, Vedretta di Adamè and the Vedretta di Salarno, see http://www.glaciologia.it/ubicazione-ghiacciai/ghiacciai.html). Numerous are also the cirque glaciers that still occupy the glacial cirques (i.e. on the left side of the Val di Fumo).

Fig. 3.2.2.7 – The northern tongue of the Ghiacciaio dell'Adamello (photo C. Baroni)

4 - Antarctica

4.1 A general overview in the global context

Antarctica is the southernmost continent on Earth, it is confined beyond the 60 ° South latitude and occupies an almost centered position with the South Pole. The limit of the Antarctic region is conventionally placed around the 52° parallel and it is included within a band of several tens of kilometers, where cold waters circum-Antarctic enter in contact with the warmer sub-Antarctic. This condition define a Oceanography limit called Antarctic Convergence.

The southern portions of the Atlantic, Pacific and Indian Oceans are located southern of the Antarctic Convergence and are called Southern Ocean or Antarctic Ocean. The cold Antarctic circum-polar current (fig. 4.1.1) keeps thermally isolated the continent (Kennett and Hodell, 1995).

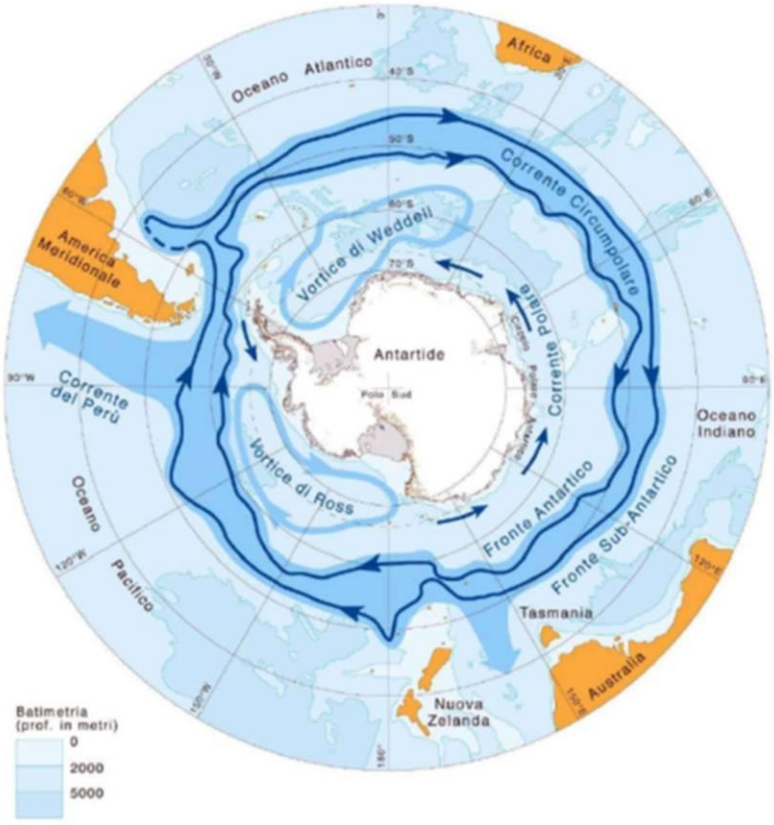

Fig. 4.1.1 - Surface circulation in Southern Ocean (after Baroni , 2001)

The Southern Ocean has an extension of about 36 million km^2, corresponding to approximately 10% of the world's oceanic masses and it

is the only great ocean without limitations by land masses. The continent covers an area of ca. 13.8 millions of km^2 and during the winter the Antarctic extension can reach 20 millions of km^2 due to the formation of a big amount of ice see surrounding the coastal areas (Baroni, 2013).

The roughly circular shape of Antarctica is interrupted by the appendix of the Antarctic Peninsula, facing the South America. The Transantarctic Mountains cross the continent for 4000 km from the Ross Sea to the Weddel Sea and divide the continent in two main sectors, the East Antarctica and the West Antarctica.

The 98% of the continent surface is covered by the Antarctic Ice Sheet that has a volume of 26.6 millions of km^3 that corresponds to the 90% of the global ice and about the 80% of the fresh water on the Earth (Vaughan *et al.,*1999).

The ice sheet average thickness is more than 2100 m with a maximum around 4000 m. This condition define Antarctica as the continent with the higer mean altitude on the planet (ca. 2300 m a.s.l.). An hypothetical melting of all the antarctic ice will correspond to an uprising of tens of meters of the world sea level (Denton *et al.*, 1991), testifying once more the important role of Antarctica in the global context.

The Antarctic Ice Sheet is not a single ice body but it's made up by two main elements (fig. 4.1.2), the east Antarctic Ice Sheet (EAIS) and the West Antarctic Ice Sheet (WAIS). The EAIS has an almost regular shape and faces mainly the Indian Ocean while the Wais is charaterized by a lower enxtension and a more complex shape. The Antarctic ice sheet covers almost the entire continent, the deglaciated areas constitute only the 2.4% of the territory (Baroni, 2013) and are concentrated mainly in the coastal areas, along the Transantarctic Mountains and on the Antarctic Peninsula. The highest rock culmination of the continent is the Vision Massif, located along the Ellsword Mountains in West Antarctica with an altitude of 4897 m a.s.l. while the most elevated in the Transantarctic Mountains is Mount Kirkpatrick (4528 m a.s.l.) in Queen Alexandra chain. Remarkable altitude are reached by the ice sheet, that culminates in some large glacial domes(i.e. the Argos Dome, 4200 m).

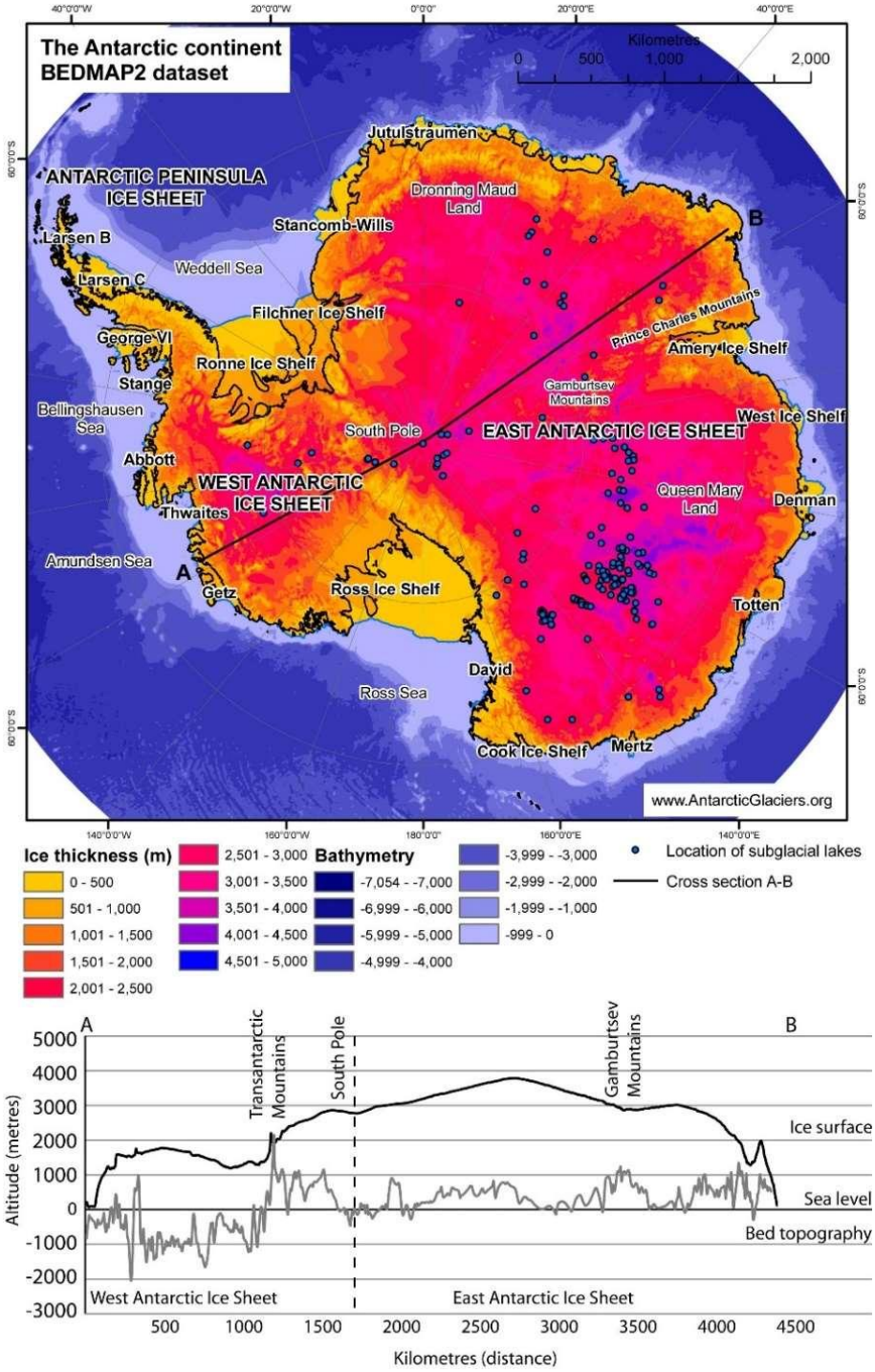

Fig. 4.1.2 - The Antarctic continent BEDMAP2 dataset show the thickness variation over Antarctica. Section A-B divides EAIS and WAIS (www.AntarcticGlaciers.org).

A series of summits and ridges allow to subdivide the ice sheets in different glacial basins. The ice masses that cover the continent are driven by their own weight in a radial way from the inner part to the coastal areas. The entity of this movement is very low in the inner part of the ice sheet (some meters per year) increasing to the coast where can reach a

velocity of 100-250 m per year (Bamber *et al.*, 2000; Rignot *et al.*, 2011). Outlet glaciers and ice streams with their dynamic behavior have a fundamental role in the drain system and stability of the ice sheet. This importance is related to the ice outflow in to the sea. Once reached the sea the glaciers, still drained by the ice sheet, fed the shelfs along the Antarctic coasts (Baroni,2001).The most important shelfs are the Ross Shelf (472.960 km^2) in the Ross Sea, The Ronne-Filchner shelf (422.420 km^2) in the Weddel Sea and the Amery Shelf (62.620km^2) in the Prydz Bay (fig. 4.1.3).

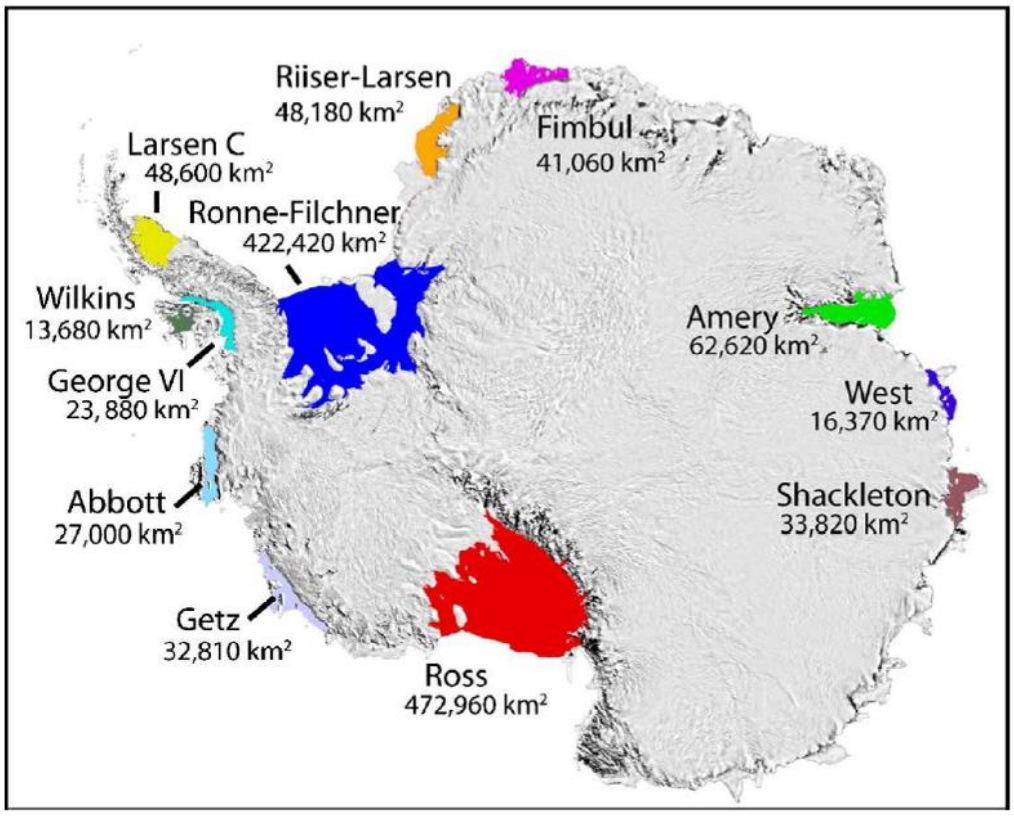

Fig. 4.1.3 - Three most important ice shelfs (Scambos *et al.*, 2007)

The huge ice mass that covers Antarctica continent had a fundamental role in the geological history of the continent.

The beginning of the glaciation started with the passing from "Greenhouse" to "Icehouse" conditions. This transition was inducted by the fragmentation of the Gondwana super-continent and by consequent dispersion of the different parts. Antarctica migrated to the South Pole and

important ocean current developed around the continent. (Kennett, 1977). These conditions led to the paleo-oceanographic insulation and to the starting of the cold climate conditions. Despite its polar position since 100 Ma Antarctica the first glaciations over Antarctica occurred ca. 50 Ma ago when it was still connected to the South America. Since that moment the antarctit climate recorded a progressive lowering of temperatures and a consequent increasing of the ice masses over the continent.

Antarctica was geographically and thermally completely insulated after the opening of the Drake Strait (36 Ma) and with the establishing of the Circum-antarctic current. Also the uplift of the Transasantarctic Mountains had a fundamental role in the glacial history of the continent with the formation of big sea basins that today are occupied by ice. The EAIS reached continental dimensions between the upper Eocene and the lower Oligocene(Barrett *et al.*, 1991; Denton *et al.*, 1991) occupying the dendric valley system previously modeled by the fluvial activity (Baroni *et al.*, 2005). The EIAS found its stability durin the middle Miocene (14.5-14 Ma). The presence of a western ice sheet durin the Oligocene is testified by a glacial diamicton and marine sediments outcropping on the Seymour Islands (Ivany *et al.*, 2006)

Other evidences of the presence of the EAIS and WAIS during the Miocene are provided by the perforations of the Ocean Drilling Program (ODP) and by geophysics surveys. (Hambrey *et al.*, 1991; Andersson, 1999).

During the middle/upper Miocene was recorded the transitino nfrom a temperate to a sub-polar/polar climate regime. (Armienti and Baroni, 1999).

Trimlines over the Transantarctic Mountains and on the outlet glacier valleys constrain the maximal glacia expansion occurred during the lower Pleistocene (Denton *et al.*, 1986). Several morphological evidences testify a thicker WAIS during the middle/lower Pleistocen compared to the present day (Denton *et al.*, 1991; Anderson, 1999).

Different expansion and contraction phases characterized the antarctic ice sheet over the entire Pleistocene. The Last Glacial Maximum (LGM) occurred 25-18/16 ka and it is correlated with the Marine Isotopic Stage 2

(MIS2). During this glaciations the EAIS thickening was bigger in the coastal areas where developed a pedemontan glacier related to the ice sheet and resting on the Ross Sea . (Orombelli *et al.*, 1990), along the Leeward side of the southern Victoria Land nunatak (Baroni *et al.*, 2008; Strasky *et al.*, 2009) and over the upper part of the Rennick Glacier basin (Meneghel *et al.*,1999).The following interglacial phase can be constrained around 11.5 and 10.5 ka for the EAIS and around 10 ka for the WAIS (Leventer *et al.*, 2006; Stone *et al.*, 2003)

Over the McMurdo area and the southern Scott Coast the deglaciation ended around 6.6 ka, 0.5 ka later than in the Terra Nova Bay (Hall *et al.*,2004; Baroni e Hall, 2004).

4.1.1 Geology

The almost total ice coverage of the continent (ca.98%) drastically reduce the geological knowledge of Antarctica. Direct geologigal investigations have been conducted mainly along mountain ranges and coastal areas. Indirect methods, like geomagnetic and geophysical surveys showed that the Antarctic region is divided into microplates and "terranes". This context testify a progressive enhancement of the crust due to the amalgamation of the geological provinces related to different paleogeographic domains.

Antarctica is divided in two main geological domains separated by the Transantarctic Mountains: the East and West Antarctica.

Eastern Antarctica is considered part of the old Gondwana continent and presents geological similarities with other continental areas of South America, Africa, India, Australia and New Zeland.

It is a craton constituted by crystalline rocks with an age ranging from 2.5 bilions to 500 Ma of years surmounted by sedimentary and volcanic rocks (fig. 4.1.1.1). Over the western margin of the craton develops layer of metamorphic rocks with an age of 500 Ma, the Ross Orogen.

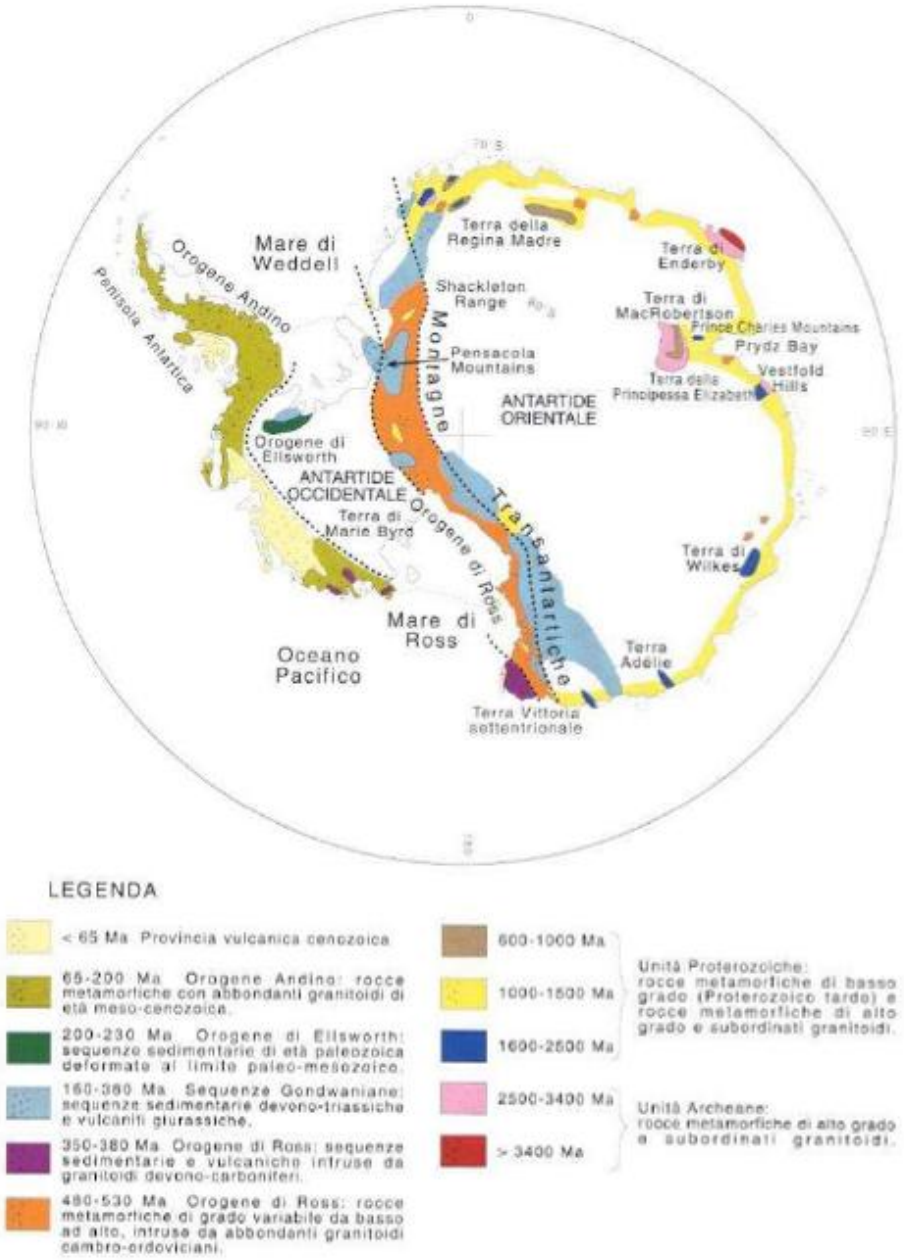

Fig. 4.1.1.1 - Antarctic gelogical pattern (Baroni, 2001)

Western Antarctica is the product of the micro-continents aggregation ad it is made of younger rocks deformed, metamorphosed and intruded by plutons.

Using a geographical and temporal criteria it is possible define two different orogenic levels. The first is the Ellsworth/Weddel Orogen with a Paleozoic-Mesozoic origin (230-180 Ma) and the Mesozoic-Cenozoic (< 100 Ma) Andean Orogen. Summarizing from East to West we recognize the old and stable zone of the eastern Antarctic craton, three metamorphic

and magmatic bands with decreasing ages from the Transantarctic Mountains to the western coast and a Cenozoic volcanic domain covering the area from the Antarctic Peninsula to the Victoria Land (Baroni, 2001).

4.2 Victoria Land

4.2.1 Geological setting

The northern Victoria Land is the pacific termination of the Ross Orogen and it is constituted by three different "Terranes": Wilson Terrane, Bowers Terrane and Robertson Bay Terrane. The terranes are separated by two big faults with a NW-SE direction, the Lanterman Fault (LF) and the Leap Year Fault (LYF) (Carmignani *et al.*, 1989).

In the northern Victoria Land the principal fault system is NW-SE oriented and generated sectors more easily erodible in which resettle the glaciers flow. The terranes emplacement derives from the lower Paleozoic Ross orogeny when new crust material was added to the East Antarctic Craton with a transpressive event. The Wilson Terrane is the most internal tectonic unit and it is characterized by the presence of Cambrian-Ordovician batholiths that intrude in Proterozoic and Cambrian metamorphic rocks. This event generated the Granite Harbour Intrusive Complex that includes granites, granodiorites, gneiss and ortogneiss(Isaac *et al.*, 1995). The presence of the granodiorites is characteristics of the Wilson Terrane and derived from the SW subduction of the Pacific Plate under the craton. (Kleinschmidt and Tessensohn, 1987; Carmignani *et al.*,1989). The Bowers Terrane (Cambrian-Ordovician) is made by volcanic and sedimentary rocks (Weaver *et al.*, 1984). The Robertson Bay Terrane is constituted by a complex and thick sequence of marine sediments from the continental shelfs called Robertson Bay Group (Cambrian-lower Ordovician). The three terranes are intruded by Devonia-Carbonifer granodiorites of the Admiraly Intrusives (Vetter and Tessensohn, 1987). The Wilson and Bower terranes were uplifted and subsequently strongly eroded with the envelop of an horizontal erosional surfacer on a regional scale (Pagliuca, 2001). The erosional suface exposed along the Transantarctic Mountains separates the crystalline basement from wo

sub-horizontal formations , the Beacon Supergroup (sedimentary) and the Ferrar Group (magmatic) (Pagliuca, 2001). The first formation is made of sedimentary levels with a continental origin and the second one is a tholeitic Jurassic succession of dolerites and basalts(Elliot and Fleming, 2004). These two groups don't outcrop in the Robertson Bay Terrane and the Ferrar Group finds expression along the Transantarctic Mountains and derives from the extensional tectonic that originated the Gondwana subdivision (ca. 180 Ma) (Fleming *et al.*, 1997), della, the formation of the western Antarctic Rift and the opening of the Ross Sea.

The most recent geological activity of the Victoria Land is related to the Cenozoic volcanism . The products of this activity are known as McMurdo volcanic group (MMVG) with a maximum age of 38-28 Ma(Armienti *et al.,* 1990, Tonarini *et al*., 1997, Rocchi *et al*.,2002). Some central volcanoes as Mount Erebus and Mount Melbourn are still in activity today.

The Cenozoic magmatism is related to the rift system of the western Antarctica and is testified by the presences of dikes and volcanoes.

The Cenozoic magmatism has two different compositional trends, the first one is characterized by alkaline transitional basalts that generated riolitic and trachytic rocks, the second one is made by alkaline basalts with a lower foid apport and erupted as pumice phonolitic at the Mount Overlor, the Mount Rittmann and on the Coulman Island or found as syenitic clasts over the Daniell Peninsula (Armienti and Baroni, 1999).

The good correlation between the isotopic data of the igneous rocks of this zone and the Erebus (Kyle, 1990), area suggest the western margin of the Ross Sea rift was interessed by uniform magmatic processes. The oldest dated rocks of the area constrained between the Priestley and Tucker glaciers have an age of 14-15 Ma and are located on the Malta and Deception plateau. This volcanic deposits are lacking of a visible volcanic structure.

A relevant igneous activity is testified by some present volcanoes, for instance the Hawkes Heights on the Coulmann Island (7,3-7,6 Ma) and Mount Overlord (7,5 Ma)with several small volcanic centers over the Malta Plateau.

The Pleiadi and the Berlin Dome are holocenic volcanoes and Mount Melbourn and Mount Rittmann are active at the present day (Armienti e Baroni, 1999).

4.2.2 Glacial evolution

The Victoria land is divided by the Terra Nova Bay in two main regions with different glacial dynamics: the southern Victoria Land and the northern Victoria Land.

The southern Victoria Land, is characterized by ice streams and outlet glaciers that cross the Transtantarctic Mountains and drain the EAIS. The Reeves and Priestley glaciers drain local mountain ice and interior East Antarctic ice from near Talos Dome. The two glaciers flow into the Nansen Ice Sheet, which floats on the western sector of the Terra Nova Bay finding the connection with the Northern Foothills, Vegetation Island, and Inexpressible Island. On the South the EAIS is drained from the Dome C and from the divide inland of Talos Dome by the huge David Glacier that terminates in the huge floating Drygalski Ice Tongue, (Orombelli *et al.*, 1990).

The northern Victoria Land presents a different setting. It is characterized by a dendritic valley networks without a direct relation to the EAIS and it is fed by ice fields and local névés. The Campbell Glacier is fed by several basins of the Southern Cross Mountains and Deep Freeze Range on the Transantarctic Mountains and terminates as the floating Campbell Glacier Tongue (Orombelli, 1989). More in detail the valley networks present natural basin features that had a fluvial origin. (Baroni *et al*., 2005)

In a climate system completely different from the present one the fluvial erosion enhanced the denudation of the area (55 Ma). A shifting from an erosional fluvial system to the temperate glacial erosion modeling occurred in several antarctic regions at the Eocene-Oligocene limit (Strand *et al.*, 2003; Sugden and Denton, 2004). The relict fluvial system was subsequently occupied by wetbased glaciers (Orombelli *et al.*, 1990; Baroni *et al.*, 2005).

An alpine topography was modeled by the glaciers erosive capability while local glaciation occured under temperate conditions and a subsequent overriding of the EAIS characterized the first phases of the glacial history in the southern Victoria Land (Sugden *et al.*, 1999; Sugden and Denton, 2004).

Hyperarid polar climate established at 13.6 Ma in southern Victoria Land while temperate glacial conditions ended at ca 8.2-7.5 Ma in northern Victoria Land (Armienti and Baroni, 1999). Since this period cold polar condition prevailed all over the Victoria Land and the preserved alpine topography was the consequence of an insignificant erosional capability (Baroni *et al.*,2005). From the Pliocene, phases of contraction and expansion of ice masses have alternated over time.

The last phase of evident expansion occurred in correspondence with the Marine oxygen Isotope Stage 2 (MIS2) ca. 20 ka BP and it is known as Last Glacial Maximum (LGM). During this phase the glaciers were thicker in the coastal areas where a series of piedmont glaciers filled the Terra Nova Bay (Orombelli *et al.,* 1990) Late glacial fluctuations are documented by lateral moraines locally preserved along Reeves, Priestley, Boomerang and Campbell glaciers. The deglaciation process interested the interval time between the end of the LGM and ca 8-7 ka when sea and land conditions were similar to the present day.. Geomorphological evidences and radiocarbon ages outline this upper limit of the deglaciation (Orombelli, 1991; Baroni and Hall, 2004).

From a geomorphological point of view the study areas are characterized by a series of main morphologies that are nunataks emerging from the ice sheet, coastal piedmonts, valleys molded by the outlet glaciers, residual tabular reliefs (mesas) and the relict alpine morphology (Orombelli *et al.*, 1990)

The Ricker Hills and the Trio Nunataks are example of the few scattered nunataks emerging from the EAIS in the area.

The coastal areas are characterized by the presence of rounded mountains (ca. 1000 m a.s.l.); examples are the Northern Foothills, Inexpressible Island, and Tarn Flat. Inexpressible Island and the Northern Foothills

present alpine cirques in the steep inland slopes and deep theater-shaped depressions cut partly below sea level in their eastern flanks. The meeting with the undulating piedmont generate a morphologic variation from steep trough walls to the piedmont surfaces

The glacial valleys developed in internal areas and are occupied by the Campbell, Priestley, and Reeves Glaciers and ranging from the sea level to the highest elevations (>3000 m), they comprise an articulated, complex drainage system, with main and tributary valleys.

The area between Priestley and Campbell glaciers is characterized by mesas relict landforms rising up to 300 m along internal margin of the Transantarctic Mountains. Glacial erosion has shaped the margins and thin ice caps cover the summits. The last stream over the mesa edges and feed cirques or tributary glaciers which drain into the main outlets.

The peaks of the Deep Freeze Range and of the Prince Albert Mountains present a relict alpine morphology. This topography developed on the valley sides and in sectors between the valleys; the alpine glaciers drain into the major outlet glaciers. They are mostly ice covered and, in the ice free areas, display sharp ridges and serrated spires.

The alpine morphology has continuity from the mesa edges to the present day tributary and outlet glaciers and it is filled with glacial ice except that in ice free areas beside Reeves and Priestley glaciers that are strongly affected by katabatic winds.

On the highest summit and on the walls of Priestley, Campbell and Reeves glaciers trimlines are well preserved. On many ridges and rock spurs it is possible to detect a double position of the trimlines. Differently from the lower one, the upper one shows a high degree of irregularity. These trimlines are superimposed on the alpine and outlet- topography and define a possible expansion of the northern Victoria Land ice cover since the erosion of the alpine topography. The entity of this expansion was lower in the upper part of the outlet glaciers and in the mountain accumulation area but was stronger along the lower reaches of the outlet glaciers. This remarkable thickening in these areas suggest an extensive grounding in the Ross Sea (Orombelli *et al.*, 1990). The inland erosion

processes of the outlet glaciers isolated and preserved parts of the original topography that are the coastal piedmont areas and the summit in the internal sectors.

The investigated area has been almost entirely shaped by glaciers that left morphologic and stratigraphic evidences of several glacial phases. In this context several glacial drift can be recognized.

The Youger Drift (Denton *et al.*, 1975) or Terra Nova Drift (Orombelli *et al.*, 1990) mantles the eastern flanks of the Northern Foothills and is commonly attributed to Late Pleistocene. It can be described as a discontinuous matrix-supported diamicton consisting of a scattering of clasts and erratic boulders directly resting on the bedrock. The Terra Nova Drift can be found in the lower part of the ice free areas in an elevation range from the coast to the interior mountain. The clast lithology includes different rocks as gneiss, micaschist, granite, amphibolite, basalt, diorite and olivine-basalt from erratics of the Mc-Murdo Volcanics. Radiocarbon dates from reworked marine fauna (shells in marine sediments and penguin remains) provide an age for this drift of 25-7 ka(Orombelli *et al.*, 1990; Baroni and Orombelli, 1991, 1994; Baroni and Hall, 2004).

Terra Nova Drift is only moderately weathered, with the erratic displaying little weathering apart from those close to the present coast.

Constructional morphologies are generally scarce. The most important exception is an end moraine at Black Ridge. This moraine is several hundreds of meters long and can be interpreted as a lateral moraine abandoned at the confluence of Corner Glacier with Priestley Glacier

At elevations above the upper limit of Terra Nova Drift different glacial drifts were identified (Baroni and Orombelli,1989; Orombelli *et al.*, 1990) .

The Terra Nova Drift II (Baroni and Orombelli, 1989) is located at intermediate altitude (up to 600 m asl at Mt Abbott, 520 m asl at Mt Browning, and 700 m asl at Mt. Keinath) and can be described as a discontinuous sheet of strongly weathered glacial sediments. The last are composed of a massive, matrix-supported diamict with a sandy-silty matrix. Clasts, from pebbles to boulders are subangular to subrounded and are composed of granitic and metamorphic rocks. At higher elevation are

located scattered isolated erratic boulders, strongly oxidized and affected by deep cavernous weathering. This deposit was called by Baroni and Orombelli (1989) Terra Nova Drift III and can be found at altitude around 700-800 m a.s.l. on the northern slope of Mount Abbott, at 720 m asl on the Mount Browning, and at an altitude of 850 m asl along the southern slope of Mount Keinath.

In 1990 Orombelli *et al.* banded together the Terra Nova Drift II and III in a single deposit called Older Drift. Different concentrations of erratic boulders at different altitude, an increasing of the weathering characteristics and a changes in the clast lithology suggest that the Older Drift could have been deposited by different glaciations (Baroni and Orombelli, 1989).The Older Drift buried a paleosol that can be referred to a pre-Pleistocene age.

Progressing to higher elevation but below the highest erosional trimline, in the coastal ice-free areas no glacial sediments or erratics can be found, The mountain tops of the coastal mountains (Mt. Keinath ,1090 m; Mt. Abbott 1022 m: Mt. Gerlache (980 m) and Mt. Crummer ,895 m) are rounded and preserved. The morphology of these coastal reliefs can be the consequence of a series of older glaciations which covered almost the entire coastal area.

The Holocene fluctuations of the glaciers are testified by moraines located close to the terminal margins of the outlet glaciers, the ice shelves and the local glaciers (Baroni and Orombelli, 1989; Chinn, 1991). Holocene moraines suggest small variations in the ice thickness for the outlet glaciers. Examples of Holocene moraines can be detected on the right side of the Reeves Glacier near Tarn Flat, on the left side of Priestley Glacier, near Black Ridge at theconfluence with Corner Glacier, at Vegetation Island, on both sides of Boomerang Glacierand in several places along the right side of Campbell Glacier.

5 -Results

5.1 Alps

The location of the sampled moraines in the Ortles Cevedale Group and Adamello Presanella Massif is depicted in fig. 5.1.1. The cosmogenic ages of 29 new alpine samples are listed in lables (see tabb. 5.1.1.1, 5.1.2.5, 5.1.2.10, 5.1.2.14, 5.1.2.15 for details).

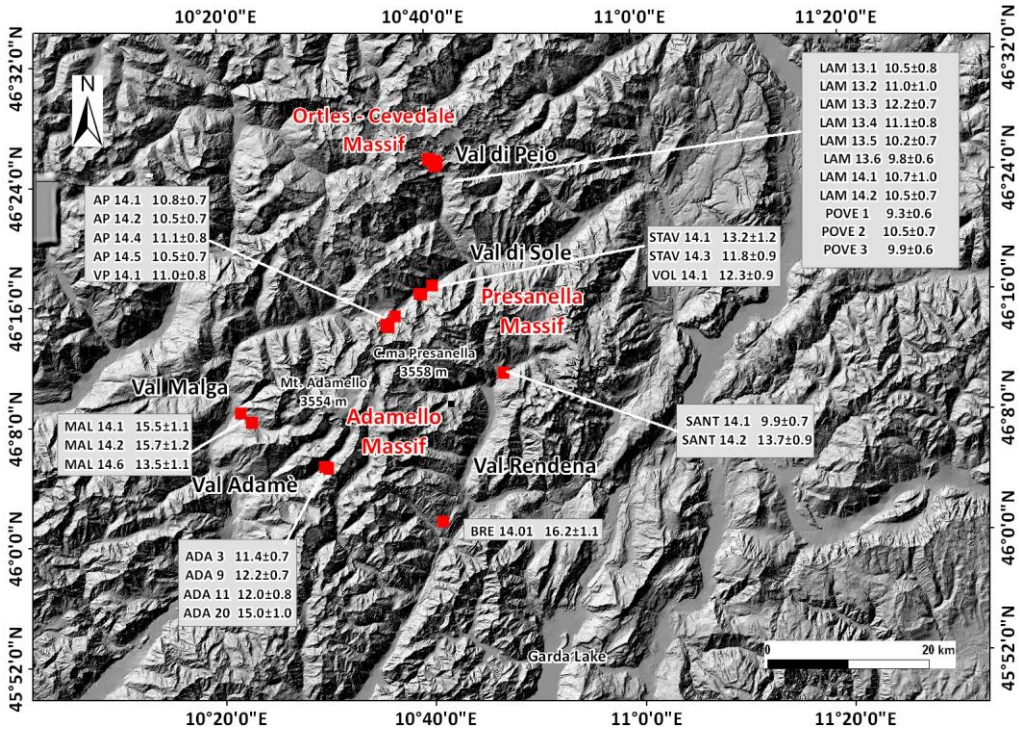

Fig. 5.1.1 – Location map of the dated moraines and Exposure Ages obtained.

5.1.1 Ortles-Cevedale Massif

Alta Val di Peio (Upper Peio Valley)

Geomorphological evidences, altogether with new geochronological data, brought to the reconstruction of the glacial history of La Mare and Careser Glaciers at the end of the Pleistocene. During this period two clear phases are identified, when La Mare and Careser glaciers occupied the most part of upper Peio Valley. Reconstructed glaciers were typical valley glaciers with compound catchment basins and well defined tongues, that reached the Pozza di Venezia area extending below the maximum Holocene limit reached during the Little Ice Age (LIA) as constrained by Carturan *et al.,* (2014). Sampled moraines are characterized by a sharp and well preserved ridge (figg. 5.1.1.1, 5.1.1.2). These moraines show evidences of deeper weathering of erratic boulders, thicker soils, and wider vegetation cover respect to the LIA moraines (GNGFG, 1986; Carturan *et al.*, 2014).

Fig. 5.1.1.1 - Sampled moraine (MLm2) in La Mare Valley (see fig. 5.1.1.3 for location)

Fig. 5.1.1.2 - Sample Lam 14_1 (see fig. 5.1.1.3 for location)

Sample ID	Quartz dissolved (g)	^{10}Be concentration	Exposure Age (Yr)	Internal uncertainty(yr) Lal(1991)/Stone(2000)	External uncertainty(yr) Lal(1991)/Stone(2000)
LAM 13.1	19.665	260200±16300	10510	670	840
LAM 13.2	19.124	274400±21700	11020	880	1030
LAM 13.3	19.358	307200±10650	12190	430	730
LAM 13.4	20.498	282200±13650	11080	540	760
LAM 13.5	20.474	258500±12700	10230	510	710
LAM 13.6	19.560	244000±10200	9760	410	630
LAM 14.1	10.677	262600±21300	10680	880	1010
LAM 14.2	17.888	254600±13100	10450	550	740
POVE 1	22.141	206900±9850	9290	450	630
POVE 2	23.295	235500±9800	10550	450	680
POVE 3	21.378	197700±8700	9940	440	650

Table 5.1.1.1 - Data and relative exposure ages of processed samples.
Reported external errors (1σ) consider internal uncertainties related to AMS measurement processing, together with the variability of the considered production rate scaling schemes.

Eleven new ^{10}Be exposure ages (tab. 5.1.1.1) were obtained from erratic boulders located on top of moraine ridges at the external limit reached during each recognized phase. The new surface exposure ages ranges from 9.2 to 12.2 ka and they allow us to chronologically constrain the identified glacial phases.

La Mare Glacier descended below Ponte di Pietra (toward Malga Mare; fig. 5.1.1.3) reaching this position before 12.2±0.7 ka (LAM 13.3 sampled on

moraine MLm1). Later on the glacier re-advanced between 11.1±0.8 ka (LAM 13.4) and 9.8±0.6 ka (LAM 13.6), this glacier position is testified by the moraine MLm4 .

On the other hand the ages obtained on moraines MC1 and MC2, related to the Careser Glacier, allow us to constrain the identified position between 10.5±0.7 ka and 9.3±0.6 ka (POVE1, POVE2). This phase can be related to the innermost reconstructed position of La Mare Glacier as reported in fig. 3.3.1.4. Furthermore in La Mare Valley the right lateral moraine MLm3, located between MLm1 and MLm4, provided ages of 10.5±0.7 ka and 11.0± 1.0 ka. These ages find a good correlation with samples LAM 14.1 (10.7±1.0 ka) and LAM 14.2 (10.5±0.7 ka), located on top of the moraine MLm2, and further enforce the considered time interval. This can support the hypothesis that La Mare Glacier was proximal to this position until at least 11.0±1.0 ka and re-used the same left lateral moraine (MLm2). The topography of the valley and the consequent main ice flow direction may have concurred in generating this asymmetry. However the dates obtained on moraines MLm2 and MLm3 are here treated as minimum ages for this phase. In fact geomorphological evidences provide to consider the latter older than the phase identified by the moraine MLm4.

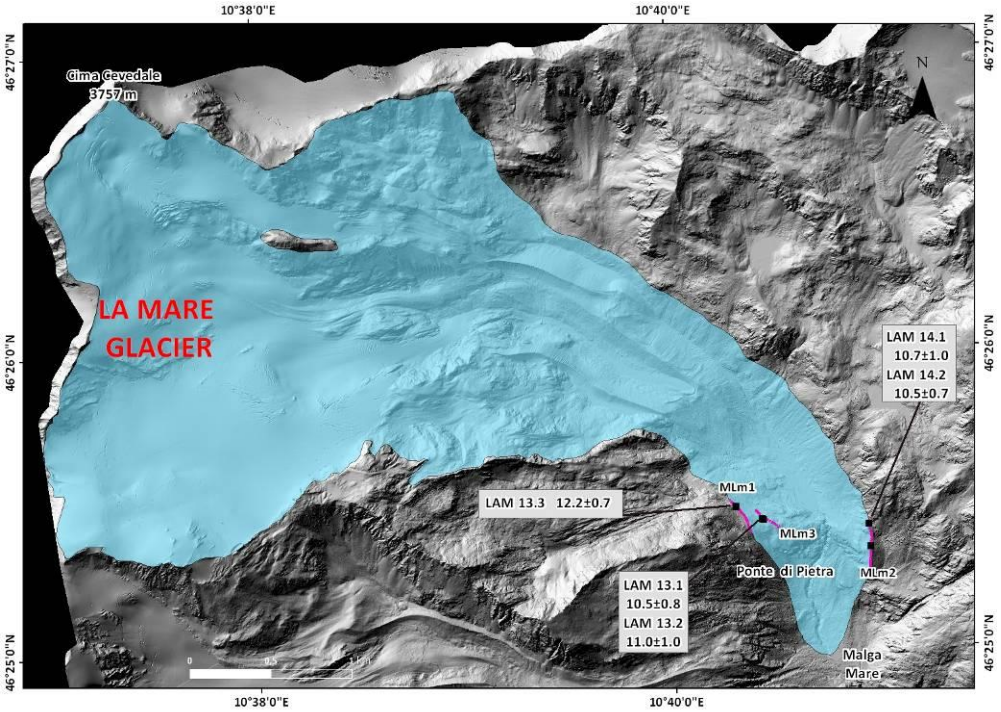

Fig. 5.1.1.3 – La Mare Glacier Ponte di Pietra I and ^{10}Be ages (ka) location. Purple lines represent the dated moraines.

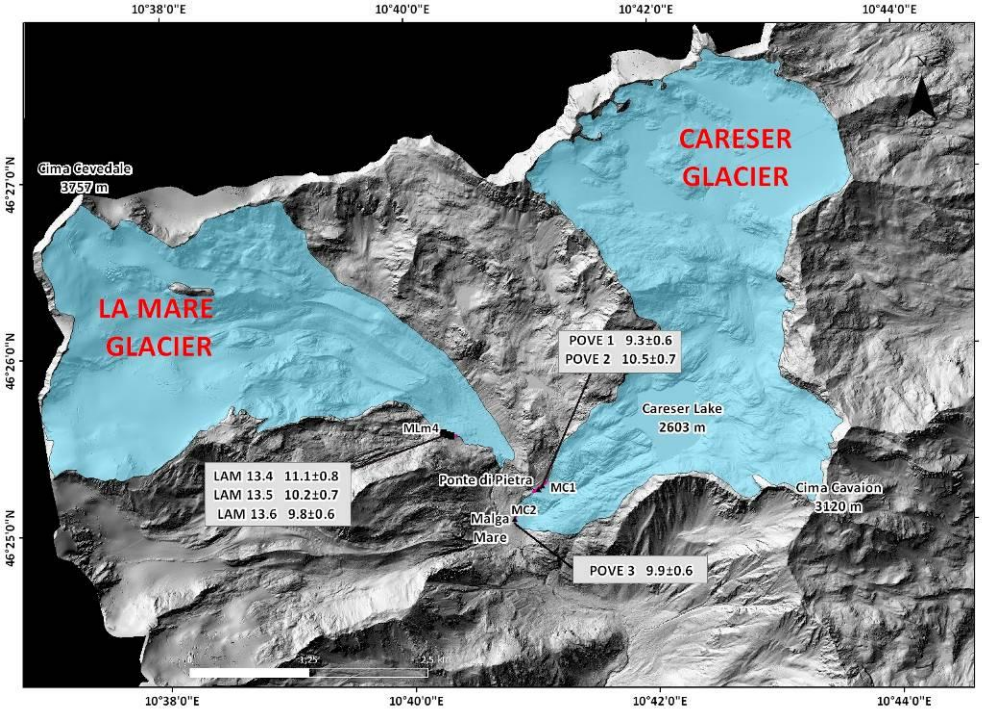

Fig. 5.1.1.4 – La Mare and Careser glaciers Ponte di Pietra II phase and ^{10}Be ages (ka) location. Purple lines represent the dated moraines.

Morphometric parameters (tab. 5.1.1.2, 5.1.1.3) of reconstructed phases lead to the estimation of areal and volume variations as well as Equilibrium Line Altitude (ELA) variations for comparison with data of the Little Ice Age maximum expansion and with present day minimal extension (Carturan *et al.,* 2013a, 2014; Salvatore *et al.,* 2015).

Glacial phase	Area (km²)		Volume variations (km³)		Minimum elevation (m a.s.l.)		Maximum length (km)	
	La Mare	Careser	La Mare	Careser	La Mare	Careser	La Mare	Careser
Ponte di Pietra I	9.1	-	0.42	-	1998	-	5.7	-
Ponte di Pietra II	8.4	10.3	0.27	0.57	2200	1996	4.9	5.5
Little Ice Age	6.1	6.3	0.13	0.27	2286	2609	4.4	3.4
Present day(2006)*	3.9*	2.1*	-	-	2652*	2868*	2.8	1.8*
&(2012)'+	3.6+	1.6'	-	-	2670+	2865'	3.0+	-

Table 5.1.1.2 - Morphometric parameters. 'Carturan *et al.,* 2013a°; +Carturan *et al.,* 2014; *Salvatore *et al.,* 2015.

During the oldest reconstructed phase La Mare glacier reached a minimum elevation of 1998 m a.s.l. and occupied the valley for 9.1 km². Compared to the maximum LIA expansion (modified from Carturan *et al.,* 2014) and to present day (Salvatore *et al.,* 2015), La Mare glacier reduced its glaciated area by 3.0 km² and 5.2 km² respectively. In terms of percent the glacier reduced its extension of ca. 8% since Ponte di Pietra I to Ponte di Pietra II

phase whereas 67% of the original extent was preserved during the LIA. During the Ponte di Pietra II phase Careser Glacier (fig. 5.1.1.4)reached with its terminus Pozza di Venezia at 1996 m a.s.l., about 870 m below the minimum elevation recorded in 2012. Since this phase until today(2012), the glacier reduced its extent from 10.3 km^2 to 1.6 km^2 (Carturan *et al.*, 2013a).

Considering an AAR of 0.67±0.005 (fig. 5.1.1.5), La Mare Glacier recorded an ELA of 2823 m a.s.l. (+9 -10) related to the Ponte di Pietra I phase. During the Ponte di Pietra II phase the ELA calculated for La Mare and Careser Glaciers reached elevations of 2912 m a.s.l. (+8,-7) and 2849 m a.s.l. (+4,-5), respectively. (tab.5.1.1.3).

Glacial phase	ELA (m a.s.l.) & ELA error (m)		Δ ELA LIA (m)	
	La Mare	Careser	La Mare	Careser
Ponte di Pietra I	2823 (+9,-10)	-	-228	-
Ponte di Pietra II	2912 (+8,-7)	2849 (+4,-5)	-139	-176
Little Ice Age	3051 (+7,-6)	3025 (+2,-1)	-	-

Table 5.1.1.3 - Equilibrium Line Altitude of reconstructed glacial phases and ELA variation compared to Little Ice Age maximum position.

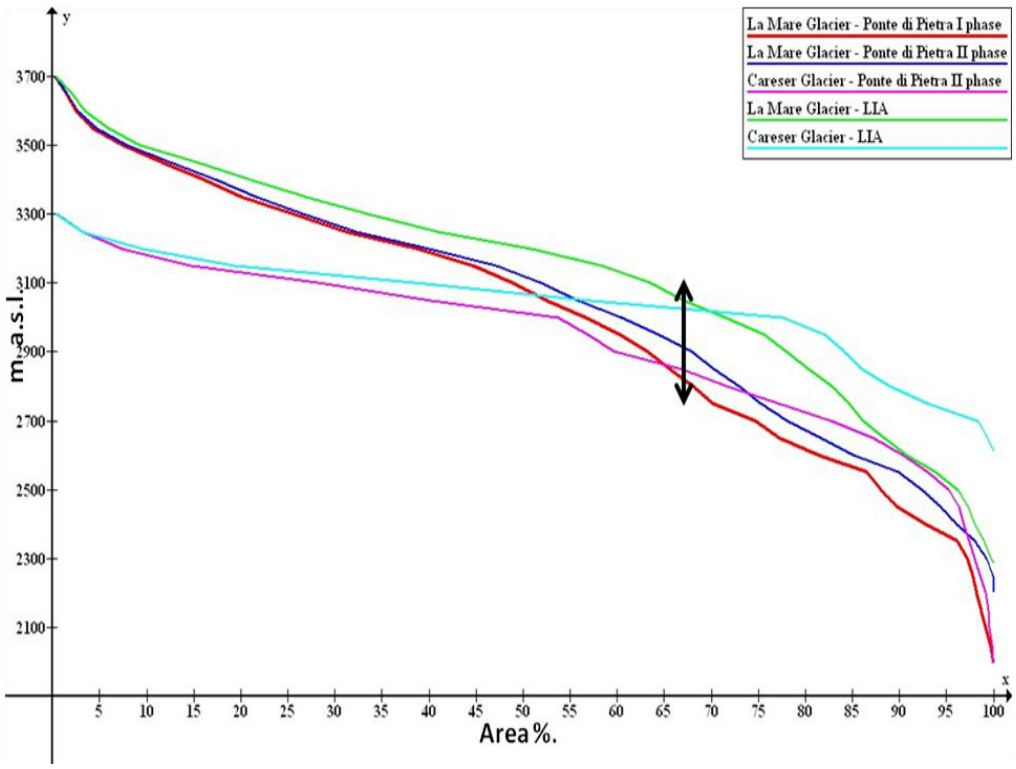

Fig. 5.1.1.5 – Hypsographic curve of La Mare and Careser glaciers reconstructed phases. The black arrow point out the Equilibrium Line Altitude position adopting an Accumulation Area Ratio (AAR) for valley glaciers of 0.67±0.005.

5.1.2 Adamello – Presanella Massif

In the Adamello-Presanella Massif, for obtaining a good distribution of the samples, six of the radial valleys departing from the summit of the mountain group were sampled. Samples were collected in Val Presena and Val Stavel (Upper Val di Sole), Val Rendena ,Val Breguzzo, Val Adamè and Val Malga see table for details and figure 2.3.3.2 for location.
In these selected sites we reconstructed the shape and timing of different glacier re-advances, related to climate deterioration events occurred at the end of the Pleistocene.

Val di Sole (Upper Sole Valley)
Val Presena and Val Stavel develop in the northernmost sector of the massif, both flowing from S to N in the upper Val di Sole where they join. To better understand the glacial evolution of this area of the mountain group, we studied the glacial evolution of the Val di Sole also focusing on some lateral valleys such as the Val Ricolonda, Val Palù and Val Barco. (fig. 5.1.2.5).

We reconstructed the extension of four different glacial phases in this area and new ^{10}Be ages, from erratic boulders located on top of moraine ridges allow us to chronologically constrain three of them for the main valley (tab. 5.1.2.5).
The phase I (Vermiglio phase, fig. 5.1.2.1) is the most extended among the reconstructed phases in the upper Val di Sole. Several valley and mountain glaciers covered a total area of ca. 50 km^2 while the volume exceeded ca. 5 km^3. Apart the Val di Sole Glacier (a compound basins valley glacier) three of the reconstructed glaciers can be classified as valley glaciers (Val Ricolonda, Val Palù, and Val di Barco W) and two as mountain glaciers (Val di Barco E and Rocca Marcia Glacier). Glacier extensions ranged from 40 km^2 for compound basins valley glacier (Val di Sole) to 0.6 km^2 for the smaller mountain glacier (Val di Barco E).
The glacier hosted in the Val di Sole was the widest with an extension of ca 80% of the total glaciated surface and a volume exceeding ca.4.4 km^3. Its front reached a minimum elevation of 1110 m a.s.l. Lateral and frontal

positions of the main Val di Sole Glacier are not supported by well shaped moraines but were reconstructed following the valley profile, the outcrop of glacial deposits and the size of the relative catchment basin.

Absolute ELA values for this phase ranged from ca 1860 (+4/-5) m for the Val di Barco W Glacier to the 2250 (+4/-3) m a.s.l. for the Rocca Marcia Glacier. The main Val di Sole Glacier has an ELA of 2205 (+17/-18) m a.s.l. (fig. 5.1.2.6). Morhometric parameters of all the reconstructed glaciers are listed in table 3.3.2.1.

Glacier	Original glacier	Glacier type	Min. altitude (m a.s.l.)	Max altitude (m a.s.l.)	Mean altitude (m a.s.l.)	Area (km^2)	Δ Volume (km^3)	ELA (m a.s.l.)
Sole	Val di Sole	Valley	1140	3550	2345	39.8	4.38	2205
Ricolonda	Val Ricolonda	Valley	1413	2885	2149	2.2	0.15	2120
Barco E	Barco E	Mnt	1823	2441	2132	0.6	0.02	2070
Palù	Palu	Valley	1587	2981	2284	2.2	0.15	1930
Rocca Marcia	Rocca Marcia	Mnt	1799	2646	2223	1.6	0.08	2250
Barco W	Val di Barco W	Valley	1170	2849	2010	2.9	0.17	1860

Table 5.1.2.1 - Morphometric parameters Vermiglio Phase.Mnt; mountain glacier.

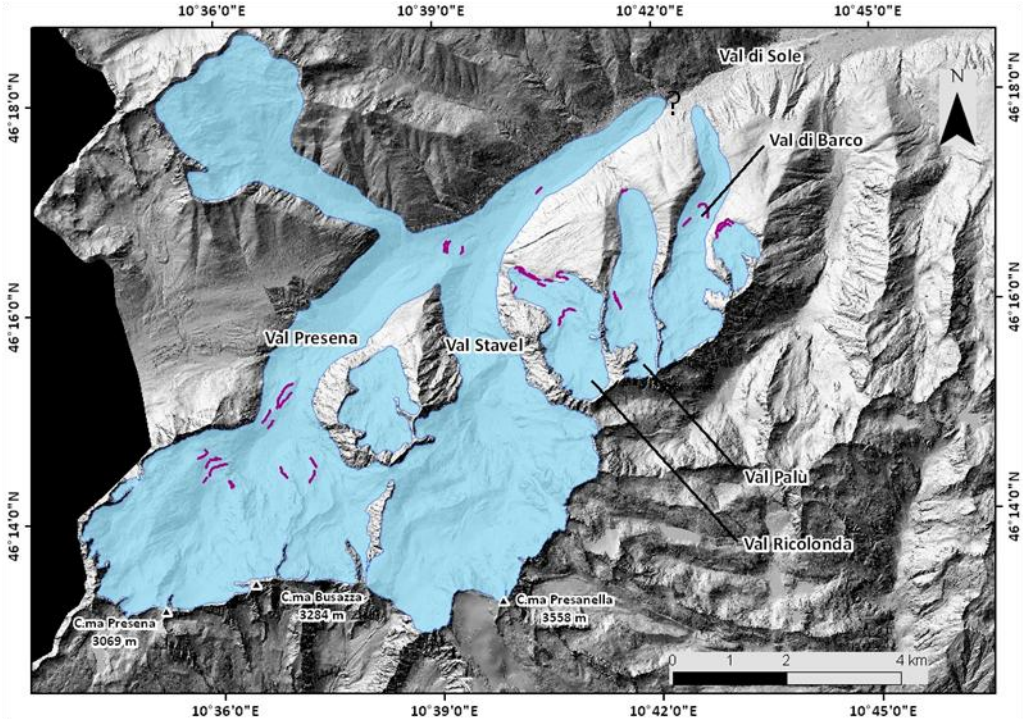

Fig. 5.1.2.1 - Vermilio phase extension. Purple lines represent the moraines.

The second phase (Volpaia phase, fig. 5.1.2.2) testified a reduction of ca. 16% (7.2 km^2) of the glacial surface in the study area and a volume reduction of ca. 2.0 km^3. The four valley glaciers and three mountain

glaciers reconstructed for this phase occupied a total area of ca. 42 km^2. The main Val di Sole Glacier had a fragmentation in two different glaciers. The biggest one preserved the characteristics of a compound basins valley glacier and still descended in the main valley (Val di Sole); the second glacier occupied the upper portion of a left lateral valley, the Val Strino. Together the Val di Sole and Val Strino Glaciers, previously connected in the main Val di sole Glacier, recorded an areal reduction of ca. 4.7 km^2 and a volume contraction of ca. 1.7 km^3. Its terminus reached 1198 m testifying a rising of ca. 100 m of the minimum frontal elevation respect to the previous Vermiglio Phase.

Absolute ELA values for the Volpaia phase ranged from ca 2110 (±4) m for the Val Palù Glacier to the 2250 (±3) m a.s.l. for the Val Strino Glacier. The main Val di Sole Glacier had an ELA of 2285(±10) m, ca. 80 m higher than in the older Vermiglio phase. Morhometric parameters of all the reconstructed glaciers are listed in table 5.1.2.2.

For this phase we dated a sample of an erratic boulder located on a right lateral moraine (mVol1) in the Volpaia area. The exposure age of 12.3±0.9 ka represents a minimum limiting age for the Volpaia Phase.

Glacier	Original glacier	Glacier type	Min. altitude (m a.s.l.)	Max altitude (m a.s.l.)	Mean altitude (m a.s.l.)	Area (km^2)	Δ Volume (km^3)	ELA (m a.s.l.)
Ricolonda	Ricolonda	Valley	1698	2881	2290	1.6	0.10	2240
Barco E	Barco	Mnt	2087	2444	2265	0.2	0.004	2250
Palù	Palù	Valley	1596	2980	2288	1.6	0.07	2110
Rocca Marcia	Rocca Marcia	Mnt	1799	2645	2222	1.6	0.06	2240
Barco W	Barco	Valley	1690	2848	2269	2.0	0.09	2115
Strino	Sole	Mnt	1941	2902	2422	4.6	0.16	2550
Sole	Sole	Valley	1198	3550	2374	30.5	2.49	2285

Table 5.1.2.2 - Morphometric parameters Volpaia Phase. Mnt; mountain glacier

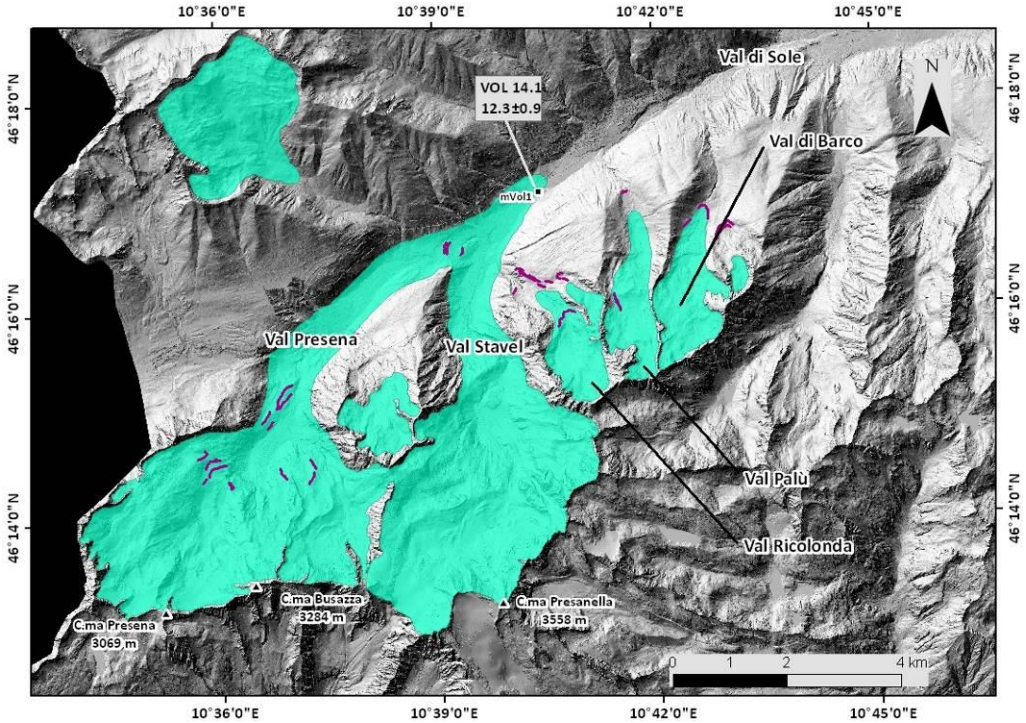

Fig. 5.1.2.2 - Volpaia phase extension and ^{10}Be exposure ages. Purple lines represent the moraines.

A third phase (Stavel phase, fig. 5.1.2.3, tab 5.1.2.3) was characterized by the presence of two valley glaciers and ten mountain glaciers. The areal extension was around 30 km^2, documenting a reduction of ca. 12 km^2 and 20 km^2 respect to the Volpaia and Vermiglio phases, respectively. As a consequence of the ice masses reduction, a fragmentation in different ice bodies was recorded. The Val Strino Glacier was divided in three small mountain glaciers (0.3-0.8 km^2) nestled in the higher portion of the valley. Rocca Marcia Glacier was fragmented in two mountain glaciers. The Val di Barco E glacier extinguished. The main Val di Sole glacier was split up in two valley glaciers hosted in Val Stavel and Val Presena. The Val Stavel Glacier was the wider glacier of this phase reaching an extension of ca. 12.9 km^2 , with a minimum and mean elevation of 1253 m and 2400 m, respectively. The Val Presena Glacier glaciated area was at about 11.9 km^2, with a mean altitude of ca. 2450 m and the front terminating at 1650 m. Adding the extensions of the these two glaciers that previously constituted the main Val di Sole Glacier we record a reduction of ca. 5.6 km^2 compared to the Volpaia phase.

ELA values ranging from 2350 (±1) m (Rocca Marcia E) to 2685 (±1) m (Strino NE) and the two principal valley glacier (Val Stavel and Val Presena glaciers) recorded an Equilibrium Line position around 2400 m , 200 m higher than the original glacier of the II phase (Volpaia Phase).

We dated two erratic boulders from two different left lateral moraines (mStav1 and mStav2) proximal to the glacier terminus area for the Stavel Glacier as well as two left lateral moraines (mPres3 and mPres4) for the Val Presena Glacier. The exposure ages constrain the Stavel phase prior to 13.2±1.2 ka (STAV14.1) and not later on 11±0.8 ka (VP14.1).

Glacier	Original glacier	Glacier type	Min. altitude (m a.s.l.)	Max altitude (m a.s.l.)	Mean altitude (m a.s.l.)	Area (km^2)	Δ Volume (km^3)	ELA (m a.s.l.)
Presena	Val di Sole	Valley	1650	3246	2448	11.9	0.71	2450
Ricolonda	Val Ricolonda	Mnt	2003	2886	2445	1.1	0.07	2375
Rocca Marcia W	Rocca Marcia	Mnt	2168	2647	2408	0.7	0.02	2405
Strino NE	Val di Sole	Mnt	2542	2898	2720	0.8	0.01	2685
Rocca Marcia E	Rocca Marcia	Mnt	2144	2587	2366	0.1	0.001	2350
Stavel	Val di Sole	Valley	1243	3550	2397	12.9	0.91	2400
Palù	Val Palu	Mnt	2097	2978	2538	0.9	0.02	2400
Barco W	Val di Barco	Mnt	2084	2848	2466	1.0	0.03	2415
Strino W	Val di Sole	Mnt	2383	2638	2511	0.3	0.004	2525
Strino NW	Val di Sole	Mnt	2393	2747	2570	0.4	0.005	2645

Table 5.1.2.3 - Morphometric parameters Stavel Phase. Mnt:mountain glacier.

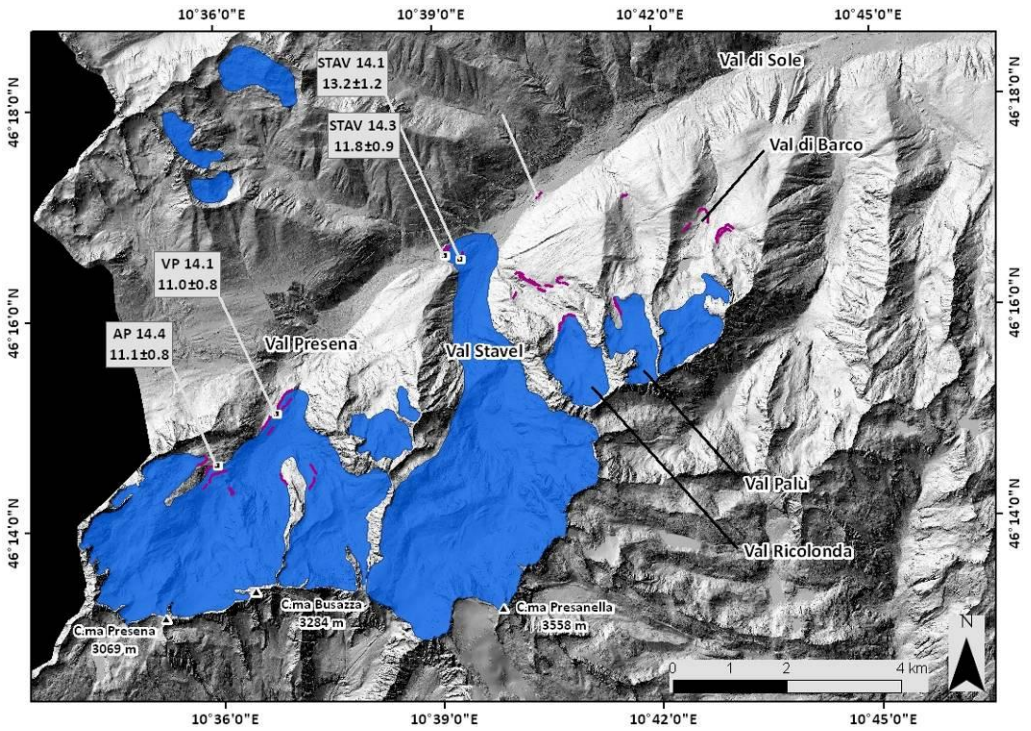

Fig 5.1.2.3 - Stavel phase extension and ^{10}Be exposure ages. Purple lines represent the moraines.

For the fourth recognized phase (Presena phase, fig. 5.1.2.4) we reconstructed the position and extension of three valley glaciers and four mountain glaciers.

These seven glaciers occupied a total area of ca. 24 km^2, about 6.5 km^2 less than during the Stavel phase. The comparison with the most vigorous and oldest reconstructed phase (Vermiglio phase) shows a reduction of the ice covered area of ca. 25.9 km^2, corresponding to ca. the 52.3% of the original extension. In terms of volume, glaciers of the Presena phase show a contraction about 0,65 km^3 and 4.3 km^3 towards the Stavel and Vermiglio phases, respectively. Any ice masses were preserved in Val Strino while the Val Presena valley glacier fragmented in two distinct ice bodies, the Val Presena W and Busazza glaciers. These two glaciers deriving from the Val Presena Glacier had an overall area of 8.6 km^2 , corresponding to the 72% of the original past glacier. Val Stavel Glacier was still most extended covering 10.6 km^2 with a minimum and mean elevation of 1800 m and 3550 m, respectively(tab. 5.1.2.4).

ELA values ranging from 2395 (+4/-3) m (Ricolonda) to 2615(±3) m (Presena W) and the biggest valley glacier (Stavel Glacier) recorded an Equilibrium Line position of ca. 2525 (+5/-3) m , 130 m higher during the Stavel phase.

^{10}Be exposure ages were obtained from a right lateral (mPres1) and a left lateral-frontal (MPres2) moraines of the Presena W Glacier. The minimum age of this moraines ranges from10.8±0.8 ka to 10.5±0.7 ka (tab. 5.1.2.5)

Glacier	Original glacier	Glacier type	Min. altitude (m a.s.l.)	Max altitude (m a.s.l.)	Mean altitude (m a.s.l.)	Area (km^2)	Δ Volume (km^3)	ELA (m a.s.l.)
Presena W	Sole	Valley	2050	3244	2647	5.7	0.38	2615
Ricolonda	Ricolonda	Mnt	2049	2873	2461	1.0	0.04	2395
Palù	Palù	Mnt	2134	2982	2558	0.7	0.01	2440
Rocca Marcia W	Rocca Marcia W	Mnt	2200	2643	2422	0.5	0.009	2440
Stavel	Sole	Valley	1800	3550	2675	10.6	0.57	2525
Busazza	Sole	Valley	1848	3272	2560	2.9	0.11	2470
Barco W	Barco	Mnt	2298	2848	2573	0.5	0.01	2490

Table 5.1.2.4 - Morphometric parameters Presena phase.Mtn: mountain glacier.

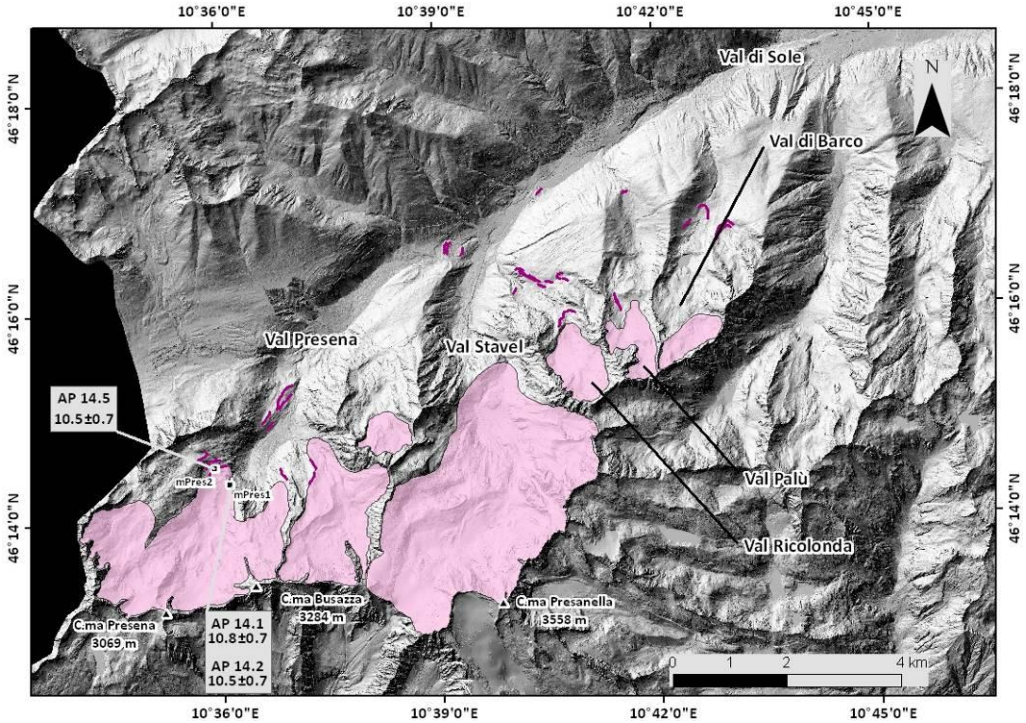

Fig. 5.1.2.4 - Presena phase extension and ^{10}Be exposure ages. Purple lines represent the moraines.

Sample ID	Quartz dissolved (g)	^{10}Be concentration (atoms/g qtz)	Exposure Age (Yr)	Internal uncertainty(yr) Lal(1991)/Stone(2000)	External uncertainty(yr) Lal(1991)/Stone(2000)
AP14.1	19.732	233600±10400	10760	480	710
AP14.2	14.830	224900±11600	10490	550	750
AP14.4	13.758	244400±12700	11150	590	790
AP14.5	17.036	222800±10600	10500	500	720
VP14.1	13.523	175000±10000	10950	630	820
VOL14.1	18.793	130000±7200	12290	680	900
STAV14.1	6.150	147300±11600	13160	1040	1220
STAV14.3	15.099	139900±7700	11850	660	870

Table 5.1.2.5 - ^{10}Be exposure ages in Val di Sole. Data and relative exposure ages of processed samples. Reported external errors (1σ) consider internal uncertainties related to AMS measurement processing, together with the variability of the considered production rate scaling schemes.

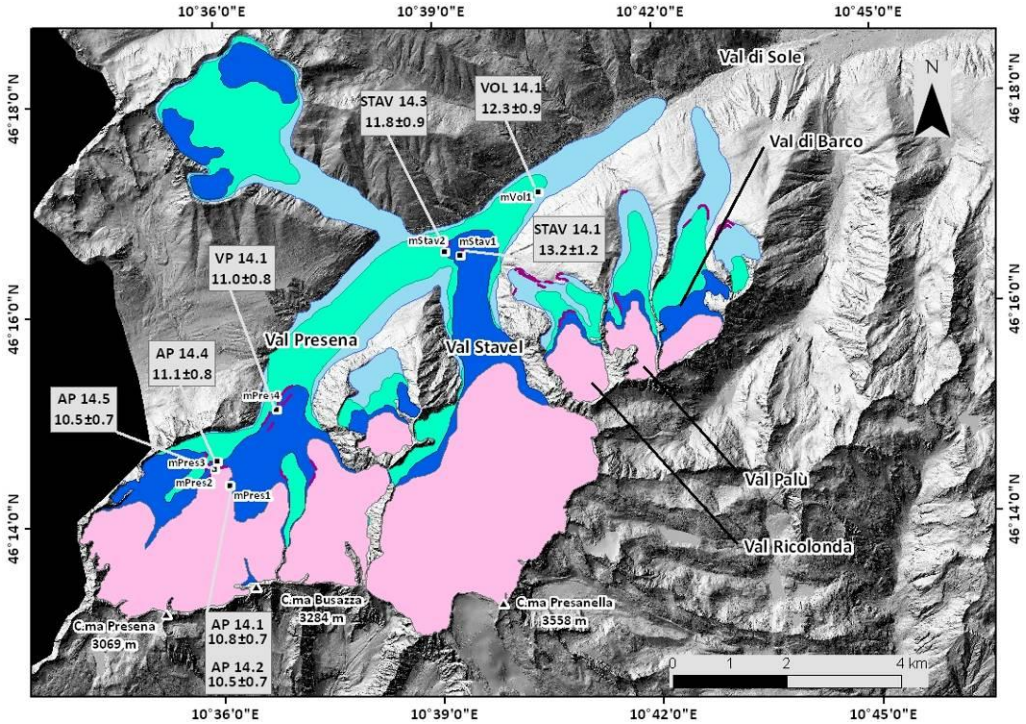

Fig. 5.1.2.5 - Reconstructed glacial phases comparison and exposure ages. Purple lines represent the moraines.

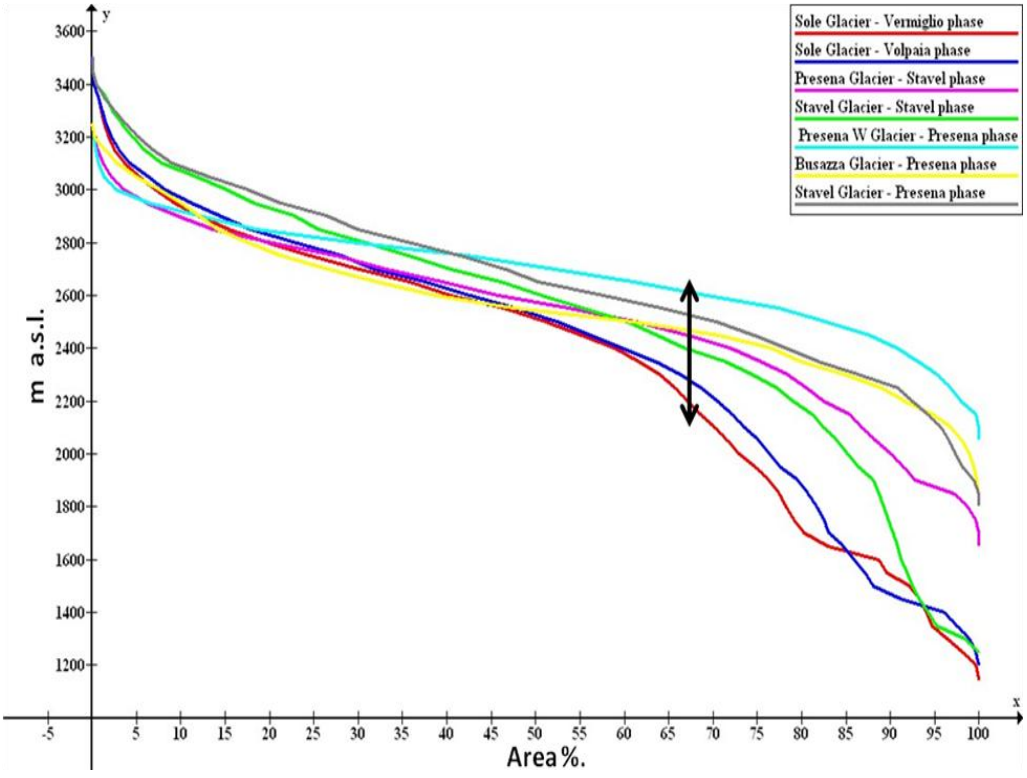

Fig. 5.1.2.6 - Hypsographic curve of the main Val di Sole glacier in the different reconstructed phases. The black arrow point out the Equilibrium Line Altitude position adopting an Accumulation Area Ratio (AAR) for valley glaciers of 0.67±0.005.

Val Malga (Malga Valley)

Moving to the western sector of the Adamello-Presanella, we reconstructed the glacial evolution of the Val Malga.

We recognized evidences of four different glacial phases, for which areal extension was reconstructed (fig. 5.1.2.11). Samples collected from erratic boulders located on top of moraines ridges, allow us to obtain ^{10}Be ages providing a chronological constrain for two of the recognized phases in the main valley (tab 5.1.2.10).

The first phase (Rino phase) reconstructed for the Val Malga shows is characterized by the presence of a single compound basins glacier that occupied the entire valley (fig 5.1.2.7).

The Rino phase was reconstructed on considering the position of well shaped lateral and frontal moraines and also following the valley profile, the presence of glacial deposits.

The Malga Glacier was characterized by a well defined tongue extended for about 5.5 km and two principal catchment basins that gave their provision from the Val Baitone and Val Miller. The glacier occupied the valley since a maximum elevation of ca. 3270 m until a minimum elevation of ca. 800 m and occupied an area of ca. 24.7 km^2 (tab. 5.1.2.6). The calculated ELA reached an elevation of 2375(±7) m (fig. 5.1.2.12).

Sample MAL14.6 taken from an erratic boulder located on a left lateral-frontal moraine (mMal2) at an altitude of 879 m constrains this phase prior to 13.5±1.1 ka.

Glacier	Original glacier	Glacier type	Min. altitude (m a.s.l.)	Max altitude (m a.s.l.)	Mean altitude (m a.s.l.)	Area (km^2)	Δ Volume (km^3)	ELA (m a.s.l.)
Malga	Malga	Valley	804	3272	2038	24.7	2.71	2375

Table 5.1.2.6 - Morphometric parameters Rino Phase.

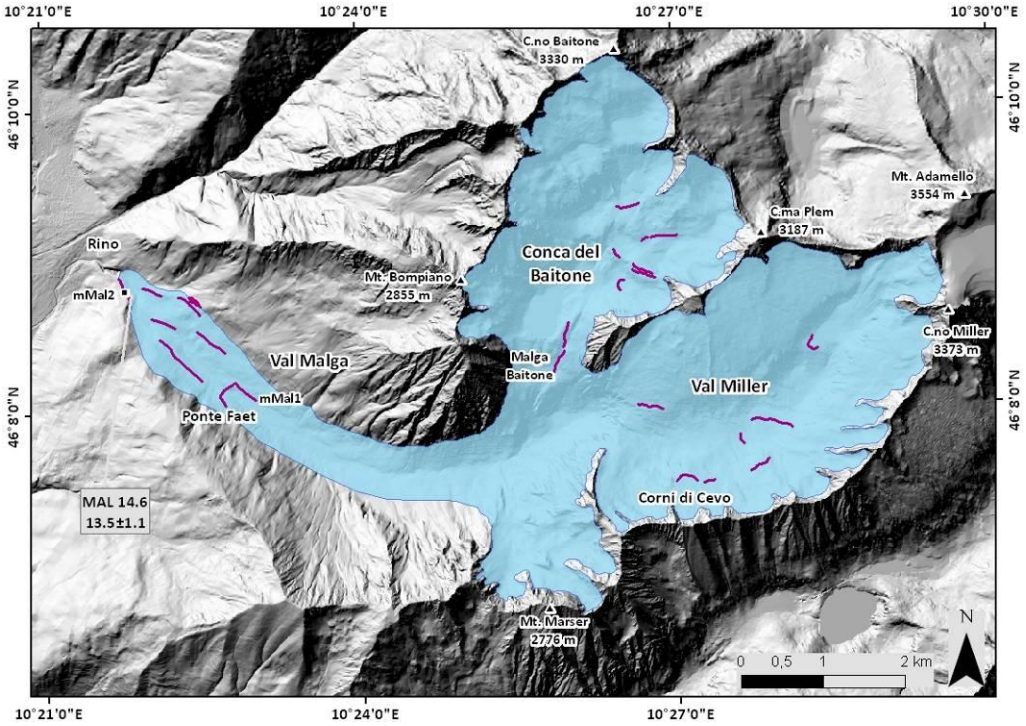

Fig. 5.1.2.7 - Rino phase extension and ^{10}Be exposure ages. Purple lines represent the moraines.

The second phase (Ponte Faet phase) was similar (tab. 5.1.2.7)to the previous Rino phase. The glaciated area was still constituted by a a single compound basins glacier that occupied the main valley (fig 5.1.2.8). The Malga Glacier had an extension of ca. 22.4 km^2 with a 2.3 km^2 reduction and a volume reduction of ca. 1.5 km^3 compared to the Rino phase. The mean altitude was of ca. 2190 m and the glacier had its terminus at an elevation of 1110 m, recording a rise of the glacier terminus of ca. 300 m. The ELA reached an elevation of 2380 (+3/-4) m.

The front of this phase is testified by the presence of a well defined moraine (mMal1), that was sampled and dated (tab. 5.1.2.10). Samples MAL14.1 and MAL14.2 provide ages of 15.5±1.1 ka and 15.7±1.2 ka, giving the minimum age for this phase.

Glacier	Original glacier	Glacier type	Min. altitude (m a.s.l.)	Max altitude (m a.s.l.)	Mean altitude (m a.s.l.)	Area (km^2)	Δ Volume (km^3)	ELA (m a.s.l.)
Malga	Malga	Valley	1109	3269	2189	22.4	1.24	2380

Table 5.1.2.7 - Morphometric parameters Ponte Faet Phase.

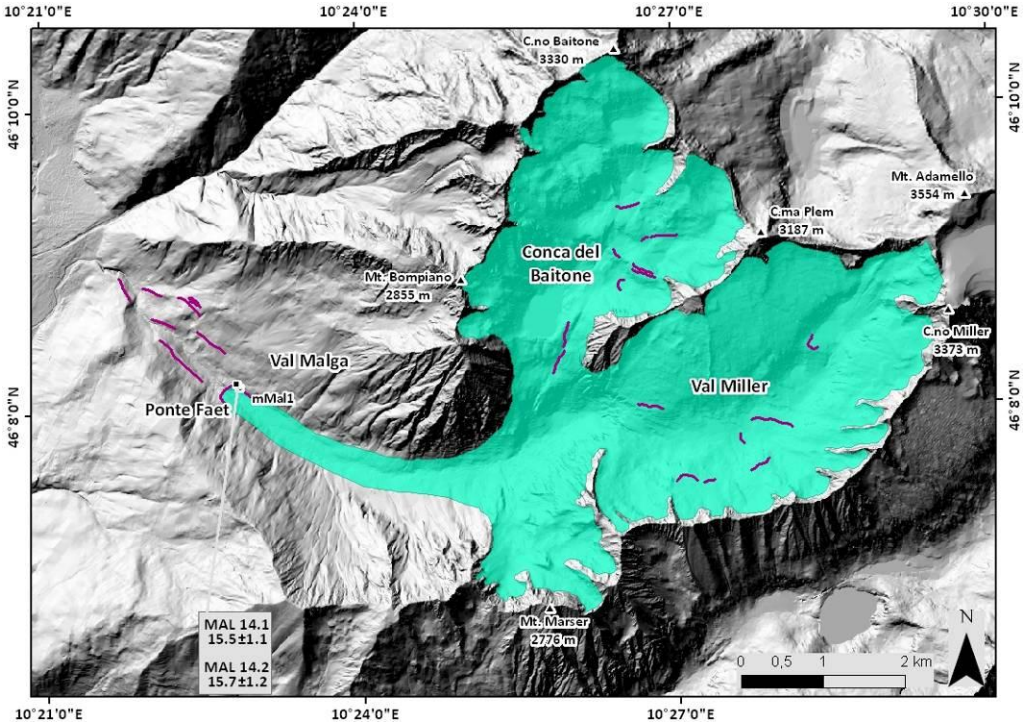

Fig. 5.1.2.8 - Ponte Faet phase extension and ^{10}Be exposure ages. Purple lines represent the moraines

The Malga Baitone phase is the third phase reconstructed (fig. 5.1.2.9) and shows the fragmentation of the main Malga Glacier in three different valley glaciers.

The Miller Glacier was the most extended during this phase covering 8.7 km^2 while the total glaciated area in the valley was about 17.3 km^2, the 30% less than the first and most extended reconstructed phase. The total volume was around 0.76 km^3, contracted by ca. the 50% compared to the Ponte Faet phase. Miller glacier reached the lowest altitude of 1800 m with its front and was characterized by a mean altitude of ca. 2515 m. The smallest Coppo Glacier was the one with the lesser mean altitude (ca. 2300 m) due to its extension constrained between 1970 m and 2650 m. The ELAs of the three glacier ranging from 2260 (+2/-3) m (Coppo) and 2590 (±3) m (Baitone S)(tab. 5.1.2.8).

Glacier	Original glacier	Glacier type	Min. altitude (m a.s.l.)	Max altitude (m a.s.l.)	Mean altitude (m a.s.l.)	Area (km^2)	Δ Volume (km^3)	ELA (m a.s.l.)
Baitone S	Malga	Valley	1976	3274	2625	7.4	0.30	2585
Miller	Malga	Valley	1800	3232	2516	8.7	0.44	2470
Coppo	Malga	Valley	1971	2647	2309	1.2	0.02	2260

Table 5.1.2.8 - Morphometric parameters Malga Baitone phase.

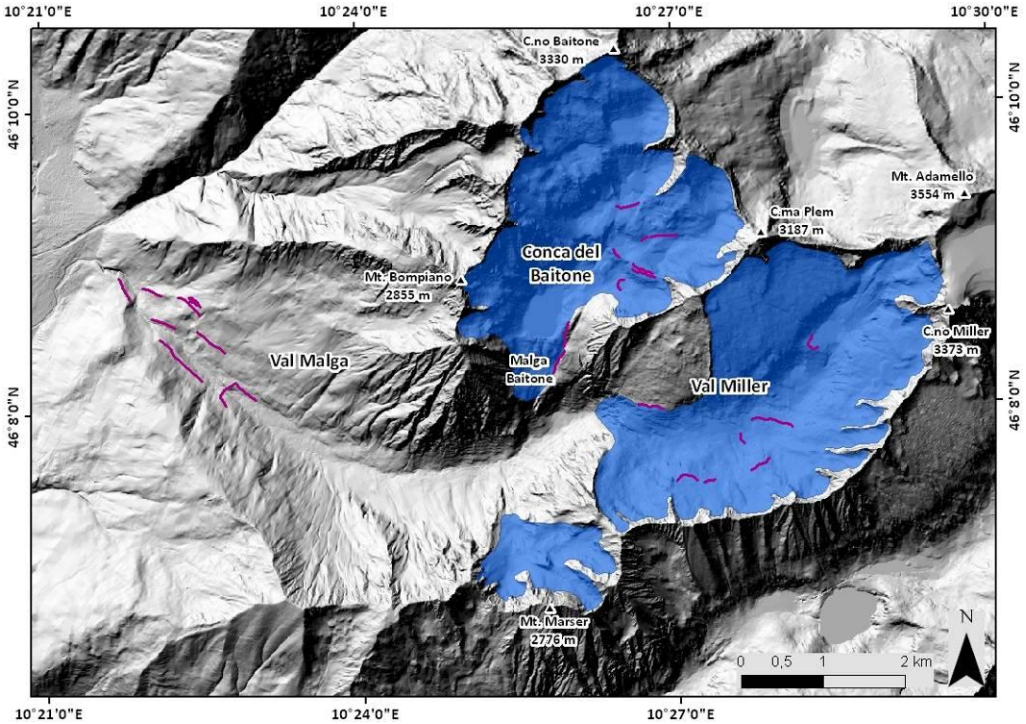

Fig. 5.1.2.9 - Malga Baitone phase extension and ^{10}Be exposure ages. Purple lines represent the moraines

A strong fragmentation of the South-West facing Baitone S Glacier is the biggest factor highlighted in the fourth (Miller phase) reconstructed phase (fig. 5.1.2.10). The valley glacier reconstructed for the third phase is replaced with six smaller mountain glaciers. The areal extension of these glaciers (tab. 5.1.2.9) had a range between 0.1 km^2 (Bonpià N and Bonpià S) and 2.1 km^2 (Baitone S) with a total glaciated are of ca. 3.8 km^2. Miller Glacier was still the most extended one, but was reduced by the 55% compared to the Malga Baitone phase. Comparing the total ice covered area of the first and fourth phases we can underline a reduction of the 65% (16 km^2) and the fragmentation of the original glacier in 8 different mountain glaciers. ELAs ranging from 2365 (+2,-3) m (Coppo) to 2890 (±1) m (Granate) with a value of 2885 (+1/-4) m and 2590 (+4,-2) m for the Baitone S and Miller glaciers, respectively that are the two biggest glaciers of this phase.

Glacier	Original glacier	Glacier type	Min. altitude (m a.s.l.)	Max altitude (m a.s.l.)	Mean altitude (m a.s.l.)	Area (km^2)	Δ Volume (km^3)	ELA (m a.s.l.)
Baitone S	Malga	Mnt	2515	3266	2891	2.1	0.08	2885
Baitone SE	Malga	Mnt	2437	3039	2738	1.1	0.03	2735
Baitone SSE	Malga	Mnt	2397	2694	2546	0.2	0.004	2560
Bonpià S	Malga	Mnt	2439	2646	2543	0.1	0.001	2580

Bonpià N	Malga	Mnt	2523	2837	2680	0.1	0.002	2635
Granate	Malga	Mnt	2789	3025	2907	0.2	0.003	2890
Miller	Malga	Mnt	2193	3224	2709	3.9	0.05	2590
Coppo	Malga	Mnt	2096	2647	2372	0.9	0.01	2365

Table 5.1.2.9 - Morphometric parameters Miller phase.Mnt: mountain glacier

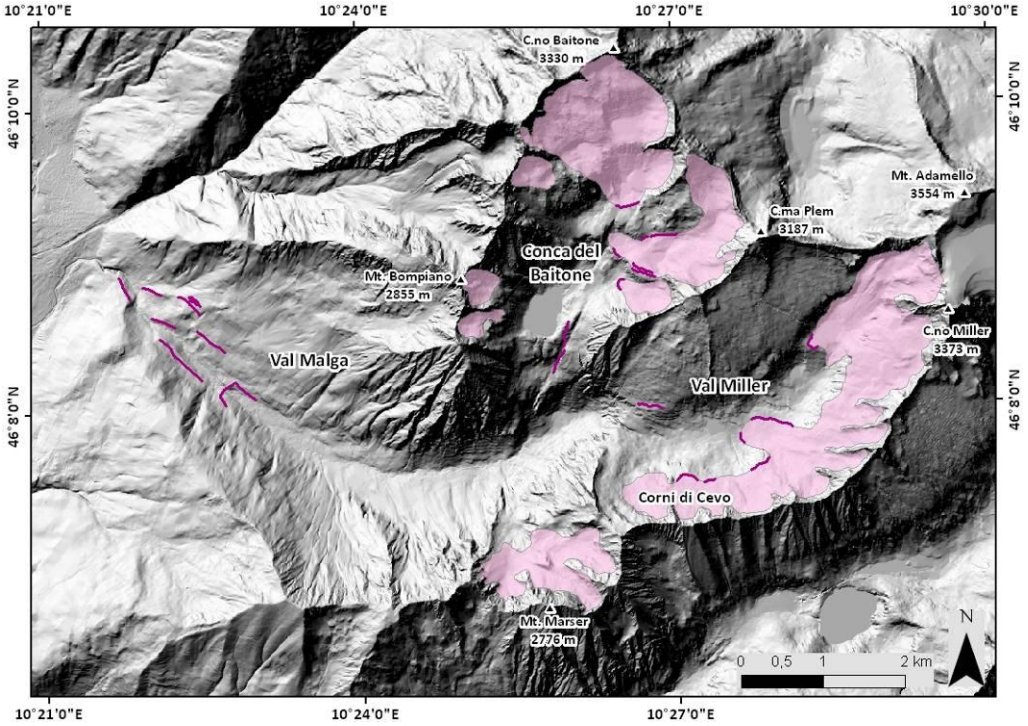

Fig. 5.1.2.10 - Miller phase extension and ^{10}Be exposure ages. Purple lines represent the moraines.

Sample ID	Quartz dissolved (g)	^{10}Be concentration (atoms/g qtz)	Exposure Age (Yr)	Internal uncertainty(yr) Lal(1991)/Stone(2000)	External uncertainty(yr) Lal(1991)/Stone(2000)
MAL14.1	16.802	1528oo±7800	15500	800	1090
MAL14.2	24.136	156000±9700	15700	980	1250
MAL14.6	10.725	107000±6900	13500	870	1090

Table 5.1.2.10 - ^{10}Be exposure ages in Val Malga. Data and relative exposure ages of processed samples. Reported external errors (1σ) consider internal uncertainties related to AMS measurement processing, together with the variability of the considered production rate scaling schemes.

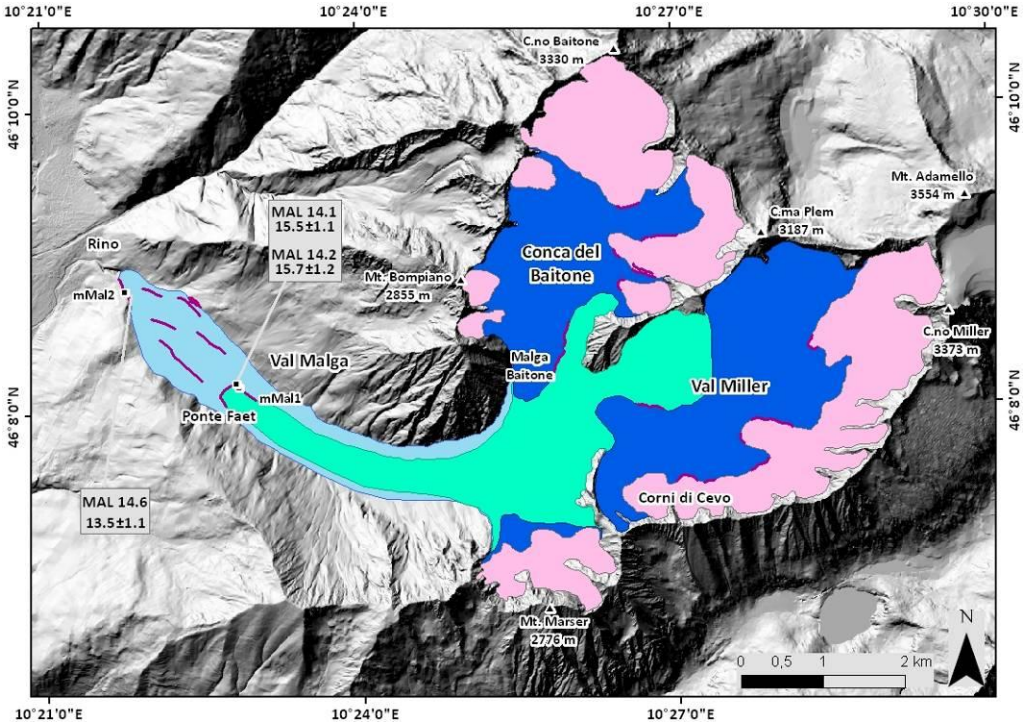

Fig. 5.1.2.11 - Reconstructed glacial phases comparison and exposure ages. Purple lines represent the moraines.

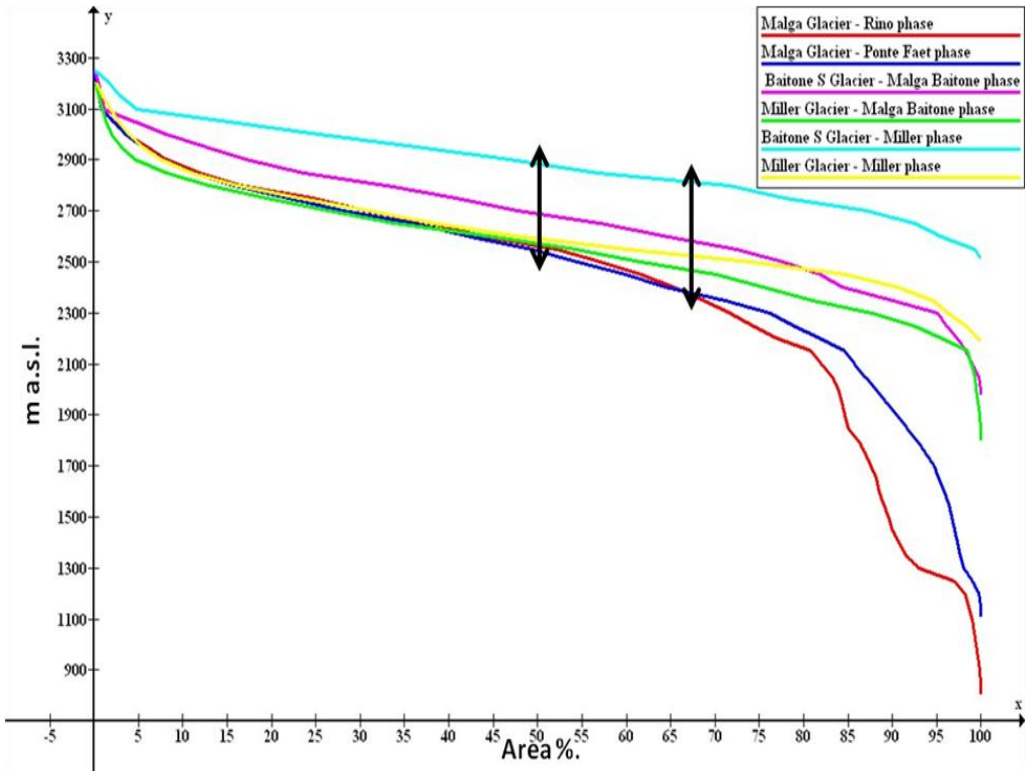

Fig. 5.1.2.12 - Hypsographic curve of the main Val Malga glaciers in the reconstructed phases. The black arrows point out the Equilibrium Line Altitude position adopting an Accumulation Area Ratio (AAR) for valley glaciers of 0.67±0.005 (Rino, Ponte Faet and Malga Baitonr phases) and for mountain glaciers of 0.50±0.005 (Miller phase) .

Val Adamè (Adamè Valley)

In the southern sector of the massif we studied the glacial history of the Val Adamè. The same approach used for the other alpine sites was applied and conducted to the reconstruction of three different glacial phases related to ice masses re-advances (fig. 5.1.2.16) One of these phases was chronologically constrained with exposure dating ages (tab. 5.1.2.14).

The most extended reconstructed phase of this area (Saviore phase) was obtained on the basis of the valley profile, the outcrop of glacial deposits and the size of the relative catchment basin.

The Saviore phase (fig. 5.1.2.13) was characterized by the presence of 2 valley glaciers and one mountain glacier that together occupied an area of ca. 22 km^2. Almost the totality of the this glaciated area was occupied by the main Adamè valley Glacier with an extension of ca. 21 km^2 and a volume estimated of ca. 2.6 km^3. The Adamè Glacier consisted of a well defined tongue reaching the lower altitude of 950 m and of a catchment basin that occupied the all Adamè Valley. The mean altitude was around 2020 m and the calculated ELA was 2325 (+8,-9) m. The other two glacier descended from the left side of the valley with small areas (0.3-08 km^2) and ELAs ranging from 2235 (±3) m and 2290 (±1) m (tab. 5.1.2.11).

Glacier	Original glacier	Glacier type	Min. altitude (m a.s.l.)	Max altitude (m a.s.l.)	Mean altitude (m a.s.l.)	Area (km^2)	Volume (km^3)	ELA (m a.s.l.)
Adamè	Adamè	Valley	949	3095	2022	21.0	2.64	2325
Monte Marosso	Monte Maroso	Mnt	2041	2547	2294	0.3	0.009	2290
Forcella di Marosso	Forcella di Marosso	Valley	1928	2750	2339	0.8	0.04	2235

Table 5.1.2.11 - Morphometric parameters of the Saviore phase. Mnt: mountain glacier.

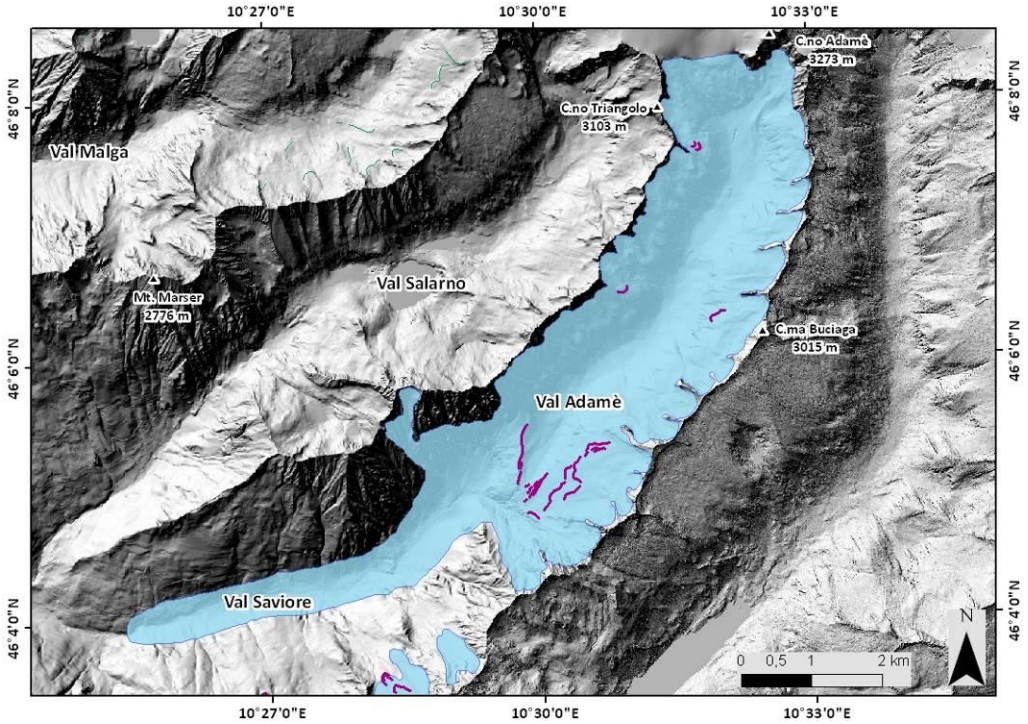

Fig. 5.1.2.13 - Saviore phase extension and ^{10}Be exposure ages. Purple lines represent the moraines.

The second reconstructed phase (Malga Adamè phase) show the presence of six glaciers (fig. 5.1.2.14) , four of which deriving from the Adamè Glacier fragmentation. Indeed on the left side of the valley it is possible underline the presence of three glacier derived from this fragmentation. Extensions of these glaciers ranged between 0.4 km^2 (Punta Forcel Rosso E and Punta Forcel Rosso W) and 1.1 km^2 (Cima Molinazzo). The wider glacier of the phase was still the Adamè glacier that occupied the biggest portion of the valley with an area of 11.5 km^2 and a rise of the minimum and mean elevation of ca. 990 m and 500 m, respectively (tab. 5.1.2.12). The sum of the extensions of the four glaciers deriving from the main glacier of the previous phase evidences a reduction of the glaciated area of the 36%. The Monte Marosso and Forcella di Marosso Glaciers reduced their extensions by the 66% and 50% respectively. ELAs of the Malga Adamè phase ranged between 2145 (+3,-4) m (Punta Forcel Rosso W) and 2545 (+3,-6) m (Adamè).

We sampled an dated four erratic boulders from two left lateral (mAda1 and MAda2) and one right lateral (mAda3) moraines. ^{10}Be ages (tab.

5.1.2.14) ranging from 15.0±1.0 ka (ADA20) to 11.4±0.7(ADA3) provide the minimum age for this phase.

Glacier	Original glacier	Glacier type	Min. altitude (m a.s.l.)	Max altitude (m a.s.l.)	Mean altitude (m a.s.l.)	Area (km^2)	Δ Volume (km^3)	ELA (m a.s.l.)
Adamè	Adamè	Valley	1937	3095	2516	11.5	2.42	2545
Cima Molinazzo	Adamè	Mnt	2087	2800	2444	1.1	0.008	2425
Punta forcel Rosso E	Adamè	Valley	1900	2732	2316	0.4	0.001	2195
Punta forcel Rosso W	Adamè	Valley	1739	2648	2194	0.4	0.04	2145
Monte Marosso	Monte Maroso	Mnt	2089	2526	2308	0.1	-	2305
Forcella di Marosso	Forcella di Marosso	Valley	2039	2750	2395	0.4	-	2285

Table 5.1.2.12 - Morphometric parameters of the Malga AdamèPhase.

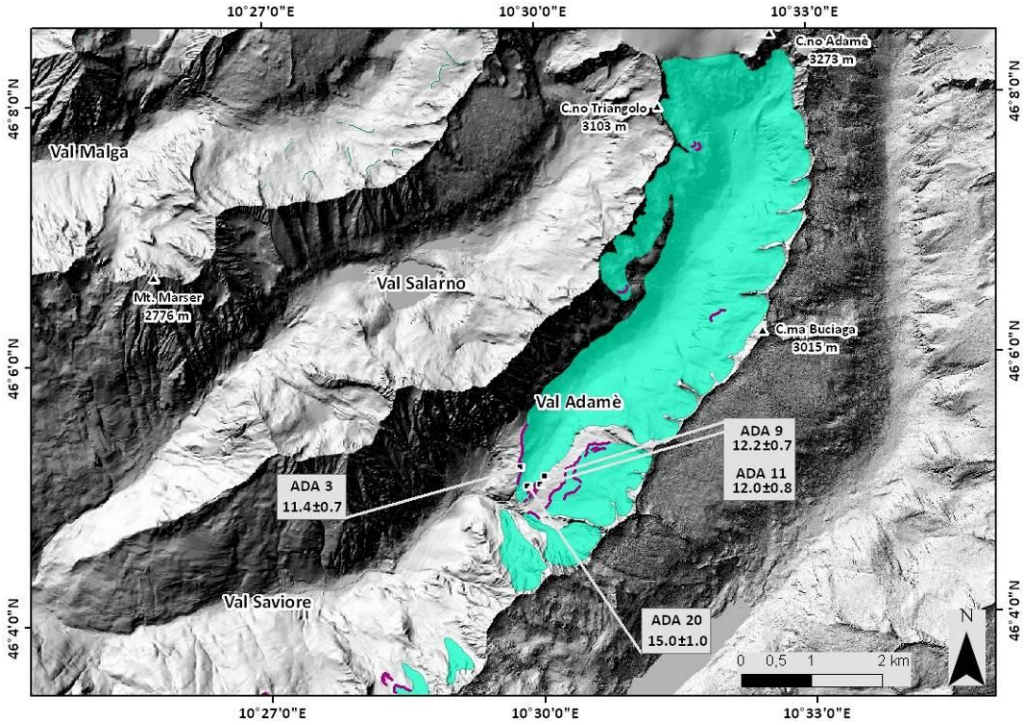

Fig. 5.1.2.14 - Malga Adamè phase extension and ^{10}Be exposure ages. Purple lines represent the moraines.

Thirteen glaciers have been reconstructed for the third (Coster phase) Lateglacial phase of this area (fig. 5.1.2.15). Eleven of them derived from the fragmentation of the wider Adamè Glacier of the Malga Adamè phase and the totality of the preserved glaciers had as original glacier, the Adamè Glacier reconstructed in the Saviore Phase. Indeed Monte Marosso and Forcella di Marosso glacier resulted extinguished. Only one glacier, the Adamè Glacier, preserved the characteristics of a valley glacier, with a

define tongue reching an altitude of 2111 m, recording a rise of the minimum altititude of ca. 405 m and 1160 m compared to the Malga Adamè and Saviore phases respectively. Its areal extension was 4.0 km^2 and the ice covered area of the thirteen glacier was only the 33% of the original Adamè Glacier (Cancè phase). The other twelve glaciers were mountain glaciers with small dimensions nestled on the upper portions of the slopes and distributed on the two lateral sides of the Val Adamè (2 right side and 10 left side). Absolute values of the ELA (tab. 5.1.2.13) show a big variability due to the position and extension of the glaciers. The ELA ranging from 2455 (±6)m (Adamè) to 2820 (±1) m (Poja Nord)

Glacier	Original glacier	Glacier type	Min. altitude (m a.s.l.)	Max altitude (m a.s.l.)	Mean altitude (m a.s.l.)	Area (km^2)	Δ Volume (km^3)	ELA (m a.s.l.)
Adamè	Adamè	Valley	2111	3095	2603	4.0	0.4	2455
Poja sud	Adamè	Mnt	2549	2889	2719	0.5	0.01	2725
Poja Nord	Adamè	Mnt	2729	2945	2837	0.06	0.002	2820
Bocchetta di Levade	Adamè	Mnt	2679	2850	2765	0.1	0.0007	2770
Pisage	Adamè	Mnt	2648	2819	2734	0.1	0.0006	2725
Artigliere N	Adamè	Mnt	2582	2820	2701	0.1	0.0006	2700
Artigliere S	Adamè	Mnt	2495	2849	2672	0.2	0.06	2700
Cima Coster N	Adamè	Mnt	2475	2853	2664	0.4	0.001	2660
Buciaga	Adamè	Mnt	2476	2840	2658	0.5	0.01	2665
Punta Forcel Rosso E	Adamè	Mnt	2231	2732	2482	0.2	0.01	2460
Cima di Molinazzo	Adamè	Mnt	2232	2771	2502	0.9	0.005	2530
Russi N	Adamè	Mnt	2449	2786	2618	0.1	0.001	2605
Russi S	Adamè	Mnt	2280	2791	2534	0.6	0.005	2555

Table 5.1.2.13 - Morphometric parameters of the Coster phase. Mnt: mountain glacier.

Sample ID	Quartz dissolved (g)	^{10}Be concentration (atoms/g qtz)	Exposure Age (Yr)	Internal uncertainty(yr) Lal(1991)/Stone(2000)	External uncertainty(yr) Lal(1991)/Stone(2000)
ADA3	17.987	226700±9600	11400	490	740
ADA9	24.794	251000±9200	12200	450	750
ADA11	17.686	239900±10200	12000	520	780
ADA20	24.17	289600±11800	15000	620	960

Table 5.1.2.14 - ^{10}Be exposure ages in Val Adamè. Data and relative exposure ages of processed samples. Reported external errors (1σ) consider internal uncertainties related to AMS measurement processing, together with the variability of the considered production rate scaling scheme.

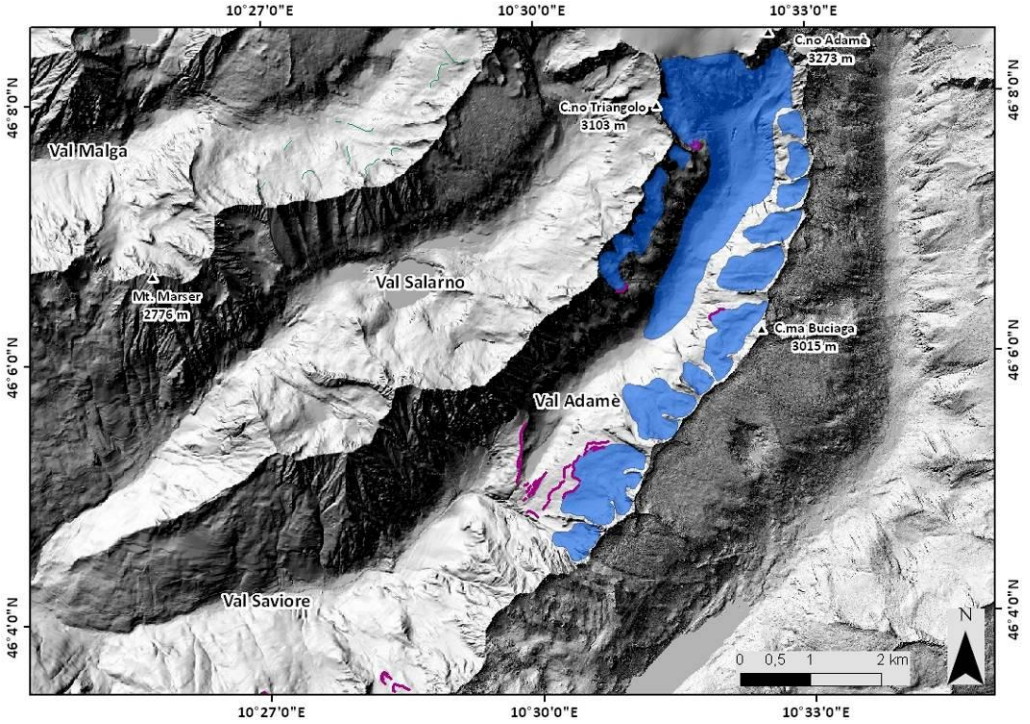

Fig. 5.1.2.15 - Coster phase extension and ^{10}Be exposure ages. Purple lines represent the moraines

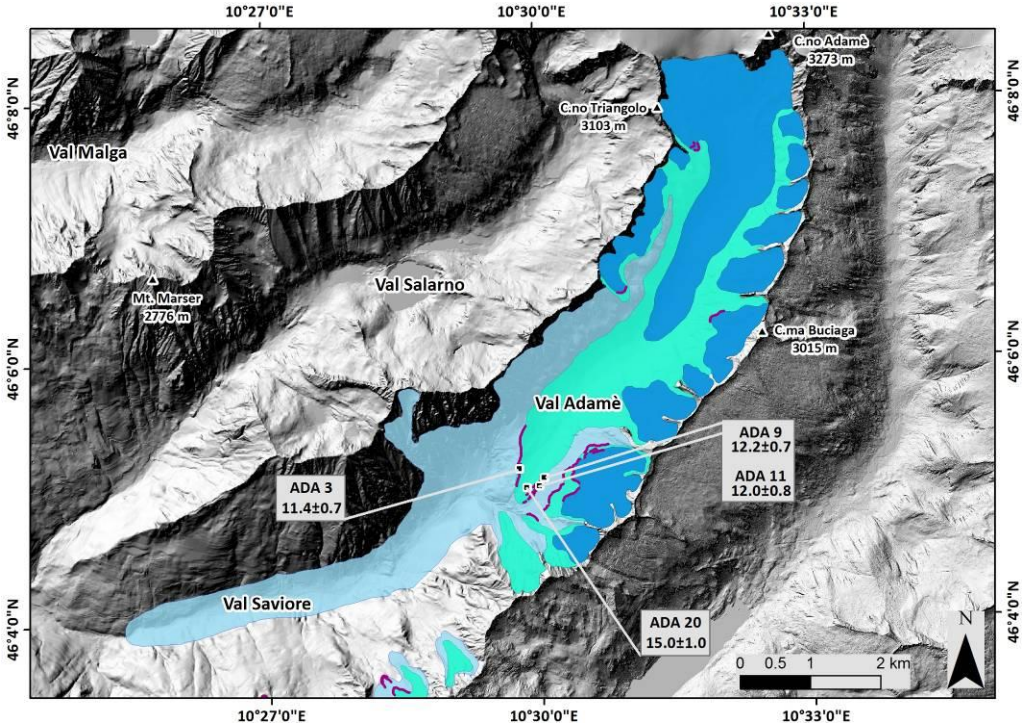

Fig. 5.1.2.16 - Reconstructed glacial phases in Val Adamè. Purple lines represent the moraines

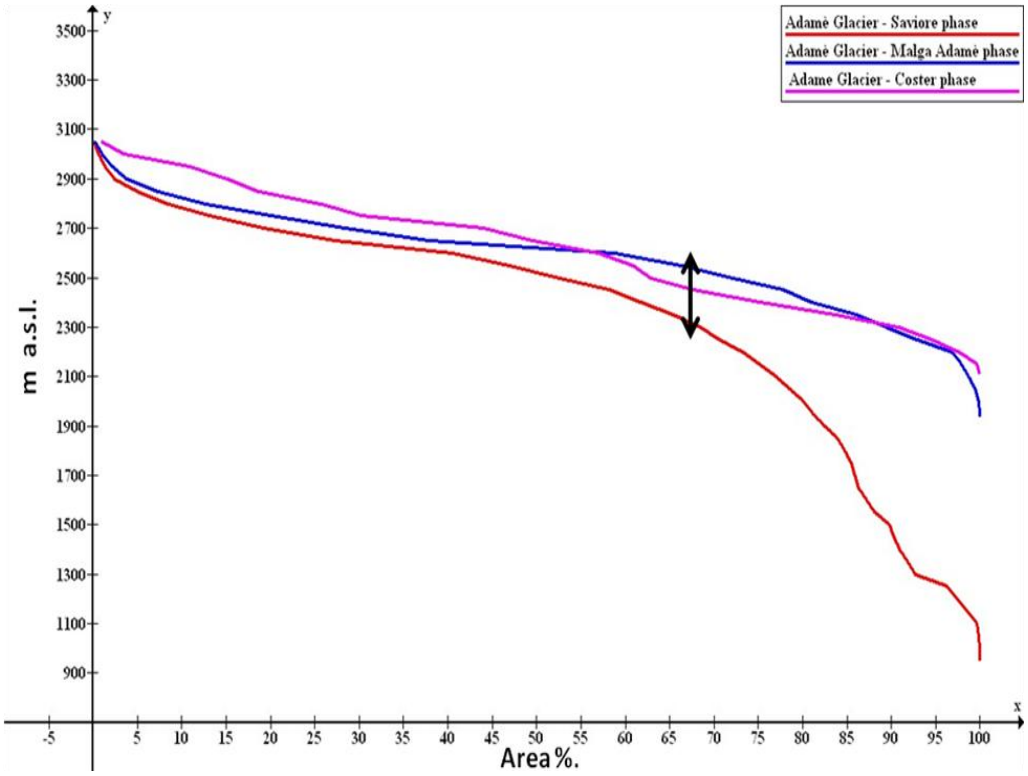

Fig. 5.1.2.17 - Hypsographic curve of the main Val Adamè glacier in the different reconstructed phases. The black arrow point out the Equilibrium Line Altitude position adopting an Accumulation Area Ratio (AAR) for valley glaciers of 0.67±0.005.

Val Rendena

In Val Rendena we dated three samples from erratic boulders (fig. 5.1.2.18) located at Sant Antonio di Mavignola (SANT14.1, SANT14.2) and in Val Breguzzo (BRE14.01). The obtained exposure ages define a range between 9.9 ka and 16.2 ka (tab. 5.1.2.15) Samples from Sant Antonio di Mavignola give ages of 9.9±0.7 ka (SANT14.1) and 13.7±0.9 ka (SANT14.2). Sample BRE14.01 is the older of the group of samples dated for the Adamello-Presanella Massif and provides an exposure age of 16.2±1.1 ka.

Sample ID	Quartz dissolved (g)	^{10}Be concentration (atoms/g qtz)	Exposure Age (Yr)	Internal uncertainty(yr) Lal(1991)/Stone(2000)	External uncertainty(yr) Lal(1991)/Stone (2000)
SANT14.1	23.136	97000±5400	9900	550	730
SANT14.2	18.076	130700±6200	13700	650	930
BRE14.01	17.656	205000±9900	16200	790	1100

Table 5.1.2.15 - ^{10}Be exposure ages in Val Rendena. Data and relative exposure ages of processed samples. Reported external errors (1σ) consider internal uncertainties related to AMS measurement processing, together with the variability of the considered production rate scaling schemes.

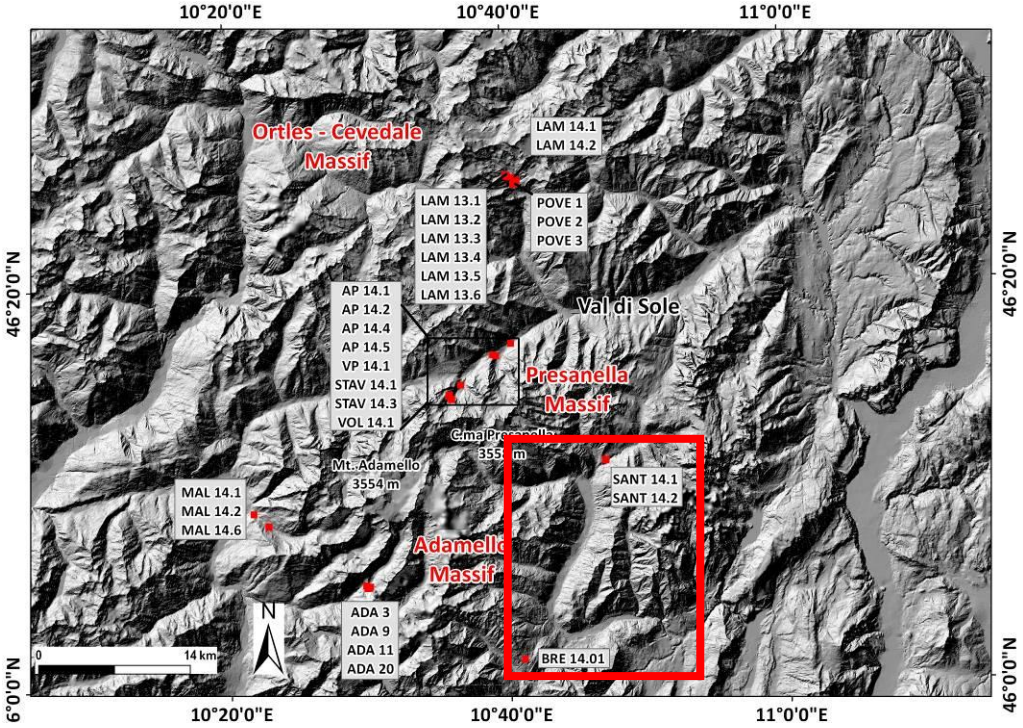

Fig. 5.1.2.18 - Location map of the dated samples. The red rectangle outline samples related to the Val Rendena.

5.2 Antarctica

5.2.1 The Antarctic Database

A result of the bibliographic work at the beginning of this project was the implementation of the database of Surface Exposure Dating ages for the Victoria Land (Antarctica). As shown in the Material and Methods chapter the goal was to homogenize data from different sources, obtained with different techniques (different cosmogenic nuclides) and make more accessible the existing dataset. We obtained a georeferenced (UTM-WGS84) shape file representative of the geographical location of the dated Antarctic samples that allow a fast view of the ages distribution on the investigated sector. A selection of available data was made and an attribute table was associated to the shape file. The information findable in the database concern the samples bibliographic references, their geographical attributes (Latitude, Longitude, altitude, locality name), some sampling factors (i.e. sample thickness, topographic shielding) and Surface Exposure Dating parameters (used cosmogenic nuclide, cosmogenic nuclide concentration, exposure age).

During several Antarctic expeditions in the framework of the Programma Nazionale di Ricerche in Antartide (PNRA) (from 1997/98 to 2012/13) Prof. Carlo Baroni and Prof. Maria Cristina Salvatore collected samples from erratic boulders and ice free bedrock portions. These samples have been included in the database and their distribution covers an area with incomplete dating information (fig. 5.2.1.1). This condition highlighted the importance of the collected samples and the necessity of their dating. In this framework 40 samples (from 2009/10 to 2012/13 expeditions) were selected and dated with the Surface Exposure Techniques and new ^{10}Be and ^{26}Al ages were obtained.

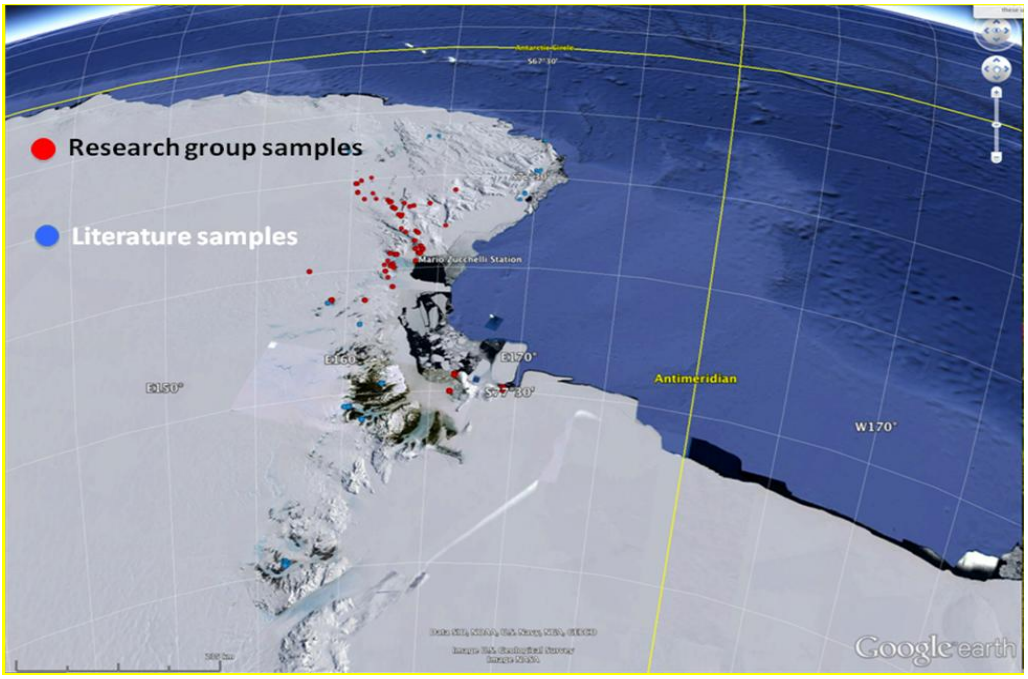

Fig. 5.2.1.1 – Location map of the literature and research group samples.

5.2.2 New evidences for the glacial evolution reconstruction

In the framework of the Antarctic part of this work we selected and dated 40 samples from sites of the Victoria Land, to better constrain the EIAS evolution over time. The geographical distribution of the samples allow us to define two macro-areas, the Northern Victoria Land and the Southern Victoria Land (fig. 5.2.2.1). We dated with Surface Exposure Dating two different typologies of glacial feature, erratic boulders and ice free bedrock portions (tab. 5.2.2.1) and we obtained new ^{10}Be and ^{26}Al ages.

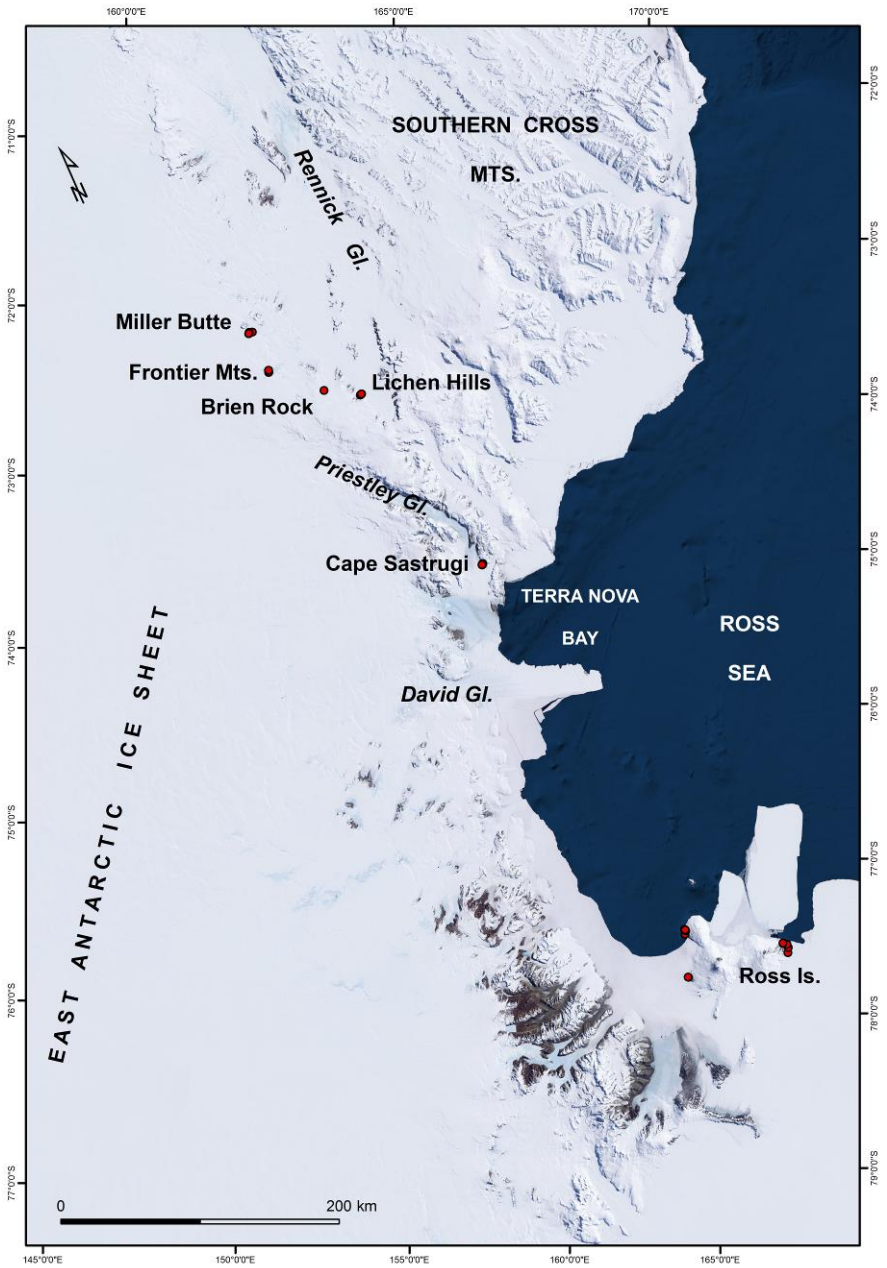

Fig. 5.2.2.1 - Location map of Antarctic dated samples.

SITE	Nr.Samples	Bedrock	Erratic boulder	TCN
Cape Sastrugi	10	1	9	^{10}Be
Lichen Hills	3	-	3	^{10}Be
Brien Rocks	1	1	-	^{10}Be, ^{26}Al
Frontier Mts.	6	3	3	^{10}Be
Miller Butte	8	5	3	^{10}Be
Ross Island	12	-	12	^{10}Be

Table 5.2.2.1 - Dated samples, glacial features and cosmogenic nuclides measured.

Northern Victoria Land

In the Northern Victoria Land we studied sites located at the border of the EIAS to better understand the glacial history of this relevant sector of the ice sheet. Here, in a first step, we analyze the data obtained in each single site and after we make a comparison to get a general overview of the glacial evolution of the ice sheet in this sector. It is important to underline once more that the obtained data are minimum ages and define the minimum time of exposition of the sample to the cosmic radiation. Samples have been corrected for the thickness factor but not for the erosion.

Cape Sastrugi

In the Cape Sastrugi area we dated ten samples of which nine are from erratic boulders and one from ice free bedrock (fig, 5.2.2.2, tab. 5.2.2.2). These samples were collected in an altitude range of 180-330 m a.s.l and allow us to define three groups of ages useful to better define the EAIS glacial history of the area.

A first group of samples (erratic boulders) has an ages range between 5.7±1.1 ka and 10.3±1.5 ka. In particular sample CB100103.03, located at

an altitude of 179 m a.s.l., has an exposure age of 5.7±1.1 ka, the sample CB100103.02 (176 m a.s.l.) give us an age of 7.5±1.0 ka and sample CB100103.04, located at the similar altitude of 185 m a.s.l., shows a minimum exposure age of 8.0±1.5 ka. In the same group we can find CB091218.06, CB100103.01 and CB100103.06 located between 168 m a.s.l. and 239 m a.s.l.. This sub-group of ages ranging from 9.0 ka to 10.3 ka. In particular sample CB100103.06 (239 m a.s.l.) has an exposure age of 9.0±1.0 ka, the sample CB100103.01 (168 m a.s.l.) shows an age of 9.3±1.8 ka and sample CB091218.06 (187 m a.s.l.) was exposed at least since 10.3±1.5 ka. A overall view of these six samples underline the presence of a glacial phase detectable around 9 ka.

The sample CB100118.04 collected from an erratic boulder at an altitude of 185 m a.s.l. is characterized with an exposure age of 16.3±2.1 ka.

Sample Id	Glacial feature	Qtz dis.	^{10}Be conc. (atoms/g)	Exposure age (yr)	Int uncert.(yr)	Ext uncert.(yr)
CB 09 12 18.03	Erratic	5.769	238600±14100	41000	2400	4600
CB 09 12 18.04	Erratic	7.876	96600±8500	16300	1400	2100
CB 09 12 18.05	Bedrock	20.492	411300±12300	70600	2100	7000
CB 09 12 18.06	Erratic	7.651	61100±6900	10300	1100	1500
CB 10 01 03.01	Erratic	6.023	54000±9000	9300	1500	1800
CB 10 01 03.02	Erratic	20.713	43900±4300	7500	700	1000
CB 10 01 03.03	Erratic	8.866	33300±5600	5700	900	1100
CB 10 01 03.04	Erratic	6.077	54400±9100	8000	1300	1500
CB 10 01 03.05	Erratic	9.568	280800±12500	41400	1800	4300
CB 10 01 03.06	Erratic	20.236	60200±4100	9000	600	1000

Table 5.2.2.2 - Cape Sastrugi ^{10}Be ages.

Going towards older exposure ages we found a group of two erratic boulders samples with ages around 40 ka and 1 bedrock sample dated around 70 ka. In detail samples CB091218.03 (183 m a.s.l.) and CB100103.05 (332 m a.s.l.) have respectively an age of 41.0±4.6 ka and 41.4±4.3 ka. The bedrock sampled with CB091218.05 (187 m a.s.l.) give us the oldest age for this study site with an exposure age of 70.6±7.0 ka.

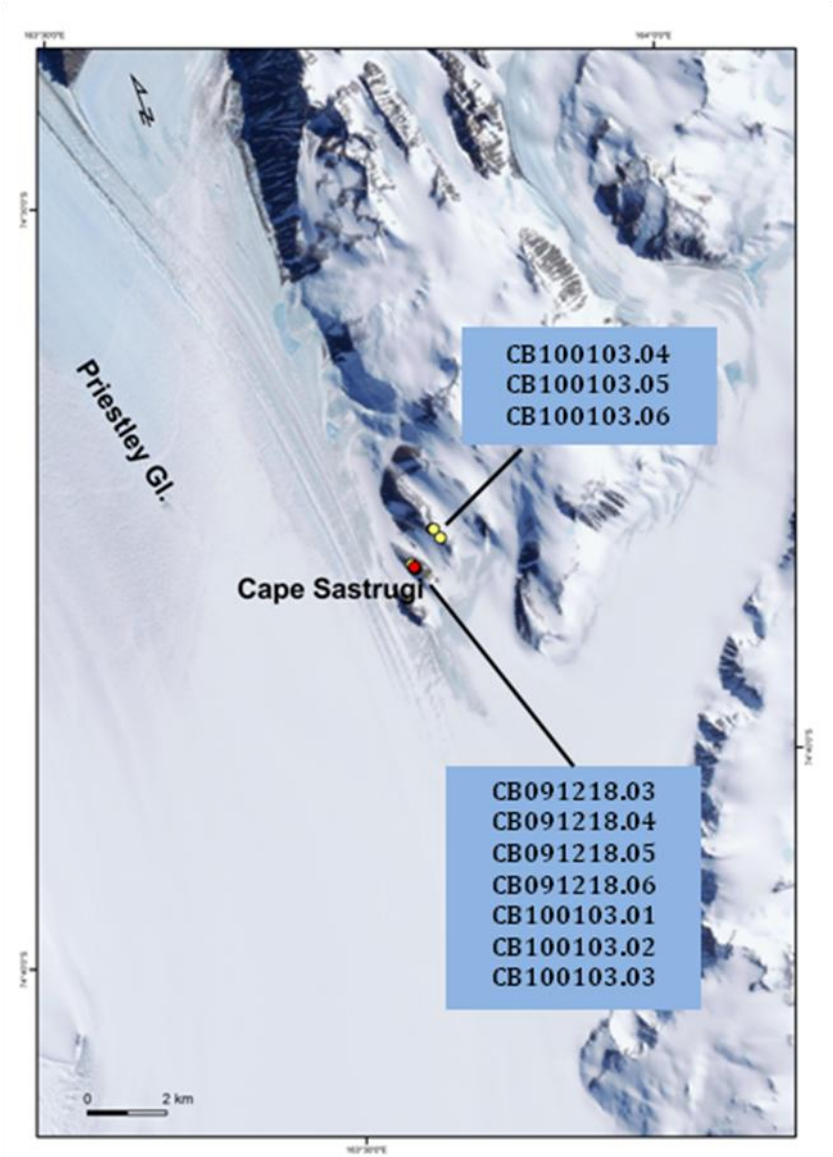

Fig. 5.2.2.2 - Location map of the Cape Sastrugi dated samples. Bedrock samples are in red and erratic boulders samples are in yellow.

Brien Rocks and Lichen Hills

Moving to more internal sites we dated 3 erratic boulder samples from the Lichen Hills and 1 bedrock sample from Brien rocks (fig. . 5.2.2.3, tab. 5.2.2.3).

The ages from the Lichen Hills site are from 54 ka to 88 ka. Samples CB091228.16 and CB091228.17 were collected at an altitude of 2059 m a.s.l. and have an age respectively of 54.9±5.5 ka and 67.9±6.7 ka while the third sample (CB091228.14) was collected at an altitude of 2347 m a.s.l. and shows an age of 88±8.7 ka.

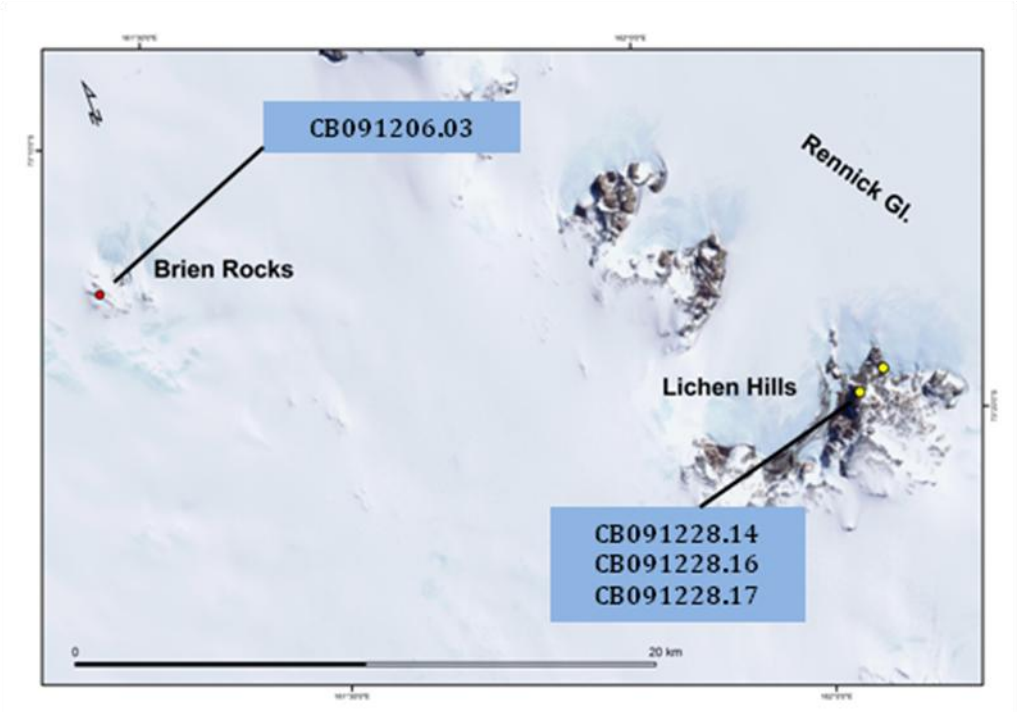

Fig. 5.2.2.3 - Location map of the Brien Rock and Lichen Hills dated samples. Bedrock samples are in red and erratic boulders samples are in yellow.

Sample Id	Glacial feature	Site	Qtz dis.	^{10}Be conc. (atoms/g)	Exposure age (yr)	Int uncert. (yr)	Ext uncert.(yr)
CB091206.03	Bed	Brien Rocks	8.339	14651900±327000	348400	8200	36300
CB 09 12 28.14	Erratic	Lichen Hills	7.641	3056000±83900	88000	2400	8700
CB 09 12 28.16	Erratic	Lichen Hills	8.870	1581600±55500	54900	1900	5500
CB 09 12 28.17	Erratic	Lichen Hills	11.721	1956500±52800	67900	1800	6700

Table 5.2.2.3 - Brien Rocks and Lichen Hills ^{10}Be ages. Bed.: bedrock.

For the Brien Rocks sample (CB091206.03) was possible to apply a multi-nuclide approach and measure ^{10}Be and ^{26}Al concentrations (tab. 5.2.2.4). The exposure ages for this portion of bedrock, located at 2734 m a.s.l., range between 338 ka and 348 ka. ^{10}Be and ^{26}Al ages highlight an exposition to the cosmic radiation at least of 348±36 ka and 338±49 ka, respectively and allow to speculate a simple exposition history.

Sample Id	Glacial feature	Site	Qtz dis.	^{26}Al conc. (atoms/g)	Exposure age (yr)	Int uncert. (yr)	Ext uncert.(yr)
CB091206.03	Bed.	Brien Rocks	8.339	89200000±7000000	338500	30400	48800

Table 5.2.2.4 - Brien Rocks ^{26}Al age. Bed.: bedrock.

Frontier Mountains

Samples collected at the Frontier Mountains (fig. 5.2.2.4, tab. 5.2.2.5) can be divided in two groups on the base of their altitude and on the glacial feature typology. The first group is made by samples deriving from erratic boulders, located at an altitude around 2600 m a.s.l.. Their exposure ages ranging from ca. 177 ka to 267 ka. In detail samples CB091206.17, CB091206.18 (both with an elevation of 2614 m a.s.l.) and CB091206.19 (2617 m a.s.l.) give dates of 177±18 ka, 267±27 ka and 181±18 ka, respectively. The second group consists on bedrock samples, collected from higher altitude, with an elevation of ca. 3200 m a.s.l.. The data from these samples tell us an older story, in the order of millions of years of exposition to the cosmic radiation. Exposure ages define a range that starts from ca. 3.4 Ma and arrives to ca. 5.1 Ma. Sample CB091206.09 (3164 m a.s.l.) has an age of 3.8±1.1 Ma, while CB091206.10 (3157 m a.s.l.) 3.4±0.9 Ma. The highest sample (CB091206.11) collected at an altitude of 3178 m a.s.l is the oldest exposure age of our new data an show an exposition period of 5.1±2.3 Ma.

Sample Id	Glacial feature	Qtz dis.	^{10}Be conc. (atoms/g)	Exposure age (yr)	Int uncert. (yr)	Ext uncert.(yr)
CB091206.09	Bedrock	5.372	100967600±2019600	3842200	196200	1105100
CB091206.10	Bedrock	4.865	96838700±1937000	3414300	156700	855800
CB091206.11	Bedrock	5.195	110121080±2202700	5137500	354700	2284000
CB091206.17	Erratic	9.976	7146100±152400	176500	3800	17600
CB091206.18	Erratic	9.879	10600000±212200	266600	5500	27000
CB091206.19	Erratic	9.901	7310700±146400	181200	3700	18000

Table 5.2.2.5 - Frontier Mountains ^{10}Be ages.

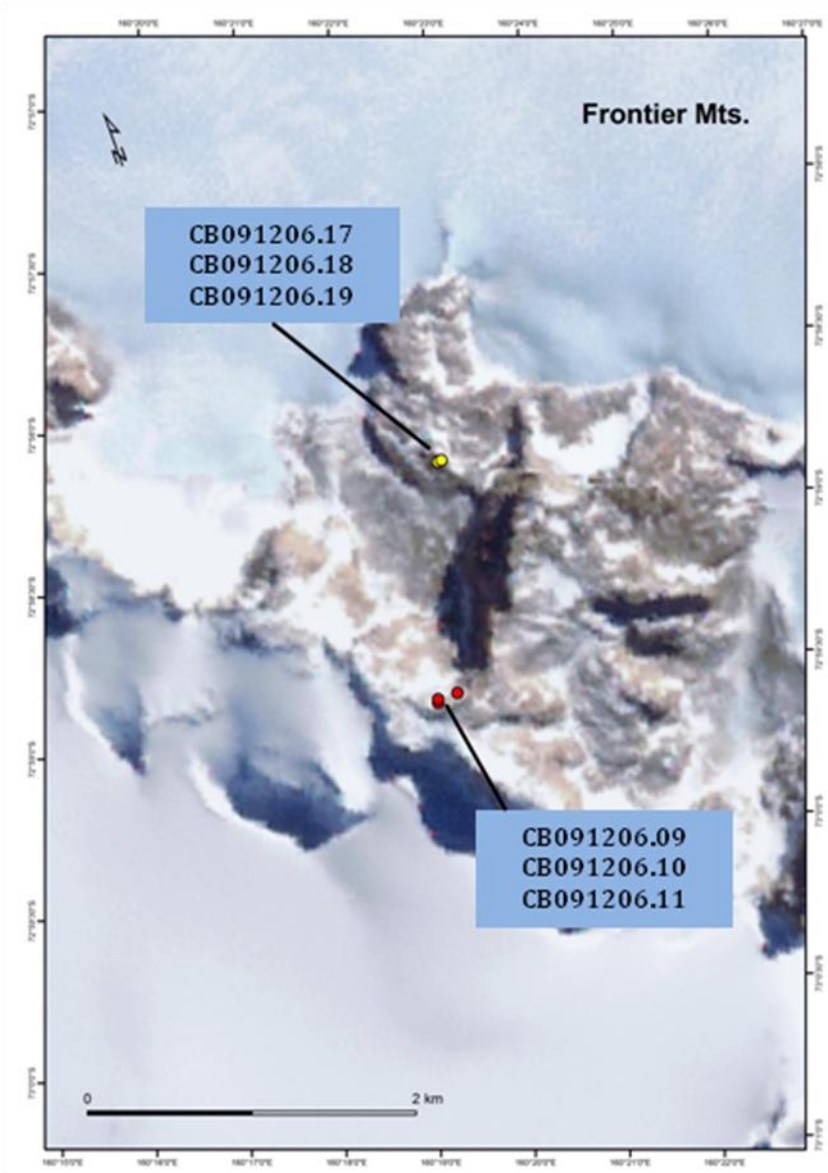

Fig. 5.2.2.4 - Location map of the Frontier Mts. dated samples. Bedrock samples are in red and erratic boulders samples are in yellow.

Miller Butte

The most internal site that we studied is related to the reliefs of Miller Butte (fig. 5.2.2.5). Also in that case it is possible to define two different groups of samples on the basis of the elevation and exposure ages values (tab. 5.2.2.6).

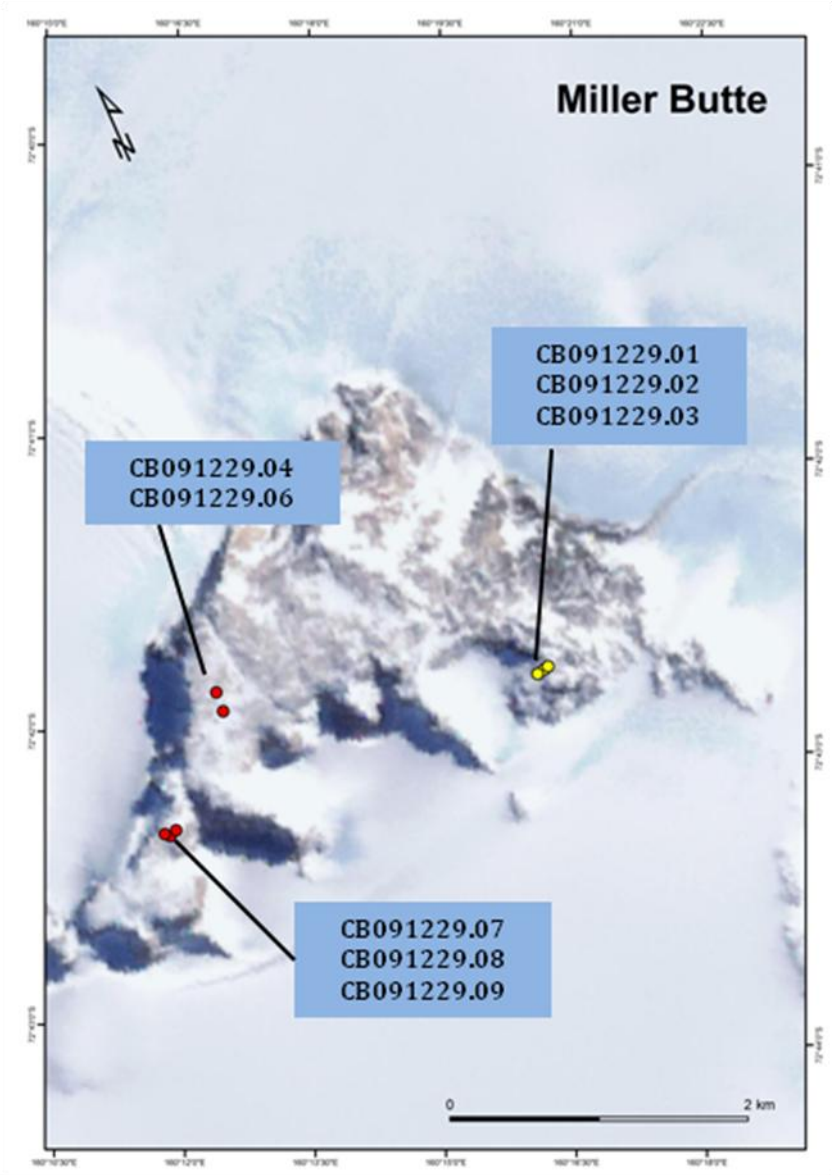

Fig. 5.2.2.5 - Location map of the Miller Butte dated samples. Bedrock samples are in red and erratic boulders samples are in yellow.

A group of three erratic boulders is located at an altitude around 2700 m a.s.l. and give ages from 121 ka to 413 ka. The youngest of the group is the sample CB091229.02 (2732 m a.s.l.) with an exposure age of 121±12 ka, followed by the sample CB091229.01(2748 m a.s.l.) with its age of 294±30 ka. The oldest the erratic boulders samples is CB091229.03 (2740 m a.s.l.) with 413±44 ka.

Sample Id	Glacial feature	Qtz dis.(g)	^{10}Be conc. (atoms/g)	Exposure age (yr)	Int uncert. (yr)	Ext uncert.(yr)
CB091229.01	Erratic	8.920	12522100±250600	293700	6100	30000
CB091229.02	Erratic	7.442	5289500±114700	120600	2600	11800
CB091229.03	Erratic	7.946	17020300±458800	413000	12000	44300

CB091229.04	Bedrock	8.584	69593500±1392000	2313200	80200	413300
CB091229.06	Bedrock	8.677	61925800±1238700	1866800	57700	292700
CB091229.07	Bedrock	9.457	34388700±687900	823200	19600	96600
CB091229.08	Bedrock	8.498	58174700±2139000	1700400	92600	267300
CB091229.09	Bedrock	10.630	45056500±901200	1175700	30500	151800

Table 5.2.2.6 - Miller Butte ^{10}Be ages.

As for the Frontier Mountains site, the 5 bedrock samples give us information about an older story of the EAIS evolution in this area. Samples are located at an altitude of ca 200 m higher than the erratic boulders and the ages obtained are from 0.8 Ma to 2.3 Ma. The youngest of this group is the sample CB091229.07 (2913 m a.s.l.) with an age of 0.8±0.1 Ma, followed by the 1.2±0.2 Ma of CB091229.09 (2904 m a.s.l.), the 1.7±0.3 Ma of CB091229.08 (2921 m a.s.l.), the 1.9±0.3 Ma of CB091229.06 (2915 m a.s.l.) and finally by the 2.3±0.4 Ma of CB091229.04 (2920 m a.s.l.).

Southern Victoria Land

Ross Island

In the Southern Victoria Land area we obtained new dates from sites of Ross Island, in particular Cape Bird, Cape Royds and Cape Crozier (fig. 5.2.2.6, tab. 5.2.2.7). Samples from Cape Bird are located at low altitude included between 90 and 340 m a.s.l. and give ages ranging from 12.4 ka to 153 ka. These samples can be divided in three groups, the first is represented by the sample CB111215.02 (88 m a.s.l.) with an age of 12.4±1.4 ka. The second one is composed by the samples CB111220.05 (338 m a.s.l.) and CB111220.07 (286 m a.s.l.) with exposure time of 17.8±2.0 ka and 15.8±1.7 ka, respectively. The last group is made by the sample CB111221.01 (169 m a.s.l.) that show an age of 153±15 ka. Cape Royds provides two new exposure ages of 18.8±2.0 ka and 12.9±1.4 ka with the samples CB120101.03 (32 m a.s.l.) and CB12010106 (54 m a.s.l.).The last studied site on Ross Island is Cape Crozier with five samples from erratic boulders that can be grouped in three different sets. The younger one is made by three samples ranging between 12 ka and 14.5 ka. Sample CB121220.03 (155 m a.s.l.) provides an age of 11.9±1.3 ka,

CB130101.02 (278 m a.s.l.) shows an exposure age of 12.5±1.0 ka and CB13010101 (271 m a.s.l.) was exposed at least for 14.±1.1 ka.

Sample Id	Glacial feature	Site	Qtz dis.	^{10}Be conc. (atoms/g)	Exposure age (yr)	Int uncert. (yr)	Ext uncert.(yr)
CB121220.03	Erratic	Cape Crozier-Hut	19.433	68000±4200	11900	700	1300
CB121220.04	Erratic	Cape Crozier-Hut	20.415	1887900±37800	328300	6900	33800
CB121220.07	Erratic	Cape Crozier	25.638	783300±18000	140700	3300	13900
CB130101.02	Erratic	Cape Crozier	20.114	81000±4700	12400	700	1400
CB130101.01	Erratic	Cape Crozier	19.787	92100±5500	14500	900	1600
CB111215.02	Erratic	Cape Bird-South colonies	21.449	65500±3900	12400	700	1400
CB111220.05	Erratic	Cape Bird-Inclusion Hil	16.540	120700±7000	17800	1000	2000
CB111220.07	Erratic	Cape Bird-Inclusion Hil	19.120	103200±5000	15800	800	1700
CB111221.06	Erratic	Cape Bird	19.796	20600±3100	4000	60o	700
CB111221.01	Erratic	Cape Bird	21.924	865700±17500	153400	3100	15100
CB120101.03	Erratic	Cape Royds	22.766	92200±4300	18800	900	2000
CB120101.06	Erratic	Cape Royds	21.065	65400±3900	12900	800	1400

Table 5.2.2.7 - Ross Island ^{10}Be ages.

The second and third sets are made by 1 sample each and highlight two different glacial phases. One phase is represented by the sample CB121220.07 (158 m a.s.l.) that gives an age of 141±14 ka and the other phase finds evidence with the 328±34 ka of the sample CB121220.04.

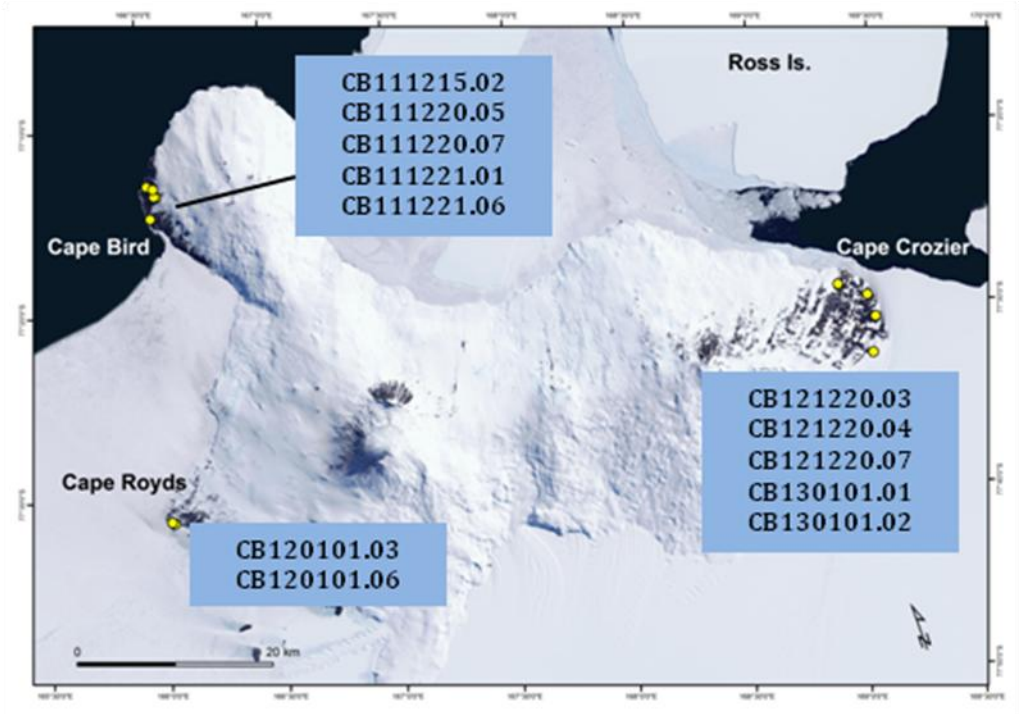

Fig. 5.2.2.6 - Location map of the Ross Island dated samples. Boulders samples are in yellow.

5.2.3 Dataset synthesis

The analysis of the new dataset allow us to define a series of group ages that are evidences of different phases of the EAIS evolution in the Victoria Land area (tab. 5.2.3.1). Starting from the younger ages we can define a family of ages around 8-9 ka highlighted by samples from Cape Sastrugi (CB100103.03, CB100103.02, CB100103.04, CB091218.06, CB100103.01 and CB100103.06).

Another phase can be constrained around 18-16 ka using samples from Ross Island (CB111220.05, CB111220.07 and CB130101.01) and Cape Sastrugi (CB100118.04). The time interval 40-70 (90) ka finds evidences in Cape Sastrugi (CB091218.03, CB100103.05 and CB091218.05) and Lichen Hills (CB091228.16, CB091228.17, CB091228.14). At least 3 different phases are recognized in the Middle Pleistocene in Brien Rocks, Frontier Mts., Miller Butte and Ross Island. These stages are focused on ca. 120-180 ka (CB091206.17, CB091206.19, CB091229.02, CB121220.07, CB111221.01), 270-330 ka (CB091206.18, CB091206.03, CB091229.01, CB121220.04), 450-500 ka (CB091229.03) and allow underline a multiphasic evolution of the Middle Pleistocene. The double cosmogenic approach used on the Brien Rock sample (CB091206.03) allow to affirm

that the dated bedrock had a constant exposition to the cosmic radiation since at least 350 ka. Focusing on the ages obtained from the samples of the Miller Butte site we underline a bedrock deglaciation (2900 m a.s.l.) prior to 2.3 Ma (CB091229.04) and not later than 0.8 Ma (CB091229.07). A comparable situation can be defined for the dated Frontier Mountains bedrock that results deglaciated since 5.1 (CB091206.11) Ma and not later than 3.4 Ma (CB091206.10).

Time interval	Site	Sample
9 ka	Cape Sastrugi	CB091218.06, CB100103.01, CB100103.02,CB100103.03, CB100103.04, CB100103.06
18-16 ka	Cape Sastrugi, Ross Island	CB100118.04, CB111220.05, CB111220.07, CB130101.01
70 (90)-40ka	Cape Sastrugi, Lichen Hills	CB091218.03, CB100103.05, CB091218.05, CB091228.16, CB091228.17 (CB091228.14)
180-120	Miller Butte, Frontier Mts., Ross Island	CB091206.17, CB091206.19, CB091229.02, CB121220.07, CB111221.01
330-270-ka	Miller Butte, Frontier Mts., Ross Island	CB091206.18, CB091206.03, CB091229.01, CB121220.04
450-400 ka	Miller Butte	CB091229.03
Millions of years	Miller Butte, Frontier Mts.	CB091229.04, CB091229.06, CB091229.07, CB091229.08, CB091229.09, CB091206.09, CB091206.10, CB091206.11

Table 5.2.3.1 - Summary of recognized phases and related samples.

6 -Discussion

6.1 Lateglacial phases in the Rhaetian Alps

The reconstruction of the glacial history of our alpine study areas provides new data for the Rhaetian Alps Lateglacial chronology. We found and dated glacial deposits related to three main glacial stages characterizing the end of the Pleistocene. The peculiarity of the investigated sites in the Rhaetian Alps consists in the possibility of reconstructing in detail the glacier dynamics since the last glacial cycle.

In the Val Malga we found evidences of repeated glacial phases that testify the answer of the glaciers to different late Pleistocene climate deteriorations. During the oldest Lateglacial phases the Val Malga was occupied by one main valley glacier. For this area we can refer to this phase as *Ponte Faet* phase. Our data from the Val Malga derive from the dating of a lateral-frontal right moraine (mMal1) and allow us to constrain this phase before 15.7±1.2 ka (MAL14.2). Sample Mal14.1 renforces this interpretation providing an age of 15.5±1.1 ka. The first Lateglacial stage has a good correlation with the Heinrich 1 IRD cooling event (H1) recorded in the North Atlantic. The H1 event had effects on a worldwide scale and can be related to the Oldest Dryas cold stage. According to other coeval chronologies in the Alps (Ivy-Ochs *et al.*, 2006b; Alvarez-Solas *et al.*, 2011; Baroni *et al.*, 2014; Guillevic *et al.*, 2014; Ivy-Ochs, 2015 and references therein) the identified glacial stage can be correlated to the alpine Gschnitz stadial.

We also recognized a glacial phase (*Rino* phase) just external respect to the Ponte Faet phase that can be tentatively correlated to a more vigorous answer of the Malga Glacier to the Oldest Dryas signal, according to Castiglioni (1961) who pointed out two distinct Gschnitz oscillations in the Val Malga.

Afterwards the early Lateglacial stage, a new glacier re-advance is testified by well preserved moraines located several hundreds of meters upvalley the *Ponte Faet* phase. This lateglacial phase is here referred as "*Malga Baitone*" and it can be tentatively related to the Daun alpine stadial phase.

In the upper part of the valley we identified a phase (*Val Miller* phase) related to a third Lateglacial advance. This phase is testified by several well preserved glacial landforms and deposits (Baroni and Carton, 1990) and can be related to the last climate deterioration event of the Pleistocene, the Younger Dryas. On this basis the *Val Miller* phase can be correlated to the Egesen Alpine stadial.

The analysis of the ELA values obtained for the reconstructed glacial phases highlight a progressive rising of the ELA from the Ponte Faet phase (2380 +4,-3 m) to the Val Miller phase (2590 +5, -2) passing through the Baitone phase that recorded an ELA at 2470 (+2, -5). These ELA values are referred to the main glaciers hosted in the valley in the different steps considered. (Val Malga/ Faet, and- Miller glaciers) Results are in agreement with Castiglioni (1961) who evaluated a snowline altitude of 2400 m for the Gschnitz phase. The same Author reconstructed a snowline at 2700 m for the Daun phase, here attributed to the Egesen advance which registered an ELA at (2590 +5, -2). The ELA of glaciers originated by the separation of the Malga Baitone phase ranges from 2560 (±2) m to 2890 (+1,-8) m.

As for the Val Malga, in Val Adamè we reconstructed different glacial phases representative of the glacial answer to climate deterioration events occurred at the end of the late Pleistocene. The Oldest Dryas cold event, and therefore the alpine Gschnitz stadial, were registered by The *Saviore* phase. The glacier occupied the entire Val Adamè and a well defined tongue descended the Val Saviore for several kilometers.

A series of well preserved moraines represent the evidence of the glacial re-advance recorded as response to the second Lateglacial cold stage, related to the Daun alpine stadial. This phase (*Malga Adamè* phase) was less vigorous than the previous one, but it was strong enough for occupying the main part of the Val Adamè. A new ^{10}Be minimum limiting age of 15.0±1.0 ka (sample ADA20 on the mAda2 moraine) allows us to correlate this phase to the alpine Daun stadial. Our hypothesis is in accordance with Castiglioni (1961) and with other authors who

chronologically confine the Daun stadial to 15.5-14.7 ka time interval (Ivy-Ochs *et al*., 2004; Favilli *et al.*, 2009; Baroni *et al*., 2014).

A phase related to the Younger Dryas cold event was identified and reconstructed. The *Coster* phase was characterized by one valley glacier hosted in the upper part of the Val Adamè (Baita Adamè) and by several mountain glaciers nestled on the glacial shoulders which characterize the valley geomorphology. Our reconstructions, according to Baroni *et al.* (2014) allow us to recognize the Coster phase as the Egesen alpine stadial expression in the Val Adamè.

A set of three more samples collected on other moraines (mAda1 and mAda3) related to the Malga adamè phase provides exposure ages ranging from 12.2±0.7 ka to 11.4±07 ka.

Giving a different interpretation to the obtained exposure ages, the Malga Adamè phase could be defined as the evidence of the Egesen stadial in the Val Adamè. In this eventuality, considering the presence of a most internal phase (Coster/Baita Adamè phase), we could assume a double glacier advance recorded during the YD as documented below for the Upper Val di Sole (Adamello-Presanella Group) and the Upper Val di Peio (Ortles-Cevedale Group).

Our data indicate an ELA rising from the Saviore phase to the Malga Adamè phase, attributed to the Gschnitz and Daun phase, respectively. Considering the main Adamè Glacier only, the ELA rose about 225 m.

On the contrary, the Coster phase, related to the Egesen alpine stadial, paradoxically registered a lowering of the ELA if we consider the main glacial body only (Baita Adamè). The morphology and configuration of the glacier during the two different phases can explain this contradiction. In fact, the glacier developed during the Malga Adamè phase received the contribution of wide portions of the catchment basins covering the shoulders and located at very high elevation. These last, on the contrary, did not contribute to the Coster phase being splitted in several mountain glaciers as a consequence of the fragmentation of the ice masses developed during the previous phase.

Also the glaciers of the Val di Sole retain traces of different glacial re-advances related to the deterioration of climate events characterizing the last part of the Late Pleistocene. The first identified phase (*Vermiglio* phase) is not directly dated but ^{10}Be ages we obtained for more recent Lateglacial phases (see below) represent minimum ages of this stage that can be interpreted as the glacial response to the Oldest Dryas stage and related to the H1 North Atlantic cooling event. If this is correct, the *Vermiglio* phase can be assumed as the expression of the alpine Gschnitz stadial in the upper Val di Sole.

Later on the glaciers of this valley recorded a new advance documenting a second Lateglacial cold event that we refer as *Volpaia* phase chronologically constrained prior to 12.3±0.9 ka (sample VOL14_1 on the mVol1 moraine, fig. 5.1.2.2). This phase is tentatively correlated to the to the Daun alpine stadial.

In the Val di Sole we identified and reconstructed a double response to the Younger Dryas (YD) the last cold event of the Late Pleistocene (fig. 6.1.1). The first answer to the YD is outlined by the *Stavel* phase that finds evidences in several dated moraines (mStav1, mStav2, mPres3, mPres4). The ^{10}Be ages define the timing of this glaciers advance prior to 13.2±1.2 ka (sample STAV14.1 on the moraine mStav1). This age seems to be too old for the Egesen stadial, but the comparison with the age obtained from the sample STAV14.3 (11.8±0.9 ka) and the analysis of the uncertainties obtained show that the two dates overlap; furthermore, the mean age from the two dates (12.5 ka) fits very well with the Egesen stadial and we tentatively correlate it to the YD event. Then a second response to the YD is depicted by a series of moraines located upstream of the most external Egesen moraines and identified a new phase, the *Presena* phase. A set of three exposure ages limit the Presena phase before 10.8±0.7 ka and can represent the glaciers response in the final phase of the YD. A multiple response of the alpine glaciers to the Younger Dryas climate deterioration was detected in several sites along the Alps (Maisch, 1987; Kerschner, 2009, Ivy-Ochs, 2015) and dated at Julier Pass (Switzerland, Ivy-Ochs *el al.*, 1996), at Schönferwall and in the Larstigtal Valley (Tyrol-Austria, Ivy-Ochs

el al., 2006, 2009), at the Belalp cirque (western Alps, Schindelwig *et al.*, 2011), at Falgin cirque and Hinteres Bergle cirque (Tyrol-Austria-Italy, Moran *et al.*, 2016) and eventually in Val di Gesso (Maritime Alps, Federici *et. al.*, 2016).

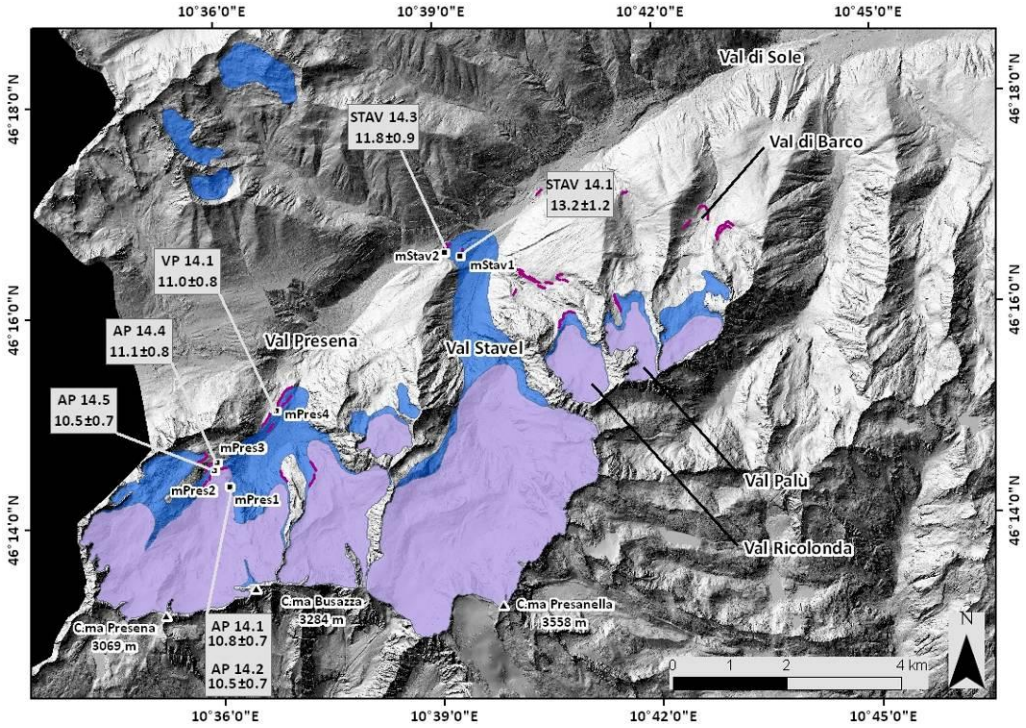

Fig. 6.1.1 - Focus on the double response of the Upper Val di Sole the Younger Dryas.

It is possible to underline a progressive rise of the ELA since the Vermiglio phase to the Presena phase. Focusing on the evolution of the main glacier of this are (Sole Glacier) and consequently on the glaciers deriving from its fragmentation, we can report an ELA rise of several hundreds of meters. In fact, since the Vermiglio phase to the Volpaia phase the Val di Sole Glacier recorded an ELA rise of ca. 80 m (the Strino Glacier derived from the fragmentation of the Sole Glacier and was nestled in the upper part of the Val Strino, with an ELA of 2550 m). The Presena and Stavel glacier of the Stavel phase had an ELA of 2450 and 2400, respectively. This condition highlight an equilibrium line variation of 200-250 m in comparison with the Vermiglio phase. Finally, the Presena phase is characterized by three glaciers deriving from the original Val di Sole Glacier. The ELA for these glaciers ranges between 2470 m and 2615 testifying a rise of 260-410 m.

In the Upper Val di Peio (upper Peio Valley-Ortles-Cevedale Group), La Mare and Careser glaciers retain traces of repeated glacier advances postdating the Last Glacial Maximum (LGM). These two glaciers have also been studied in detail for recustructing their Holocene variations (GNGFG, 1986; Carturan *et al.*, 2013a, 2014). Furthermore, the glaciers hosted in this group provide the longest record of mass-balance monitoring giving therefore the opportunity to investigate how local factors can lead to different responses to the same climate signal (Carturan *et al.*, 2013a, 2014, 2016).

During the latest Lateglacial phase the upper Peio Valley was widely glaciated. The two Lateglacial phases detected and dated with SED for La Mare Glacier (Ponte di Pietra I phase and Ponte di Pietra II phase) allow to identify a double response to the Younger Dryas.

Geomorphological evidences, supported by Surface Exposure Dating, allow us to identify the traces of the Egesen alpine stadial of La Mare Glacier, correlated to the Younger Dryas cold stage. The moraine related to this phase supplied a minimum age of 12.2±0.7 ka. Our chronological constraint of the Egesen stadial finds support and good correlation with exposure ages from the Val di Rabbi (Favilli *et al.*, 2009). In this area, located some kilometers North-East of the Upper Val di Peio authors define the timing for the Egesen around 11.7±1.2 ka. Moreover in the Upper Val di Peio (La Mare Glacier), as for the Upper Val di Sole, a multiple response to the YD can be depicted (fig. 6.1.2). In fact, a well defined position of La Mare Glacier, represented by the moraine MLm4, located in between the first Egesen ones (Ponte di Pietra I phase) and the LIA, stabilized no later than 11.1±0.5 ka. This glacier position can represent a glaciers expression of the final phase of the Egesen related to a delayed effect of the YD event. Furthermore, the exposure ages related to the moraine MLm3, located just internally to the MLm1 and constrained before 11.0±0.9 ka, enforce our hypothesis providing a further minimum age for the phase represented by MLm4.

The second response to the YD signal in La Mare Valley (Ponte di Pietra II phase) finds its correspondent in Val Venezia, where the Careser Glacier settled its terminus ca. 600 m below the LIA extent before 10.5±0.4 ka.

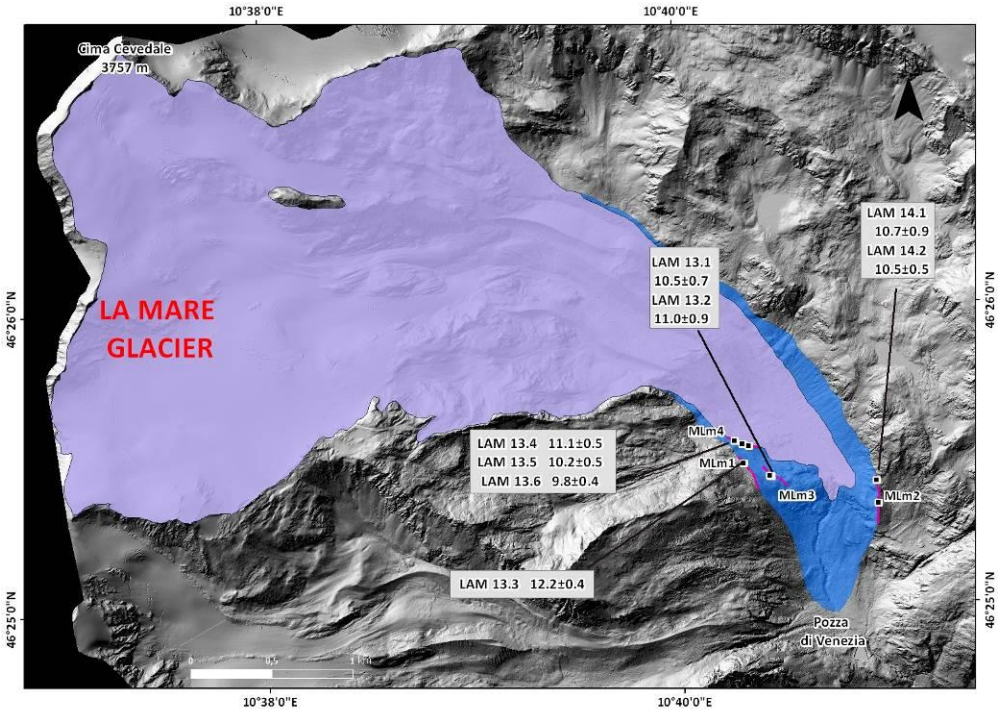

Fig. 6.1.2 - Focus on the double response of the Upper Val di Peio (La Mare Glacier)to the Younger Dryas.

After the Egesen, glaciers in upper Peio Valley melted back to minimal Holocene positions. The timing of the deglaciation is provided by a radiocarbon date obtained by Carturan *et al.* (2014) from an organic layer directly on top of glacial deposits. The section is located just internal to the reconstructed Ponte di Pietra II phase position of La Mare Glacier and testifies that the glacier retreated before 9215±125 ^{14}C yr BP, corresponding to 10,167-10,737 cal BP. Since then on, the Pian di Venezia area was deglaciated.

The ELA of La Mare Glacier recorded at the Egesen stadial was depressed by ca. 230 m compared to the LIA maximum extension. The ELA calculated for the Egesen phase is related to the most advanced reconstructed position of La Mare Glacier and stands at lower altitude of ca. 600 m and 395 m compared to the median altitude of the northernmost and southernmost ice body of present day (2012) glacier (Carturan *et al.*,

2014). Median altitude is approximately equal to the balanced-budget Equilibrium Line Altitude (Braithwaite and Raper 2009, in Carturan *et al.*, 2014). Our results are supported by data from different sites on the alpine chain (figg. 6.1.3, 6.1.4). Similar values of ΔELA LIA are recorded in the central sector of the Alps, clustered between -220 m and -250 m.

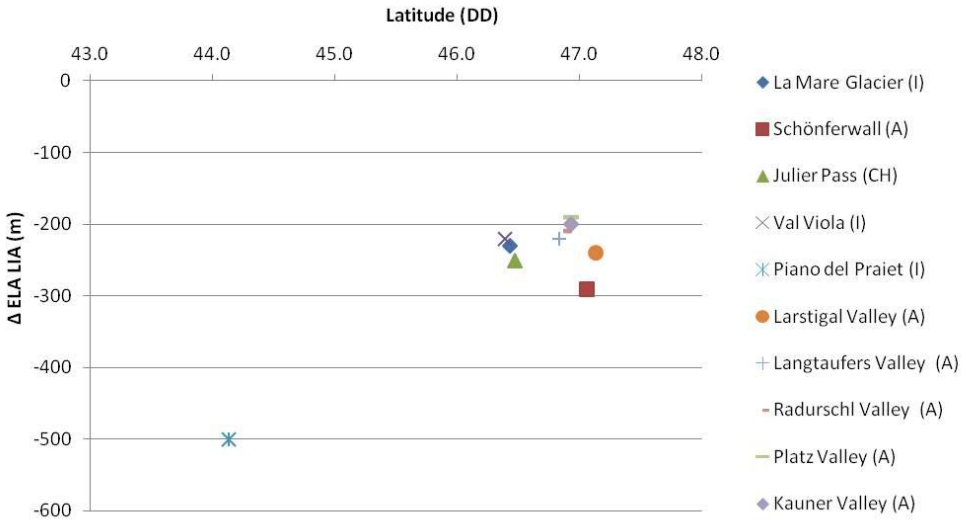

Fig. 6.1.3 - Egesen ΔELA distribution related to the latitude. Values of ELA and references are reported in Table 6.1.1.

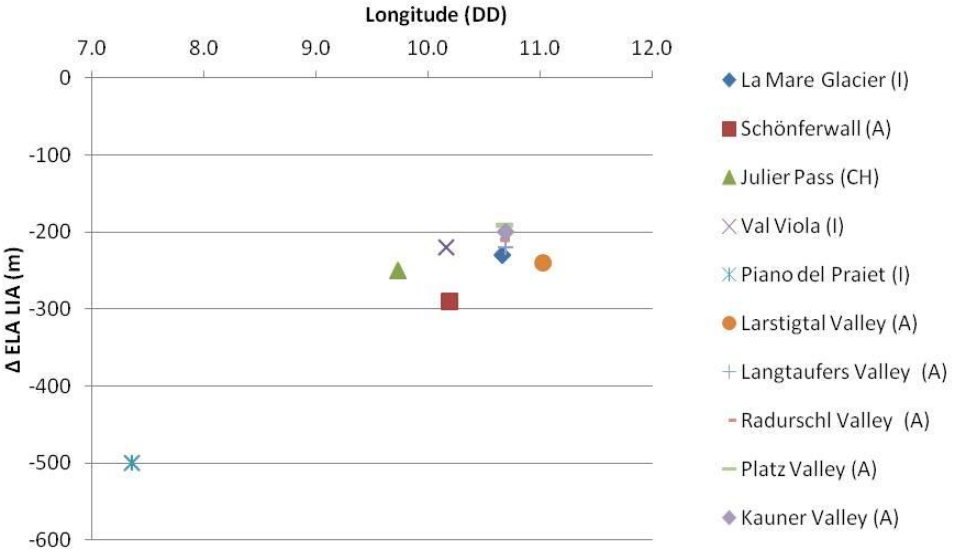

Fig. 6.1.4 - Egesen ΔELA distribution related to the longitude. Values of ELA and references are reported in Table 6.1.1.

Site	Associated phase	ELA(m a.s.l.)	ELA LIA(m a.s.l.)	ΔELA LIA (m)	Reference
La Mare Glacier	Egesen(Ponte di Pietra I)	2823	3051	-228	This work
La Mare Glacier	Egesen(Ponte di Pietra II)	2912	3051	-139	This work
Careser Glacier	Egesen(Ponte di Pietra II)	2849	3025	-176	This work
Schönfewall	Egesen	-	-	-290	Ivy-Ochs *et al.*,2006
Julier Pass	Egesen	-	-	-250	Ivy-Ochs *et al.*, 1996,2006
Val Viola	Egesen	-	-	-220	Hormes *et al.*, 2008 in Ivy-Ochs *et al.*, 2009
Piano del Praiet	Egesen	2305	2810	-505	Federici *et al.*,2016
Largistal Valley	Egesen	2480	2720	-240	Ivy-Ochs *et al.*, 2009
Langtaufers Valley	Egesen	2650	2870	-220	Moran *et al.*, 2016
Radurschl Valley	Egesen	2610	2820	-210	Moran *et al.*, 2016
Platz Valley	Egesen	2590	2780	-190	Mauntner, 2012 in Moran *et al.*, 2016
Kauner Valley	Egesen	2660	2870	-210	Kerschner, 1979 in Moran *et al.*, 2016

Table 6.1.1 -. Reconstructed ELA based on the accumulation area ratio of 0.67. ΔELA is based on LIA ELA as reference

In terms of absolute ELA, values recorded on La Mare Glacier result ca. 200 m higher compared to the available data from published studies (tab.6.1.1). The southernmost location and aspect of the glacier could explain this remarkable difference of ELA elevation. Comparing the two Egesen reconstructed phases of La Mare Glacier we can recognise an ELA rising of 90 m, an areal reduction of ca. 0.7 km^2, and a volume variation estimated in 0.15 km^3.

6.2 Antarctica

6.2.1 LGM and deglaciation of the Victoria Land

As it concerns the Antarctic section of this research project we studied the glacial evolution of key sectors of the Victoria Land. We obtained new data concerning the glacial history of: i) the southern Victoria land, where ice streams and outlet glaciers cross the Transantarctic Mountains and drain the EAIS (to the South of Terra Nova Bay), and ii) the northern Victoria Land (to the North of Terra Nova Bay), where a dendritic network of glacial valleys has no direct relation with the EAIS and is fed by extensive ice fields and local névés. We found new evidences of several glacial phases registered by the complex Antarctic system in the Victoria Land. New data enrich our knowledge on the glacial dynamics embracing a long

time interval of the Late Cenozoic (spanning from thousands to millions of years)

In terms of timing and extension of glacial bodies in Antarctica, the last glacial maximum (LGM) was not homogeneous over the entire continent. The ice sheets did not reach everywhere the continental shelf and the deglaciation was not synchronous all over the Antarctic margin (Clark *et al*., 2009; The RAISED Consortium, 2014).

Nevertheless we can affirm that during the LGM the EAIS and WAIS advanced over the Ross Sea for ca. 1000 km, occupying almost the entire continental shelf (Stuiver *et al.,* 1981; Orombelli *et al.*, 1990; Denton and Hughes, 2000; Anderson *et al*., 2002, 2014; The RAISED Consortium, 2014 and references therein). The grounding line was located in proximity of Coulman Island (western coast, 73°S) and glaciers hundreds of meters thicker than today (i.e in the Terra Nova Bay area, Orombelli *et al.*, 1990) covered the coastal areas. Several thousands of years after the LGM, the Victoria Land sector registered a progressive deglaciation. According to Conway *et al.* (1999), the LGM condition in the Ross Sea were maintained from ca 27.8 to 12.8 ka. These dates are strongly supported by a huge set of data from the Dry Valleys (Denton and Hughes, 2000; Denton and Marchant, 2000; Dochat *et al.,*2000; Hall and Denton, 2000a,b; Hall *et al.*, 2000) where the LGM was bracketed in a similar interval of ca. 26.9-12.7 ka (Denton and Marchant, 2000) with the Ross ice sheet extended North of Ross Island and across the McMurdo Sound to Taylor Valley at 16.6-12.7 ka. The ice sheet remained mostly intact until 8.3 ka when the deglaciation process started (Hall and Denton, 2000a).

Since about 12.8 to 3.2 ka the grounding line of the Ross IceShelf retreated from Coulman Island to its present position (Conway *et al.*, 1999). Along the Victoria Land coast, deglaciation was accomplished at about 8 ka BP (Baroni and Orombelli, 1991, 1994; Baroni and Hall, 2004) while deglaciation was completed on the Scott Coast about 500-700 years later (Hall and Denton, 2000, Hall *et al.*, 2004). At Terra Nova Bay, on the Northern Foothills, the LGM is bracketed by a maximum limiting age of 25.6 ka furnished by shells collected in the younger drift and by minimum

limiting ages of 7.5-8 ka supplied by shells in marine sediments and penguin remains collected from relict colonies in coastal areas (Orombelli *et al.*, 1990; Baroni and Orombelli, 1991; 1994).

New data here presented strongly enrich the already existing glacial chronology for the Victoria Land. In fact, we obtained evidences of the LGM signal, related to the Marine Isotope Stage 2 (MIS2), but also of the subsequent deglaciation process.

Concerning the southern Victoria Land, set of four ages from samples collected on Ross Island (CB111220.05, CB111220.07, CB120101.03 and CB130101.01) identify the transition between the LGM and the beginning of the deglaciation. ^{10}Be ages clustered this time interval between 18.9±1.3 ka and 14.6±1.1 ka (tab.5.2.2.7, fig. 5.2.2.6). The latter date can be assumed as minimum limiting age for the LGM in the study area. It is worthy to note that a group of other four dates (CB111215.02, CB120101.06, CB121220.03, CB130101.02) cluster between 12.9 and 11.9 ka.

These latter ages can be interpreted as minimum limiting ages for enforcing the interpretation of a prolonged permanence of the marine based Ross Ice Sheet in the Mc Murdo Sound area (Denton and Hughes, 2000; Denton and Marchant, 2000; Dochat *et al.,*2000; Hall and Denton, 2000a,b; Hall *et al.*, 2000).

The bracketing limiting ages of the LGM in this area are indicated in previous works (Orombelli *et al.,* 1990; Di Nicola *et al.*, 2009) and new data from this work allow us to constrain LGM time extension from 26 ka to ca 15 ka. In fact, radiocarbon dates from shells included in the Terra Nova Drift provided maximum ages for the beginning of the LGM of ca. 25.6±0.2 ka BP (Orombelli *et al.*, 1990). The date of 16.3 ka at Cape Sastrugi would represents a minimum limiting age for the maximum extension of glacial bodies in the lower margin of the Priestley Glacier. Another ^{10}Be age from Black Ridge (recalculated with the parameters adopted at ETH after April 2010 and with the 2.3 version of Cronus Earth) furnishes a similar minimum age (14.6 ka) for the LGM in the Terra Nova Bay area (Oberholzer *et al*. 2003; Balco *et al.*, 2009).

Landscape features and glacial deposits related to Lateglagial re-advances are not yet nor clearly recognized nor chronologically constrained on the Antarctic continent. The entity of the contribute of the Antarctic Cold Reversal to glacial readvance is still under debate. This event that interrupted the last deglaciation trend and correspond to a well identified cold period, finds expression in the ice cores and can be bracketed between 14.7 and 13 ka (Pedro *et al.*, 2016) In this framework, four dates (CB111215.02, CB120101.06, CB121220.03, CB130101.02;(see tab 5.2.2.7 and fig. 5.2.2.6) that we obtained from erratic boulders located in the Ross Island area provide ages ranging between 12.9 ka and 11.9 ka can be tentatively interpreted as minimum ages for constraining the readvance eventually If our interpretation is correct, we are dealing with the first identification of evidence related to the response of the Antarctic ice sheet to the Antarctic Cold Reversal.

In any case, the deglaciation processes occurred after the LGM endured also until the Early Holocene and followed complex dynamics. Along the East Antarctic margin there are evidences of a different timing of glacial retreat retreat (RAISED Consortium, 2014). Concerning the study area we are able to assert that the deglaciation of the coastal areas started ca. 17/16 ka and was completed ca. 7-8 ka. Several ^{14}C dating on penguin guano, animal remains and marine shells outlined an age for the Terra Nova Bay raised beaches of 7-8 ka (Orombelli *et al.*, 1990; Baroni and Orombelli, 1991; Baroni and Hall, 2004).

In this framework we obtained a set of six ages from erratic boulders from Cape Sastrugi that provide new data about the glacier regression after the LGM. In fact, these samplesidentified a glacial limit attested around 8 ka that can be interpreted as a period of permanence or eventually of short readvance (?) of the glaciers registered in a general retreat trend during the Early Holocene (fig. 5.2.2.2, tab. 5.2.2.2). The latter glacial limit is outlined by the distribution of ^{10}Be apparent exposure ages (fig. 6.2.1.1) obtained from Cape Sastrugi erratic boulders. During this time interval the coastal areas were also under deglaciation and reached characteristics similar to the present day conditions only at about 7.5 ka (Orombelli *et al.*,

1990; Anderson *et al.* 2014). New dated samples from Cape Sastrugi come from previously glaciated benches (at 170-330 m a.s.l.) that became ice free after about 8 ka. They document a rapid lowering of the glacial surface of at least 100-200 m in a very short time interval, approximately confined at less than 1 ka (between ca 8 and 7.5 ka).

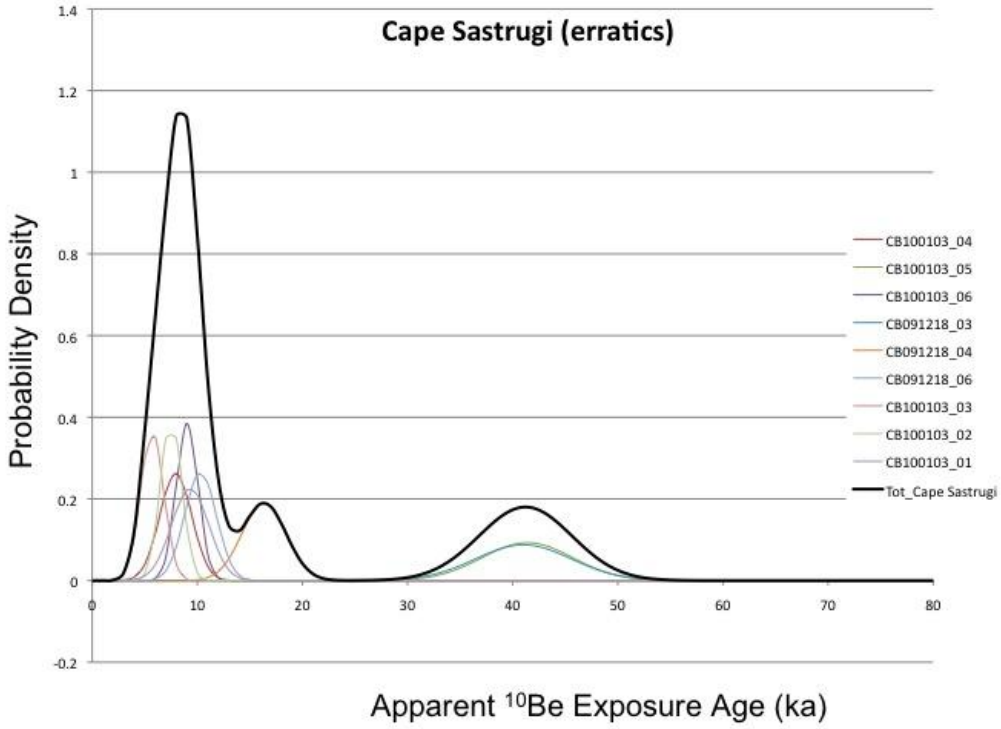

Fig. 6.2.1.1 – Probability density plot ^{10}Be apparent exposure ages of Cape Sastrugi erratics. Thin lines are probability curves for individual samples. Bold black line is the summed probability. The probability density shows two different glacial phases attested around 8 ka and 40 ka, respectively

6.2.2 Late Pleistocene polyphasic glacier advances (pre-dating the LGM)

The dating of a set of samples (5) collected in the Cape Sastrugi area and at the Lichen Hills define a time interval of (90)70-40 ka. In this time interval we are able to identify at least two, possibly three distinct glacial phases. Two erratic boulders (CB091218.03, CB100103.05) collected from the Cape Sastrugi area provide an age of ca. 40 ka (fig. 6.2.1.1), documenting a glacial advance and pre-dating the LGM and the Marine Isotope Stage 2 (MIS2). Two ages from the Lichen Hills (CB091228.16, CB 091228.17-erratic boulders; tab 5.2.2.3, fig. 5.2.2.3) provide evidence of a glacial

phase occurred before 54.9±6 ka. This phase can be related to the Marine Isotope Stage 4 (MIS4). A third glacial phase is documented by an exposure age of 88±9 ka obtained from a boulder related to the younger drift on the Lichen Hills (fig. 6.2.1.2). If this interpretation is correct, the drift dated at >90 ka can be related to the oldest cold period occurred during the early Late Pleistocene.

On the basis of new dates, the glacial phases described above evidence a polyphasic evolution of the Younger Drift, also indicated as Terra Nova Drift I (Denton *et al.*, 1975; Stuiver *et al.*, 1981; Orombelli *et al.*, 1990). The younger drift was deposited by glaciers ticker than the present ones and related to the advance of the marine based Ross Ice Sheet (Denton *et al.*, 1989; Orombelli *et al.*, 1990). The identified glacial phases can be assumed as evidences of different glacial advances embracing the entire Late Pleistocene. This interpretation can be further confirmed by a multi nuclide approach, but our interpretation of the multitemporal origin of the Younger Drift finds support in other dates previously obtained in the same area. In fact, deposits with similar characteristics have been dated in several sites of the Victoria Land (i.e. Mount Keinath, Anderson Ridge, Mount Emison, Ricker Hills) providing ages ranging between 50 ka and 70 ka. (Oberholzer *et al.*, 2003; Di Nicola, 2007; Strasky, 2008; Strasky *et al.*, 2009). In some cases the surface exposure dates underline a complex exposure history of the studied sites (Northern Foothills, Di Nicola *et al.*, 2009), but other cases support the interpretation that the drift was deposited during different glacial phases ranging from the LGM to older phases (Oberholzer *et al.*, 2003; Di Nicola, 2007).

6.2.3 Middle Pleistocene

A set of ages obtained from erratic boulders (9) and bedrock (1) collected in the northern Victoria Land (Frontier Mountains, Miller Butte and Brien Rocks) and southern Victoria Land (Ross Island), provided dates referable to the Middle Pleistocene spanning from ca. 120 ka to ca. 400-450 ka.

These ages are grouped for evidencing different glacial phases occurred during the depicted time interval.

The first group is constituted by ages obtained from samples collected at the Frontier Mountains (CB091206.17, CB091206.19) and Miller Butte (CB091229.02) Exposure ages range between 186±10 ka and 123±7 ka (tabb. 5.2.2.5, 5.2.2.6, 5.2.2.5.7) The latter time interval enable us to propose a glacial phase occurred around **180-120 ka**. Two dates from Ross Island (CB121220.07, CB111221.01) further confirm the identification of this glacial phase also recordeb by the marine-based Ross Ice Sheet. In fact, this "180-120" glacial phase finds correspondence in other studied sites ib the Terra Nova Bay area. ^{10}Be ages from Mount Abbott and Mount Browning provide time intervals of 165±11-135±13 ka and 136±11-128±12 ka, respectively (Di Nicola *et al.*, 2009) for the advance of the marine based Ross Ice Sheet on the Northern Foothills (Orombelli *et al.*, 1990). A ^{21}Ne age from Black Ridge of 145±33 ka enforces this interpretation also considering the contribute of the Priestley outlet Glacier (Oberholzer *et al*., 2003).

Also a second group of exposure dates is defined by the ages obtained at Frontier Mountains (CB091206.18), Miller Butte (CB091229.01) and Ross Island (CB121220.04) sites. These dates identify a time interval spanning from 332±19 ka to 273±15 ka and can be correlated to glaciation attested around **280** ka (fig. 6.2.1.2), tentatively correlable to MIS 8.

Furthermore, on Brien Rocks, the bedrock sample (CB091206.03) dated with a multi-nuclides approach furnished ^{10}Be and ^{26}Al ages of 348±36 ka and 338±49 ka, respectively. The good data correlation between the two nuclides allow us to speculate a simple exposure history and consequently that the ice sheet did not override the sampled area since at least 348±36 ka. This date represents a minimum limiting age for the glacial phase responsible of the areal scouring (MIS 10?). The multinuclide dates obtained at Brien Rocks strongly support the evidence that the Priestley Névé, and consequentely the EAIS did not overrode the area after ca 350 ka. Therefore, during the last three glacial cycles the elevation and thickness of the EAIS at the head of the Priestley Glacier and in the vicinity of Talos Dome did not increase more than ca 100 m.

A sample from Miller Butte (CB091229.03) presented an exposure age of 413±44 ka that could be an evidences of an older glacial advance, eventually supported by a similar age obtained at Mount Abbott (473±30 ka, Di Nicola *et al*. 2009).

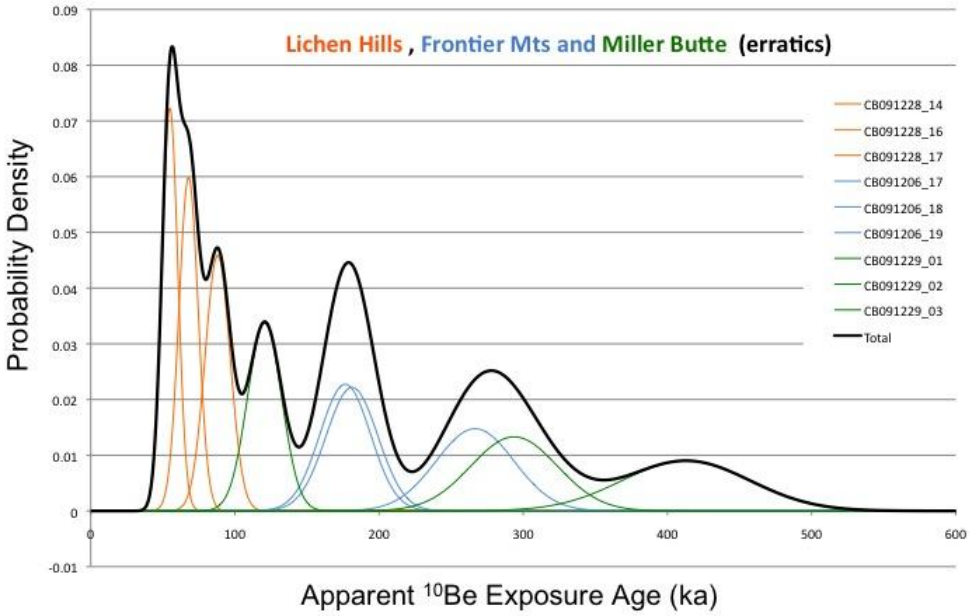

Fig. 6.2.1.2 – Probability density plot ^{10}Be apparent exposure ages of Lichen Hills, Frontier Mts. And Miller Butte erratics. Thin lines are probability curves for individual samples. Bold black line is the summed probability.

6.2.4 Relict surfaces

Exposure ages from relict surfaces collected on the Miller Butte and Frontier Mountains tell us an older story, in the order of millions of years (tabb. 5.2.2.5, 5.2.2.6; fig. 5.2.2.4, 5.2.2.5). The five dates obtained from the Miller Butte range from 823±97 ka (CB091229.07) to 2.3±0.4 Ma (CB091229.04). These results indicate that the sampled portions (ca. 2900 m a.s.l.) of the nunatak are ice free at least since 2.3±0.4 Ma (CB091229.04), an age much older if we would correct the dates for the erosion rate. Also applying a minim erosion rate of 5 cm/ Ma as calculated for the Mt. Pollock and Archamboldt Ridge, the new obtained age would be ca. 3 Ma.

The oldest bedrock surface was dated at the Frontier Mountains. The ages obtained cover a time interval of 3.4±0.9 Ma (CB091206.10) to 5.1±2.3 Ma.

(CB091206.11). Also in this case an erosion correction would provide a much older age. Applying a very low erosion rate of 5 cm/Ma the two oldest samples of this group (CB091206.09, CB091206.11) are close to the application limit of the method, and the data calculation system is not capable to provide the ages. This evidence indirectly confirms the very long exposition time of the samples. Instead the same correction for erosion rate applied on sample CB091206.10 supplied an age of ca 6.4±3.6 Ma supporting the hypothesis of a prolonged exposition to the cosmic radiation.

These samples were collected at higher altitude (ca. 3200 m a.s.l) compared to the Miller Butte samples and allow us to assert that the ice sheet did not surmount the reliefs during at least the last 6 Ma. Multinuclides dates from similar landscape features further testify that the relict surfaces are continuosly exposed since a very long time. This evidence is very common in the Victoria land as previously documented at Mount Keinath and Mount Abbot that provided minimum exposure ages of 2.6 Ma and 3.5 Ma, respectively (Oberholzer *et al.*, 2003, 2008).

Furthermore, Di Nicola *et al.* (2009) obtained exposure ages of 5.8±0.4 Ma for Mount Abbott and of 6.1±0.6 Ma for Mount Keinath (this value was obtained recalculating the ages obtained by Oberholzer *et al.*, 2003). The same authors (Di Nicola *et al.*, 2012) indicate that the relict landscape features of the highest peaks (Mount Pollock, Archambault Ridge) of the Deep Freeze Range were exposed since 5-7 Ma with a denudation rate in the order of 5cm/Ma.

On this basis we can speculate that over the studied areas a regime of cold and arid desert characterized by very low erosion rates persists since a period at lest of 5-7 Ma and that cold-based glacial condition at the margin of the EAIS in northern Victoria Land endured since at least the Late Miocene.

7 -Conclusions

The availability of dated continental proxies provides the possibility to constrain and correlate palaeoclimatic events along wide and different geographical domains. This can contribute in investigating the dynamics of the cryosphere response to the climate changes both at local and global scale. The high detail provided by continental records of past glaciers in key sites of the Rhaetian Alps turns out as a crucial element to enrich the knowledge about the Lateglacial evolution of the glaciers in the Central Italian Alps and about the correlation with relevant palaeoclimatic events occurred during the Late Pleistocene. At the same time the dating of glacial features of selected sites of the Victoria Land (Antarctica) furnish new evidences on the behavior of the EAIS along a huge time interval.

In this work the Lateglacial history of sectors of the Ortles-Cevedale and Adamello-Presanella massifs is reconstructed and constrained by Surface Exposure Dating. Furthermore we propose evidences of the northern and southern Victoria Land Late Cenozoic glacial evolution. The obtained data represent a new relevant piece in the comprehension of the evolution of the glacial system in the investigated sectors. In particular ^{10}Be (^{26}Al) ages obtained for the Antarctic continent cover a time range since the late Miocene to the Holocene.

The conclusions of this thesis are synthetically described here below

- A quantitative reconstruction of glaciers in key sites of the Ortles-Cevedale (Upper Val di Peio) and Adamello-Presanella (Val di Sole, Val Malga, Val Adamè) massifs. Glaciers maximum positions and relative ELAs were reconstructed for each phase and chronologically constrained in the Lateglacial context with the support of Surface Exposure Dating.

- A polyphasic Lateglacial evolution of the studied alpine areas. Geomorphological and glacial-geolocical evidences, supported by a set of ^{10}Be ages allow us to identify three main stages that find correlation with the most relevant climate deterioration

events occurred at the end of the Pleistocene that testify periodical changes in the North Atlantic circulation. We detected also a double response of the glaciers (Val di Sole, Alta Val di Peio) to the Younger Dryas cold stage.

- A georeferenced GIS database of the SED ages available for the Victoria Land that contains data related to the samples characteristics, exposure ages obtained and relative bibliographic references.

- New evidences for the EAIS evolution chronology. ^{10}Be and ^{26}Al dates allow us to identify different glacial phases in a large time interval, providing new data on the EAIS evolution. We present ages constraining the LGM and the subsequent deglaciation evolution in the southern and northern Victoria Land. The poliphasic evolution of the Younger Drift is outlined by a series of glacial phases occurred also before the LGM. We also provide evidences of different glacial advances occurred during the Middle Pleistocene. The dating of relict surfaces confirms a prolonged exposure history of the sampled reliefs and the permanence of cold and arid climate conditions since million years.

Alps

A polyphasic Lateglacial evolution of the glaciers in the study sites at the end of the Pleistocene is outlined. A first Lateglacial stage was reconstructed and constrained for three valleys of the Adamello-Presanella Massif. During this early Lateglacial stage the reconstructed glaciers reached an extension of ca. 94 km^2. This phase is here confined by ^{10}Be before 15.7±1.2 ka (Ponte Faet phase, Val Malga) and is related to the Oldest Dryas cold stage and to the Alpine Gschnitz stadial.

Subsequent to a general reduction that followed the first Lateglacial stage, the glaciers recorded a new re-advance. This second Lateglacial stage is reconstructed for the studied Adamello-Presanella valleys and presents a

total extension of ca. 73 km^2. Comparing the ice covered areas of the two phases it is possible underline a difference of ca. 22% of glacial extension. This re-advance is constrained prior to. 15±1.0 ka (Malga Adamè phase, Val Adamè) and can be tentatively related to the Alpine Daun stadial.

The glacial answer to the Younger Dryas signal is identified and constrained in the four valleys. In the Adamello-Presanella sectors, the glaciers reached an overall extension of ca. 41 km^2, corresponding to the 44% of the Gschnitz stadial extension. This phase is bracketed between 13.2±1.2 and 10.5±0.8 ka and is referable to the Egesen Alpine stadial.

A double response to the Younger Dryas is identified in the Val Di Sole (Adamello-Presanella) and in the Alta Val di Peio (Ortles-Cevedale). This phase can be considered as a second Egesen stadial and finds expression in well preserved moraines located between the LIA and the most external Egesen moraines. This phase is here limited between 11.1±0.8 and 9.9±0.6 ka. The latter re-advance can be correlated to the the final phase of the YD signal and the glacier reached extensions proximal to the most extended Egesen positions.

During the Egesen stadial the ELA in the upper Val di Peio was ca. 2820 m a.s.l. (Ponte di Pietra I phase) , about 200 m higher than other sites in the innermost Alps. Instead, in terms of ΔELA results are in agreement with different sites on the Alpine chain (Maisch, 1987; Kerschner, 2009, Ivy-Ochs, 2015, Ivy-Ochs *el al.*, 1996, 2006, 2009; Schindelwig *et al.*, 2011, Moran *et al.*, 2016). At the end of the Late Pleistocene (during the Ponte di Pietra II phase) glaciers in the upper Peio Valley recorded a rising of the ELA of less than 100 m compared to the first and most vigorous expression of the Egesen stadial (Ponte di Pietra I phase).

During the Lateglacial phases, La Mare and Careser glaciers had a similar behavior. The two glaciers reacted differently to the same climate change only since the LIA, due to different ELA variation of the two glaciers. In fact, today La Mare Glacier preserve ca. 45% of its latest Pleistocene extension, compared to the 20% of Careser Glacier (Carturan *et al.*, 2013, 2014; Salvatore *et al.*, 2015). Aspect and topography of the hosting valleys

are relevant factors in driving the glacier evolutions since last decades but they did not induce a different behavior during the Lateglacial.

Antarctica

The dating of glacial features in selected sites of the Victoria Land (East Antarctica) provides evidences about several glacial phases of the Antarctic Ice Sheets evolution.

We present data concerning the LGM signal, related to the Marine Isotope Stage 2 (MIS2). In southern Victoria Land the 18.8-14.5 ka time interval indicate the permanence on Ross Island of the marine based Ross Ice Sheet. In the same area, a set of dates identifies a time period between 12.9 and 11.9 ka that can be assumed as minimum limiting age for further permanence of the marine-based Ross Ice Sheet in the McMurdo Sound area. On the other hand, this dates can tentatively be interpreted as the first evidence on land of a glacial advance of Antarctic glaciers in response to the Antarctic Cold Reversal.

Concerning the northern Victoria Land a 26/15 ka time interval is proposed for limiting the LGM. Since then, glacial reduction was ongoing; a period of interruption of the general deglaciation trend (or eventually a slight re-advance) is detected at ca 8 ka in the Cape Sastrugi area referring to the Priestley outlet Glacier . This evidence support the hypothesis that the coastal areas reached conditions similar to the present day only at 8-7.5 ka. A lowering of the glacial surface of ca. 100-200 m occurred in a very short time interval (less than 1 ka from ca 8 ka to 7.5 ka).

A polyphasic evolution of the Younger Drift is detected and defined with two or even three glacial phases. Our data identify a phase (ca. 40 ka, Cape Sastrugi) that pre-date the Marine Isotope Stage 2 (MIS2) with glacier condition similar to those registered at ca 8 ka. A second phase (before 55 ka), identified at Lichen Hills is correlable to the Marine Isotope Stage 4 (MIS4). A third phase can be tentatively constrained at ca. 90 ka (Lichen Hills). If confirmed, the latter phase can be correlated to the oldest cold period occurred during the early Late Pleistocene. These conditions outline three distinct glacial phases occurred during the Late Pleistocene.

Multiple glacial phases characterized the Middle Pleistocene glacial dynamics of the study areas. The obtained ages span over the 420-120 ka time interval and can be interpreted as evidences of different glacial phases along the entire Victoria Land. A younger, glacial advance testified by ages obtained from Miller Butte, Frontier Mountains and Ross Island, can be limited in the 180-120 ka time interval and is tentatively correlable to MIS 6. A second phase finds expression in the same sectors and could be attested around 280 ka (MIS 8). The multinuclide approach applied on the Brien Rocks sample support the hypothesis that the Priestley Névé and the EAIS did not overrode the area after ca 350 ka (MIS 10?). This condition allow us to speculate that the elevation and thickness of the EAIS at the head of the Priestley Glacier did not recorded an increasing bigger than ca 100 m during the last three glacial cycles. A third phase can be speculated with an age older than 400 ka.

The dating of relict surfaces located at high elevations (2900-3200 m a.s.l.) of the Miller Butte and Frontier Mountains reliefs testify a prolonged exposition to the cosmic radiation. The oldest age obtained indicate that the Frontier Mountains sampled area is continuously ice free since 5.1±2.3 Ma. The new data, correlated with available ages from other sites (i.e. Mount Abbot, Mount Keinath, Mount Pollok, Archambault Ridge), demonstrate conditions of cold and arid desert persisting since at least 5-7 Ma along the Victoria Land both in coastal areas and at the margin of the East Antarctic Ice Sheet.

8 -References

Ajassa, R., Biancotti, A., Biasini, A., Brancucci, G., Caputo, C., Pugliese, F., Salvatore, M.C. (1994) - *Il Catasto dei Ghiacciai Italiani: Primo Confronto tra* i dati 1958 e 1989. Il Quaternario, AIQUA, 7(1), 497-502.

Ajassa, R., Biancotti, A., Biasini, A., Brancucci, G., Carton, A., Salvatore, M. C. (1997) - *Changes in the number and area of Italian alpine glaciers between 1958 and 1989*. Geografia Fisica e Dinamica Quaternaria, 20, 293 – 297, 6 figg., 4 tabb.

Akçar, N., Yavuz, V., Ivy-Ochs, S., Kubik, P.W., Vardar, M., Schlüchter, C. (2007) - *Paleoglacial records from Kavron valley, NE Turkey: field and cosmogenic exposure dating evidence.* Quaternary International, 164-165, 170-183.

Akçar, N., Yavuz, V., Ivy-Ochs, S., Reber, R., Kubik, P. W., Zahno, C., Schlüchter, C. (2014) - *Glacier response to the change in atmospheric circulation in the eastern Mediterranean during the Last Glacial Maximum.* Quaternary Geochronology, 19, 27-41.

Akçar, N., Yavuz, V., Yeşilyurt, S., Ivy-Ochs, S., Reber, R., Bayrakdar, C., Kubik, P.W., Zahno, C., Schlunegger, F., Schlüchter, C. (2016) - *Synchronous Last Glacial Maximum across the Anatolian peninsula.* In: Hughes, P. D. and Woodward, J. C., Eds. (2016) - Quaternary Glaciation in the Mediterranean Mountains. Geological Society, London, Special Publications, 433, SP433-7.

Álvarez-Solas, J., Montoya, M., Ritz, C., Ramstein, G., Charbit, S., Dumas, C., Ganopolski, A. (2011) - *Heinrich event 1: An example of dynamical ice-sheet reaction to oceanic changes.* Climate of the Past, 7(4), 1297-1306. doi:10.5194/cp-7-1297-2011

Anderson, J.B. (1999) - *Antarctic Marine Geology*. Cambridge, Cambridge University Press, pp. 289

Anderson, J.B., Bartek, L.R. (1992) - *Cenozoic glacial history of the Ross Sea revealed by intermediate resolution seismic data combined with drill information.* Antarctic Research Series 56, 231-263.

Anderson, J.B., Conway, H., Bart, P.J., Vitus, A.E., Greenwood, S.L., McKay, R.M., Hall, B.L., Ackert, R.P., Licht, K., Jakobsson, M, Stone, J.O. (2014) - *Ross Sea paleo-icesheet drainageand deglacial historyduring and since LGM.* Quaternary Science Review 100 (2014), 31-54.

Anderson, J.B., Shipp, S.S., Lowe, A.L., Wellner, J.S., Mosola, A.B. (2002) - *The Antarctic Ice Sheet during the Last Glacial Maximum and its subsequent retreat history: a review.* Quaternary Science Reviews 21, 49-70.

Armienti, P. and Baroni, C. (1999) - *Cenozoic climatic change in Antarctica recorded by Volcanic activity and landscape evolution.* Geology 27, 617-620.

Armienti, P., Ghezzo, C., Innocenti, F., Manetti P., Rocchi, S., Tonarini S. (1990) - *Paleozoic and Cainozoic intrusives of Wilson Terrane: geochemical and isotopic data.* Mem. Soc. Geol. It., 43, 67-75.

Balco, G., Briner, J., Finkel, R.C., Rayburn, J.A., Ridge, J.C., Schaefer, J.M. (2009) - *Regional beryllium-10 production rate calibration for late-glacial northeastern North America.* Quaternary Geochronology, 4, 93-107.

Balco, G., Stone, J.O., Lifton, N.A., Dunai, T.J. (2008) - *A complete and easily accessible means of calculating surface exposure ages or erosion rates from ^{10}Be and ^{26}Al measurements.* Quaternary Geochronology, 3, 174-195.

Ballantyne, C.K. and Stone, J.O. (2012) - *Did large ice caps persist on low ground in northwest Scotland during the lateglacial interstade?* Journal of Quaternary Science, 27, 297-306.

Bamber, J. L., Vaughan, D. G., and Joughin, I. (2000) - *Widespread complex flow in the interior of the antarctic ice sheet*. Science, 287, 1248−1250.

Baroni, C. (1987) - *Geomorphologic map of the Northern Foothills near the Italian Station, (Terra Nova Bay, Antarctica).* Memorie della Società Geologica Italiana 33, 195-211.

Baroni, C. (2001) - *Antartide, terra di scienza e riserva naturale.* Terra Antartica publication, pp. 280.

Baroni, C. (2010) – *La risposta dei ghiacciai alpini alle variazioni climatiche.* Geoitalia, vol. 32, Settembre, 50 – 52.

Baroni, C. (2013) - *Climate change impacts on cold climates.* In: Shroder, J. (Editor in Chief), Giardino, R., Harbor, J. (Eds.), Treatise on Geomorphology. Academic Press, San Diego, CA, vol. 8, Glacial and Periglacial Geomorphology, 430−459.

Baroni, C., Armiraglio, S., Gentili, R., Carton, A. (2007) - *Landform–vegetation units for investigating the dynamics and geomorphologic evolution of Alpine composite debris cones (Valle dell'Avio, Adamello Group, Italy).* Geomorphology, 84, 59–79.

Baroni, C., Carton, A., Seppi, R. (2004) - *Distribution and behaviour of rock glaciers in the Adamello–Presanella Massif (Italian Alps).* Permafrost Periglac. Process 15, 243–259. http://dx.doi.org/10.1002/ppp.497.

Baroni, C. and Carton, A. (1990) - *Holocene variations of the vedrett della lobbia, adamello group, central alps. [Variazioni oloceniche della Vedretta della Lobbia (Gruppo dell'Adamello, Alpi Centrali)]*. Geografia Fisica e Dinamica Quaternaria, 13(2), 105-119.

Baroni, C. and Carton, A. (1996) - *Geomorfologia dell'alta V. di Genova (Gruppo dell'Adamello, Alpi Centrali). (With Geomorphological Map at the Scale of 1:15,000).* Geografia Fisica e Dinamica Quaternaria, 19(1), 3–17.

Baroni, C. and Hall, B.L. (2004) - *A new relative sea-level curve for Terra Nova Bay, Antarctica.* Journal of Quaternary Science 19(4), 377-396.

Baroni, C. and Orombelli, G. (1989) - *Glacial geology and geomorphology of Terra Nova Bay (Victoria Land, Antarctica).* Memorie della Società Geologica Italiana 33 (1987), 171-193.

Baroni, C. and Orombelli, G. (1991) - *Holocene raised beaches at Terra Nova Bay (Victoria Land, Antarctica).* Quaternary Research 36, 157–177.

Baroni, C. and Orombelli, G. (1994) - *Abandoned Penguin Rookeries as Holocene paleoclimatic indicators in Antarctica.* Geology 22, 23−26.

Baroni, C. and Salvatore, M. C. (2010) - in *Rapporto sulla Campagna Antartica, Estate Australe 2009-2010, Venticinquesima Spedizione.*

Baroni, C., Fasano, F., Giorgetti, G., Salvatore, M.C., Ribecai, C. (2008) - *The Ricker Hills tillite provides evidence of Oligocene warm-based glaciation in Victoria Land, Antarctica.* Global and Planetary Change 60 (3-4), 457-470.

Baroni, C., Martino, S., Salvatore, M.C., Scarascia Mugnozza, G., Schilirò, L. (2014) - *Thermomechanical stress-strain numerical modelling of deglaciation since the Last Glacial Maximum in the Adamello Group (Rhaetian Alps, Italy).* Geomorphology, 226, 278-299.

Baroni, C., Noti, V., Ciccacci, S., Righini, G., Salvatore, M.C. (2005) - *Fluvial Origin of the valley system in northern Victoria Land (Antarctica) from quantitative geomorphic analysis.* Geological Society of America Bulletin 117 (1-2), 212-228.

Barret, P.J, Hambrey, M.J., Robinson, P.R. (1991) - *Cenozoic glacial and tectonic history fromCIROS-1, McMurdo Sound.* In: Thomson, M.R.A., Crame, J.A. and Thomson, J.W. (eds),Geological Evolution of Antarctica. Cambridge: Cambridge University Press, 651-656.

Bentley, M.J., Anderson, J.B. (1998) - *Glacial and marine geological evidence for the ice sheet configuration in the Weddell Sea-Antarctic Peninsula region during the Last Glacial Maximum.* Antarctic Science 10, 309-325.

Bentley, M. J., Ocofaigh, C., Anderson, J. B., Conway, H., Davies, B., Graham, A. G. C.,Hillebrandt, C.D., Hodgson, D.A., Jamieson, S.S.R., Larter, R.D., Mackintosh, A., Smith, J.A., Verleyen, E., Ackert, R.P., Bart, P.J., Berg, S., Brunstein, D., Canals, M., Colhoun, E.A., Crosta, X., Dickens, W.A., Domack, E., Dowdeswell, J.A., Dunbar, R., Ehrmann, W., Evans, J., Favier, V., Fink, D., Fogwill; C.J., Glasser, N.F., Gohl, K., Golledge, N.R., Goodwin, I., Gore, D.B., Greenwood, S.L., Hall, B.L., Hall, K., Hedding, D.W., Hein, A.S., Hocking, E.P., Jakobsson, M., Johnson, J.S., Jomelli, V., Jones, R.S, Klages, J.P., Kristoffersen, Y., Kuhn, G., Leventer, A., Licht, K., Lilly, K., Lindow, J., Livingstone, S.J., Massè, G., McGlone, M.S., McKay, R.M., Melles, M., Miura, H., Mulvaney, R., Nel, W., Nitsche, F.O., O'Brien, P.E., Post, A.L., Roberts, S.J., Saunders, K.M., Selkirk, P.M., Simms, A.R., Spiegel, C., Stolldorf, T.D., Sugden, D.E., Van der Putten, N., Van Ommen, T., Verfaillie, D., Vyverman, W., Wagner, B., White, D.A., Witus, A.E., Zwartz, D. (2014) (The RAISED Consortium) - *A community-based geological reconstruction of antarctic ice sheet deglaciation since the last glacial maximum.* Quaternary Science Reviews, 100, 1-9. doi:10.1016/j.quascirev.2014.06.025

Blunier, T., Chappellaz, J., Schwander, J., Dallenbach, A., Stauffer, B., Stocker, T.F.,Raynaud, D. (1998) - *Asynchrony of Antarctic and Arctic climate change during the lastglacial period*. Nature 394, 793-743.

Braithwaite, R.J. and Muller, F. (1980) - *On the parameterization of glacier equilibrium line altitude.* IAHS Publication 126 (Riederalp Workshop 1978 –World Glacier Inventory), 263–271.

Braithwaite, R. and Raper, S. (2009) - *Estimating equilibriumline altitude (ELA) from glacier inventory data.* Annals of Glaciology, 50 (53), 127–132

Briner, J.P., Young, N.E., Goehring, B.M., Schaefer, J.M. (2012) - *Constraining Holocene ^{10}Be production rates in Greenland.* Journal of Quaternary Science, 27, 2-6.

Brunetti, M., Maugeri, M., Monti, F., and Nanni, T. (2006) - *Temperature and precipitation variability in Italy in the last two centuries from homogenized instrumental time series.* Int. J. Climatol, 26, 345-381.

Callegari E., Dal Piaz G. B., Gatto G. O. (1998) - *Carta Geologica del Gruppo Adamello – Presanella, alla scala di 1:50.000*. S.EL.CA. – Firenze.

Cape Roberts Science Team (2000) - *Studies from the Cape Roberts Project, Ross Sea, Antarctica*. Initial Report on CRP-3: Terra Antarctica 7, 1–209.

Carmignani, L., Ghezzo, C., Gosso, G., Lombardo, B., Meccheri, M., Montrasio, A., Pertusati, P.C., Salvini, F. (1989) - *Geological Map of the area between David and Mariner Glaciers. Victoria Land Antarctica*. In Ricci, C.A., ed., Proceedings meeting Geosciences in Victoria Land, Antarctica, Siena, 2−3 September 1987: Memorie Società Geologica Italiana, v. 33, 77−97.

Carminati, E., Lustrino, M., and Doglioni, C. (2012) - *Geodynamic evolution of the central and western mediterranean: Tectonics vs. igneous petrology constraints.* Rendiconti Online Societa Geologica Italiana, 21(PART 1), 119-120.

Carturan, L. (2010) - *Climate change effects on the cryosphere and hydrology of a high-altitude watershed.* PhD diss., TeSAF, University of Padova, Italy.

Carturan, L., Baroni C., Becker M., Bellin A., Cainelli O., Carton A., Casarotto C., Dalla Fontana G., Godio A., Martinelli T., Salvatore M.C., Seppi R. (2013a) - *Decay of a long-term monitored glacier: Careser Glacier (Ortles-Cevedale, European Alps)*. The Cryosphere, 7, 1819-1838.

Carturan L., Baroni C., Brunetti M., Carton A., Dalla Fontana G., Salvatore M.C., Zanoner T. and Zuecco G. (2016) - *Analysis of the mass balance time series of glaciers in the Italian Alps.* The Cryosphere, 10, 695-712; doi:10.5194/tc-10-695-2016.

Carturan, L., Baroni C., Carton C., Cazorzi F., Dalla Fontana G., Del Pero C., Salvatore M.C., Seppi R., Zanoner T. (2014) - *Reconstructing fluctuations of La Mare Glacier (Eastern Italian Alps) in the Late Holocene: new evidence for a Little Ice Age maximum around 1600 AD.* Geografiska Annaler, Series A: Physical Geography, 96 (3), 287- 306.

Carturan, L., Cazorzi, F., and Fontana, G. D. (2009) - *Enhanced estimation of glacier mass balance in unsampled areas by means of topographic data.* Annals of Glaciology, 50(50), 37-46. doi:10.3189/172756409787769519

Carturan, L., Dalla Fontana, G. and Borga, M. (2012) - *Estimation of winter precipitation in high-altitude catchment of the Eastern Italian Alps: validation by means of Glacier mass balance observations.* Geografia Fisica e Dinamica Quaternaria, 35, 37-48.

Carturan, L., Filippi, R., Seppi, R., Gabrielli, P., Notarnicola, C., Bertoldi, L., Paul, F., Rastner, P., Cazorzi, F., Dinale, R. and Dalla Fontana, G. (2013b) - *Area and volume loss of the glaciers in the Ortles-Cevedale group (Eastern Italian Alps): controls and imbalance of the remaining glaciers.* The Cryosphere, 7, 1819-1838.

Castiglioni, G.B. (1961) - *I depositi morenici del gruppo AdamelloPresanella, conparticolare riguardo agli stadi glaciali postwurmiani.* Mem. Ist. Geol. Miner. Univ. Padova 23, 1–122.

Cavallin, A., Baroni, C., Bini, A., Carton, A., Marchetti, M., Orombelli, G., Pelfini, M. and Zanchi, A. (1997) - *Guide for the excursion - Geomorphology of the Central and Southern Alps.* Supplementi Di Geografia Fisica E Dinamica Quaternaria, III T.2, 13-47.

Ceriani, M., Carelli, M. (1999) -. *Carta delle precipitazioni medie, massime e minime annue del territorio alpino della Regione Lombardia (registrate nel periodo 1891–1990).* Servizio Geologico Regione Lombardia, Milano.

Ciais, P., Jouzel, J., Petit, J.R., Lipenkov, V., White, J.W.C. (1994) - *Holocene temperature variations inferred from six Antarctic ice cores*. Annals of Glaciology 20, 427-436.

Chiesa S., Micheli P., Cariboni M., Tognini P., Motta D., Longhin M.Zambotti G., Marcato E., Ferrario A. (2010) – *Note Illustartive dellla Carta Geologica d'Italia 1:50.000, Foglio "Ponte di Legno". Servizio Geologico d'Italia, Progetto CARG*. 160 pp.

Chiesa S., Micheli P., Cariboni M., Tognini P., Motta D., Longhin M., Zambotti G., Marcato E., Ferrario A. (a cura di) (in stampa) - *Note illustrative della Carta Geologica d'Italia alla scala 1:50.000, Foglio 041 Ponte di Legno. Servizio Geologico d'Italia* - ISPRA – Regione Lombardia, 1-169.

Chinn, T.J. (1991) - *Polar glacier margin and debris features.* Memorie Società Geologica Italiana 46, 25-44.

Christl, M., Vockenhuber, C., Kubik, P. W., Wacker, L., Lachner, J., Alfimov, V., Synal, H. A. (2013) - *The ETH Zurich AMS facilities: Performance parameters and reference materials.* Nuclear Instruments and Methods in Physics Research Section B: Beam Interactions with Materials and Atoms, 294, 29-38.

Clark, P.U., Dyke, A.S., Shakum, J.D., Carlson, A.E., Clark, J., Wohlfarth, B., Mitrovica, J.X., Hostetler, S.W., McCabe, A.M. (2009) - *The Last Glacial Maximum*. Science 325 (5941), 710e714.

Conway, H., Hall, B.L., Denton, G.H., Gades, A.M., Waddington, E.D. (1999) - *Past and future grounding-line retreat of the West Antarctic Ice Sheet*. Science286, 280–283.

Dal Piaz, G. V., Bistacchi, A. and Massironi, M. (2003) - *Geological outline of the alps.* Episodes, 26(3), 175-180.

Dal Piaz G. B. and Venturelli G. (1983) – *Brevi riflessioni sul magmatismo post – ofiolitico nelquadro dell'evoluzione spazio – temporale delle Alpi*. Mem. Soc. Geol. It., 26, 5 – 19, 1 fig.

Delmas, M., Calvet, M., Gunnell, Y., Braucher, R., Bourlès, D. (2011) - *Palaeogeography and 10Be exposure-age chronology of Middle and Late Pleistocene glacier systems in the northern Pyrenees: implications for reconstructing regional palaeoclimates.* Palaeogeography, Palaeoclimatology, Palaeoecology, 305(1), 109-122.

Denton, G.H., Bockheim, J.G., Wilson, S.C., Stuiver, M. (1989) - *Late Wisconsin and Early Holocene glacial history, inner Ross Embayment, Antarctica.* Quaternary Research, 31, 151-182.Denton, G.H., Borns, H.W. Jr., Grosswald, M.G., Stuvier, M., Nichols, R.L. (1975) - *Glacial History of the Ross Sea*. Ant. Journa. of the U.S. 10, 160-164.

Denton, G.H., Hughes, T.J. (2000) - *Reconstruction of the Ross ice drainage system, Antarctica, at the last glacial maximum.* Geografiska Annaler 82A, 143-166.

Denton, G.H., Marchant, D.R. (2000) - *The geologic basis for a reconstruction of a grounded ice sheet in McMurdo Sound, Antarctica, at the last glacial maximum.* Geografiska Annaler 82A, 167-212.

Denton, G.H., Prentice, M.L., Burckle (1991) - *Cenozoic history of the Antarctic ice sheet*. In: Tingey, R.J. (Ed.), Geology of Antarctica. Oxford: Oxford University Press, 365- 433.

Desio, A. (1967) - *I ghiacciai del Gruppo Ortles-Cevedale.* Consiglio Nazionale delle Ricerche, Comitato Glaciologico Italiano, Torino. [In Italian].

Di Nicola, L. (2007) - *Multiple cosmogenic nuclide dating of Late Cenozoic rock surfaces and glacial drifts in the Terra Nova Bay region (Antarctica).* Scuola di Dottorato di Ricerca in Scienze Polari, Università degli Studi di Siena, PhD thesis.

Di Nicola, L., Baroni, C., Strasky, S., Salvatore, M. C. Schlüchter, C., Akçar, N., Kubik, P.W., Wieler, R. (2012) - *Multiple cosmogenic nuclides document the stability of the East Antarctic Ice Sheet in northern Victoria Land since the Late Miocene (5-7 Ma).* Quaternary Science Reviews 57 (2012) 85-94.

Di Nicola, L., Strasky, S., Schlüchter, C., Salvatore, M.C., Akçar, N., Kubik, P.W., Christl, M., Kasper, H.U., Wieler, R., Baroni, C. (2009) - *Multiple cosmogenic nuclides document complex Pleistocene exposure history of glacial drifts in Terra Nova Bay (northern Victoria Land, Antarctica).* Quaternary Research, 71, 83-92.

Diolaiuti, G., Bocchiola, D., D'agata, C., Smiraglia, C. (2012) - *Evidence of climate change impact upon glaciers' recession within the Italian Alps: The case of Lombardy glaciers.* Theoretical and Applied Climatology, 109 (3-4), 429-445.

Dochat, T.M., Marchant, D.R. and Denton, G.H. (2000) - *Glacial geology of Cape Bird, Ross Island, Antarctica.* Geografiska Annaler, 82 A: 237–247.

Domack, E., Levanter, A., Gilbert, R., Brachfeld, S., Ishman, S., Camerlenghi, A., Gavahan, K., Carlson, D., Barkoukis, A. (2001) - *Cruise reveals history of Holocene Larsen Ice Shelf*.EOS, 82(2), 13 and 16-17.

Domack, E.W., Jull, A.J.T., Donahue, D.J. (1991) - *Holocene chronology for the unconsolidated sediments at Hole 740A: Prydz Bay, East Antarctica. Proceedings of theOcean Drilling Program Scientific Results* 119B (207), 1-7.

Elliot, D.H. and Fleming, T.H. (2004) - *Occurrences and dispersal of magmas in the JurassicFerrar large igneous province, Antarctica.* Gondwana Research, 7, 223−237.

Elverhøi, A. (1981) - *Evidence for a late Wisconsin glaciation of the Weddell Sea*. Nature 293, 641-642.

EPICA Community Members (2004) - *Eight glacial cycles from an Antarctic ice core.* Nature 429, 623-628 (10 June 2004)

EPICA Community Members (2006) - *One-to-one coupling of glacial climate variability in Greenland and Antarctica.* Nature, 444, 195-198.

Favilli, F., Egli, M., Brandova, D., Ivy-Ochs, S., Kubik, P., Cherubini, P., Mirabella, A., Sartori, G., Giaccai, D., Haeberli, W. (2009) – *Combined use of relative and absolute dating techniques for detecting signals of Alpine landscape evolution during the late Pleistocene and early Holocene.* Geomorphology, 112, 48-66.

Federici, P. R., Ribolini, A. and Spagnolo, M. (2016) - *Glacial history of the Maritime Alps from the Last Glacial Maximum to the Little Ice Age.* In: Hughes, P. D. and Woodward, J. C., Eds. (2016) - Quaternary Glaciation in the Mediterranean Mountains. Geological Society, London, Special Publications, 433, SP433-9.

Fenton, C.R., Hermanns, R.L., Blikra, L.H., Kubik, P.W., Bryant, C., Niedermann, S., Meixner, A., Goethals, M.M. (2011) - *Regional ^{10}Be production rate calibration for the past 12 ka deduced from the radiocarbon-dated Grøtlandsura and Russenes rock avalanches at 69_ N, Norway.* Quaternary Geochronology, 6, 437-452.

Fleming, T.H., Heimann, A., Foland, K.A., Elliot, D.H. (1997) - *$^{40}Ar/^{39}Ar$ geochronology of Ferrar Dolerite sills from the Transantarctic Mountains, Antarctica: Implications for the age and origin of the Ferrar magmatic province.* GSA Bullettin. V.109, 533-546.

Frei, C. and Schar, C. (1998) - *A precipitation climatology of the Alps from high-resolution raingauge observations, Int.* J. Climatol., 18, 873-900.

Froitzheim, N., Schmid, S. M. and Frey, M. (1996) - *Mesozoic paleogeography and the timing of eclogitefacies metamorphism in the alps: A working hypothesis.* Eclogae Geologicae Helvetiae, 89(1), 81-110.

Gabrieli, J., Decet, F., Luchetta, A., Valt, M., Pastore, P. and Barbante, C. (2010) - *Occurence of PAHs in seasonal snowpack of Eastern Italian Alps.* Environ. Pollut., 158, 3130-3137.

GNGFG-CNR (Gruppo Nazionale Geografia Fisica e Geomorfologia – Consiglio Nazionale delle Ricerche) (1986) – *Ricerche geomorfologiche nell'alta Val di Pejo (Gruppo del Cevedale) [Geomorfological research in*

upper Val di Pejo (Cevedale Group)]. Geografia Fisica e Dinamica Quaternaria, 9, 137-191.

Goehring, B.M., Lohne, Ø.S., Mangerud, J., Svendsen, J.I., Gyllencreutz, R., Schaefer, J., Finkel, R. (2012) - *Late glacial and Holocene ^{10}Be production rates for western Norway.* Journal of Quaternary Science, 27, 89-96.

Gosse, J.C., Grant, D.R., Klein, J., Lawn, B. (1995) - *Cosmogenic ^{10}Be and 26Al constraints on weathering zone genesis, ice cap basal conditions, and Long Range Mountain (Newfoundland) glacial history*. CANQUA-CGRG Conference Abstracts, Memorial University of Newfoundland, St. Johns, CA19.

Gosse, J.C., Phillips, F.M. (2001) - *Terrestrial in situ cosmogenic nuclides: theory and application.* Quaternary Science Reviews, 20, 1475-1560.

Guillevic, M., Bazin, L., Landais, A., Stowasser, C., Masson-Delmotte, V., Blunier, T., Eynaud, F., Falourd, S., Michel, E., Minster, B., Popp, T., Prié, F. and Vinther, B. M. (2014) - *Evidence for a three-phase sequence during heinrich stadial 4 using a multiproxy approach based on greenland ice core records.* Climate of the Past, 10(6), 2115-2133. doi:10.5194/cp-10-2115-2014.

Hall, B.L., Baroni, C., Denton, G.H. (2004) - *Holocene relative sea-level history of the Southern Victoria Land Coast, Antarctica.* Global and Planetary Change 42, 241−263.

Hall, B.L. and Denton, G.H. (2000a) - *Radiocarbon chronology of Ross Sea drift, eastern Taylor Valley, Antarctica: Evidence for a grounded ice sheet in the Ross Sea at the last glacial maximum.* Geografiska Annaler, 82 A: 305–336.

Hall, B.L. and Denton, G.H. (2000b) - *Extent and chronology of the Ross Sea ice sheet and the Wilson Piedmont Glacier along the Scott Coast at and since the last glacial maximum*. Geografiska Annaler, 82 A: 337–363.

Hall, B.L., Denton, G.H., Hendy, C. (2000) - *Evidence from Taylor Valley for a grounded ice sheet in the Ross Sea, Antarctica.* Geogr. Ann. 82A, 275e304.

Hambrey, M.J., Ehrmann, W.U. and Larsen, B. (1991) - *Cenozoic glacial record of the Prydz Bay continental shelf, East Antarctica. Proceedings of the Ocean Drilling* Programme, Scientific Results, 119, 77-132.

Heinrich, H. (1988) - *Origin and consequences of cyclic ice rafting in the northeast Atlantic Ocean during the past 130,000 years.* Quaternary Research, 29(2), 142-152.

Heyman, J. (2014) - *Paleoglaciation of the Tibetan Plateau and surrounding mountains based on exposure ages and ELA depression estimates.* Quaternary Science Reviews, 91, 30-41.

Hippe, K., Ivy-Ochs, S., Kober, F., Zasadni, J., Wieler, R., Wacker, L., Kubik, P. W., Schlüchter, C. (2014) - *Chronology of Lateglacial ice flow reorganization and deglaciation in the Gotthard Pass area, Central Swiss Alps, based on cosmogenic ^{10}Be and in situ 14C.* Quaternary Geochronology, 19, 14-26.

Huang, B., Banzon, V. F., Freeman, E., Lawrimore, J., Liu, W., Peterson, T. C., Smith, T. M., Thorne, P. W., Woodruff, S. D. and Zhang, H.M. (2015) - *Extended Reconstructed Sea Surface Temperature Version 4 (ERSST.v4).* Part I: Upgrades and Intercomparisons. Journal of Climate, 28:3, 911-930.

Huss, M. (2013) - *Density assumptions for converting geodetic glacier volume change to mass change.* The Cryosphere, 7, 877–887.

IPCC (Intergovernmental Panel on Climate Change) (2007) - *Climate change. The physical science basis.* In: Solomon, S., Qin, D., Manning, M., Chen, Z., Marquis, M., Averyt, K. B., Tignor, M., Miller, H.L. (Eds.), Contribution of Working Group I to the Fourth Assessment Report of the Intergovernmental Panel on Climate Chang. Cambridge Univ. Press, Cambridge, UK.

IPCC − Intergovernmental Panel on Climate Change (2013) - *Climate Change 2013:* The Physical Science Basis. In: Stocker T. F., Qin D., Plattner G. K., Tignor M., Allen S. K., Boschung J., Nauels A., Xia Y., Bex V. and Midgley P. M. (Eds.) Contribution of Working Group I to the Fifth Assessment Report of Intergovernmental Panel on Climate Change. Cambridge University Press, Cambridge, pp. 1535.

Isaac, M.J., Chinn, T.J., Edbrooke, S.W., forsyth, P.J. (1995) - *Geology of the Olympus Range area, southern Victoria Land, Antarctica. 1:50 000.* Lower Hutt, New Zealand: New Zealand Institute of Geological and Nuclear Sciences, Geological map 20, 1sheet +60 pp.

Ivany, L.C., Van Simaeys, S., Domaci, E.W., Samson, S.D. (2006) - *Evidence for an earliest Oligocene ice sheet on the Antarctic Peninsula.* Geology 34 (5) 377–380.

Ivy-Ochs, S. (1996) - *The Dating of Rock Surfaces Using in Situ Produced ^{10}Be, ^{26}Al and ^{36}Cl, with Examples from Antarctica and the Swiss Alps.* Ph.D. thesis, ETH Zürich.

Ivy-Ochs, S. (2015) - *Glacier variations in the European Alps at the end of the last glaciation.* Cuadernos de investigación geográfica, 41(2), 295-315.

Ivy-Ochs, S., Kerschner, H., Kubik, P.W., Schlüchter, C. (2006b) - *Glacier response in the European Alps to Heinrich event 1 cooling: The Gschnitz stadial.* Journal of Quaternary Science, 21, 115–130.

Ivy-Ochs, S., Kerschner, H., Maisch, M., Christl, M., Kubik, P.W. and Schlüchter, C. (2009) – *Latest Pleistocene and Holocene glaciers in the European Alps.* Quaternary Science Reviews, 28, 2137-2149.

Ivy-Ochs, S., Kerschner, H., Reuther, A., Maisch, M., Sailer, R., Schaefer, J., Kubik, P.W., Synal, H., Schlüchter, C. (2006a) - *The timing of glacier advances in the northern European Alps based on surface exposure dating with cosmogenic ^{10}Be, ^{26}Al, ^{36}Cl, and ^{21}Ne.* In: Siame, L.L., Bourlès, D.L., Brown, E.T. (Eds.), In Situ e Produced Cosmogenic Nuclides and Quantification of Geological Processes. Geological Society of America Special Paper, 415, 43-60.

Ivy-Ochs, S., Kerschner, H., Reuther, A., Preusser, F., Heine, K., Maisch, M., Kubik, P.W., Schlüchter, C. (2008) - *Chronology of the last glacial cycle in the European Alps.* Journal of Quaternary Science, 23, 559-573.

Ivy-Ochs, S., Kerschner, H., Schlüchter, C. (2007) - *Cosmogenic nuclides and the dating of Lateglacial and Early Holocene glacier variations: the Alpine perspective.* Quaternary International, 164-165, 53–63.

Ivy-Ochs, S. and Kober, F. (2008) – *Surface exposure dating with cosmogenic nuclides.* Eiszeitalter und Gegenwart, 57, 179-209.

Ivy-Ochs, S., Schäfer, J., Kubik, P.W., Synal, H.A., Schlüchter, C. (2004) - *Timing of deglaciation on the northern Alpine foreland (Switzerland).* Eclogae Geol. Helv. 97 (1), 47–55. http://dx.doi.org/10.1007/s00015-004-1110-0.

Ivy-Ochs, S., Schlüchter, C., Kubik, P.W., Beer, J., Kerschner, H. (1996) -*The exposure age of an Egesen moraine at Julier Pass measured with the cosmogenic radionuclides ^{10}Be, ^{26}Al and ^{36}Cl.* Eclogae geologicae Helvetiae, 89, 1049-1063.

Jouzel, J., Masson-Delmotte, V., Cattani, O., Dreyfus, G., Falourd, S., Hoffmann, G., Wolff, E. W. (2007) - *Orbital and millennial antarctic climate variability over the past 800,000 years.* Science, 317(5839), 793-796. doi:10.1126/science.1141038

Kelly, M.A., Buoncristiani, J. F., Schlüchter, F. (2004) - *A reconstruction of the last glacial maximum (LGM) ice-surface geometry in the western Swiss Alps and contiguous Alpine regions in Italy and France.* Eclogae geologicae Helvetiae, 97, 57-75.

Kennett, J.P. (1977) - *Cenozoic Evolution of Antarctic Glaciation, the Circum-Antarctic Ocean, and Their Impact on Global Paleoceanography.* Journal of Geophysical Research 82, 3843- 3860.

Kennett, J.P. and D.A. Hodell (1995) - *Stability or Instability of Antarctic Ice Sheets During Warm Climates of the Pliocene.* GSA Today, 5 (1), 1-22.

Kerschner, H. (2009) - *Gletscher und Klima im Alpinen Spätglazial und frühen Holozän*. In: Schmidt, R., Matulla, C., Psenner, R., Eds. (2009) - Klimawandel in Österreich–Die letzten 20.000 Jahre und ein Blick voraus. Innsbruck university press, 5-26.

Kohl, C.P. and Nishiizumi, K. (1992) - *Chemical isolation of quartz for measurement of insitu -produced cosmogenic nuclides.* Geochimica et Cosmochimica Acta, 56, 3583-3587.

Kyle P.R. (1990) - *McMurdo Volcanic Group western Ross Embayment*. In: Volcanoes of the Antarctic Plate and Southern Oceans: LeMasurier and Thomson (eds.): AGU Antarctic Research Series., p.487.

Lal, D. (1991) - *Cosmic ray labeling of erosion surfaces: in situ nuclide production rates and erosion models.* Earth and Planetary Science Letters, 104, 424-439.

Lemke, P., Ren, J., Alley, R.B., Allison, I., Carrasco, J., Flato, G., Fujii, Y., Kaser, G., Mote, P., Thomas, R.H. and Zhang, T. (2007) - *Observations: Changes in*

Snow, Ice and Frozen Ground. In Solomon, S., Qin, D., Manning, M., Chen, Z., Marquis, M., Averyt, K.B., Tignor, M. and Miller, H.L., eds. Climate Change 2007: The Physical Science Basis. Contribution of Working Group I to the Fourth Assessment Report of the Intergovernmental Panel on Climate Change. Cambridge: Cambridge University Press, 337–383.

Leventer, A., Domack, E., Dunbar, R., Pike, J., Stickley, C., Maddison, E., Brachfeld, S., Manley, P., McClennen, C. (2006) - *Marine sediment record from the East Antarctic margin reveals dynamics of ice sheet recession.* Geological Society of America Today 16 (12), 4−10.

Li, Y. (2013) - *Determining topographic shielding from digital elevation models for cosmogenic nuclide analysis: a GIS approach and field validation.* Journal of Mountain Science, 10 (3), 355-362.

Licht, K.J., Jennings, A.E., Andrews, J.T., Williams, K.M. (1996) - *Chronology of the late Wisconsin ice retreat from the western Ross Sea, Antarctica.* Geology 24, 223-226.

Maisch, M. (1987) - *Zur Gletschergeschichte des Alpinen Spaetglazials: analyse und Interpretation von Schneegrenzdaten*. Geogr. Helv. 42 (2), 63–71.

Marroni, M., Molli, G., Ottria, G. and Pandolfi, L. (2001) - *Tectono-sedimentary evolution of the external liguride units (Northern Appennines, Italy): Insights in the pre-collisional history of a fossil ocean-continent transition zone*. Geodinamica Acta, vol. 14, no. 5, 307-320.

Masarik, J., Frank, M., Schäfer, J.M., Wieler, R. (2001) - *Correction of in situ cosmogenic nuclide production rates for geomagnetic field intensity variations during the past 800,000 years.* Geochimica et Cosmochimica Acta, 65, 2995-3003.

Masson, V., Vimeux, F., Jouzel, J., Morgan, V., Delmotte, M., Ciais, P., Hammer, C., Johnsen, S., Lipenkov, V.Y., Mosley-Thompson, E., Petit, J.R., Steig, E.J., Stievenard, M., Vaikmae, R. (2000) - *Holocene climate variability in Antarctica based on 11 ice-core isotopic records.* Quaternary Research 54, 348-358.

Matulla, C., Briffa, K., Jones, PD., Efthymiadis, D., Brunetti, M., Nanni, T., Maugeri, M., Mercalli, L., Mestre, O., Moisselin, J-M., Begert, M., Müller, Westermeier, G., Kveton, V., Bochnicek, O., Stastny, P., Lapin, M., Szalai, S., Szentimrey, T., Cegnar, T., Dolinar, M., Gajic-Capka, M., Zaninovic, K., Majstorovic, Z., Nieplova, E. (2007) - HISTALP − *Historical instrumental climatological surface time series of the greater Alpine region 1760-2003.* International Journal of Climatology, 27, 17-46, DOI: 10.1002/joc.1377.

Mayer A., Cortiana G., Dal Piaz G. V., Deloule E., De Pieri R., Jobstraibizer P. G. (2003) - *U – Pb single zircon ages of the Adamello Batholith, Southern Alps.* Mem. Sc. Geol. Padova, 55, 151 – 167, 8 figg., 2 tabb.

Meneghel, M., Bondesan, A., Salvatore, M. C., Orombelli, G. (1999) - *A model of theglacial retreat of upper Rennick Glacier, Victoria Land, Antarctica.* Ann. Glaciol., 29, 225-230.

Miller, G.H., Briner, J.P., Lifton, N.A., Finkel, R.C. (2006) - *Limited ice-sheet erosion and complex exposure histories derived from in situ cosmogenic 10Be, 26Al, and 14C on Baffin Island, Arctic Canada.* Quaternary Geochronology 1, 74–85 Research paper

Mojsisovics (1865) - *Ein streifzug durchdie Ortler Alpen.* Jahrb. D. Oe. Alpenvereins, I, 257 – 289, Wien.

Moran, A.P., Ivy-Ochs, S., Schum, M., Christl, M. and Kerschner, H. (2016) – *Evidence of central Alpine glacier advances during the Younger Dryas-early Holocene transition period.* Boreas

Nishiizumi, K., Imamura, M., Caffee, M.W., Southon, J.R., Finkel, R.C., McAninch, J. (2007) - *Absolute calibration of ^{10}Be AMS standards.* Nuclear Instruments and Methods in Physics Research, B 258, 403-413.

Oberholzer, P. (2004) - *Reconstructing paleoclimate and landscape history in Antarctica and Tibet with cosmogenic nuclides*. PhD thesis, ETH Zurich.

Oberholzer, P., Baroni, C., Salvatore, M.C., Baur, H., Wieler, R. (2008) - *Dating late Cenozoic erosional surface in Victoria Land, Antarctica, with cosmogenic neon in pyroxenes.* Antarctic Science, 20 (1), 89-98.

Oberholzer, P., Baroni, C., Schaefer, J., Orombelli, G., Ivy-Ochs, S. ,Kubik, P. W., Baur, H., Weiler, R. (2003) - *Limited Pliocene /Pleistocene glaciation in Deep Freeze Range, northern Victoria Land, Antarctica, derived from in situ cosmogenic nuclides.* Antartic Science 15 (4), 493-502.

Oerlemans, J. (2001) - *Glaciers and climate change.* Balkema Publishers, Lisse.

Ohmura, A., Kasser, P., Funk, M. (1992) - *Climate at the equilibrium line of glaciers.* Journal of Glaciology, 38, 397–411.

Orombelli, G. (1989) - *Terra Nova Bay: A geographic overview.* In Ricci, C.A., (ed), Geosciences in Victoria Land, Antarctica. Memorie della Società Geologica Italiana 32 (1987), 69–75.

Orombelli G. (1991) - *Glaciers and glacial morphology at Terra Nova Bay: an opportunity for significant studies on environmental and climatic global changes.* Memorie della Società Geologica Italiana, 46, 9-16.

Orombelli G., Baroni, C., Denton, G.H. (1990) - *Late Cenozoic glacial history of the Terra Nova Bay region, northern Victoria Land, Antarctica*. Geografia Fisica e Dinamica Quaternaria 13 (1990), 139-163.

Pagliuca, N.M. (2001) - *L' evoluzione tettonica del continente antartico* Quaderni di Geofisica, 19, 21-25.

Pedro, J. B., Bostock, H. C., Bitz, C. M., He, F., Vandergoes, M. J., Steig, E. J., Chase, B.M., Krause, C.E., Rasmussen, S.O., Markle, B.R. and Cortese, G. (2016) - *The spatial extent and dynamics of the antarctic cold reversal.* Nature Geoscience, 9(1), 51-55. doi:10.1038/ngeo2580

Pine, P.D., Kiser, J.D. (2003) – *Aerial photography and image interpretation.* Wiley, John Wiley and sons, Inc.

Peel, M.C., Finlayson, B.L., McMahon, T.A. (2007) - *Updated world map of the Köppen-Geiger climate classification.* Hydrol. Earth Syst. Sci., 11, 1633-1644.

Pelfini, M. (1992) - *Le fluttuazioni glaciali Oloceniche nel Gruppo Ortles-Cevedale (settore lombardo).* Università degli Studi di Milano. Dip. Sc. Terra, Tesi di Dottorato IV ciclo, A.A. 1990-1991, 1-211.

Petit, J.R., Jouzel, J., Raynaud, D., Barkov, N.I., Barnola, J-M., Basile, I., Bender, M., Chappallaz, J. (1999) - *Climate and atmospheric history of the past 420,000 years from the Vostok ice core, Antarctic.* Nature 399, 429-436.

Porter, S.C. (1975) - *Equilibrium line altitudes of late Quaternary glaciers in the Southern Alps, New Zealand*. Quaternary Research, 5, 27-47.

Porter, S. C. and Orombelli, G. (1982) - *Late-glacial ice advances in the western Italian Alps.* Boreas, 11, 125–140.

Ranzi, R., Baroni, C., Pepe, M., Rossi, E., Vantadori, F., Salvatore, M. C. (2013) - *GLIMS-IT: contributo italiano al progetto GLIMS di monitoraggio satellitare dei ghiacciai del globo.* Atti 17a Conferenza Nazionale ASITA − Riva del Garda 5-7 novembre 2013, 1126-1132.

Ranzi, R., Grossi, G., Gitti, A., Taschner, S. (2010) - *Energy and mass balance of the Mandrone Glacier (Adamello, Central Alps).* Geografia Fisica e Dinamica Quaternaria, 33, 45 – 60.

Rignot, E., Mouginot, J. Scheuchl, B. (2011) - *Ice Flow of the Antarctic Ice Sheet.* Science, V. 333, Issue 6048, 1427-1430, DOI: 10.1126/science.120833

Rocchi, S., Armenti, P., D'Orazio, M., Tonarini, S., Wijbrans, J. R., Di Vincenzo, G. (2002) - *Cenozoic magmatism in the western Ross Embayment: Role of mantle plume versus plate dynamics in the development of the West Antarctic Rift System.* Journal of Geophysical Research 107(B9), 2195, doi: 10.1029/2001JB000515, 2002.

Salerno, F., Gambelli, S., Viviano, G., Thakuri, S., Guyennon, N., D'Agata, C., Diolaiuti, G., Smiraglia, C., Stefani, F., Bocchiola, D., Tartari, G. (2014) - *High alpine ponds shift upwards as average temperatures increase: A case study of the Ortles−Cevedale mountain group (Southern Alps, Italy) over the last 50 years.* Global and Planetary Change, Vol. 120, 81-91.

Salomon W. - *Die Adamello Gruppe.* Abhandl. K. u. K. Geol. Reichsanst, vol. XXI, fasc. 2 (1910), 1-603.

Salvatore, M.C., Zanoner, T., Baroni, C., Carton, A., Banchieri, F.A., Viani, C., Giardino, M., Perotti, L. (2015) - *The state of Italian glaciers: A snapshot of the 2006-2007 hydrological period.* Geografia Fisica e Dinamica Quaternaria, 38 (1), 175-198.

Scambos, T., A., Haran, T. M., Fahnestock, M. A., Painter, T. H., and Bohlander, J. (2007) - *MODIS-based mosaic of antarctica (MOA) data sets:*

Continent-wide surface morphology and snow grain size. Remote Sensing of Environment, 111(2), 242-257. doi:10.1016/j.rse.2006.12.020

Schindelwig, I., Akc_ar, N., Kubik, P. W. and Schluchter, C. (2011) – *Lateglacial and early Holocene dynamics of adjacent valley glaciers in the Western Swiss Alps.* Journal of Quaternary Science 27, 114– 124.

Schwarb, M. (2000) - *The Alpine precipitation climate: evaluation of a high-resolution analysis scheme using comprehensive raingauge data.* Diss. ETHZ 13'911, Zürcher Klimaschriften, Heft 80, Institut für Klimaforschung ETH, Verlag Institut für Klimaforschung ETH Zürich.

Seppi, R., Carton, A., and Baroni, C. (2010) - *Relict rock glaciers and past permafrost distribution in the adamello presanella group (central Alps). [Rock glacier relitti e antica distribuzione del permafrost nel Gruppo Adamello Presanella (Alpi Centrali)]* Alpine and Mediterranean Quaternary, 23(1), 137-144.

Shipp, S.J., Anderson, J.B. (1994) - *High-resolution seismic survey of the Ross Sea continental shelf: implications for ice-sheet retreat behaviour.* Antarctic Journal of the United States 29(5), 137-138.

Shulmeister, J., Fink, D., Hyatt, O. M., Thackray, G. D., Rother, H. (2010) - Cosmogenic 10Be and 26Al exposure ages of moraines in the Rakaia Valley, New Zealand and the nature of the last termination in New Zealand glacial systems. Earth and Planetary Science Letters, 297(3), 558-566.

Steig, E.J., Morse, D.L., Waddington, E.D., Stuiver, M, Grootes, P.M., Mayewski, P.A., Twickler, M.S., Whitlow, S.I. (2000) - *Wisconsinan and Holocene climate history from an ice core at Taylor Dome, western Ross Embayment, Antarctic*. Geografiska Annaler A 82, 213-232.

Steffensen, J. P., Andersen, K. K., Bigler, M., Clausen, H. B., Dahl-Jensen, D., Fischer, H., Goto-Azuma, K., Hansson, M., Johnsen, S.J., Jouzel, J., Masson-Delmotte, V., Popp, T., Rasmussen, S.O., Rothlisberger, R., Ruth, U., Stauffer, B., Siggaard-Andersen, M.L., Sveinbjornsdòttir, A.E., Svensson, A., White, J. W. C. (2008) - *High-resolution greenland ice core data show abrupt climate change happens in few years.* Science, 321(5889), 680-684. doi:10.1126/science.1157707

Steig, E.J., Wolfe, A.P., Miller, G.H. (1998) - *Wisconsinan refugia and the glacial history of eastern Baffin Island, Arctic Canada: Coupled evidence from cosmogenic isotopes and lake sediments.* Geology 26, 835-838.

Stone, J.O. (2000) - *Air pressure and cosmogenic isotope production.* Journal of Geophysical Research, 105, 23753-23759.

Stone, J.O., Balco, G.A., Sugden, D.E., Caffee, M.W., Sass, L.C., Cowdery, S.G., Siddoway, C. (2003) - *Holocene Deglaciation of Marie Byrd Land, West Antarctica*. Science 299, 99−102.

Strand, K., Passchier, S., Näsi, J. (2003) - *Implications of quartz grain microtextures for onset Eocene/ Oligocene glaciation in Prydz Bay, ODP site 1166*. Antarctica: Palaeogeography, Palaeoclimatology, Palaeoecology 198, 101–111, doi: 10.1016/S0031-0182(03)00396-1.

Strasky, S. (2008) - *Glacial response to global climate changes: cosmogenic nuclide chronologies from high and low latitudes.* Ph.D. thesis, ETH Zürich.

Strasky, S., Di Nicola, L., Baroni, C., Salvatore, M.C., Baur, H., Kubik, P.W., Schlüchter, C., Wieler, R. (2009) - *Surface exposure ages imply multiple low-amplitude Pleistocene variations in East Antarctic Ice Sheet, Ricker Hills, Victoria Land.* Antarctic Science, 21 (1), 59-69.

Stuiver, M., Denton, G.H., Hughes, T.J. and Fastook, J.L. (1981) - *History of the marine ice sheet in West Antarctica during the last glaciation: A working hypothesis*. In: Denton, G.H. and Hughes, T.J. (eds): The Last Great Ice Sheets. Wiley-Interscience. New York. 319–436.

Sugden, D.E., Denton, G.H. (2004) - *Cenozoic landscape evolution of the Convoy Range to Mackay Glacier area, Transantarctic Mountains: Onshore to offshore synthesis.* GSA Bulletin, 116, 840-857.

Sugden, D.E., Summerfield, M.A., Denton, G.H., Wilch, T.I., McIntosh, W.C., Marchant, D.R., Rutford, R.H. (1999) - *Landscape development in the Royal Society Range, southern Victoria Land, Antarctica: Stability since the middle Miocene.* Geomorphology 28, 181– 200.

Thompson, L.G., Davis, M.E., Mosley-Thompson, E., Sowers, T.A., Henderson, K.A., Zagorodnov, V.S., Lin, P.N., Mikhalenko, V.N., Campen, R.K., Bolzan, J.F., Cole-Dai, J., Francou, B. (1998) - *A 25,000-year tropical climate history from Bolivian ice cores.* Science 282, 1858-1864.

Tonarini, S., Rocchi, S., Armienti, P., and Innocenti, F.(1997) - *Constraints on timing of Ross Sea rifting inferred from Cainozoic intrusions from northern Victoria Land, Antarctica,* in Ricci, C. A., ed., The Antarctic Region: Geological evolution and processes, Terra Antartica Pubbl., p. 511-521

Vaughan, D.G:, Bamber, J.L., Giovinetto, M., Russell, J., Cooper, P.R. (1999) - *Reassessment of net surface mass balance in Antarctica.* Journal of Climate 12, 933-946.

Vetter, U., and Tessenshon, F. (1987) - *S-and I-Type granitoids of North Victoria Land, Antarctica, and Their inferred geotectonic setting.* Geologische Rundschau, 76, 233- 43.

Weaver, S.D., Bradshaw, J.D., Laird, M.G. (1984) - *Geochemistry of Cambrian volcanism in northern Victoria land, Antarctica.* Earth and Planet. Sci. Letters 68, 128-40.

WGMS (World Glacier Monitoring Service) 1989 – *World Glacier Inventory -Status 1988.* Haeberli, W., Bösch, H., Scherler, K., Østrem, G. and Wallén, C.C. (eds), IAHS (ICSI)/UNEP/UNESCO, World Glacier Monitoring Service, Zurich, 458 p.

WGMS (2008) - *Fluctuations of Glaciers 2000-2005 (Vol. IX).* In: Haeberli, W., Zemp, M., Kääb, A., Paul, F., Hoelzle, M., Eds., (2008) - ICSU (FAGS) / IUGG (IACS) / UNEP / UNESCO / WMO, World Glacier Monitoring Service, Zurich, Switzerland: pp. 266 Publication based on database version: doi:10.5904/wgms-fog-2008-12.

WGMS (2014) - *Fluctuations of Glaciers Database.* World Glacier Monitoring Service, Zurich, Switzerland. Online access: http://dx.doi.org/10.5904/wgms-fog-2014-09.

Wirsig, C. (2015) - *Constraining the timing of deglaciation of the High Alps and rates of subglacial erosion with cosmogenic nuclides.* Doctoral dissertation, Diss., Eidgenössische Technische Hochschule ETH Zürich, Nr. 22978.

Wirsig, C., Zasadni, J., Ivy-Ochs, S., Christl, M., Kober, F., Schlüchter, C. (2016) - *A deglaciation model of the Oberhasli, Switzerland.* Journal of Quaternary Science, 31(1), 46-59.

Young, N.E., Schaefer, J.M., Briner, J.P., Goehring, B.M. (2013) - *A ^{10}Be production-rate calibration for the Arctic.* Journal of Quaternary Science, 28, 515-526.

Appendix I – Thin sections

LAM 13.1

Petrographic Description / Analysis

Medium-fine grained metamorphic rock with heteroblastic structure and schistose texture given by lepidoblastic and granoblatic layers irregular alternation, with prevailing granoblastic layers. Lepidoblastic layers are mainly constituted by white mica, chlorite, and subordinate quartz. Granoblastic layers are made-up of quartz with garnet with subordinate feldspar-albite. Accessory minerals like oxides and sulphides are present.

Modal Analysis	(% estimated)
Quartz	45
White mica	25
Chlorite	15
Garnet	8
Feldspar+Albite	<5
Accessory (oxides-sulphides)	1

Petrographic Classification (IUGS)

GARNET MICASCHIST

Pictures

left nicols // right nicols X – Picture dimension 2,5 X 1,8 mm

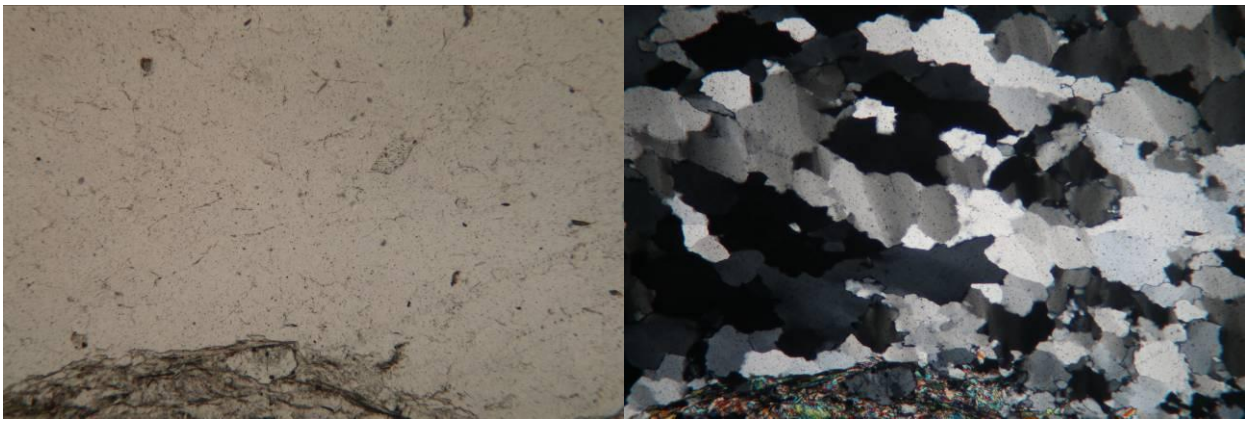

General view: granoblastic layer (quartz and feldspar) and lepidoblastic layer (white mica, garnet,).

LAM 13.2

Petrographic Description / Analysis

Medium-fine grained metamorphic rock with heteroblastic structure and schistose texture given by lepidoblastic and granoblatic layers irregular alternation, with prevailing granoblastic layers. Lepidoblastic layers are mainly constituted by white mica, chlorite, and subordinate quartz. Granoblastic layers are made-up of quartz with minor garnet and blue amphibole with subordinate feldspar-albite. Accessory minerals like oxides and sulphides are present.

Modal Analysis	(% estimated)
Quartz	40
White mica	25
Chlorite	15
Blue amphibole	8
Garnet	6
Feldspar+Albite	<5
Accessory (oxides-sulphides)	1

Petrographic Classification (IUGS)

GARNET-BLUE AMPHIBOLE MICASCHIST

Pictures

left nicols // right nicols X – Picture dimension 2,5 X 1,8 mm

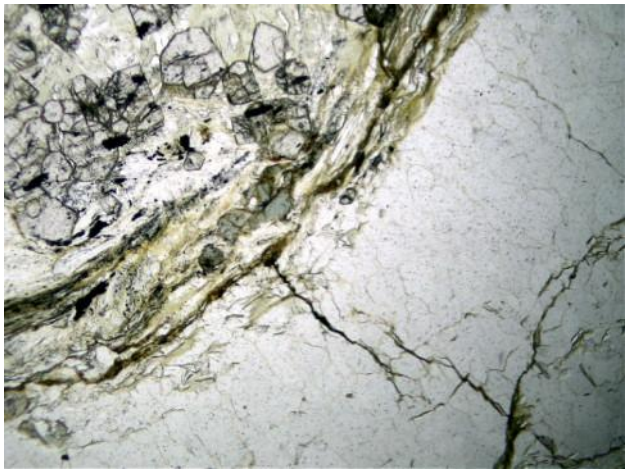

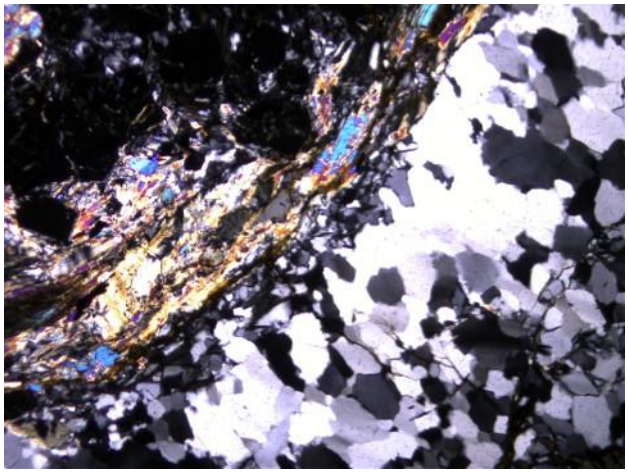

General view: granoblastic layer (quartz and feldspar) and lepidoblastic layer (white mica, garnet, blue amphibole and chlorite).

LAM 13.3

Petrographic Description / Analysis

Medium-fine grained metamorphic rock with heteroblastic structure and schistose texture given by lepidoblastic and granoblatic layers irregular alternation, with prevailing granoblastic layers. Lepidoblastic layers are mainly constituted by white mica, chlorite,tourmaline and subordinate quartz and organic matter. a Granoblastic layers are made-up of quartz with garnet. Accessory minerals like oxides and sulphides are present.

Modal Analysis	(% estimated)
Quartz	45
White mica	25
Chlorite	15
Garnet	10
Tourmaline	3
Organic Matter	1
Accessory (oxides-sulphides)	1

Petrographic Classification (IUGS)

GARNET MICASCHIST

Pictures

left nicols // right nicols X – Picture dimension 2,5 X 1,8 mm

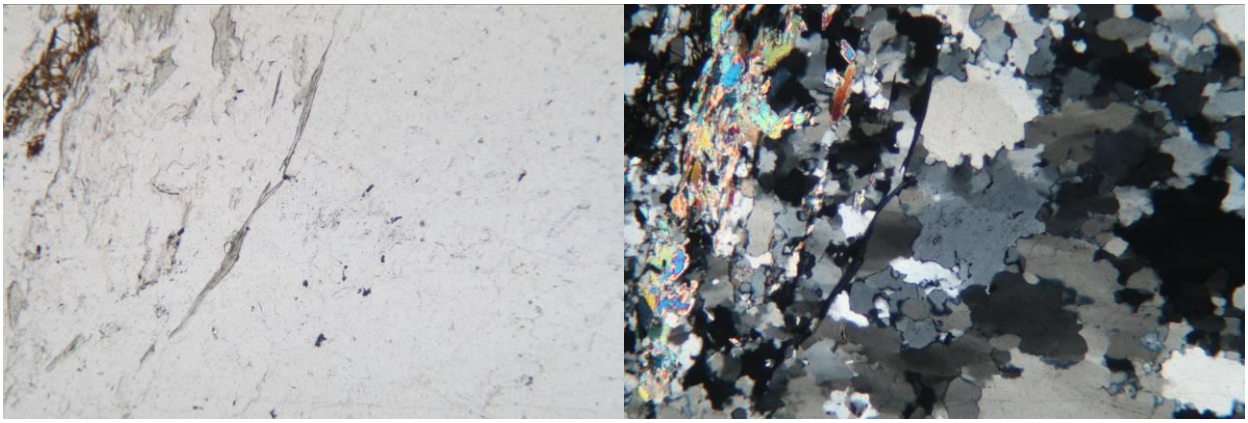

General view: granoblastic layer (quartz) and lepidoblastic layer (white mica, garnet,).

LAM 13.4

Petrographic Description / Analysis

Medium-fine grained metamorphic rock with heteroblastic structure and schistose texture given by irregular alternation of thin and rare lepidoblastic layers and prevailing granoblatic layers. Lepidoblastic layers are mainly constituted by chlorite with minor white mica. Granoblastic layers are made-up of quartz. Accessory minerals like tourmaline, oxides and sulphides are present.

odal Analysis	(% estimated)
Quartz	80
Chlorite	15
White mica	<5
Accessory (oxides-sulphides)	<1

Petrographic Classification (IUGS)

QUARTZITE

Pictures

left nicols // right nicols X – Picture dimension 2,5 X 1,8 mm

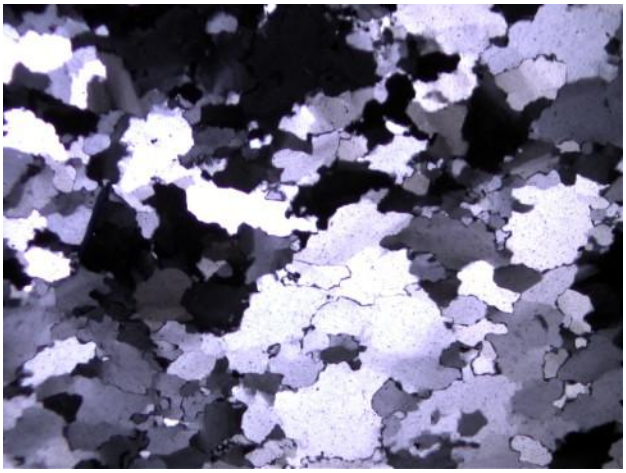

General view: granoblastic layers (quartz) with subordinate chlorite.

LAM 13.5

Petrographic Description / Analysis

Medium-fine grained metamorphic rock with heteroblastic structure and schistose texture given by lepidoblastic and granoblatic layers irregular alternation, with prevailing granoblastic layers. Lepidoblastic layers are mainly constituted by white mica, chlorite, and subordinate quartz and. a Granoblastic layers are made-up of quartz with garnet. Accessory minerals like oxides and sulphides are present.

Modal Analysis	(% estimated)
Quartz	45
White mica	25
Chlorite	17
Garnet	11
Accessory (oxides-sulphides)	2

Petrographic Classification (IUGS)

GARNET MICASCHIST

Pictures

left nicols // right nicols X – Picture dimension 2,5 X 1,8 mm

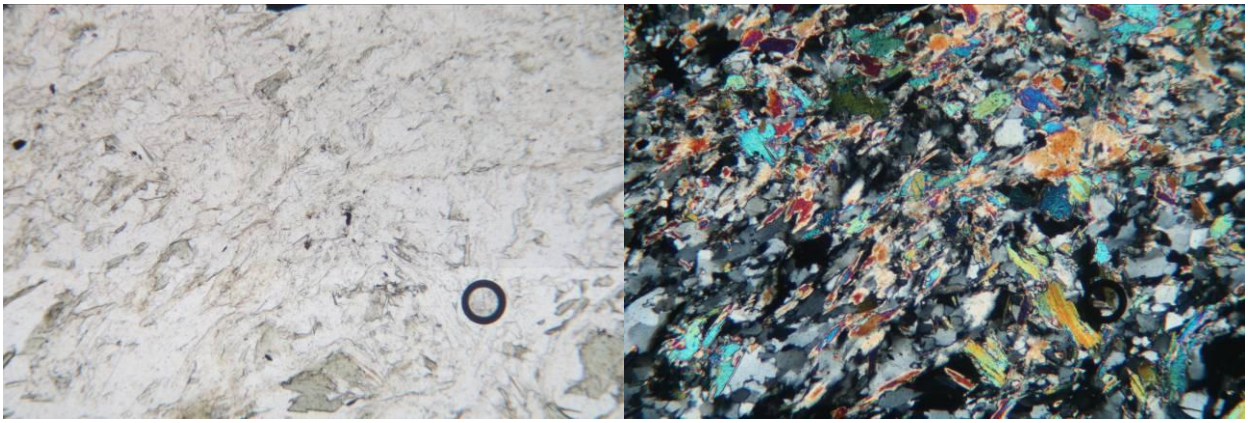

General view: granoblastic layer (quartz) and lepidoblastic layer (white mica, garnet,chlorite).

LAM 13.6

Petrographic Description / Analysis

Medium-fine grained metamorphic rock with heteroblastic structure and schistose texture given by lepidoblastic and granoblatic layers irregular alternation, with prevailing granoblastic layers. Lepidoblastic layers are mainly constituted by white mica, chlorite, and subordinate quartz and. a Granoblastic layers are made-up of quartz with garnet. Accessory minerals like oxides and sulphides are present.

Modal Analysis	(% estimated)
Quartz	43
White mica	26
Chlorite	17
Garnet	11
Accessory (oxides-sulphides)	3

Petrographic Classification (IUGS)

GARNET MICASCHIST

Pictures

left nicols // right nicols X – Picture dimension 2,5 X 1,8 mm

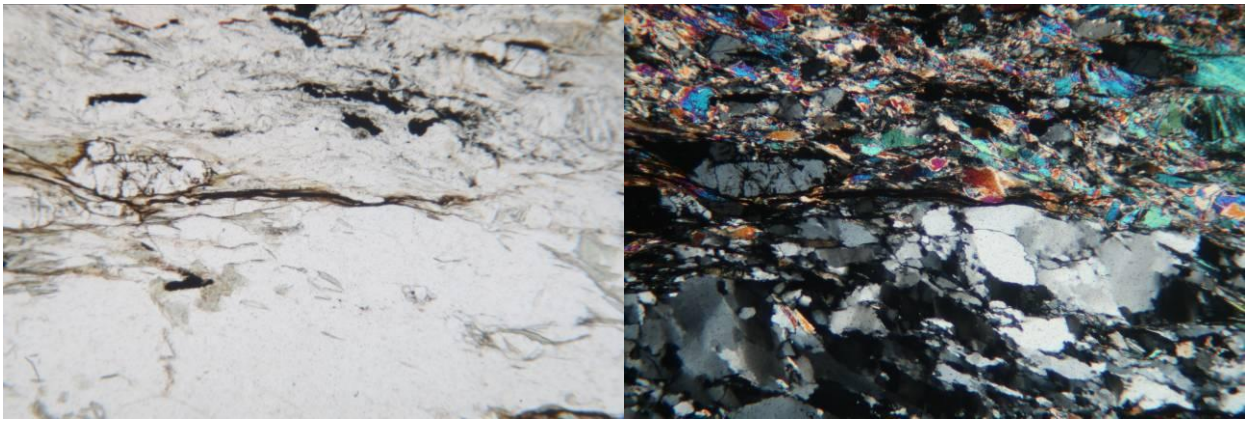

General view: granoblastic layer (quartz) and lepidoblastic layer (white mica, garnet,chlorite).

LAM 14.1

Petrographic Description / Analysis

Medium-fine grained metamorphic rock with heteroblastic structure and schistose texture given by lepidoblastic and granoblatic layers irregular alternation, with prevailing granoblastic layers. Lepidoblastic layers are mainly constituted by white mica, chlorite, and subordinate quartz. Granoblastic layers are made-up of quartz with minor garnet with subordinate feldspar-albite. Accessory minerals like oxides and sulphides are present.

Modal Analysis	(% estimated)
Quartz	42
White mica	25
Chlorite	18
Garnet	8
Feldspar+Albite	<5
Accessory (oxides-sulphides)	2

Petrographic Classification (IUGS)

GARNET MICASCHIST

Pictures

left nicols // right nicols X – Picture dimension 2,5 X 1,8 mm

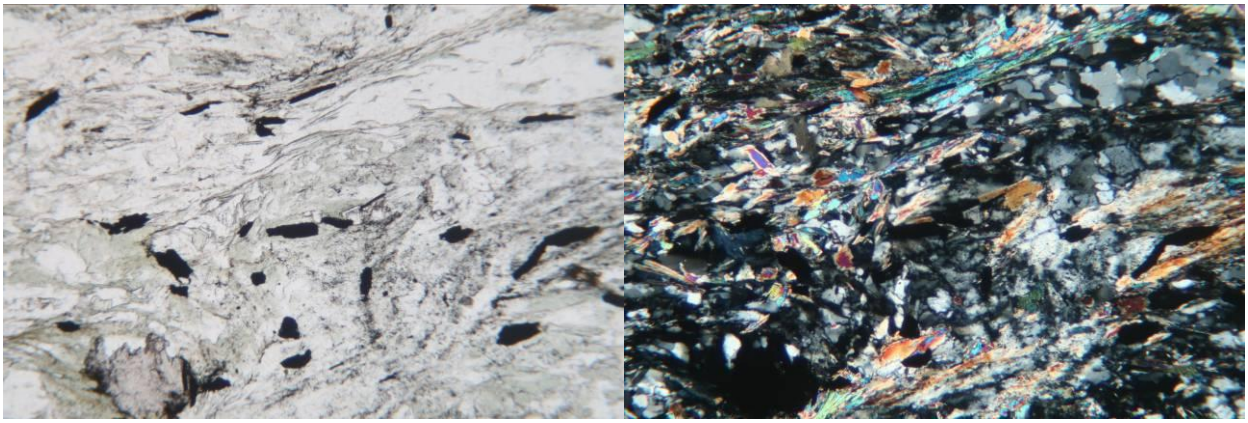

General view: granoblastic layer (quartz and feldspar) and lepidoblastic layer (white mica, garnet and chlorite).

LAM 14.2

Petrographic Description / Analysis

Medium-fine grained metamorphic rock with heteroblastic structure and schistose texture given by lepidoblastic and granoblatic layers irregular alternation, with prevailing granoblastic layers. Lepidoblastic layers are mainly constituted by white mica, chlorite,biotite, epidote and subordinate quartz. Granoblastic layers are made-up of quartz with minor garnet with subordinate feldspar-albite. Accessory minerals like oxides and sulphides are present.

Modal Analysis	(% estimated)
Quartz	40
Biotite	5
White mica	20
Chlorite	18
Garnet	10
Epidote	1
Feldspar+Albite	<5
Accessory (oxides-sulphides)	1

Petrographic Classification (IUGS)

GARNET MICASCHIST

Pictures

left nicols // right nicols X – Picture dimension 2,5 X 1,8 mm

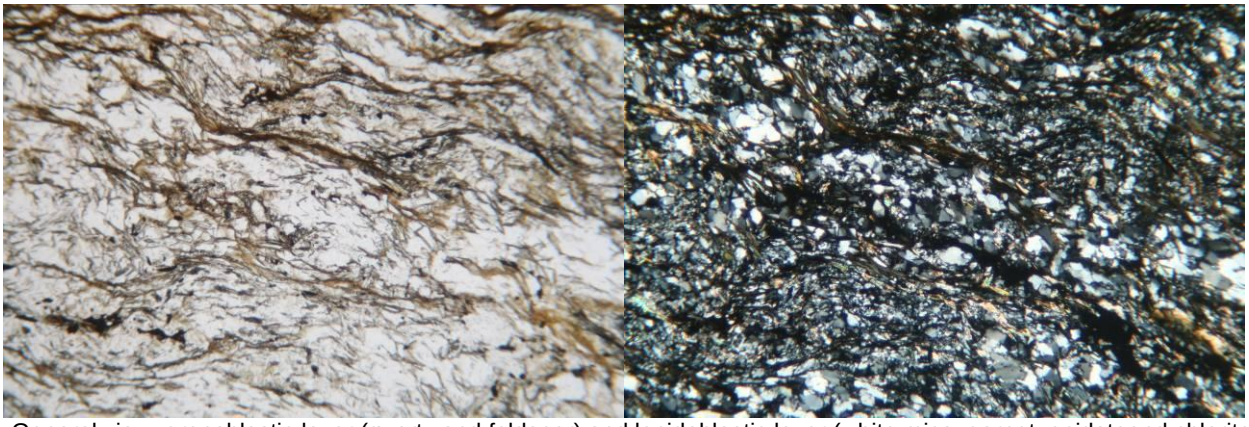

General view: granoblastic layer (quartz and feldspar) and lepidoblastic layer (white mica, garnet, epidoteand chlorite).

POVE 1

Petrographic Description / Analysis

Medium-fine grained metamorphic rock with heteroblastic structure and schistose texture given by lepidoblastic and granoblatic layers irregular alternation, with prevailing granoblastic layers. Lepidoblastic layers are mainly constituted by white mica, chlorite, and subordinate quartz. Granoblastic layers are made-up of quartz with minor garnet with subordinate Accessory minerals like oxides and sulphides are present.

Modal Analysis	(% estimated)
Quartz	45
White mica	24
Chlorite	18
Garnet	12
Accessory (oxides-sulphides)	1

Petrographic Classification (IUGS)

GARNET MICASCHIST

Pictures

left nicols // right nicols X – Picture dimension 2,5 X 1,8 mm

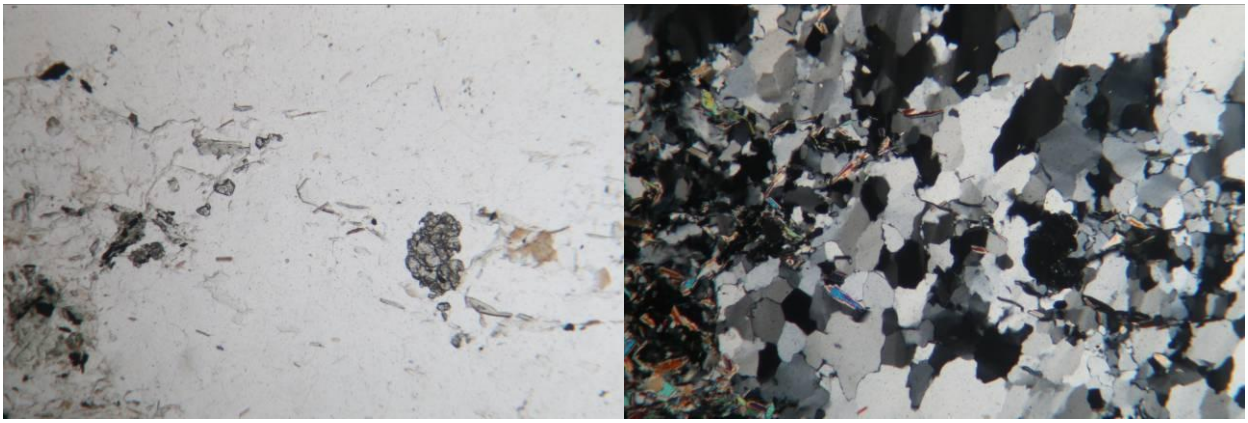

General view: granoblastic layer (quartz, garnet) and lepidoblastic layer (white mica, garnet and chlorite).

POVE 2

Petrographic Description / Analysis

Medium-fine grained metamorphic rock with heteroblastic structure and schistose texture given by lepidoblastic and granoblatic layers irregular alternation, with prevailing granoblastic layers. Lepidoblastic layers are mainly constituted by white mica, chlorite, organic matter and subordinate quartz and feldspar-albite. Granoblastic layers are made-up of quartz with minor feldspar-albite and subordinate white mica with chlorite. Accessory minerals like oxides and sulphides are present.

Modal Analysis	(% estimated)
Quartz	45
White mica	25
Chlorite	20
Feldspar+Albite	5
Organic matter	4
Accessory (oxides-sulphides)	<1

Petrographic Classification (IUGS)

MICASCHIST

Pictures

left nicols // right nicols X – Picture dimension 2,5 X 1,8 mm

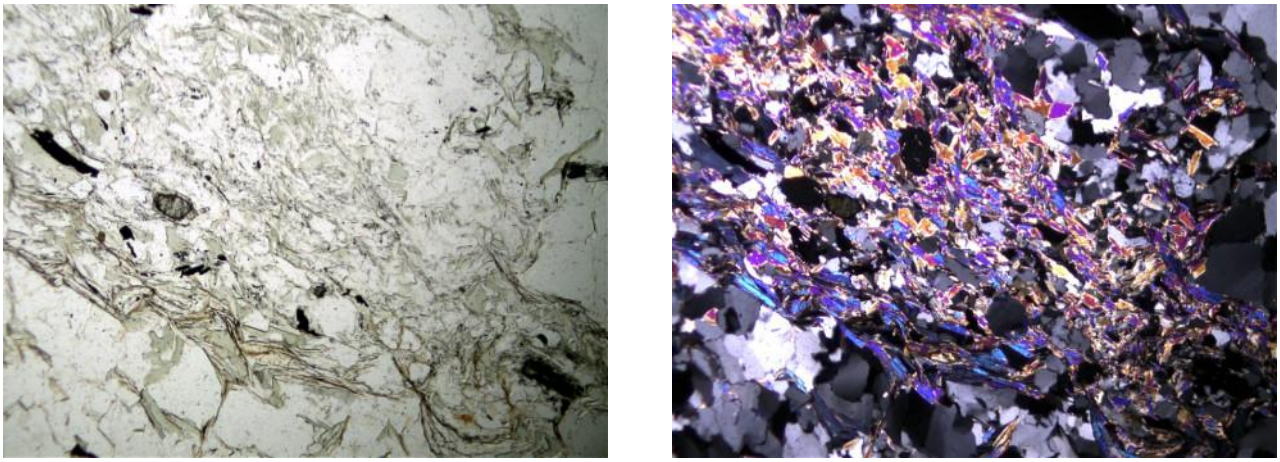

General view: granoblastic layers (quartz and feldspar) with subordinate lepidoblastic layers (white mica, chlorite and organic matter).

POVE 3

Petrographic Description / Analysis

Medium-fine grained metamorphic rock with heteroblastic structure and schistose texture given by lepidoblastic and granoblatic layers irregular alternation, with prevailing granoblastic layers. Lepidoblastic layers are mainly constituted by white mica, chlorite, and subordinate quartz. Granoblastic layers are made-up of quartz with minor garnet with subordinate feldspar-albite. Accessory minerals like oxides and sulphides are present.

Modal Analysis	(% estimated)
Quartz	42
White mica	24
Chlorite	15
Garnet	12
Feldspar+Albite	<5
Accessory (oxides-sulphides)	2

Petrographic Classification (IUGS)

GARNET MICASCHIST

Pictures

left nicols // right nicols X – Picture dimension 2,5 X 1,8 mm

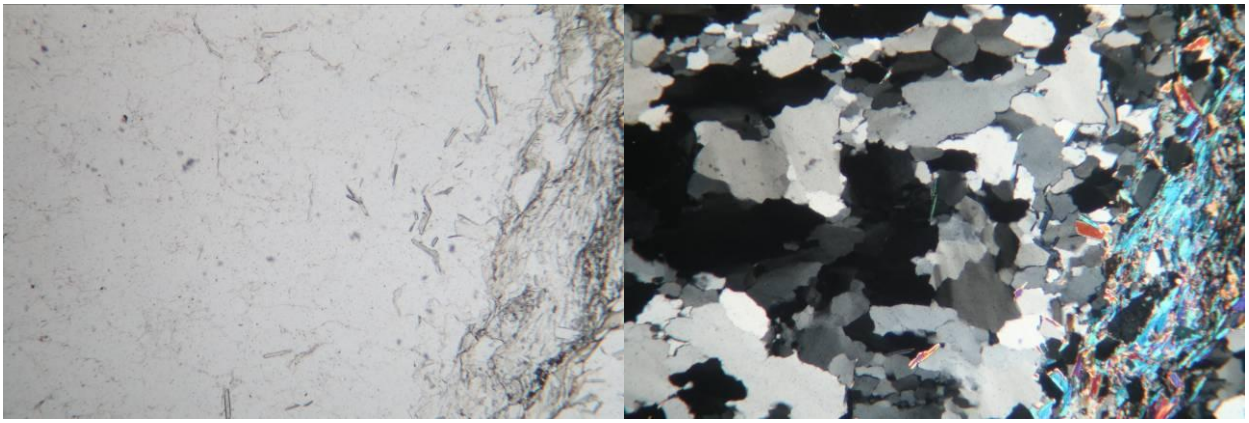

General view: granoblastic layer (quartz and feldspar) and lepidoblastic layer (white mica, garnet and chlorite).

AP 14.1

Petrographic Description / Analysis

Medium grained igneous rock with phaneritic texture (holocrystalline seriate). Crystals do not show preferred orientation (isotropic texture). Main minerals are plagioclase, biotite, quartz and amphibole. Accessory minerals are zircon, apatite and oxides. Secondary (from alteration) minerals are chlorite (on biotite and amphibole), epidote (on plagioclase, biotite and amphibole), sericite and white mica (on plagioclase).

Modal Analysis	(% estimated)
Plagioclase	40
Biotite	20
Quartz	15
Amphibole (hornebl)	18
Accessory Minerals	<5
Secondary Minerals	<2

Petrographic Classification (IUGS)

TONALITE

Pictures

left nicols // right nicols X – Picture dimension 2,5 X 1,8 mm

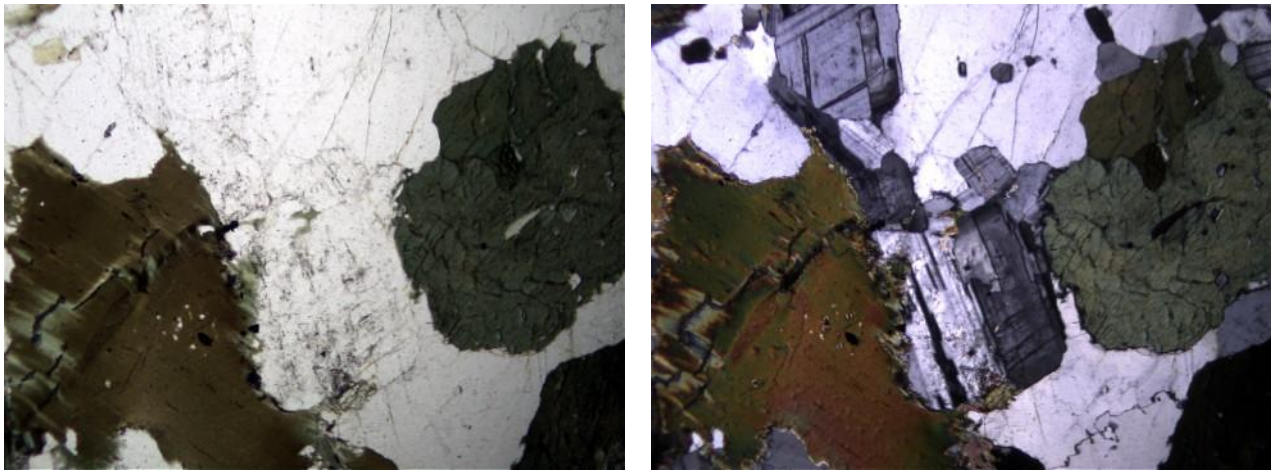

General view: Holocristalline seriate texture with plagioclase, quartz, biotite and plagioclase. Chlorite and sericite are also present.

AP 14.2

Petrographic Description / Analysis

Medium grained igneous rock with phaneritic texture (holocrystalline seriate). Crystals do not show preferred orientation (isotropic texture). Main minerals are plagioclase, biotite, quartz and amphibole. Accessory minerals are zircon, apatite and oxides. Secondary (from alteration) minerals are chlorite (on biotite and amphibole), epidote (on plagioclase and amphibole), sericite and white mica (on plagioclase).

Modal Analysis	(% estimated)
Plagioclase	45
Chlorite	5
Quartz	22
Amphibole (hornebl)	20
Accessory Minerals	<5
Secondary Minerals	<3

Petrographic Classification (IUGS)

TONALITE

Pictures

left nicols // right nicols X – Picture dimension 2,5 X 1,8 mm

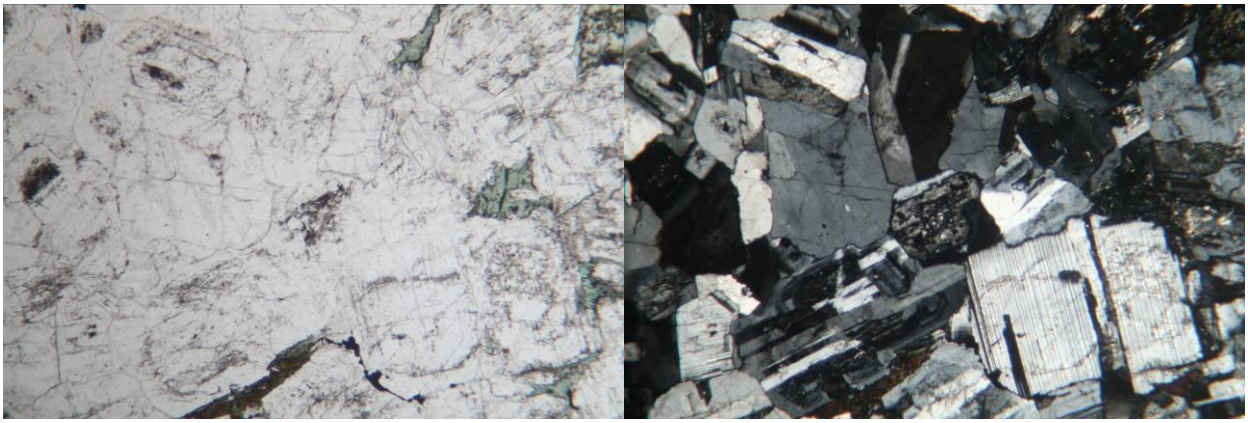

General view: Holocristalline seriate texture with plagioclase, quartz, biotite and plagioclase. Chlorite and sericite are also present.

AP 14.4

Petrographic Description / Analysis

Medium grained igneous rock with phaneritic texture (holocrystalline seriate). Crystals do not show preferred orientation (isotropic texture). Main minerals are plagioclase, biotite, quartz and amphibole. Accessory minerals are zircon, apatite and oxides. Secondary (from alteration) minerals are chlorite (on biotite and amphibole), pistacite, sericite and white mica (on plagioclase)..

Modal Analysis	(% estimated)
Plagioclase	38
Biotite	22
Quartz	15
Amphibole (hornebl)	18
Accessory Minerals	<5
Secondary Minerals	<2

Petrographic Classification (IUGS)

TONALITE

Pictures

left nicols // right nicols X – Picture dimension 2,5 X 1,8 mm

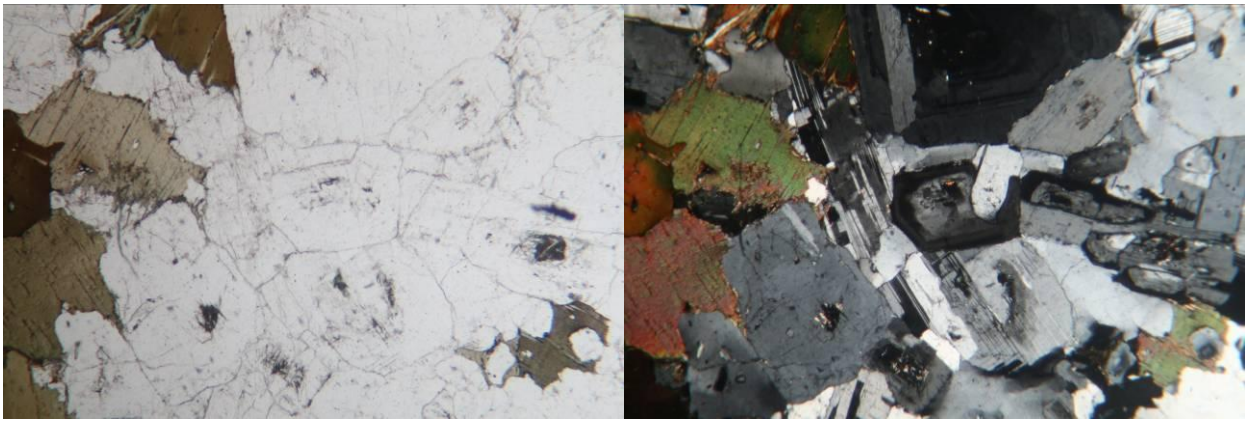

General view: Holocristalline seriate texture with plagioclase, quartz, biotite and plagioclase. Chlorite and sericite are also present.

AP 14.5

Petrographic Description / Analysis

Medium grained igneous rock with phaneritic texture (holocrystalline seriate). Crystals do not show preferred orientation (isotropic texture). Main minerals are plagioclase, biotite, quartz and amphibole.

Modal Analysis	(% estimated)
Plagioclase	40
Biotite	22
Quartz	20
Amphibole (hornebl)	18

Petrographic Classification (IUGS)

TONALITE

Pictures

left nicols // right nicols X – Picture dimension 2,5 X 1,8 mm

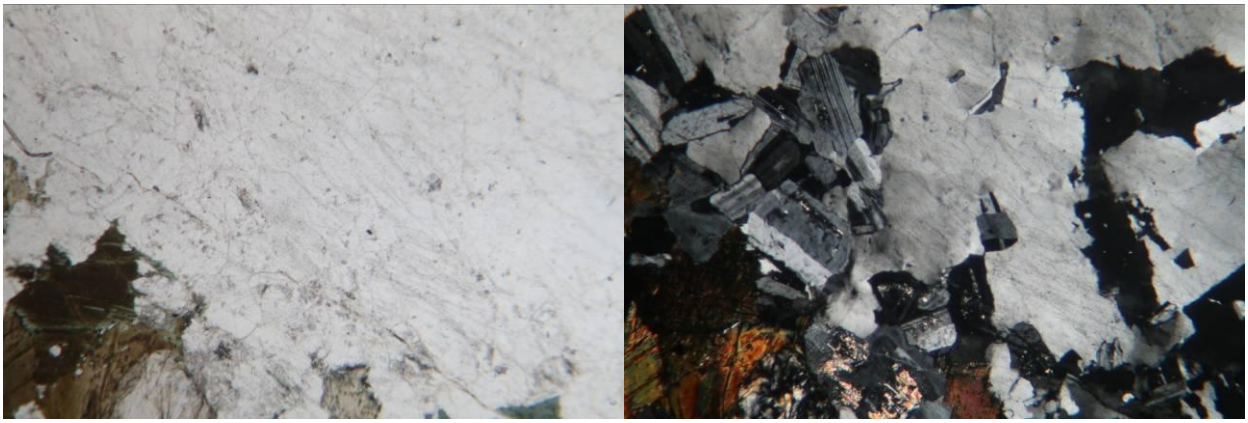

General view: Holocristalline seriate texture with plagioclase, quartz, biotite and plagioclase.

VP 14.1

Petrographic Description / Analysis

Medium grained igneous rock with phaneritic texture (holocrystalline seriate). Crystals do not show preferred orientation (isotropic texture). Main minerals are plagioclase,white mica biotite, quartz and amphibole. Accessory minerals are oxides. Secondary (from alteration) minerals are chlorite (on biotite and amphibole),

Modal Analysis	(% estimated)
Plagioclase	40
Biotite	20
Quartz	20
Amphibole (hornebl)	12
Accessory Minerals	<5
Secondary Minerals	<3

Petrographic Classification (IUGS)

TONALITE

Pictures

left nicols // right nicols X – Picture dimension 2,5 X 1,8 mm

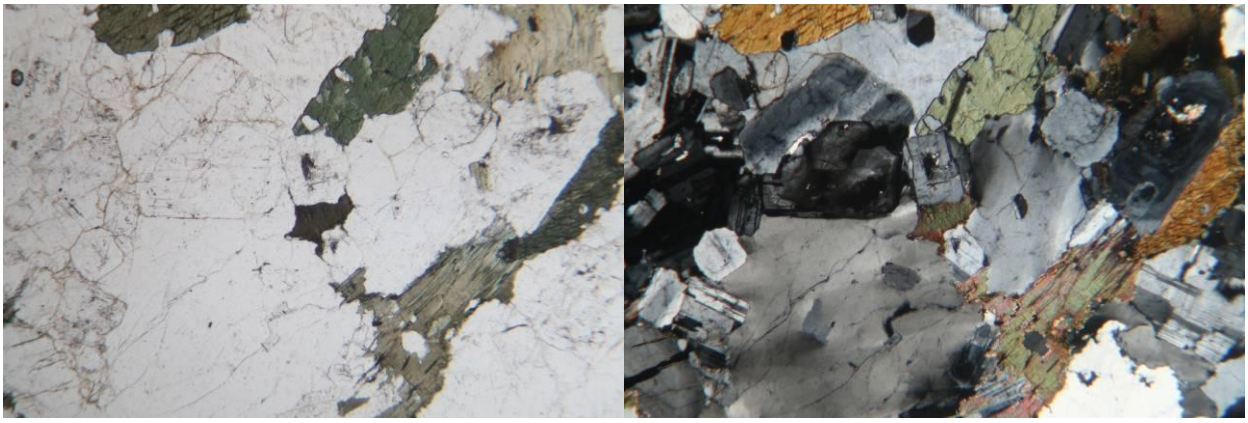

General view: Holocristalline seriate texture with plagioclase, quartz and biotite.

STAV 14.1

Petrographic Description / Analysis

Medium grained igneous rock with phaneritic texture (holocrystalline seriate). Crystals do not show preferred orientation (isotropic texture). Main minerals are plagioclase, biotite, quartz and amphibole. Accessory minerals are zircon, apatite and oxides. Secondary (from alteration) minerals are chlorite (on biotite and amphibole), epidote (on plagioclase, biotite and amphibole), sericite and white mica (on plagioclase). Traces of cataclastic deformation.

Modal Analysis	(% estimated)
Plagioclase	40
Biotite	18
Quartz	17
Amphibole (hornebl)	18
Accessory Minerals	<5
Secondary Minerals	<2

Petrographic Classification (IUGS)

TONALITE

Pictures

left nicols // right nicols X – Picture dimension 2,5 X 1,8 mm

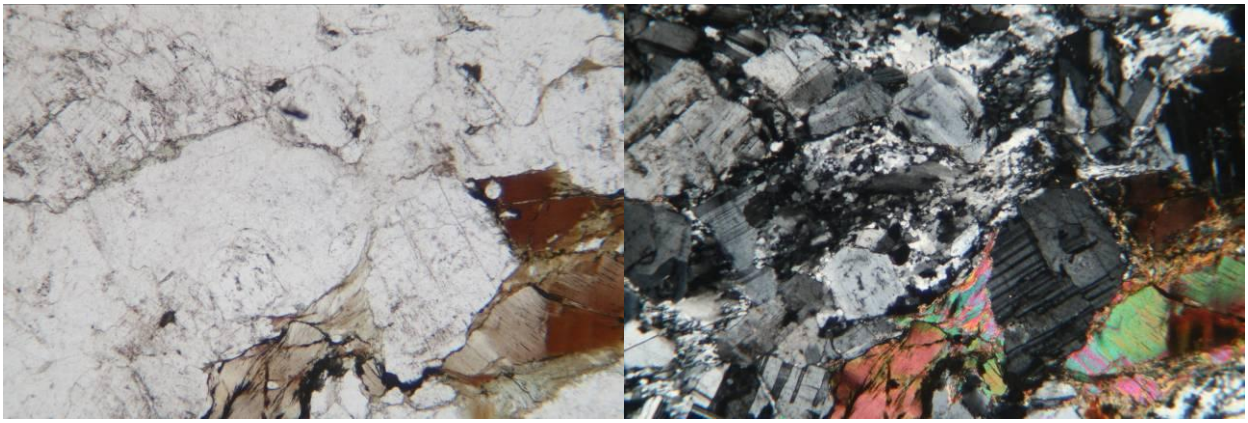

General view: Holocristalline seriate texture with plagioclase, quartz, biotite and plagioclase. Chlorite and sericite are also present.

STAV 14.3

Petrographic Description / Analysis

Medium grained igneous rock with phaneritic texture (holocrystalline seriate). Crystals do not show preferred orientation (isotropic texture). Main minerals are plagioclase, biotite, quartz and amphibole. Accessory minerals are, apatite and oxides. Secondary (from alteration) minerals are chlorite (on biotite and amphibole), epidote (on plagioclase, biotite and amphibole), sericite and white mica (on plagioclase).

Modal Analysis	(% estimated)
Plagioclase	40
Biotite	20
Quartz	18
Amphibole (hornebl)	15
Accessory Minerals	<5
Secondary Minerals	<2

Petrographic Classification (IUGS)

TONALITE

Pictures

left nicols // right nicols X – Picture dimension 2,5 X 1,8 mm

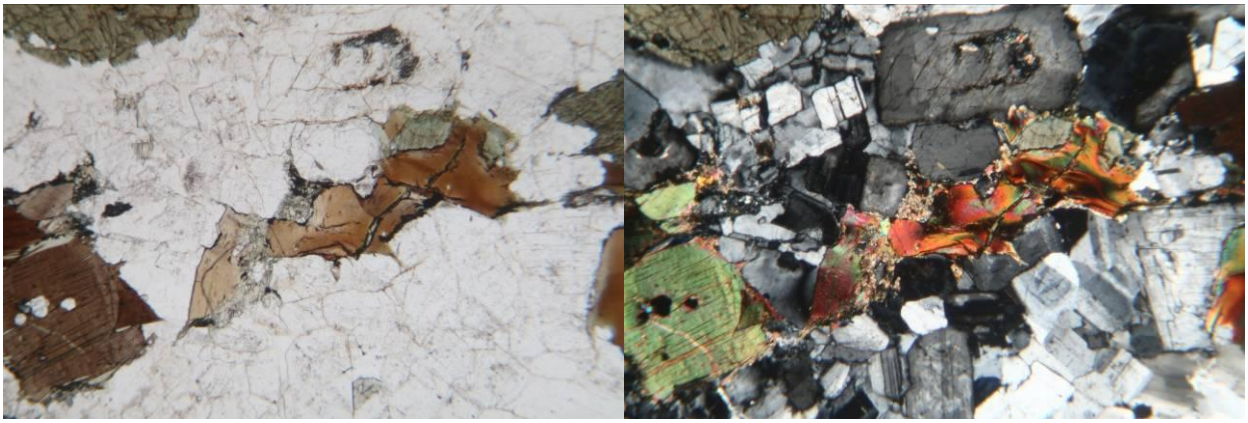

General view: Holocristalline seriate texture with plagioclase, quartz, biotite and plagioclase. Chlorite and sericite are also present.

VOL 14.1

Petrographic Description / Analysis

Medium grained igneous rock with phaneritic texture (holocrystalline seriate). Crystals do not show preferred orientation (isotropic texture). Main minerals are plagioclase, biotite, quartz and amphibole. Accessory minerals are zircon, and oxides. Secondary (from alteration) minerals are chlorite (on biotite and amphibole), zircon and zoisite

Modal Analysis	(% estimated)
Plagioclase	40
Biotite	18
Quartz	20
Amphibole (hornebl)	15
Accessory Minerals	<5
Secondary Minerals	<2

Petrographic Classification (IUGS)

TONALITE

Pictures

left nicols // right nicols X – Picture dimension 2,5 X 1,8 mm

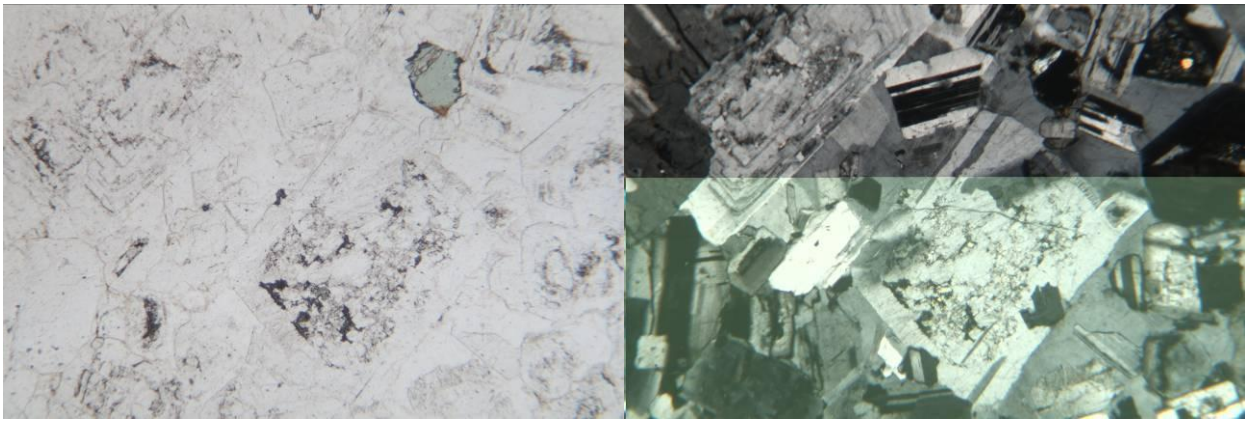

General view: Holocristalline seriate texture with plagioclase, quartz, biotite and plagioclase.

MAL 14.1 *Petrographic Description / Analysis*

Medium-fine grained metamorphic rock with heteroblastic structure and schistose texture given by lepidoblastic and granoblatic layers irregular alternation, with prevailing granoblastic layers. Lepidoblastic layers are mainly constituted by white mica, chlorite, tourmaline,biotite, organic matter and subordinate quartz and feldspar-albite. Granoblastic layers are made-up of quartz with minor feldspar-albite and subordinate white mica with chlorite. Accessory minerals like oxides and sulphides are present.

Modal Analysis	(% estimated)
Quartz	40
White mica	25
Tourmaline	2
Biotite	4
Chlorite	20
Feldspar+Albite	7
Organic matter	1
Accessory (oxides-sulphides)	<1

Petrographic Classification (IUGS)

MICASCHIST

Pictures

left nicols // right nicols X – Picture dimension 2,5 X 1,8 mm

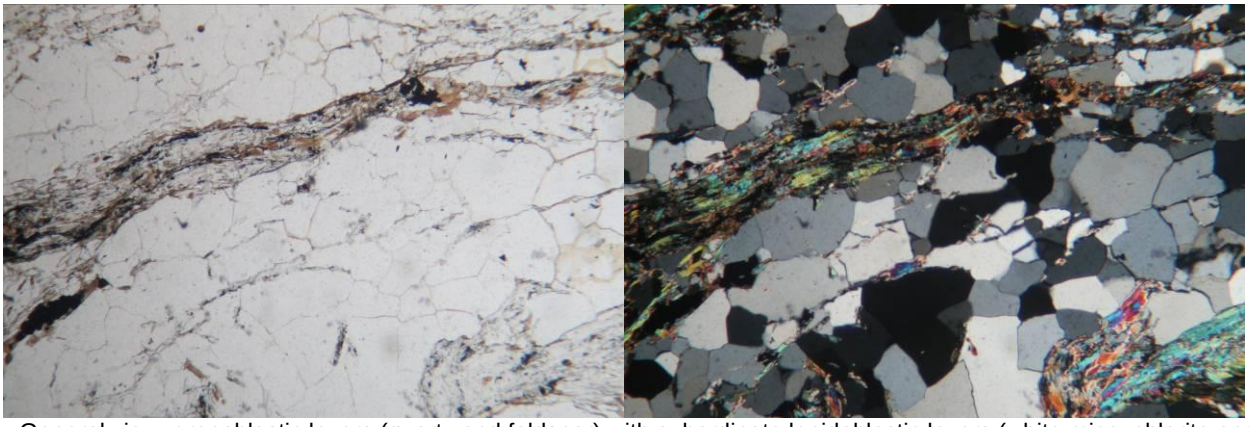

General view: granoblastic layers (quartz and feldspar) with subordinate lepidoblastic layers (white mica, chlorite and organic matter).

MAL14.2

Petrographic Description / Analysis

Medium-fine grained metamorphic rock with heteroblastic structure and schistose texture given by lepidoblastic and granoblatic layers irregular alternation, with prevailing granoblastic layers. Lepidoblastic layers are mainly constituted by white mica, chlorite, tourmaline,biotite, and subordinate quartz and feldspar-albite. Granoblastic layers are made-up of quartz with minor feldspar-albite and subordinate white mica with chlorite. Accessory minerals like oxides and sulphides are present.

Modal Analysis	(% estimated)
Quartz	40
White mica	25
Tourmaline	2
Biotite	4
Chlorite	20
Feldspar+Albite	8
Accessory (oxides-sulphides)	<1

Petrographic Classification (IUGS)

MICASCHIST

Pictures

left nicols // right nicols X – Picture dimension 2,5 X 1,8 mm

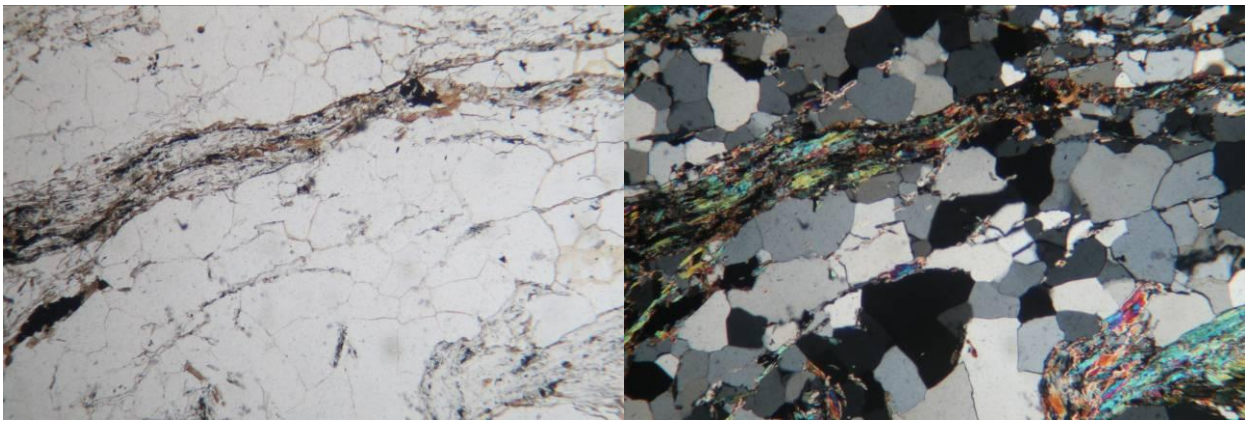

General view: granoblastic layers (quartz and feldspar) with subordinate lepidoblastic layers (white mica, chlorite and biotite).

MAL 14.6

Petrographic Description / Analysis

Medium-fine grained metamorphic rock with heteroblastic structure and gneissic texture given by thin and discontinuos lepidoblastic layers wrapping prevailing granoblatic layers. Granoblastic layers are made-up of feldspar+albite, quartz and sillimanite (fibrous and prismatic). Lepidoblastic layers are mainly constituted by biotite, white mica and chlorite. Accessory minerals like oxides and sulphides are present.

Modal Analysis	(% estimated)
Feldspar+Albite	35
Quartz	25
Sillimanite	20
Biotite	10
White mica	5
Chlorite	4
Accessory (oxides-sulphides)	1

Petrographic Classification (IUGS)

SILLIMANITE GNEISS

Pictures

left nicols // right nicols X – Picture dimension 2,5 X 1,8 mm

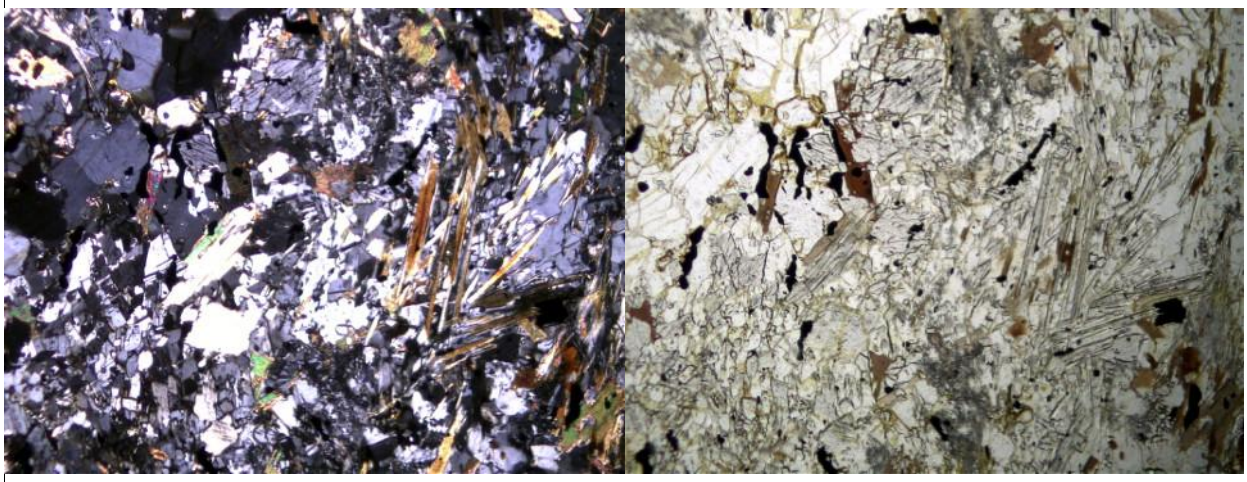

General view: granoblastic layers (quartz, sillimanite and albite-feldspar) with subordinate discontinuos lepidoblastic layers (biotite, white mica and chlorite).

SANT 14.1

Petrographic Description / Analysis

Medium grained igneous rock with phaneritic texture (holocrystalline seriate). Crystals do not show preferred orientation (isotropic texture). Main minerals are plagioclase, biotite, quartz and amphibole. Accessory minerals are zircon, apatite, titanite and oxides. Secondary (from alteration) minerals are chlorite (on biotite and amphibole), epidote (on plagioclase, biotite and amphibole), and white mica (on plagioclase).

Modal Analysis	(% estimated)
Plagioclase	40
Biotite	20
Quartz	18
Amphibole (hornebl)	15
Accessory Minerals	<5
Secondary Minerals	<2

Petrographic Classification (IUGS)

TONALITE

Pictures

left nicols // right nicols X – Picture dimension 2,5 X 1,8 mm

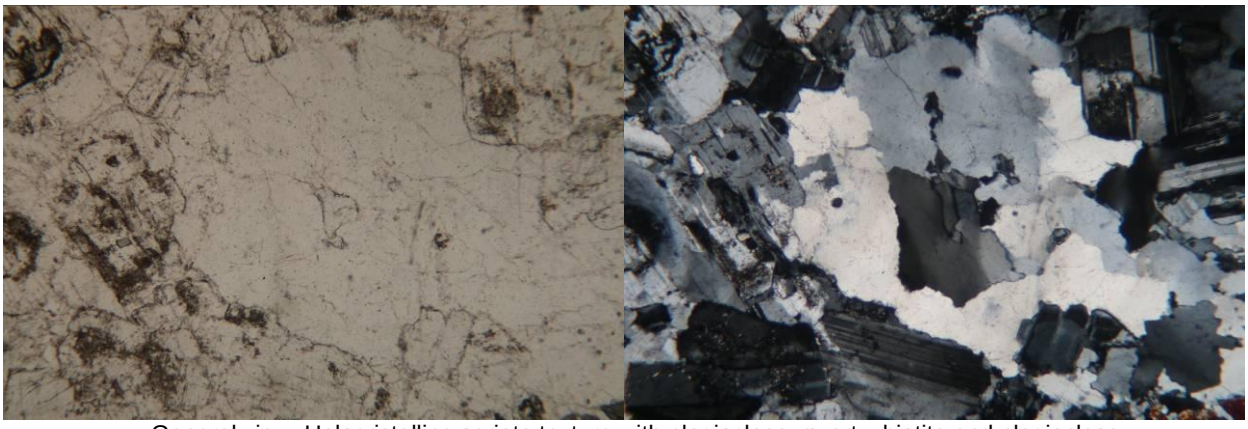

General view: Holocristalline seriate texture with plagioclase, quartz, biotite and plagioclase.

SANT 14.2

Petrographic Description / Analysis

Medium grained igneous rock with phaneritic texture (holocrystalline seriate). Crystals do not show preferred orientation (isotropic texture). Main minerals are plagioclase, biotite, quartz and amphibole. Accessory minerals are zircon, apatite, titanite and oxides. Secondary (from alteration) minerals are chlorite (on biotite and amphibole), epidote (on plagioclase, biotite and amphibole), and sericite.

Modal Analysis	(% estimated)
Plagioclase	40
Biotite	20
Quartz	20
Amphibole (hornebl)	12
Accessory Minerals	<5
Secondary Minerals	<3

Petrographic Classification (IUGS)

TONALITE

Pictures

left nicols // right nicols X – Picture dimension 2,5 X 1,8 mm

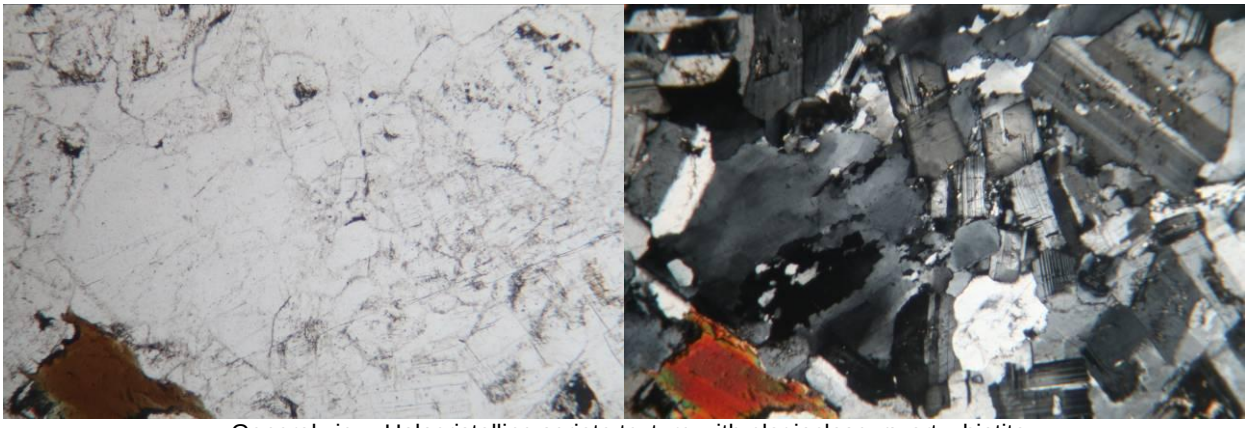

General view: Holocristalline seriate texture with plagioclase, quartz, biotite ..

BRE 14.01

Petrographic Description / Analysis

Medium grained igneous rock with phaneritic texture (holocrystalline seriate). Crystals do not show preferred orientation (isotropic texture). Main minerals are plagioclase, biotite, quartz and amphibole. Accessory minerals are zircon, apatite, titanite and oxides. Secondary (from alteration) minerals are chlorite (on biotite and amphibole), epidote (on plagioclase, biotite and amphibole), sericite and white mica (on plagioclase).

Modal Analysis	(% estimated)
Plagioclase	40
Biotite	18
Quartz	20
Amphibole (hornebl)	15
Accessory Minerals	<5
Secondary Minerals	<2

Petrographic Classification (IUGS)

TONALITE

Pictures

left nicols // right nicols X – Picture dimension 2,5 X 1,8 mm

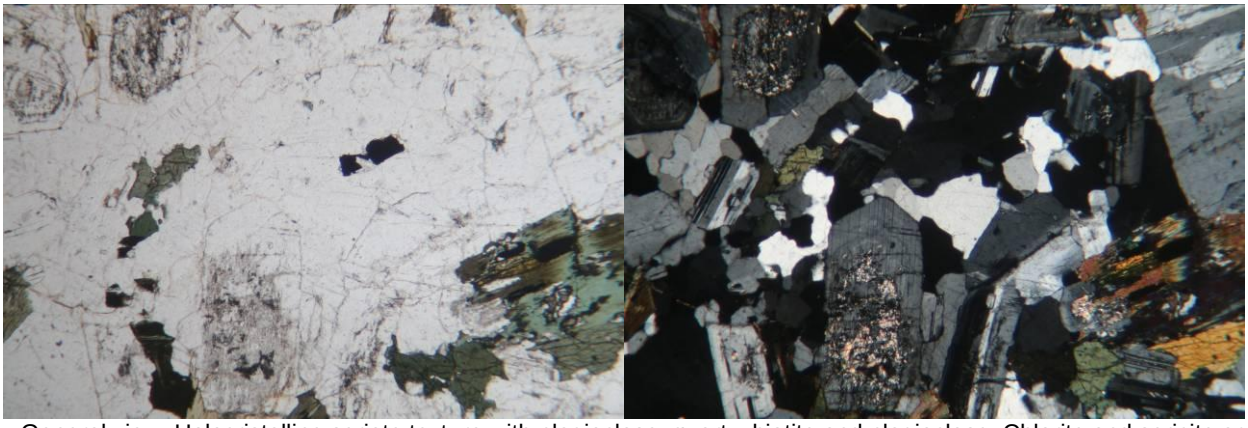

General view: Holocristalline seriate texture with plagioclase, quartz, biotite and plagioclase. Chlorite and sericite are also present.

CB 091206.03

Petrographic Description / Analysis

Medium grained igneous rock with phaneritic texture (holocrystalline seriate). Crystals show no preferred orientation. Main minerals are plagioclase, quartz, feldspar and muscovite. Accessory minerals are tourmaline, zircon, apatite and oxides. Secondary minerals (derived from alteration's process) are represented by sericite/muscovite on plagioclase.

Modal Analysis	(% estimated)
Plagioclase	40
Quartz	35
Muscovite	12
Feldspar	10
Accessory Minerals	2
Secondary Minerals	1

Petrographic Classification (IUGS)

TONALITE

Pictures

left nicols // right nicols X – Picture dimension 2,5 X 1,8 mm

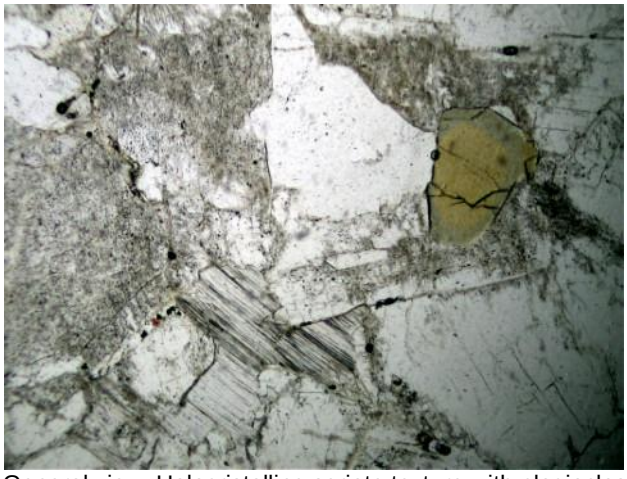

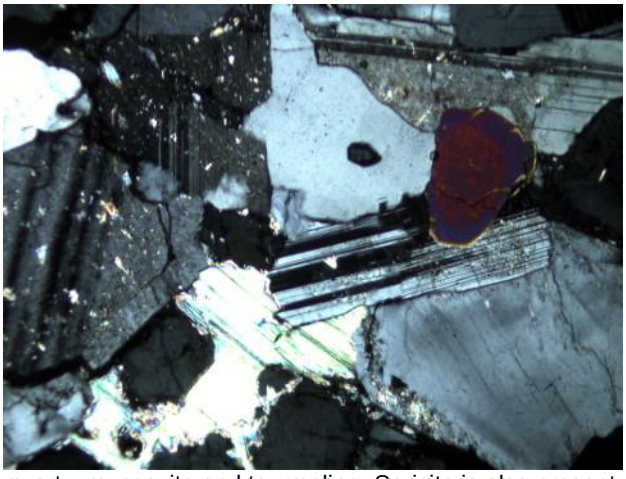

General view: Holocristalline seriate texture with plagioclase, quartz, muscovite and tourmaline. Sericite is also present.

CB 091206.09

Petrographic Description / Analysis

Medium grained igneous rock with phaneritic texture (holocrystalline seriate). Crystals do not show preferred orientation (isotropic texture). Main minerals are feldspar, quartz, plagioclase, biotite and muscovite. Accessory minerals are zircon, tourmaline, apatite and oxides. Secondary minerals are sericite and saussurrite (on plagioclase and feldspar) and chlorite (on biotite).

Modal Analysis	(% estimated)
Feldspar	40
Quartz	30
Plagioclase	15
Biotite	8
Muscovite	4
Accessory Minerals	2
Secondary Minerals	<1

Petrographic Classification (IUGS)

SYENOGRANITE

Pictures

left nicols // right nicols X – Picture dimension 2,8 X 2,1 mm

General view: Holocristalline seriate texture with feldspar, quartz, plagioclase and biotite. Sericite,saussurrite (on feldspar and plagioclase) and chlorite (on biotite) are also present.

CB 091206.10

Petrographic Description / Analysis

Medium grained igneous rock with phaneritic texture (holocrystalline seriate). Crystals do not show preferred orientation (isotropic texture). Main minerals are feldspar, quartz, plagioclase, biotite and muscovite. Accessory minerals are zircon, tourmaline, apatite and oxides. Secondary minerals are sericite and saussurrite (on plagioclase and feldspar) and chlorite (on biotite).

Modal Analysis	(% estimated)
Feldspar	36
Quartz	30
Plagioclase	18
Biotite	10
Muscovite	3
Accessory Minerals	2
Secondary Minerals	<1

Petrographic Classification (IUGS)

SYENOGRANITE

Pictures

left nicols // right nicols X – Picture dimension 2,8 X 2,1 mm

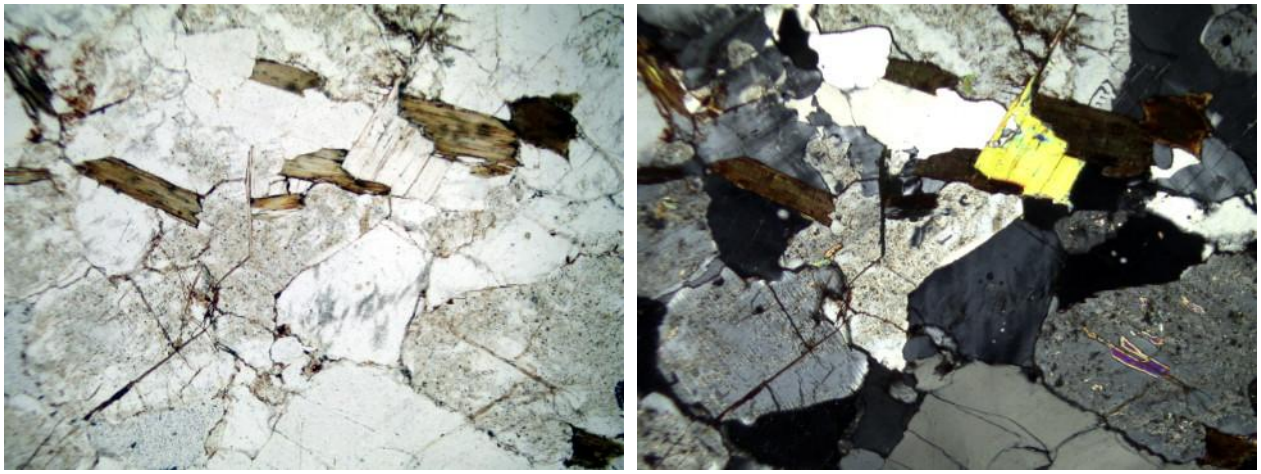

General view: Holocristalline seriate texture with feldspar, quartz, biotite and muscovite. Sericite,saussurrite (on feldspar and plagioclase) and chlorite (on biotite) are also present.

CB 091206.11

Petrographic Description / Analysis

Medium grained igneous rock with phaneritic texture (holocrystalline seriate). Crystals do not show preferred orientation (isotropic texture). Main minerals are feldspar, quartz, plagioclase, biotite and muscovite. Accessory minerals are tourmaline, apatite and oxides. Secondary minerals are epidote, sericite and saussurrite (on plagioclase and feldspar) and chlorite (on biotite).

Modal Analysis	(% estimated)
Feldspar	35
Quartz	35
Plagioclase	15
Biotite	6
Muscovite	6
Accessory Minerals	1
Secondary Minerals	2

Petrographic Classification (IUGS)

SYENOGRANITE

Pictures

left nicols // right nicols X – Picture dimension 2,8 X 2,1 mm

General view: Holocristalline seriate texture with feldspar, quartz, plagioclase biotite and muscovite. Sericite,saussurrite (on feldspar and plagioclase) and chlorite (on biotite) are also present.

CB 091206.17

Petrographic Description / Analysis

Medium grained igneous rock with phaneritic texture (holocrystalline seriate). Crystals do not show preferred orientation (isotropic texture). Main minerals are feldspar, quartz, plagioclase, biotite and muscovite. Accessory minerals are tourmaline, apatite and oxides. Secondary minerals are sericite (on plagioclase and feldspar) and chlorite (on biotite).

Modal Analysis	(% estimated)
Feldspar	40
Quartz	30
Plagioclase	15
Biotite	7
Muscovite	6
Accessory Minerals	1
Secondary Minerals	1

Petrographic Classification (IUGS)

SYENOGRANITE

Pictures

left nicols // right nicols X – Picture dimension 2,8 X 2,1 mm

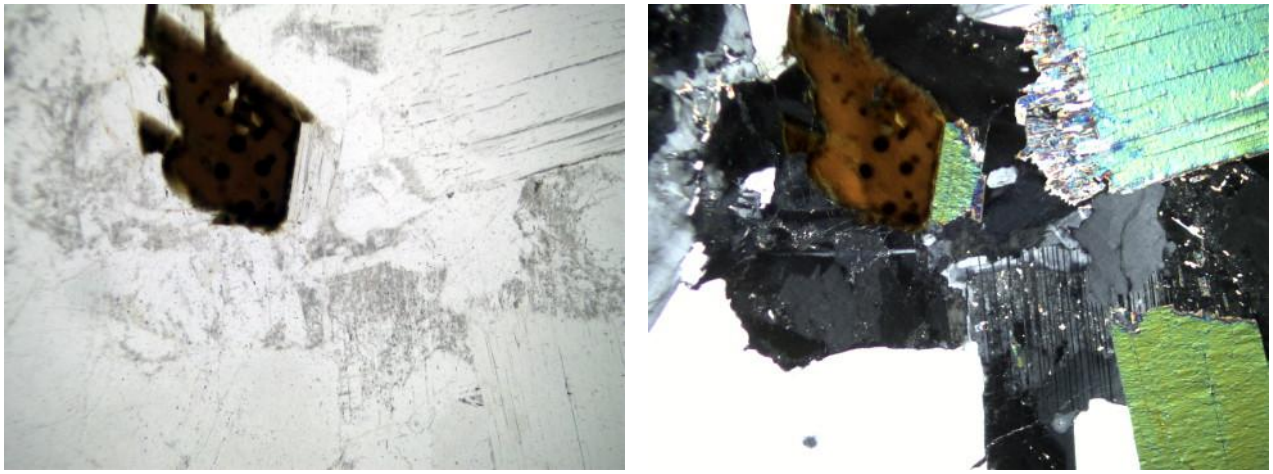

General view: Holocristalline seriate texture with feldspar, quartz, plagioclase biotite and muscovite. Sericite (on feldspar and plagioclase) and chlorite (on biotite) are also present.

CB 091206.18

Petrographic Description / Analysis

Medium grained igneous rock with phaneritic texture (holocrystalline seriate). Crystals do not show preferred orientation (isotropic texture). Main minerals are feldspar, quartz, plagioclase, biotite and muscovite. Accessory minerals are tourmaline, apatite and oxides. Secondary minerals are epidote, sericite and muscovite (on plagioclase and feldspar) and chlorite (on biotite).

Modal Analysis	(% estimated)
Feldspar	35
Quartz	30
Plagioclase	18
Muscovite	8
Biotite	7
Accessory Minerals	1
Secondary Minerals	1

Petrographic Classification (IUGS)

SYENOGRANITE

Pictures

left nicols // right nicols X – Picture dimension 2,8 X 2,1 mm

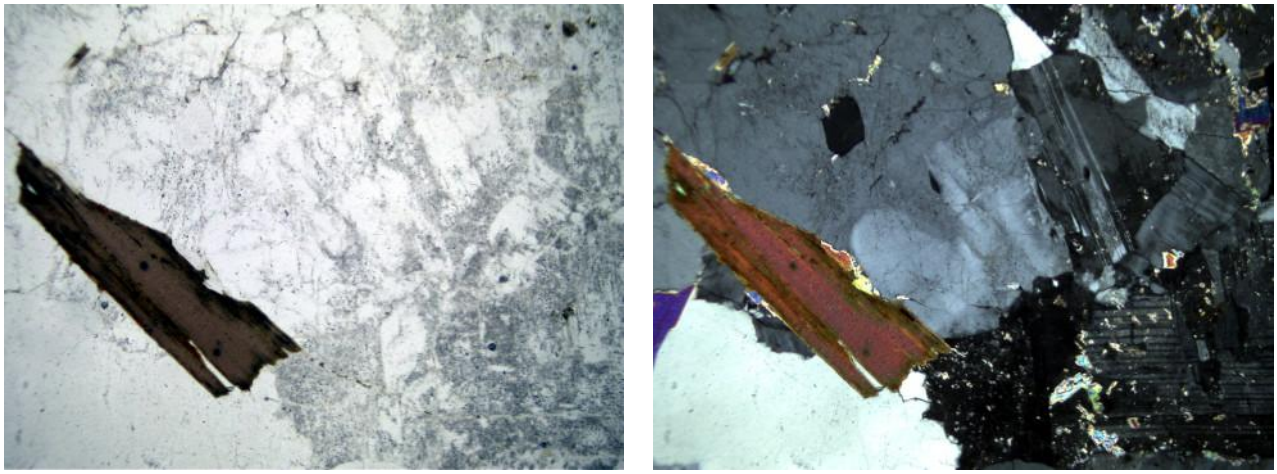

General view: Holocristalline seriate texture with feldspar, quartz, plagioclase biotite and muscovite. Sericite and muscovite (on feldspar and plagioclase) are also present.

CB 091206.19

Petrographic Description / Analysis

Medium grained igneous rock with phaneritic texture (holocrystalline seriate). Crystals do not show preferred orientation (isotropic texture). Main minerals are feldspar, quartz, plagioclase, biotite and muscovite. Accessory minerals are apatite and oxides. Secondary minerals are epidote, sericite and muscovite (on plagioclase and feldspar) and chlorite (on biotite).

Modal Analysis	(% estimated)
Feldspar	35
Quartz	30
Plagioclase	18
Biotite	8
Muscovite	7
Accessory Minerals	1
Secondary Minerals	1

Petrographic Classification (IUGS)

SYENOGRANITE

Pictures

left nicols // right nicols X – Picture dimension 2,8 X 2,1 mm

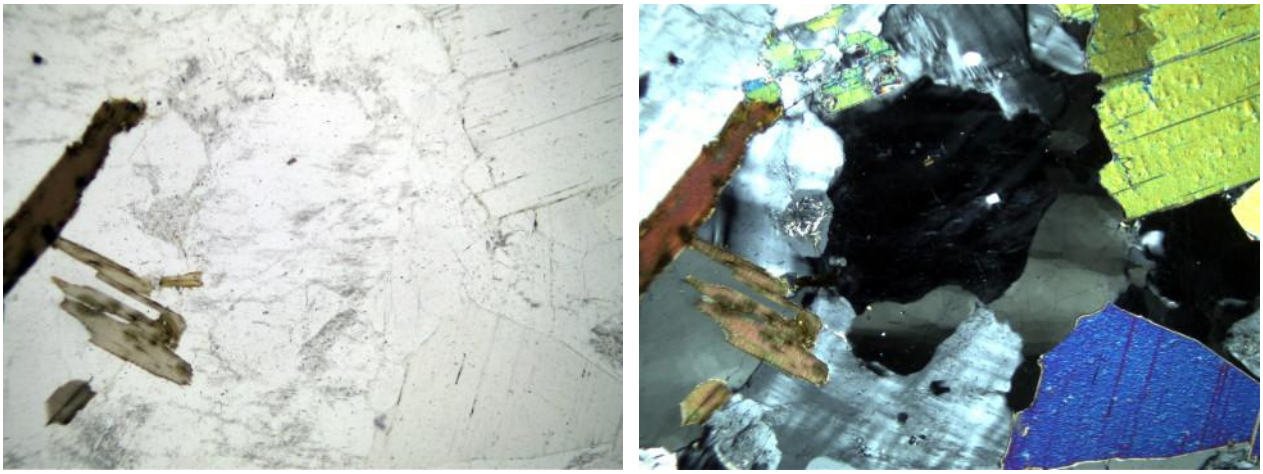

General view: Holocristalline seriate texture with feldspar, quartz, biotite and muscovite. Sericite and muscovite (on feldspar and plagioclase) are also present.

CB 091218.03

Petrographic Description / Analysis

Medium grained igneous rock with phaneritic texture (holocrystalline seriate). Crystals do not show preferred orientation (isotropic texture). Main minerals are quartz, plagioclase, feldspar, biotite and muscovite. Accessory minerals are zircon, apatite and oxides.

Modal Analysis	(% estimated)
Quartz	35
Plagioclase	35
Feldspar	15
Biotite	10
Muscovite	<5
Accessory Minerals	<1

Petrographic Classification (IUGS)

GRANODIORITE

Pictures

left nicols // right nicols X – Picture dimension 2,5 X 1,8 mm

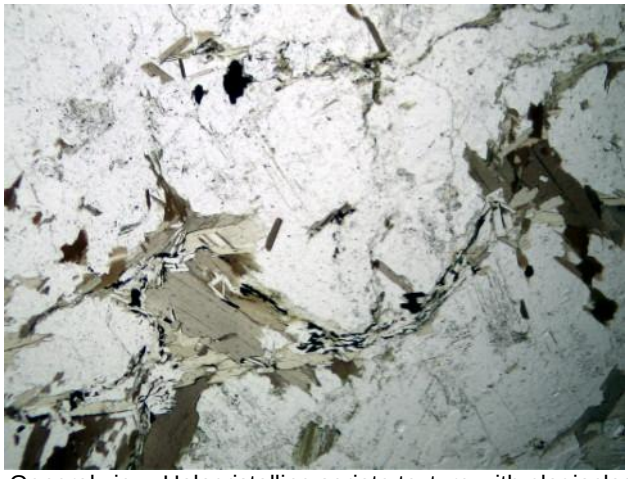

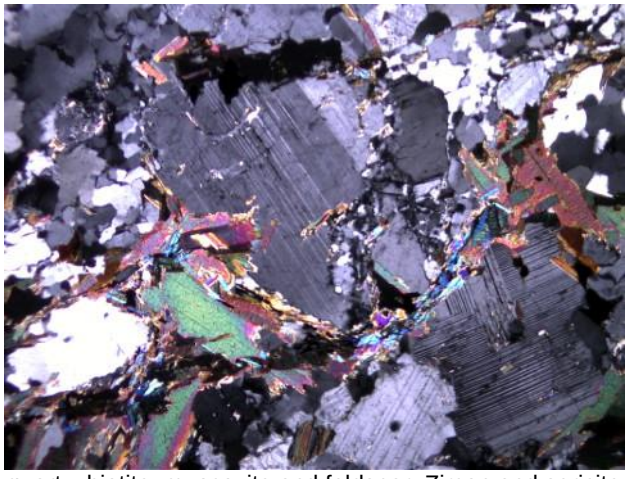

General view: Holocristalline seriate texture with plagioclase, quartz, biotite, muscovite and feldspar. Zircon and sericite are also present.

CB 091218.04

Petrographic Description / Analysis

Medium grained igneous rock with phaneritic texture (holocrystalline seriate). Crystals do not show preferred orientation (isotropic texture). Main minerals are quartz, plagioclase, feldspar and biotite. Accessory minerals are zircon (very abundant), apatite and oxides. Secondary (from alteration) minerals are chlorite (on biotite), epidote (on plagioclase and biotite), sericite and white mica (on feldspar). Quartz crystals show dynamic recrystallization and ductile deformation, whilst plagioclase and feldspar show no recrystallization and only brittle deformation.

Modal Analysis	(% estimated)
Quartz	35
Plagioclase	30
Feldspar	20
Biotite	9
Accessory Minerals	<5
Secondary Minerals	<1

Petrographic Classification (IUGS)

META-MONZOGRANITE

Pictures

left nicols // right nicols X – Picture dimension 2,5 X 1,8 mm

General view: Holocristalline seriate texture with plagioclase, quartz, biotite and feldspar. Zircon and sericite are also present.

CB 091218.05 *Petrographic Description / Analysis*

The sample shows the transition from a coarse grained igneous rock with pegmatitic texture to a subordinate medium grained igneous rock with holocrystalline seriate texture. Crystals do not show preferred orientation (isotropic texture). In the pegmatite main minerals are feldspar, quartz, muscovite and biotite. Accessory minerals are zircon and oxides. Secondary minerals are sericite (on feldspar) and chlorite (on biotite). In the medium grained portion main minerals are plagioclase, quartz, feldspar and muscovite. Accessory minerals are tourmalina and oxides. Secondary minerals are sericite and saussurrite (on plagioclase).

Modal Analysis	(% estimated)	
	AF Granite	Granodiorite
Feldspar	65	15
Quartz	20	30
Plagioclase	0	40
Muscovite	10	10
Biotite	3	0
Accessory Minerals	1	3
Secondary Minerals	<1	2

Petrographic Classification (IUGS)

Pegmatite: **ALKALI FELDSPAR GRANITE**
Medium grained rock: **GRANODIORITE**

Pictures
left nicols // right nicols X – Picture dimension 2,8 X 2,1 mm


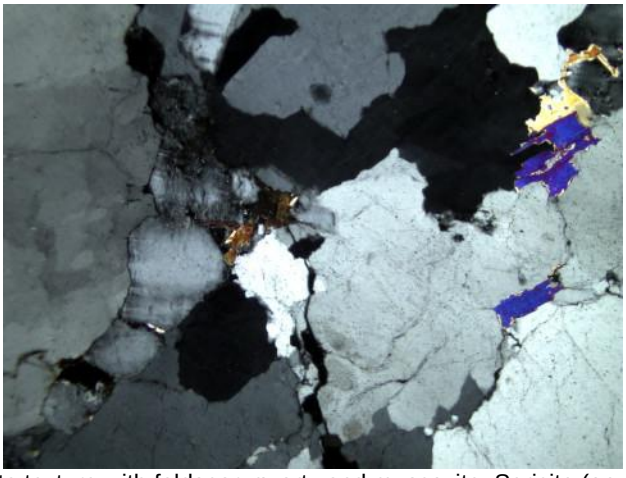

Alkali Feldspar Granite general view: Holocristalline seriate texture with feldspar, quartz and muscovite. Sericite (on feldspar) is also present.


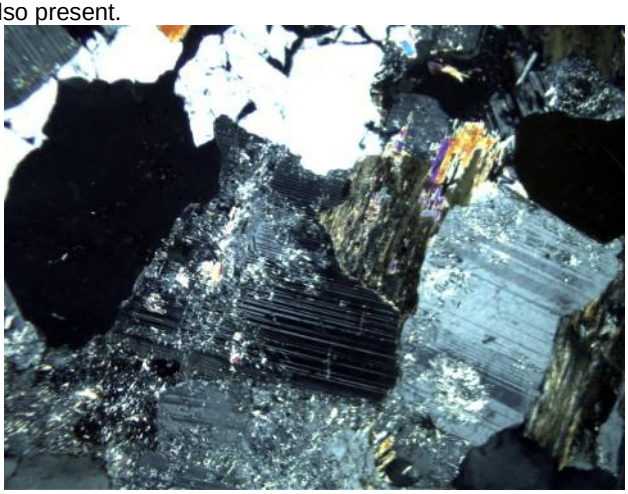

Granodiorite general view: Holocristalline seriate texture with plagioclase, quartz, feldspar and muscovite. Tourmaline crystal and sericite (on feldspar and plagioclase) are also present

CB 091218.06

Petrographic Description / Analysis

Medium grained metamorphic rock with phaneritic texture (holocrystalline seriate). Crystals show preferred orientation leading to irregular and discontinuos foliation (gneissic structure). Main minerals are quartz, plagioclase, feldspar and muscovite. Accessory minerals are zircon, apatite and oxides. Secondary minerals (derived from alterations process) are sericite on plagioclase and chlorite on muscovite. Quartz crystals show dynamic recrystallization and ductile deformation.

Modal Analysis	(% estimated)
Quartz	45
Plagioclase	35
Feldspar	10
Muscovite	8
Accessory Minerals	1
Secondary Minerals	1

Petrographic Classification (IUGS)

ORTHO-GNEISS
(MONZOGRANITE)

Pictures

left nicols // right nicols X – Picture dimension 2,5 X 1,8 mm

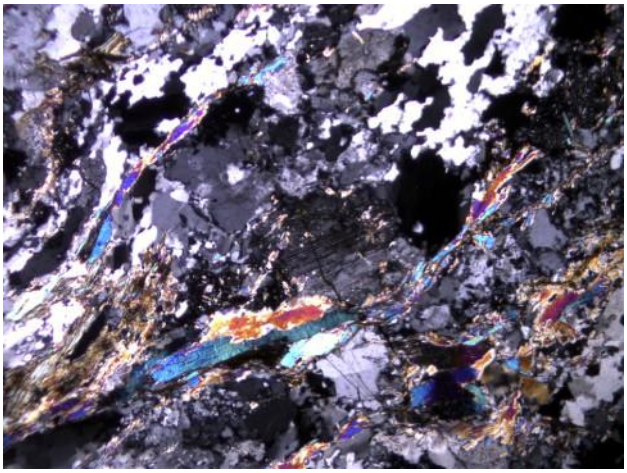

General view: Gneissic texture with plagioclase, quartz, muscovite and feldspar. Sericite is also present. Muscovite layers point out discontinuos foliation.

CB 091228.14

Petrographic Description / Analysis

Medium grained igneous rock with phaneritic texture (holocrystalline seriate). Crystals do not show preferred orientation (isotropic texture). Main minerals are plagioclase, feldspar, quartz, biotite and muscovite. Accessory minerals are zircon, apatite and oxides. Secondary minerals are sericite (on plagioclase and feldspar) and chlorite (on biotite).

Modal Analysis	(% estimated)
Plagioclase	35
Quartz	30
Feldspar	20
Biotite	8
Muscovite	5
Accessory Minerals	1
Secondary Minerals	<1

Petrographic Classification (IUGS)

GRANODIORITE

Pictures

left nicols // right nicols X – Picture dimension 2,5 X 1,8 mm

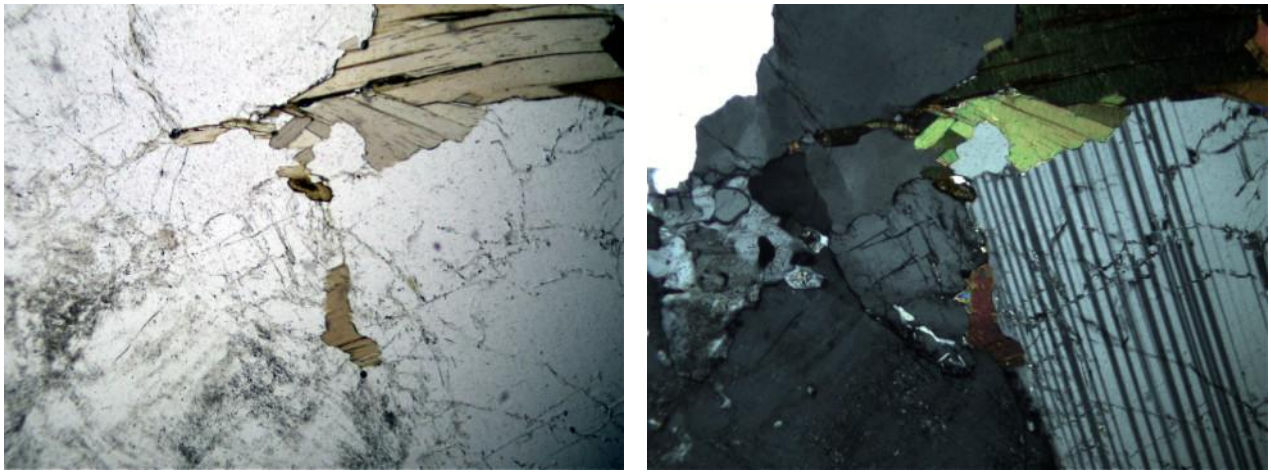

General view: Holocristalline seriate texture with plagioclase, quartz, biotite and feldspar. Sericite is also present.

CB 091228.16

Petrographic Description / Analysis

Medium grained igneous rock with phaneritic texture (holocrystalline seriate). Crystals do not show preferred orientation (isotropic texture). Main minerals are feldspar, quartz, plagioclase, biotite and muscovite. Accessory minerals are zircon, apatite and oxides. Secondary minerals are sericite (on plagioclase and feldspar) and chlorite (on biotite).

Modal Analysis	(% estimated)
Feldspar	35
Quartz	25
Plagioclase	25
Biotite	8
Muscovite	5
Accessory Minerals	1
Secondary Minerals	<1

Petrographic Classification (IUGS)

MONZOGRANITE

Pictures

left nicols // right nicols X – Picture dimension 2,5 X 1,8 mm

General view: Holocristalline seriate texture with feldspar, quartz, plagioclase, biotite and muscovite. Sericite and chlorite are also present.

CB 091228.17

Petrographic Description / Analysis

Medium grained igneous rock with phaneritic texture (holocrystalline seriate). Crystals do not show preferred orientation (isotropic texture). Main minerals are feldspar, quartz, plagioclase, biotite and muscovite. Accessory minerals are zircon, apatite and oxides. Secondary minerals are sericite (on plagioclase and feldspar) and chlorite (on biotite).

Modal Analysis	(% estimated)
Feldspar	36
Quartz	32
Plagioclase	15
Biotite	10
Muscovite	5
Accessory Minerals	1
Secondary Minerals	<1

Petrographic Classification (IUGS)

SYENOGRANITE

Pictures

left nicols // right nicols X – Picture dimension 2,5 X 1,8 mm

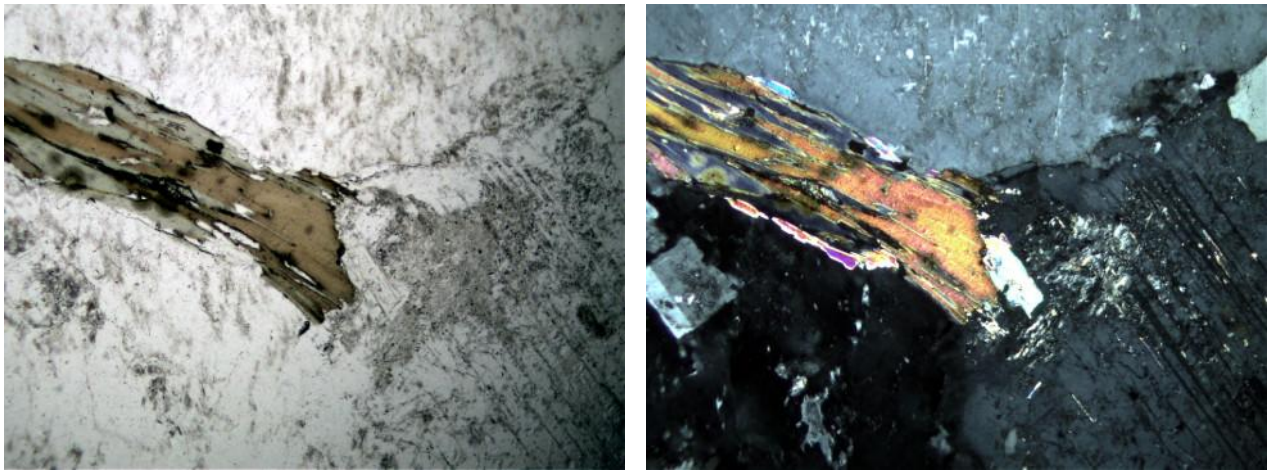

General view: Holocristalline seriate texture with feldspar, quartz, plagioclase and biotite. Zircon, sericite and chlorite are also present.

CB 091229.01

Petrographic Description / Analysis

Medium grained igneous rock with phaneritic texture (holocrystalline seriate). Crystals do not show preferred orientation (isotropic texture). Main minerals are quartz, feldspar, plagioclase, muscovite and biotite. Accessory minerals are zircon, apatite and oxides. Secondary minerals are sericite (on plagioclase and feldspar) and chlorite (on biotite).

Modal Analysis	(% estimated)
Quartz	40
Feldspar	30
Plagioclase	12
Muscovite	10
Biotite	6
Accessory Minerals	1
Secondary Minerals	1

Petrographic Classification (IUGS)

SYENOGRANITE

Pictures

left nicols // right nicols X – Picture dimension 2,5 X 1,8 mm

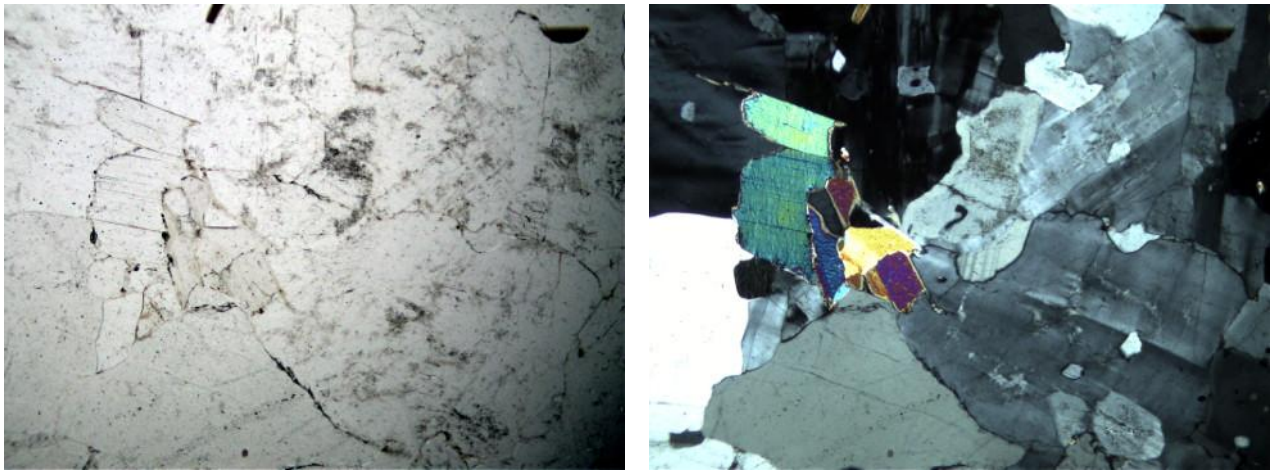

General view: Holocristalline seriate texture with feldspar, quartz, plagioclase and muscovite.

CB 091229.02

Petrographic Description / Analysis

Medium grained igneous rock with phaneritic texture (holocrystalline seriate). Crystals do not show preferred orientation (isotropic texture). Main minerals are quartz, feldspar, plagioclase, muscovite and biotite. Accessory minerals are zircon, apatite and oxides. Secondary minerals are represented by sericite (on plagioclase and feldspar).

Modal Analysis	(% estimated)
Quartz	40
Feldspar	30
Plagioclase	10
Muscovite	10
Biotite	8
Accessory Minerals	1
Secondary Minerals	1

Petrographic Classification (IUGS)

SYENOGRANITE

Pictures

left nicols // right nicols X – Picture dimension 2,5 X 1,8 mm

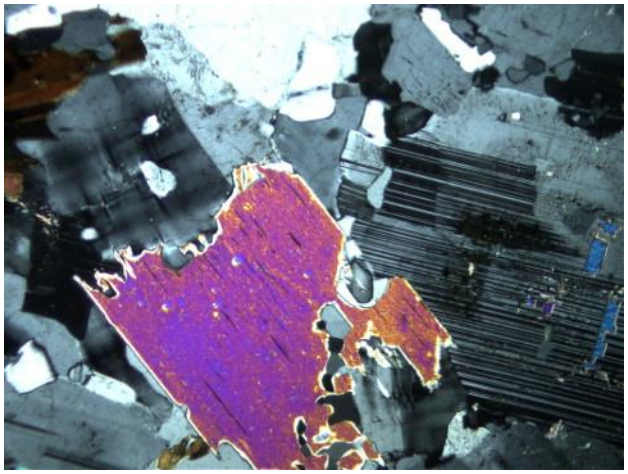

General view: Holocristalline seriate texture with feldspar, quartz, plagioclase, muscovite and biotite. Sericite is also present.

CB 091229.03

Petrographic Description / Analysis

Medium grained igneous rock with phaneritic texture (holocrystalline seriate). Crystals do not show preferred orientation (isotropic texture). Main minerals are quartz, feldspar, plagioclase, muscovite and biotite. Accessory minerals are zircon, apatite and oxides. Secondary minerals are represented by sericite (on plagioclase and feldspar) and chlorite (on biotite).

Modal Analysis	(% estimated)
Quartz	35
Feldspar	25
Plagioclase	20
Muscovite	10
Biotite	7
Accessory Minerals	1
Secondary Minerals	*2*

Petrographic Classification (IUGS)

MONZOGRANITE

Pictures

left nicols // right nicols X – Picture dimension 2,5 X 1,8 mm

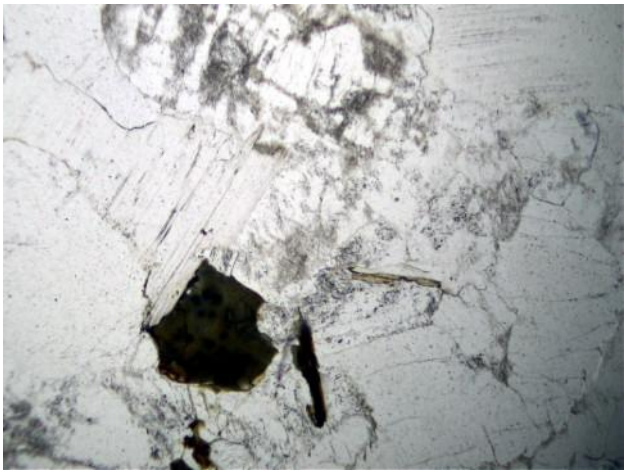

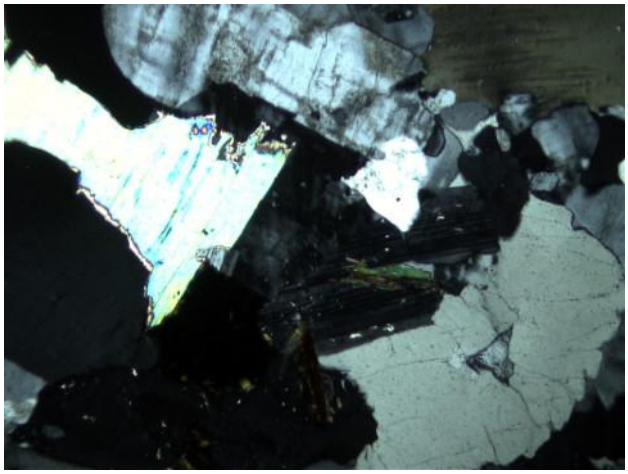

General view: Holocristalline seriate texture with feldspar, quartz, plagioclase, muscovite and biotite. Sericite is also present.

CB 091229.04

Petrographic Description / Analysis

Medium grained igneous rock with phaneritic texture (holocrystalline seriate). Crystals do not show preferred orientation (isotropic texture). Main minerals are quartz, feldspar, plagioclase, muscovite and biotite. Accessory minerals are tourmaline, zircon, apatite and oxides. Secondary minerals are represented by saussurite (on feldspar and plagioclase) sericite (on plagioclase and feldspar) and chlorite (on biotite). Cataclastic bands are present.

Modal Analysis	(% estimated)
Quartz	36
Feldspar	32
Plagioclase	10
Muscovite	10
Biotite	7
Accessory Minerals	1
Secondary Minerals	4

Petrographic Classification (IUGS)

SYENOGRANITE

Pictures

left nicols // right nicols X – Picture dimension 2,8 X 2,1 mm

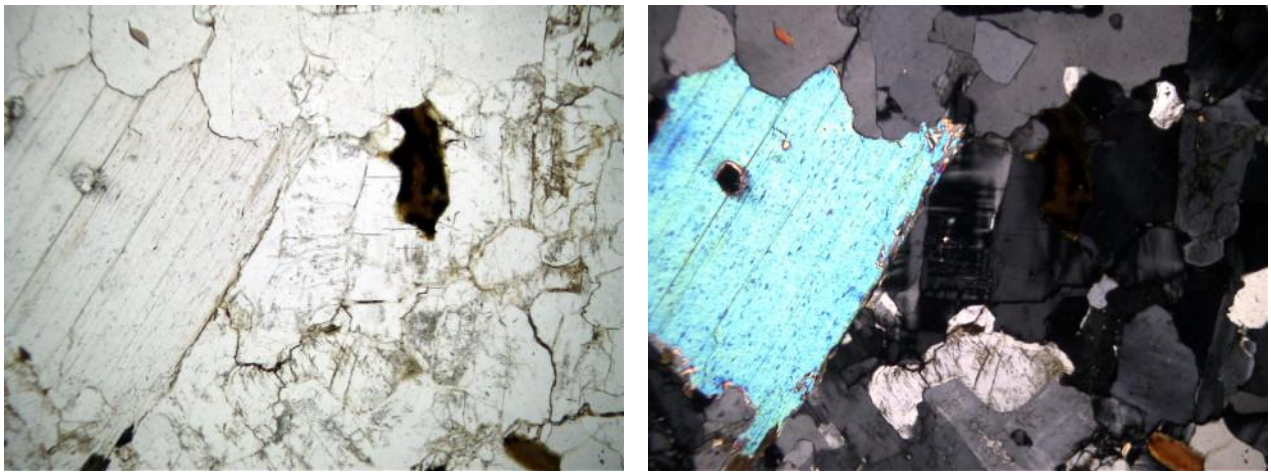

General view: Holocristalline seriate texture with feldspar, quartz, plagioclase, muscovite and biotite. Saussurite and sericite are also present.

CB 091229.06

Petrographic Description / Analysis

Medium grained igneous rock with phaneritic texture (holocrystalline seriate). Crystals do not show preferred orientation (isotropic texture). Main minerals are quartz, feldspar, plagioclase, muscovite and biotite. Accessory minerals are tourmaline, zircon, apatite and oxides. Secondary minerals are represented by saussurite (on feldspar and plagioclase) sericite (on plagioclase and feldspar) and chlorite (on biotite).

Modal Analysis	(% estimated)
Quartz	30
Feldspar	25
Plagioclase	25
Muscovite	10
Biotite	5
Accessory Minerals	2
Secondary Minerals	3

Petrographic Classification (IUGS)

MONZOGRANITE

Pictures

left nicols // right nicols X – Picture dimension 2,8 X 2,1 mm

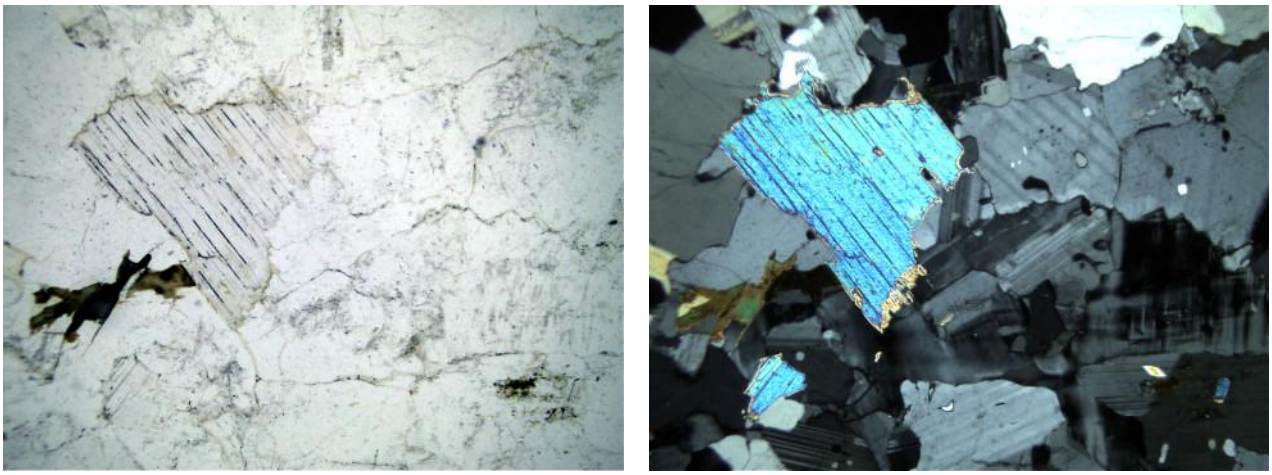

General view: Holocristalline seriate texture with feldspar, quartz, plagioclase, muscovite and biotite.

CB 091229.07

Petrographic Description / Analysis

Medium grained igneous rock with phaneritic texture (holocrystalline seriate). Crystals do not show preferred orientation (isotropic texture). Main minerals are quartz, feldspar, plagioclase, muscovite and biotite. Accessory minerals are tourmaline, zircon, apatite and oxides. Secondary minerals are represented by saussurite (on feldspar and plagioclase) sericite (on plagioclase and feldspar) and chlorite (on biotite).

Modal Analysis	(% estimated)
Quartz	35
Feldspar	25
Plagioclase	20
Muscovite	10
Biotite	4
Accessory Minerals	3
Secondary Minerals	3

Petrographic Classification (IUGS)

MONZOGRANITE

Pictures

left nicols // right nicols X – Picture dimension 2,8 X 2,1 mm

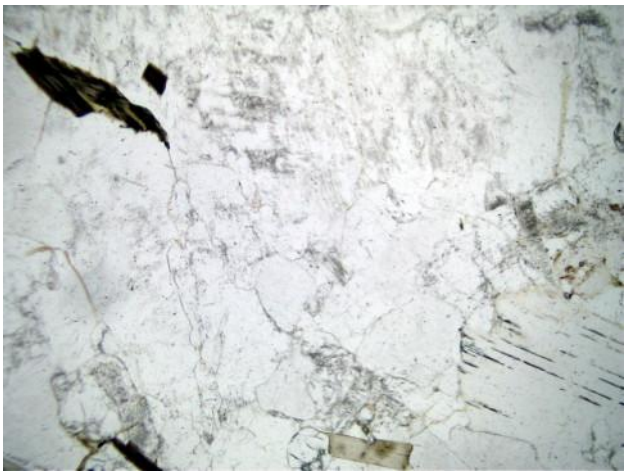

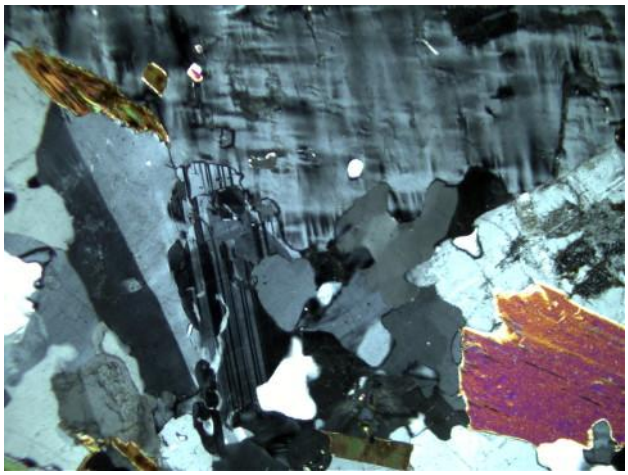

General view: Holocristalline seriate texture with feldspar, quartz, plagioclase, muscovite and biotite. Saussurrite is also present.

CB 091229.08

Petrographic Description / Analysis

Medium grained igneous rock with phaneritic texture (holocrystalline seriate). Crystals do not show preferred orientation (isotropic texture). Main minerals are quartz, feldspar, plagioclase, muscovite and biotite. Accessory minerals are tourmaline, zircon, apatite and oxides. Secondary minerals are represented by saussurite (on feldspar and plagioclase) sericite (on plagioclase and feldspar) and chlorite (on biotite).

Modal Analysis	(% estimated)
Quartz	35
Feldspar	25
Plagioclase	20
Muscovite	7
Biotite	7
Accessory Minerals	3
Secondary Minerals	3

Petrographic Classification (IUGS)

MONZOGRANITE

Pictures

left nicols // right nicols X – Picture dimension 2,8 X 2,1 mm

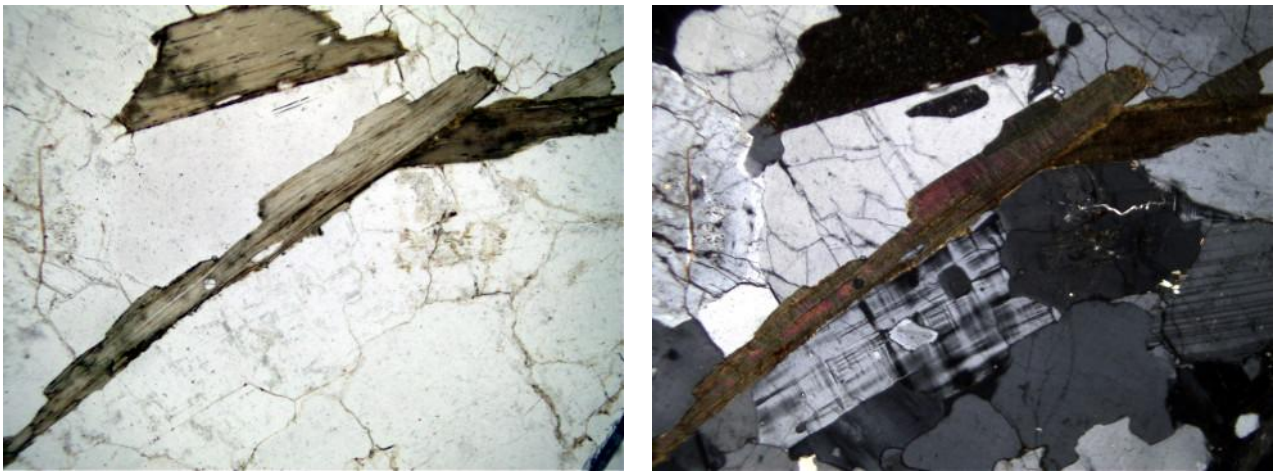

General view: Holocristalline seriate texture with feldspar, quartz, plagioclase, muscovite and biotite.

CB 091229.09

Petrographic Description / Analysis

Medium grained igneous rock with phaneritic texture (holocrystalline seriate). Crystals do not show preferred orientation (isotropic texture). Main minerals are quartz, feldspar, plagioclase, muscovite and biotite. Accessory minerals are tourmaline, zircon, apatite and oxides. Secondary minerals are represented by saussurite (on feldspar and plagioclase) sericite (on plagioclase and feldspar) and chlorite (on biotite).

Modal Analysis	(% estimated)
Quartz	40
Feldspar	20
Plagioclase	20
Muscovite	8
Biotite	7
Accessory Minerals	3
Secondary Minerals	2

Petrographic Classification (IUGS)

MONZOGRANITE

Pictures

left nicols // right nicols X – Picture dimension 2,8 X 2,1 mm

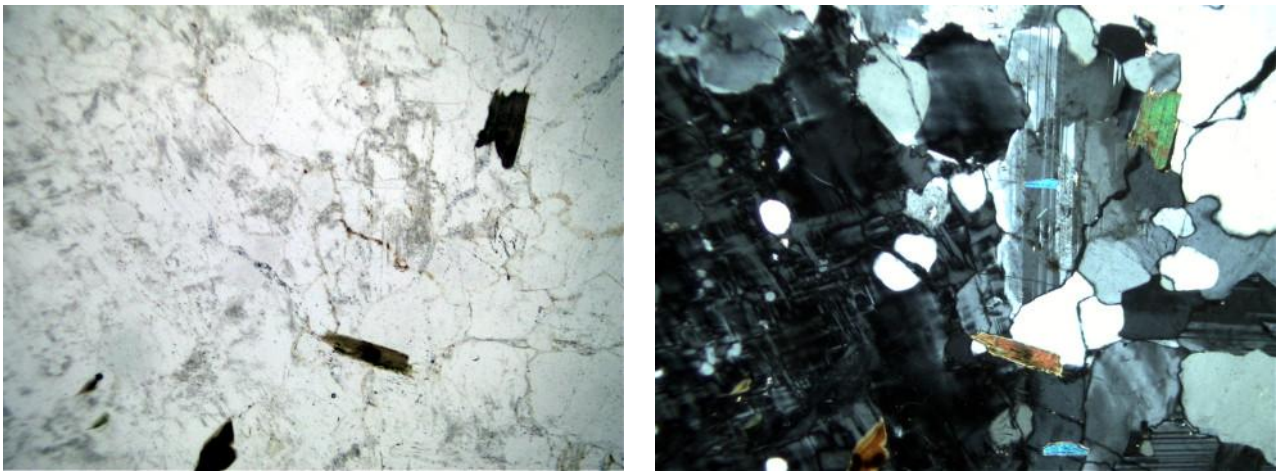

General view: Holocristalline seriate texture with feldspar, quartz, plagioclase, muscovite and biotite.

CB 100103.01

Petrographic Description / Analysis

Medium grained igneous rock with phaneritic texture (holocrystalline seriate). Crystals show no preferred orientation. Main minerals are quartz, plagioclase, biotite and amphibole (horneblend). Accessory minerals are titanite, zircon, apatite and oxides. Secondary minerals (derived from alteration's process) are sericite/muscovite on plagioclase and chlorite on biotite.

Modal Analysis	(% estimated)
Plagioclase	45
Quartz	33
Biotite	10
Amphibole	10
Accessory Minerals	1
Secondary Minerals	1

Petrographic Classification (IUGS)

TONALITE

Pictures

left nicols // right nicols X – Picture dimension 2,5 X 1,8 mm

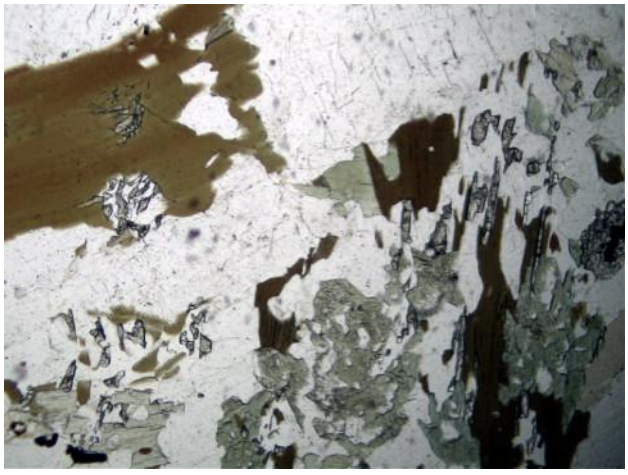

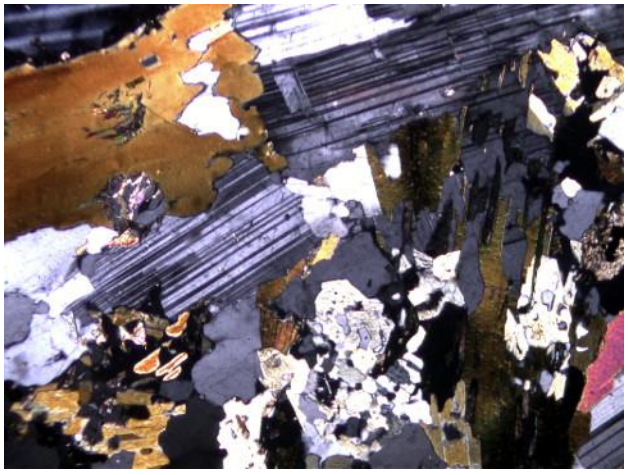

General view: Holocristalline seriate texture with plagioclase, quartz, biotite, amphibole and titanite. Sericite is also present.

CB 100103.02

Petrographic Description / Analysis

Medium grained igneous rock with phaneritic texture (holocrystalline seriate). Crystals do not show preferred orientation (isotropic texture). Main minerals are plagioclase, quartz, feldspar, biotite and amphibole. Accessory minerals are zircon, apatite and oxides. Secondary minerals (from alteration's process) are sericite and muscovite on plagioclase and chlorite on biotite and amphibole.

Modal Analysis	(% estimated)
Plagioclase	35
Quartz	30
Biotite	15
Amphibole	10
Feldspar	8
Accessory Minerals	1
Secondary Minerals	<1

Petrographic Classification (IUGS)

GRANODIORITE

Pictures

left nicols // right nicols X – Picture dimension 2,8 X 2,1 mm

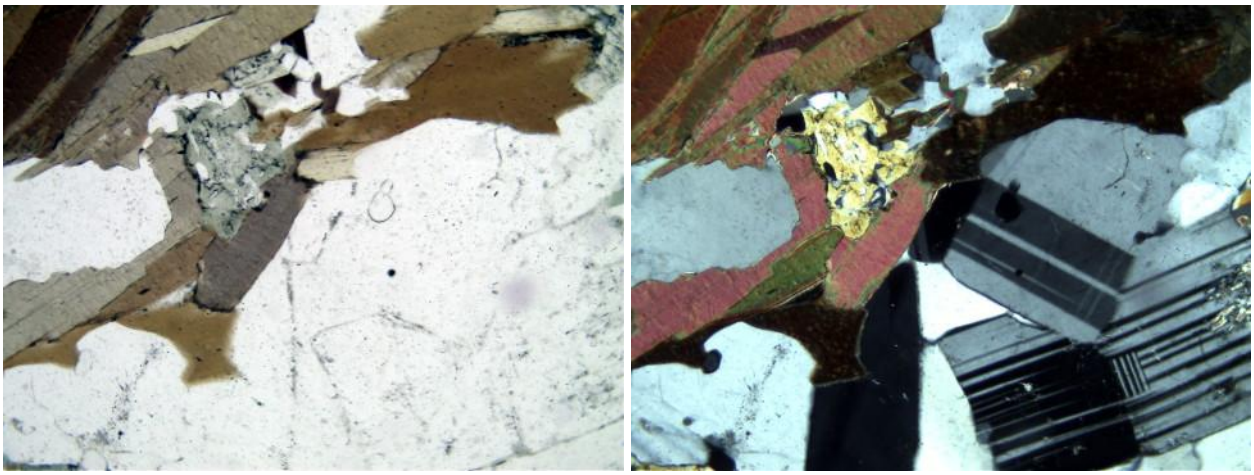

General view: Holocristalline seriate texture with plagioclase, quartz, biotite, amphibole. Apatite is also present.

CB 100103.03

Petrographic Description / Analysis

Medium grained igneous rock with phaneritic texture (holocrystalline seriate). Crystals show no preferred orientation. Main minerals are quartz, plagioclase, biotite and amphibole (horneblend). Accessory minerals are titanite, zircon, apatite and oxides. Secondary minerals (derived from alteration's process) are sericite/muscovite on plagioclase.

Modal Analysis	(% estimated)
Plagioclase	45
Quartz	30
Biotite	12
Amphibole	10
Accessory Minerals	2
Secondary Minerals	1

Petrographic Classification (IUGS)

TONALITE

Pictures

left nicols // right nicols X – Picture dimension 2,5 X 1,8 mm

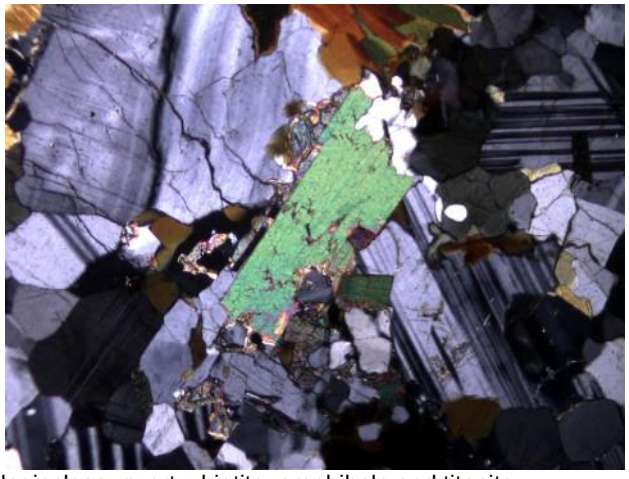

General view: Holocristalline seriate texture with plagioclase, quartz, biotite, amphibole and titanite.

CB 100103.04

Petrographic Description / Analysis

Medium grained metamorphic rock with phaneritic texture (holocrystalline seriate). Crystals show preferred orientation leading to irregular and discontinuos foliation (gneissic structure). Main minerals are feldspar, quartz, plagioclase, muscovite and biotite. Accessory minerals are zircon, apatite and oxides. Secondary minerals (derived from alterations process) are sericite on plagioclase and chlorite on muscovite. Quartz crystals show dynamic recrystallization and ductile deformation.

Modal Analysis	(% estimated)
Feldspar	40
Quartz	35
Plagioclase	10
Muscovite	8
Biotite	5
Accessory Minerals	1
Secondary Minerals	1

Petrographic Classification (IUGS)

ORTHO-GNEISS
(SYENOGRANITE)

Pictures
left nicols // right nicols X – Picture dimension 2,5 X 1,8 mm

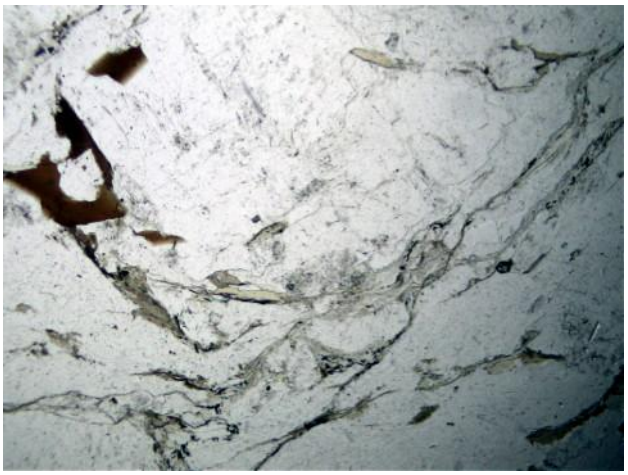

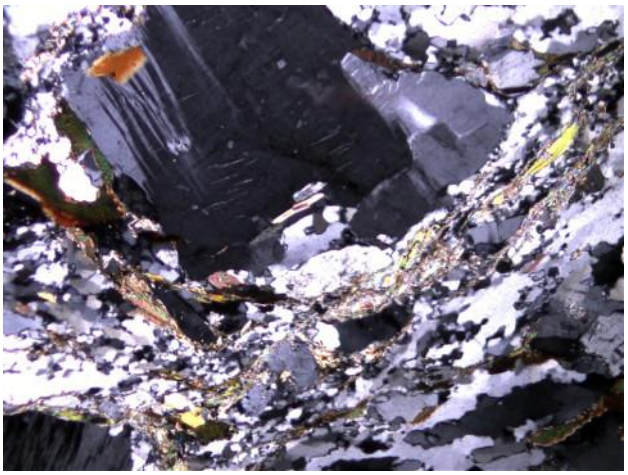

General view: Gneissic texture with plagioclase, quartz, muscovite biotite and feldspar. Muscovite layers point out discontinuos foliation.

CB 100103.05

Petrographic Description / Analysis

Medium grained igneous rock with phaneritic texture (holocrystalline seriate). Crystals do not show preferred orientation (isotropic texture). Main minerals are plagioclase, quartz, feldspar, biotite and muscovite. Accessory minerals are sillimanite (both fibrous and prismatic), zircon, apatite and oxides. Secondary minerals (from alteration's process) are sericite on plagioclase and chlorite on biotite.

Modal Analysis	(% estimated)
Quartz	35
Plagioclase	35
Feldspar	15
Biotite	10
Muscovite	<5
Accessory Minerals	<1

Petrographic Classification (IUGS)

GRANODIORITE

Pictures

left nicols // right nicols X – Picture dimension 2,5 X 1,8 mm

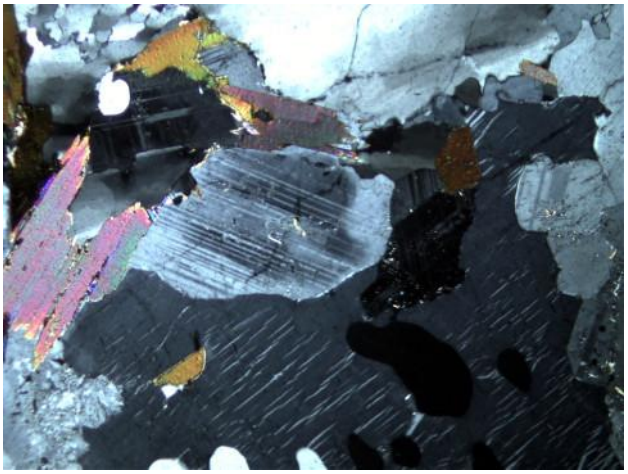

General view: Holocristalline seriate texture with plagioclase, quartz, biotite, muscovite and feldspar. Zircon is also present.

CB 100103.06

Petrographic Description / Analysis

Medium grained igneous rock with phaneritic texture (holocrystalline seriate). Crystals do not show preferred orientation (isotropic texture). Main minerals are plagioclase, quartz, feldspar, and biotite. Accessory minerals are calcite, apatite, zircon and oxides. Secondary minerals (from alteration's process) are sericite and muscovite on plagioclase and chlorite on biotite.

Modal Analysis	(% estimated)
Plagioclase	40
Quartz	26
Biotite	16
Feldspar	13
Accessory Minerals	4
Secondary Minerals	<1

Petrographic Classification (IUGS)

GRANODIORITE

Pictures

left nicols // right nicols X – Picture dimension 2,8 X 2,1 mm

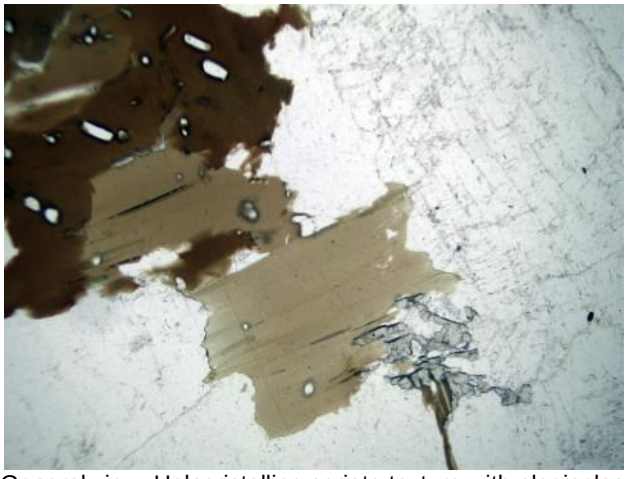

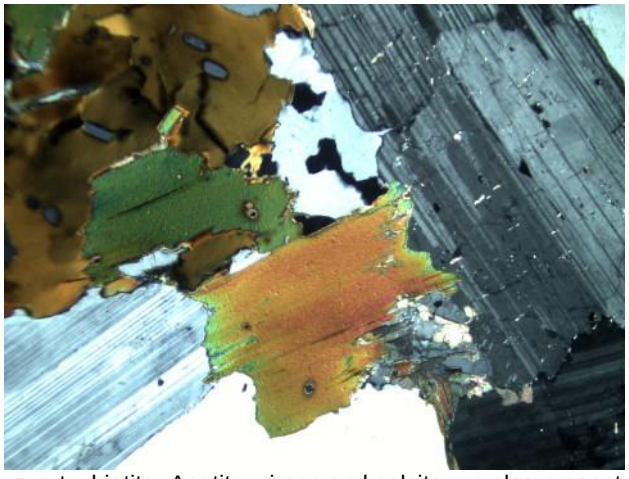

General view: Holocristalline seriate texture with plagioclase, quartz, biotite. Apatite, zircon and calcite are also present.

CB 111215.02

Petrographic Description / Analysis

Medium grained igneous rock with phaneritic texture (holocrystalline seriate). Crystals do not show preferred orientation. Main minerals are feldspar, quartz, plagioclase and biotite. Accessory minerals are zircon, apatite and oxides. Secondary minerals are sericite (on plagioclase and feldspar) and chlorite (on biotite).

Modal Analysis	(% estimated)
Feldspar	35
Quartz	35
Plagioclase	18
Biotite	10
Accessory Minerals	1
Secondary Minerals	<1

Petrographic Classification (IUGS)

SYENOGRANITE

Pictures

left nicols // right nicols X – Picture dimension 2,8 X 2,1 mm

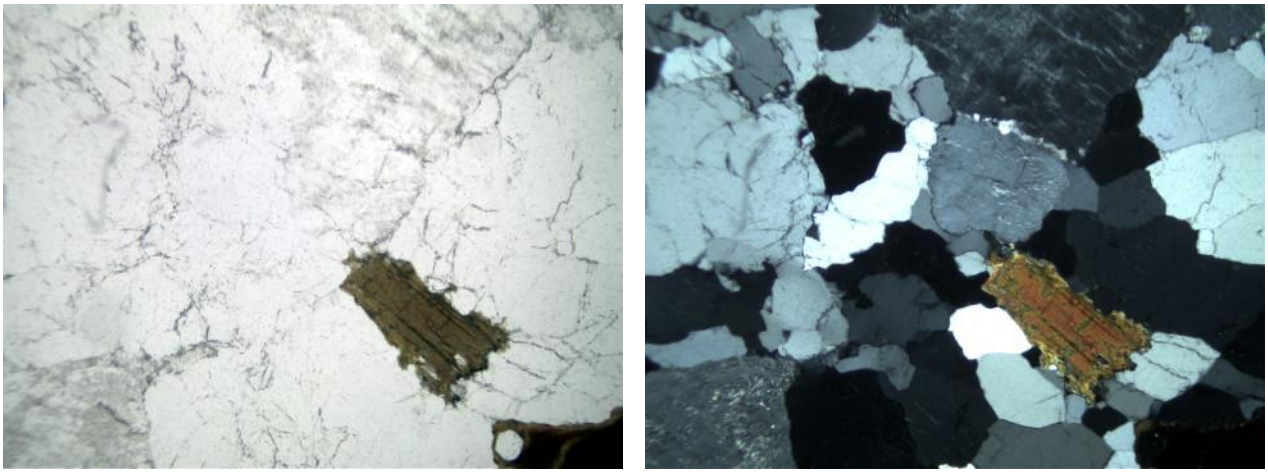

General view: Holocristalline seriate texture with feldspar, quartz, plagioclase and biotite. Apatite and sericite (on feldspar) are also present.

CB 111220.05

Petrographic Description / Analysis

Medium grained igneous rock with phaneritic texture (holocrystalline seriate). Crystals do not show preferred orientation (isotropic texture). Main minerals are plagioclase, quartz, feldspar, biotite and amphibole. Accessory minerals are calcite, zircon, apatite and oxides. Secondary minerals (from alteration's process) are sericite on plagioclase and chlorite on biotite and amphibole.

Modal Analysis	(% estimated)
Plagioclase	35
Quartz	28
Biotite	15
Feldspar	10
Amphibole	8
Accessory Minerals	3
Secondary Minerals	<1

Petrographic Classification (IUGS)

GRANODIORITE

Pictures

left nicols // right nicols X – Picture dimension 2,8 X 2,1 mm

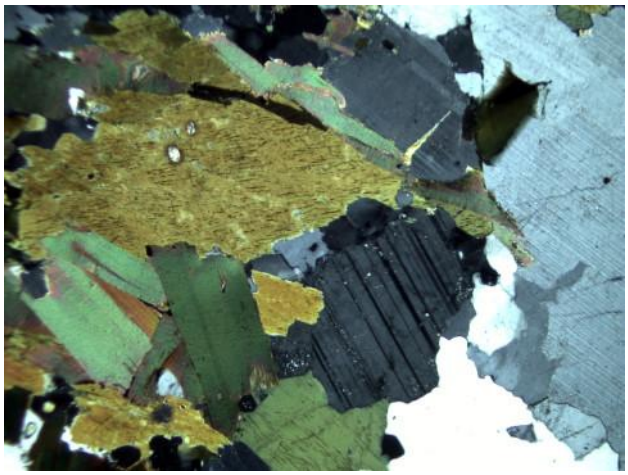

General view: Holocristalline seriate texture with plagioclase, quartz, biotite, amphibole. Apatite and zircon are also present.

CB 111220.07

Petrographic Description / Analysis

Medium grained igneous rock with phaneritic texture (holocrystalline seriate). Crystals do not show preferred orientation (isotropic texture). Main minerals are plagioclase, quartz, feldspar, and biotite. Accessory minerals are tourmaline, apatite and oxides. Secondary minerals (from alteration's process) are sericite and saussurrite on plagioclase and chlorite on biotite.

Modal Analysis	(% estimated)
Plagioclase	35
Quartz	35
Feldspar	15
Biotite	12
Accessory Minerals	2
Secondary Minerals	<1

Petrographic Classification (IUGS)

GRANODIORITE

Pictures

left nicols // right nicols X – Picture dimension 2,8 X 2,1 mm

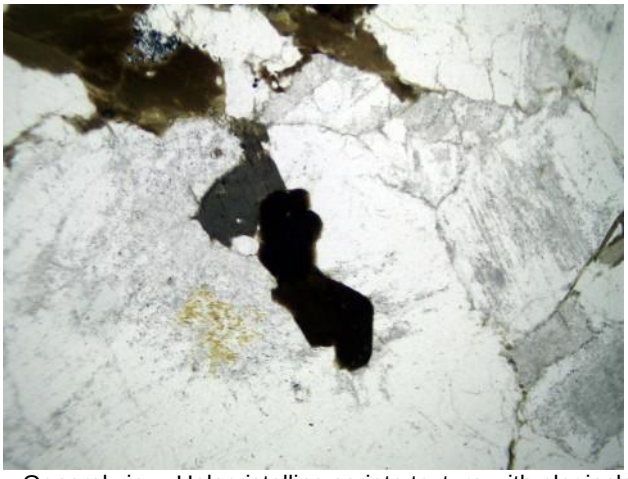

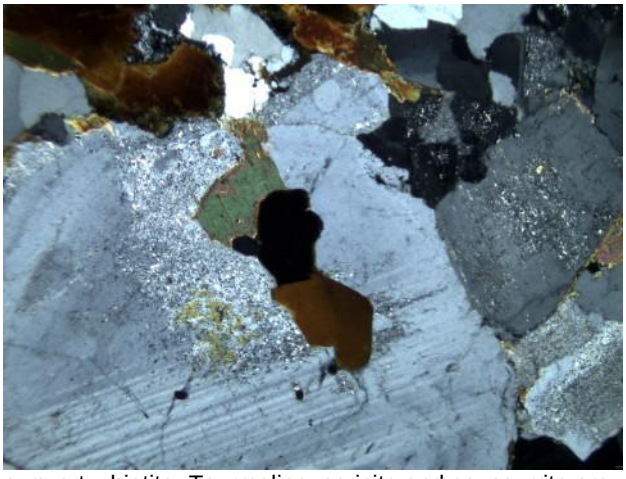

General view: Holocristalline seriate texture with plagioclase, quartz, biotite. Tourmaline, sericite and saussurrite are also present.

CB 111221.01

Petrographic Description / Analysis

Medium grained igneous rock with phaneritic texture (holocrystalline seriate). Crystals do not show preferred orientation (isotropic texture). Main minerals are quartz, plagioclase, feldspar, and biotite. Accessory minerals are zircon, apatite, calcite, tourmaline and oxides. Secondary minerals are sericite (on plagioclase and feldspar) and chlorite (on biotite).

Modal Analysis	(% estimated)
Quartz	35
Plagioclase	30
Feldspar	20
Biotite	12
Accessory Minerals	2
Secondary Minerals	<1

Petrographic Classification (IUGS)

MONZOGRANITE

Pictures

left nicols // right nicols X – Picture dimension 2,8X 2,1 mm

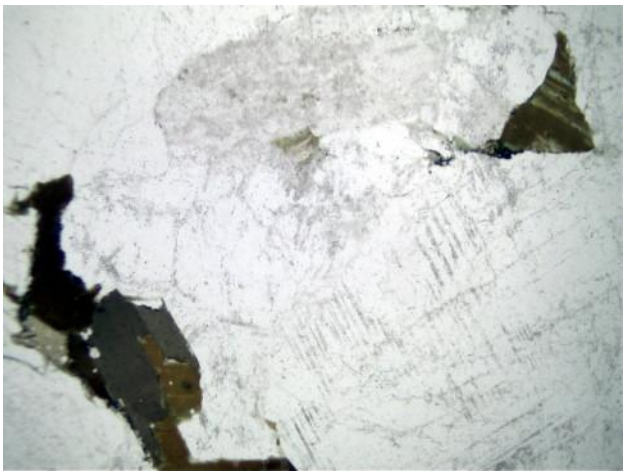

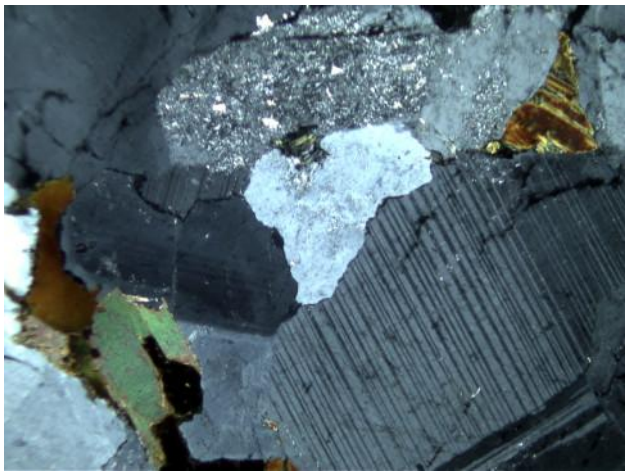

General view: Holocristalline seriate texture with feldspar, quartz, plagioclase and biotite. Sericite and chlorite are also present.

CB 111221.06

Petrographic Description / Analysis

Medium grained igneous rock with phaneritic texture (holocrystalline seriate). Crystals show weak preferred orientation. Main minerals are feldspar, quartz, plagioclase, biotite and amphibole. Accessory minerals are zircon, apatite, calcite and oxides. Secondary minerals are epidote, sericite (on plagioclase and feldspar) and chlorite (on biotite). Quartz crystals show dynamic recrystallization and ductile deformation.

Modal Analysis	(% estimated)
Feldspar	35
Quartz	30
Plagioclase	15
Biotite	10
Amphibole	8
Accessory Minerals	1
Secondary Minerals	<1

Petrographic Classification (IUGS)

SYENOGRANITE

Pictures

left nicols // right nicols X – Picture dimension 2,8 X 2,1 mm

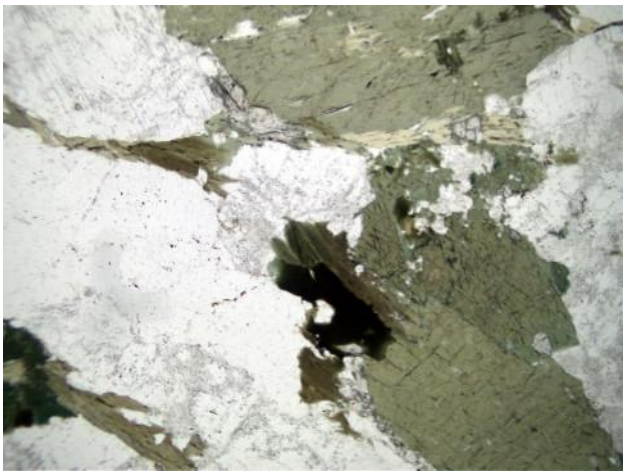

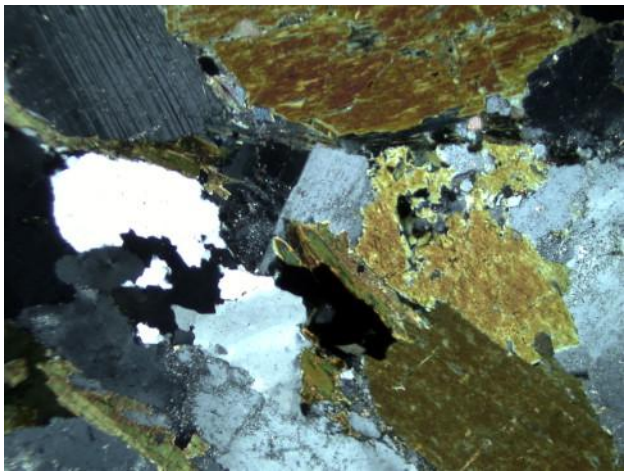

General view: Holocristalline seriate texture with feldspar, quartz, plagioclase amphibole and biotite. Sericite (on feldspar) and chlorite (on biotite) are also present.

CB 120101.03

Petrographic Description / Analysis

Medium grained igneous rock with phaneritic texture (holocrystalline seriate). Crystals do not show preferred orientation (isotropic texture). Main minerals are quartz, plagioclase, feldspar, amphibole and biotite. Accessory minerals are zircon, apatite, calcite and oxides. Secondary minerals are sericite (on plagioclase and feldspar) and chlorite (on biotite). Quartz crystals show dynamic recrystallization and ductile deformation.

Modal Analysis	(% estimated)
Quartz	35
Plagioclase	28
Feldspar	20
Biotite	10
Amphibole	5
Accessory Minerals	1
Secondary Minerals	<1

Petrographic Classification (IUGS)

MONZOGRANITE

Pictures

left nicols // right nicols X – Picture dimension 2,8X 2,1 mm

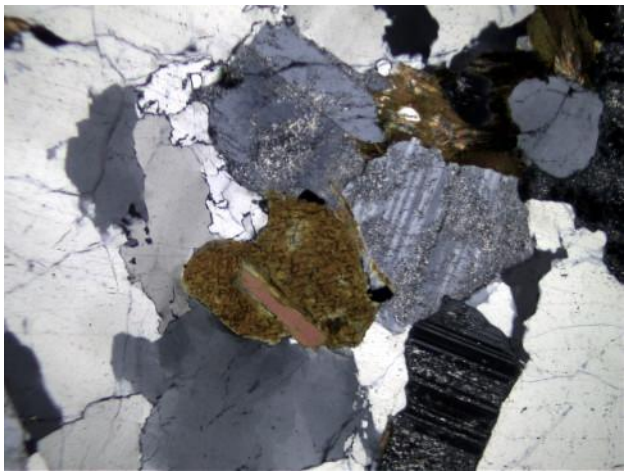

General view: Holocristalline seriate texture with feldspar, quartz, plagioclase, amphibole and biotite. Sericite and chlorite are also present.

CB 120101.06

Petrographic Description / Analysis

Medium grained igneous rock with phaneritic texture (holocrystalline seriate). Crystals do not show preferred orientation (isotropic texture). Main minerals are quartz, plagioclase, feldspar, amphibole and biotite. Accessory minerals are zircon, apatite and oxides. Secondary minerals are sericite (on plagioclase and feldspar) and chlorite (on biotite).

Modal Analysis	(% estimated)
Quartz	32
Plagioclase	28
Feldspar	22
Biotite	10
Amphibole	5
Accessory Minerals	2
Secondary Minerals	<1

Petrographic Classification (IUGS)

MONZOGRANITE

Pictures

left nicols // right nicols X – Picture dimension 2,8X 2,1 mm

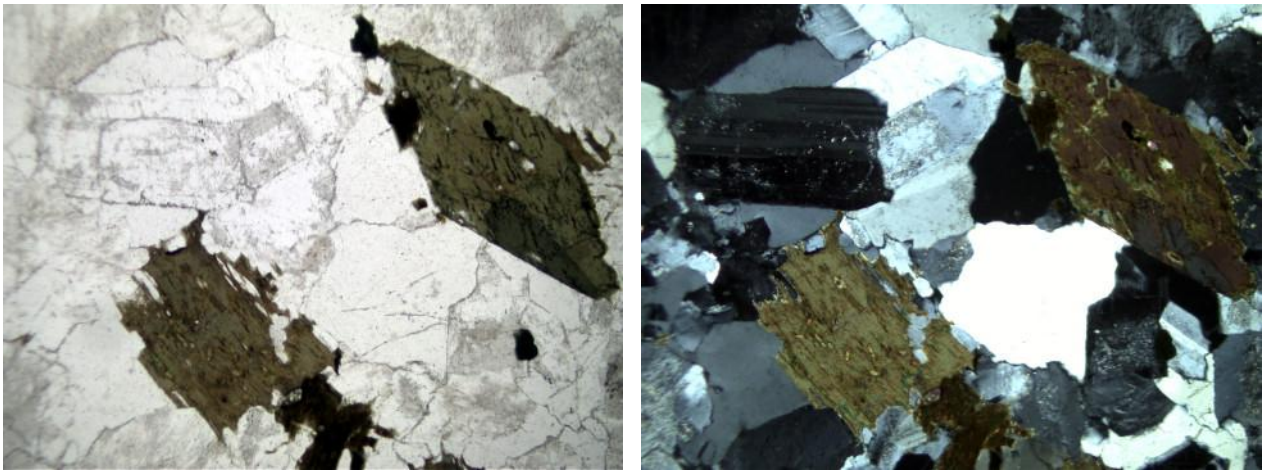

General view: Holocristalline seriate texture with feldspar, quartz, plagioclase, amphibole and biotite. Sericite and chlorite are also present.

CB 121220.03 *Petrographic Description / Analysis*

Medium-coarse grained igneous rock with phaneritic texture (holocrystalline seriate). Crystals do not show preferred orientation. Main minerals are feldspar, quartz, plagioclase, biotite and amphibole. Accessory minerals are zircon, apatite, tourmaline and oxides. Secondary minerals are sericite and saussurrite (on feldspar), chlorite (on biotite) and hematite (on amphibole). An **inclusion** made of fine grained igneous rock is also present. Crystals do not show preferred orientation. Main minerals are plagioclase, amphibole and quartz. Accessory minerals are epidote and oxides. Secondary minerals are sericite and muscovite (on plagioclase) and hematite (on amphibole).

Modal Analysis	(% estimated)	
	Syenogranite	Tonalite
Feldspar	40	0
Quartz	35	15
Plagioclase	10	45
Amphibole	8	30
Biotite	5	0
Accessory Minerals	1	2
Secondary Minerals	<1	8

Petrographic Classification (IUGS)

SYENOGRANITE
(Inclusion: **TONALITE**)

Pictures
left nicols // right nicols X – Picture dimension 2,8 X 2,1 mm

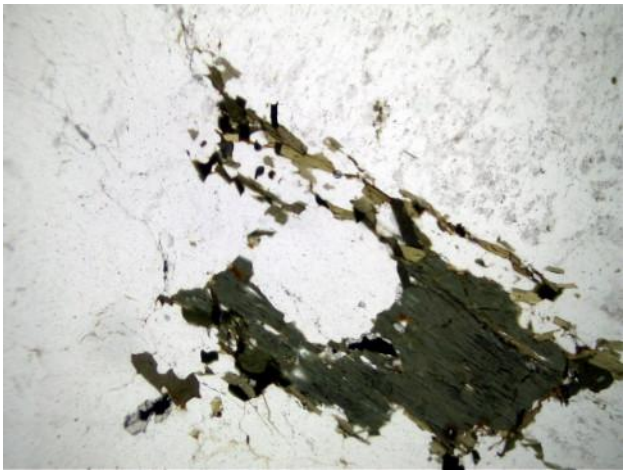

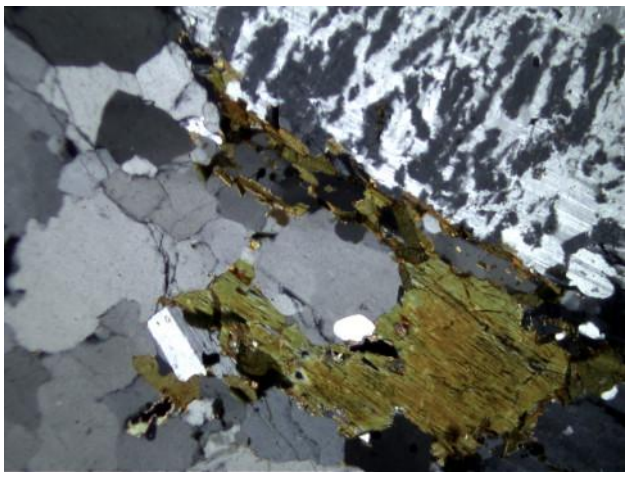

Syenogranite general view: Holocristalline seriate texture with feldspar, quartz, amphibole and biotite. Sericite (on feldspar) and chlorite (on biotite) are also present.

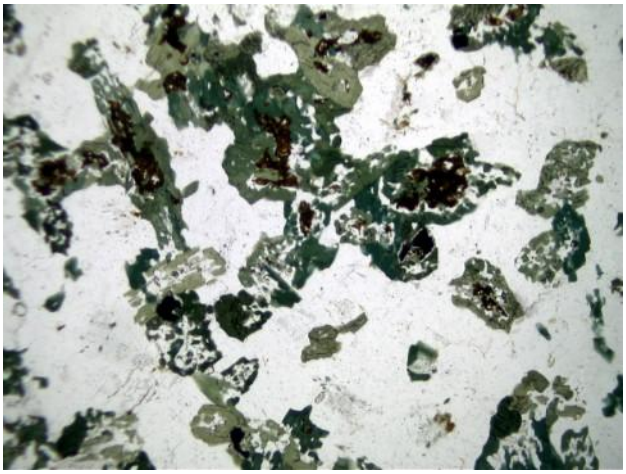

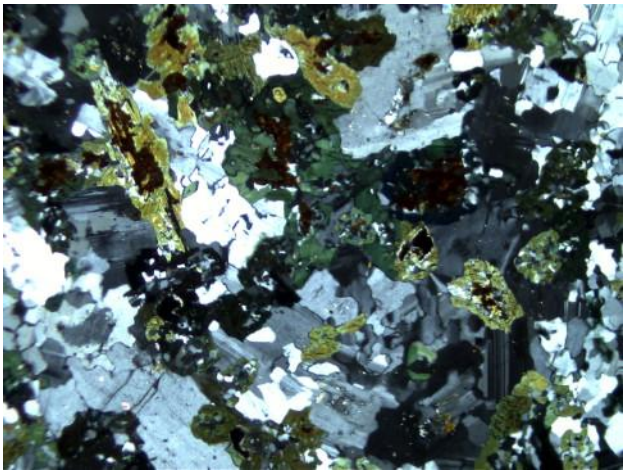

Tonalite (inclusion) general view: Holocristalline seriate texture with plagioclase, amphibole and quartz. Hematite (on amphibole) is also present.

CB 121220.04

Petrographic Description / Analysis

Medium grained igneous rock with phaneritic texture (holocrystalline seriate). Crystals do not show preferred orientation (isotropic texture). Main minerals are plagioclase, quartz, feldspar, biotite and amphibole. Accessory minerals are zircon, blue tourmaline, apatite and oxides. Secondary minerals (from alteration's process) are sericite and muscovite on plagioclase and chlorite on biotite and amphibole.

Modal Analysis	(% estimated)
Plagioclase	32
Quartz	30
Feldspar	15
Biotite	11
Amphibole	10
Accessory Minerals	1
Secondary Minerals	<1

Petrographic Classification (IUGS)

GRANODIORITE

Pictures

left nicols // right nicols X – Picture dimension 2,8 X 2,1 mm

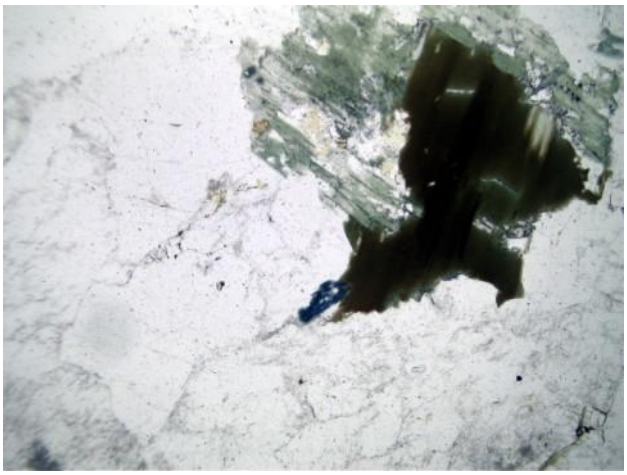

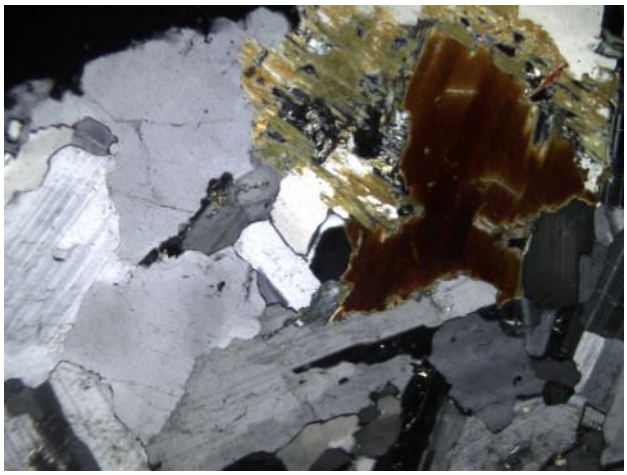

General view: Holocristalline seriate texture with plagioclase, feldspar, quartz, biotite and amphibole. Blue tourmaline is also present.

CB 121220.07

Petrographic Description / Analysis

Medium grained igneous rock with phaneritic texture (holocrystalline seriate). Crystals do not show preferred orientation. Main minerals are feldspar, quartz, plagioclase and biotite. Accessory minerals are zircon, apatite and oxides. Secondary minerals are sericite and muscovite (on plagioclase and feldspar) and chlorite (on biotite).

Modal Analysis	(% estimated)
Feldspar	38
Quartz	32
Plagioclase	16
Biotite	11
Accessory Minerals	1
Secondary Minerals	2

Petrographic Classification (IUGS)

SYENOGRANITE

Pictures

left nicols // right nicols X – Picture dimension 2,8 X 2,1 mm

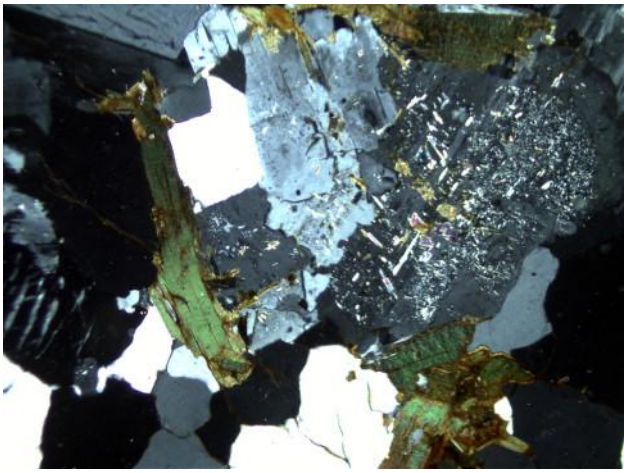

General view: Holocristalline seriate texture with feldspar, quartz, plagioclase and biotite. Sericite and muscovite (on feldspar) are also present.

CB 130101.01

Petrographic Description / Analysis

Medium grained igneous rock with phaneritic texture (holocrystalline seriate). Main minerals are quartz, plagioclase, feldspar, amphibole and biotite. Biotite crystals show preferred orientation. Accessory minerals are zircon, apatite, epidote and oxides. Secondary minerals are sericite and muscovite (on plagioclase and feldspar) and chlorite (on biotite).

Modal Analysis	(% estimated)
Quartz	40
Feldspar	20
Plagioclase	15
Biotite	16
Amphibole	5
Accessory Minerals	1
Secondary Minerals	*3*

Petrographic Classification (IUGS)

MONZOGRANITE

Pictures

left nicols // right nicols X – Picture dimension 2,8X 2,1 mm

General view: Holocristalline seriate texture with feldspar, quartz, plagioclase, amphibole and biotite. Sericite and chlorite are also present.

CB 130101.02

Petrographic Description / Analysis

Medium grained igneous rock with phaneritic texture (holocrystalline seriate). Crystals do not show preferred orientation. Main minerals are feldspar, quartz, plagioclase and biotite. Accessory minerals are zircon, apatite and oxides. Secondary minerals are sericite and muscovite (on plagioclase and feldspar) and chlorite (on biotite). Quartz crystals show dynamic recrystallization and ductile deformation.

Modal Analysis	(% estimated)
Quartz	38
Feldspar	30
Plagioclase	14
Biotite	14
Accessory Minerals	1
Secondary Minerals	3

Petrographic Classification (IUGS)

SYENOGRANITE

Pictures

left nicols // right nicols X – Picture dimension 2,8 X 2,1 mm

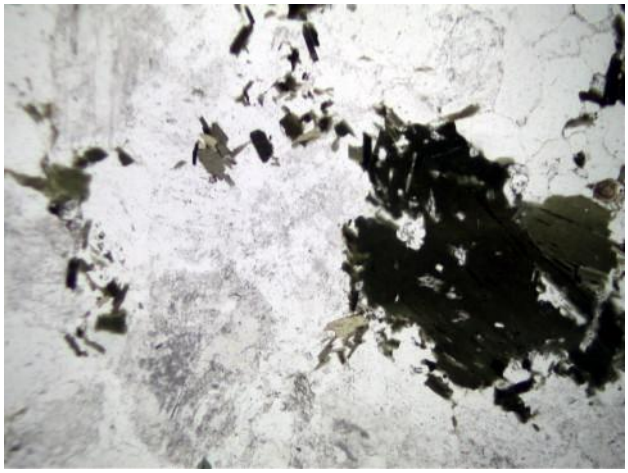

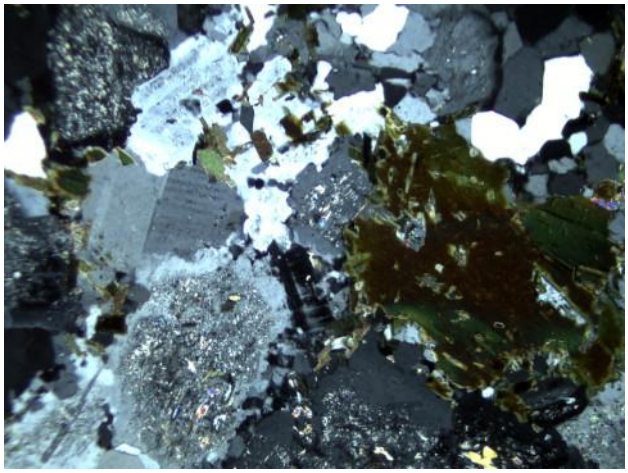

General view: Holocristalline seriate texture with feldspar, quartz, plagioclase and biotite. Sericite and muscovite (on feldspar) and chlorite (on biotite) are also present.

Ringraziamenti

Grazie a …

Professor Carlo Baroni, per aver creduto in me ed avermi permesso di intraprendere questo percorso. Grazie per essere sempre disponibile a condividere la sua grande cultura e per avermi insegnato (anche se devo ancora fare parecchia strada) ad interpretare e discutere il dato scientifico. Grazie per non essere mai banale nelle spiegazioni e per trasmettere una grande passione e dedizione verso il proprio lavoro.

Professoressa Maria Cristina Salvatore per avermi aiutato in tante situazioni dedicandomi molto tempo nonostante i sempre numerosi impegni. Grazie per mostrare costantemente il rigore scientifico ed il vivo interesse necessari per la risoluzione di qualunque problema. Grazie per aver mostrato una dedizione e passione per la didattica che terrò sempre da esempio. Infine, grazie per essere sempre disponibile nell'ascoltare e comprendere problemi anche a livello personale.

PD Dr. Susan Ivy-Ochs per avermi accolto e fatto sentire il benvenuto a Zurigo, lavorare nel suo laboratorio è stata un'esperienza molto importante e formativa. Grazie per essere sempre positiva e per i preziosi consigli utili a migliorare questa tesi.

Dr. Marcus Christl per aver misurato tutti i campioni presenti in questa tesi e per essere stato sempre positivo e disponibile nel dare consigli.

Professor Hans-Arno Synal per avermi accolto presso il Laboratory of Ion Beam Physics.

Grazie ai miei genitori, nulla di quello che ho ottenuto sarebbe stato possibile senza il vostro supporto.

Giulia e Riccardo, compagni di viaggio insostituibili.

La mia famiglia e gli amici di sempre.

Gli amici conosciuti a Pisa e con i quali ho condiviso questi anni; Fernanda, Karen, Alessandro, Salvatore, Ana, Francesca, Alberto.

Gli amici di Zurigo che mi hanno accolto e fatto sentire sempre a casa; Nuria, Anita, Nora, Belen, Martina, Olivia, Ingrid, Cristina, Ewelina, Laura, Chrisi, Maria, Caro, David, Sascha, Chris, Matze, Noldi, Daniele, Daniel, Adam.

E naturalmente…tutti quelli che ho dimenticato.

Thanks

Thanks to ...

Professor Carlo Baroni, for believing in me and allowing me to take this path. Thanks for being always available to share his great culture, and for teaching me (although I still have a long way) to interpret and discuss the scientific data. Thank you for never being banal in the explanations and to convey the great passion and dedication for his work.

Professor Maria Cristina Salvatore for helping me in many situations devoting much time despite the increasingly busy schedules. Thanks to show constantly the scientific rigor and keen interest necessary for the resolution of any problem. Thanks for showing dedication and passion for teaching that I will always by example. Finally, thanks for being always available to listen to and understand problems even on a personal level.

PD Dr. Susan Ivy-Ochs for welcoming me and made to feel at home in Zurich, working in your laboratory was very important and formative. Thanks for being always positive and thank you for the valuable advice useful to improve this thesis.

Dr. Marcus Christl for all samples measured in this thesis and for being always positive and helpful in giving advice.

Professor Hans-Arno Synal for welcoming me at the Laboratory of Ion Beam Physics.

Thanks to my parents, nothing of what I have achieved would have been possible without you.

Giulia and Riccardo, friends in this journey.

My family and the old friends.

The friends met in Pisa and with whom I shared the last three years; Fernanda, Karen, Alessandro, Salvatore, Ana, Francesca, Alberto.

The Zurich friends who welcomed me and made me feel at home; Nuria, Anita, Nora, Belen, Martina, Olivia, Ingrid, Cristina, Ewelina, Laura, Chrisi, Maria, Caro, David, Sascha, Chris, Matze, Noldi, Daniele, Daniel, Adam.

And of course ... everyone I've forgotten.